UNIVERSITÀ DELLA CALABRIA

Dottorato di Ricerca in
Ingegneria dei Materiali e delle Strutture
- Ciclo XX -

Simplified Methods for Dynamic Analysis of Structures under Blast Loading

by

Manuel Campidelli

November 2007

UNIVERSITÀ DELLA CALABRIA

Dottorato di Ricerca in
Ingegneria dei Materiali e delle Strutture
- Ciclo XX -

Simplified Methods for Dynamic Analysis of Structures under Blast Loading

by

Manuel Campidelli

A dissertation submitted in fulfillment
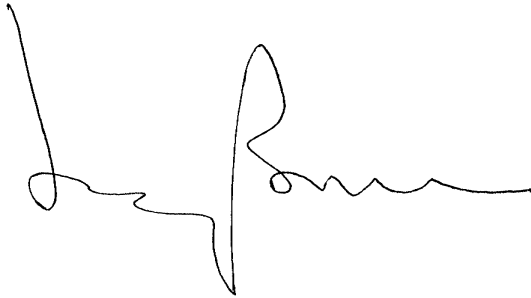of the requirements for the degree of

Doctor of Philosophy

ADVISOR
Professor Erasmo Viola

PH.D. COORDINATOR
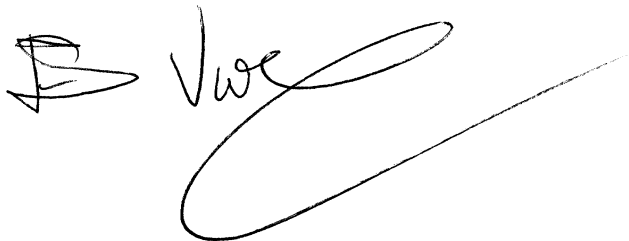Professor Domenico Bruno

November 2007

The dissertation of Manuel Campidelli is approved:

	25.11.07
Professor Domenico Bruno	Date

	25.11.07
Professor Erasmo Viola	Date

	Date

Università della Calabria, Rende

November 2007

Simplified Methods for Dynamic Analysis
of Structures under Blast Loading

ABSTRACT

Simplified Methods for Dynamic Analysis
of Structures under Blast Loading
by
Manuel Campidelli

The increasing threat of extremely severe loading conditions caused by a number of explosive sources made engineers and scientists developing, during the last half century, several methods of analysis and design of blast–resistant structures. Simple, intermediate, and advanced computational approaches have been adopted, requiring increasing computational resources. These efforts led to the publication of several manuals and guidelines for the analysis and design of blast–resistant reinforced concrete and steel structures, mostly based on simple considerations derived from Single Degree of Freedom (SDOF) models. Although the development of future guidelines based on advanced numerical techniques is desirable, typical design activities cannot be effectively carried out by applying complex methods, because of their large demand of resources. Therefore the necessity to develop simplified, low time consuming, methods of analysis, capable of supporting a daily design activity and, at the same time, takeing into account issues usually neglected, such as a strong non linear material behavior and the influence of the strain rate caused by a blast load on the structural response. The development of such design tools is the object of this study. The first part of this thesis deals with the influence of the blast load shape on the dynamic response of an undamped linear elastic oscillator. Response spectrum and pressure–impulse diagrams are shown for several shape parameters, and a sensitivity analysis of the results with respect to the computational parameters is also presented. A method validation is carried out via genetic algorithms, through a careful calibration of all the genetic parameters, such as crossover fraction and number of elite elements. Non linear material modeling and strain rate dependent constitutive laws are objects of the second part of this dissertation. A non linear oscillator made of displacement, velocity, and acceleration dependent springs and dampers, under an arbitrary dynamic load, is proposed. Spring and damper constitutive laws have no restrictions as well as the load–time function, and the dynamic analysis is accomplished by a piecewise linear approximation of any input function. Numerical problems are dealt with by applying the Newton–Raphson method, in such a way that enables the error range to be estab-

lished "a priori". Any possible drawback of this method is carefully avoided, and a quadratic speed of convergence is always ensured. Since the model provides velocity dependent springs, strain rate effects of blast loads on the structural response are taken into account by including strain rate dependent constitutive laws within the problem definition.

"The truth will set you free,
but first it will make you miserable."
J. A. Garfield

ACKNOWLEDGMENTS

I would like to thank my advisor, Erasmo Viola, for giving me so much freedom to explore new areas of structural dynamics.

I would also like to thank all the people who have been supportive over the years of my fellowship and while I was writing this thesis.

Contents

Chapter 1

Introduction

1.1 Scope and objectives of the research

Since after World War II, the effects of both conventional and non–conventional explosives have been well documented. The increasing hazard of terrorist attacks, as well as major catastrophes resulting from petro–chemical explosions, aircraft crashes, nuclear leakage, and large magnitude earthquakes, threaten military and civil structures with extreme and extraordinary loading conditions, which require a better understanding of blast effects and how they may be mitigated. Due to the threat from such severe loading conditions, efforts have been made during the last half century to develop techniques of design and structural analysis to resist blast loads. Simple, intermediate, and advanced computational approaches have been used, requiring increasing computational resources. Single Degree of Freedom (SDOF) models and Multi–degree of Freedom (MDOF) models have been widely used as simple methods, based on linear, or very simple non linear, structural behavior assumptions. Among the intermediate approaches, it is worth recalling the Timoshenko beam and Mindlin plate formulations, capable to provide detailed behavior information despite modest computational resources. Advanced methods include many finite element, finite difference, and hybrid codes. These efforts led to the publication of several manuals and guidelines for the analysis and design of blast–resistant reinforced concrete and steel structures, such as the U.S. manual TM 5-1300, mostly based on simple SDOF considerations. Although the development of future guidelines based on advanced numerical techniques is desirable, typical design activities cannot be effectively carried out by applying complex methods, because of their large demand of resources. Therefore the necessity to develop simplified, low time consuming, methods of analysis, capable of supporting a daily design activity

and, at same time, taking into account issues usually neglected, such as a strong non linear behavior and the influence of the strain rate caused by a blast load on the characteristics of the material the target structure is made of. The development of such structural design tools is pursued in this thesis.

1.2   Outlines of the thesis

Chapter 2 reports a literature review of blast phenomena including the basic characteristics of blast waves yielded by several explosion sources, the interaction of blast waves with different type of structures, the effects of air blast loads resulting from external explosions, internal explosions, and ground shocks.

Failure mechanisms induced by blast loads and corresponding damage criteria are reviewed in chapter 3. The effects of strain rate on the dynamic strength of concrete, reinforcing steel, and reinforced concrete are also highlighted.

Chapter 4 is focused on the dynamic response of a linear undamped oscillator, with special attention to the limits of structural response. The first part of this chapter deals with the problem of finding a response spectrum of such system under several load shapes, while the second part concerns the representation of the damage level via pressure–impulse diagrams. A sensitivity analysis is also carried out in order to survey how the structural response is affected by the computational parameters. Finally, a method validation is accomplished via genetic algorithms, through a careful calibration of all the genetic parameters, such as crossover fraction and number of elite elements.

A more complex structural model is proposed in chapter 5. It consists of a non linear oscillator made of displacement, velocity, and acceleration dependent springs and dampers, under an arbitrary dynamic load. Spring and damper constitutive laws have no restrictions as well as the load–time function, and the dynamic analysis is accomplished by a piecewise linear approximation of any input function. Numerical problems are dealt with by applying the Newton–Raphson method, in such a way that enables the error range to be established "a priori". Any possible drawback of this method is carefully avoided, and a quadratic speed of convergence is always ensured. Full details of Newton's method applications are presented in appendix B. Since the model provides velocity dependent springs, strain rate effects of blast loads on the structural response are taken into account by including strain rate dependent constitutive laws within the problem definition.

Conclusions and recommendations for future work are given in Chapter 6.

Appendices A and B present a brief review of the Newton–Raphson method and its application to a single–variable problem. Speed of convergence, efficiency, and drawbacks of this method are highlighted in appendix A. Four lemmas are proposed in appendix B, each of them showing an application of Newton's method involving a speed of convergence at least quadratic. Since such lemmas are the key to solve the non linear model proposed in chapter 5, original proofs of any of them have been developed, though a more extensive literature survey might make them unnecessary.

Appendix C reports some recurrent trigonometric identities.

Chapter 2

Blast Phenomena

2.1   Historical background

The most common artificial explosives are chemical explosives, usually involving a rapid and violent oxidation reaction that produces large amounts of hot gas. Gunpowder was the first explosive to be discovered and put to use. Other notable early developments in chemical explosive technology were Frederick Augustus Abel's development of nitrocellulose (guncotton) in 1865 and Alfred Nobel's invention of dynamite (stabilized nitroglycerin) in 1866. A new order of explosive, the nuclear bomb, was invented in 1945 by Allied scientists. In 1952, the US military developed the first fusion bomb.

2.2   Natural and artificial explosions

An explosion is a sudden increase in volume and release of energy, usually with the generation of high temperatures and the release of gases. Explosions do not commonly occur in nature. On Earth, most natural explosions are caused by volcanic processes. Explosive volcanic eruptions occur when magma rising from the mantle below the Earth crust contains large quantities of dissolved gas; the reduction of pressure as the magma rises causes the gas to bubble out of solution, resulting in a rapid increase in volume. Explosions also occur as a result of Earth impacts. Solar flares are an example of explosion common on the Sun, and presumably on many other stars. Among the largest known explosions in the universe are supernovae, which result from stars exploding and gamma ray bursts.

Artificial explosions, on the other hand, are unfortunately much more common and may have many different sources. The rapture of a vessel containing a pres-

surized liquid causes a rapid increase in volume as the liquid evaporates, which may lead to a boiling liquid expanding vapour explosion. A high current electrical fault may create an electrical explosion by forming a high energy electrical arc which rapidly vaporizes metal and insulation material. Excessive magnetic pressure within an ultra–strong electromagnet may cause a magnetic explosion. It is well known the risk of accidental explosions in many workplaces which may contain, or have activities that produce, an explosive or potentially explosive atmosphere, that is a mixture of dangerous substances with air under atmospheric conditions, in the form of gases, vapours, mist or dust in which, after ignition has occurred, combustion spreads to the entire unburned mixture. Examples include places where work activities create or release flammable gases or vapours, such as vehicle paint spraying, workplaces where fine organic dusts such as grain flour or wood are handled, and petroleum refineries or chemical plants, which process hydrocarbons and other inflammable fuels. Although some of these workplaces are designed to minimize the occurrence of accidental explosions, when they do occur the consequences might be extremely severe, particularly for buildings not specifically designed to withstand blast effects.

Intentional explosion are obtained by the ignition of several kind of explosive compounds, which may be defined as materials that either are chemically or otherwise energetically unstable. Upon initiation, such materials undergo a chemical decomposition or a nuclear reaction (fission or fusion), which causes a sudden volume expansion usually accompanied by the production of heat and large changes in pressure (and typically also a flash and/or loud noise). Chemical explosives are classified as low or high explosives according to their rates of decomposition; low explosives burn rapidly (or deflagrate), while high explosives undergo detonations. No sharp distinction exists between low and high explosives, because of the difficulties inherent in precisely observing and measuring rapid decomposition. A low explosive is usually a mixture of a combustible substance and an oxidant that decomposes rapidly (deflagration); unlike most high explosives, which are compounds. Under normal conditions, low explosives undergo deflagration at rates that vary from a few centimeters per second to approximately 400 meters per second. However, it is possible for them to deflagrate very quickly, producing an effect similar to a detonation, but not an actual detonation; this usually occurs when ignited in a confined space. Low explosives are normally employed as propellants. Included in this group are gun powders and pyrotechnics such as flares and illumination devices. High explosives are normally employed in mining, demolition, and military warheads. They undergo

detonation at rates of 1,000 to 9,000 meters per second. High explosives may be conventionally subdivided into three classes differentiated by sensitivity. Primary explosives are extremely sensitive to mechanical shock, friction, and heat, to which they will respond by burning rapidly or detonating. Secondary explosives, also called base explosives, are relatively insensitive to shock, friction, and heat. They may burn when exposed to heat or flame in small, unconfined quantities, but detonation can occur. These are sometimes added in small amounts to blasting caps to boost their power. Dynamite, TNT, RDX, PETN, HMX, and others are secondary explosives. PETN is often considered a benchmark compound, with materials that are more sensitive than PETN being classified as primary explosives. Tertiary explosives, also called blasting agents, are so insensitive to shock that they cannot be reliably detonated by practical quantities of primary explosive, and instead require an intermediate explosive booster of secondary explosive. Examples include an ammonium nitrate/fuel oil mixture (ANFO) and slurry or "wet bag" explosives. These are primarily used in large-scale mining and construction operations.

2.3 Detonation process

A detonation is an extremely rapid release of energy in the form of light, heat, sound, and a shock wave. A shock wave consists of highly compressed air traveling radially outward from the source at supersonic velocities. As the shock wave expands, pressures decrease rapidly (with the cube of the distance) and, when it meets a surface that is in line–of–sight of the explosion, it is reflected and amplified by a factor of up to thirteen (see Kinney and Graham [1] for more details). Pressures also decay rapidly over time (i.e., exponentially) and have a very brief span of existence, measured typically in milliseconds. Diffraction effects, caused by corners of a building, may act to confine the air–blast, prolonging its duration. Late in the explosive event, the shock wave becomes negative, creating suction. Behind the shock wave, where a vacuum has been created, air rushes in, creating a powerful wind or drag pressure on all surfaces of the building. This wind picks up and carries flying debris in the vicinity of the detonation. In an external explosion, a portion of the energy is also imparted to the ground, creating a crater and generating a ground shock wave analogous to a high–intensity, short–duration earthquake.

2.4   Regular and Mach reflection

The blast load acting on the target structure is strongly affected by the angle of incidence α_1 of the blast wave on the target surface. When $\alpha_1 = 0°$, the blast wave impinges on the surface at zero angle of incidence. The reflection occurs when the forward moving gas molecules are stopped and compressed above the incident pressure, inducing a reflected blast wave. In case of $\alpha_1 = 90°$ the incident blast wave front, traveling at velocity U_s parallel to the structure surface, does not undergo any reflection and the target is loaded by the incident overpressure. Regular and Mach reflections take place when α_1 lies within the intervals $[0°, \alpha_{lim}]$ and $[\alpha_{lim}, 90°]$ respectively, where α_{lim} is a threshold value depending on the medium the blast wave is propagating in. For air this angle is approximately $40°$. Mach reflection is a complex process and is sometimes described as a "spurt–type" effect where the incident wave skims off the reflecting surface rather than bouncing on it (Smith and Hetherington [2]). It occurs when the reflected wave catch up with the incident wave at some point above the reflecting surface, yielding a third wave called Mach stem. The point where the three waves meet together is called triple point, and it follows a path shown in Fig. 2.1 (b).

The target location with respect to the triple point affects the blast load undergone by the structure. Targets above the triple point path undergo the effects of both the incident and reflected waves, whereas structures below such path are under a single vertical shock Mach stem propagating parallel to the reflecting surface. Examples requiring the Mach stem effects to be taken into account are detonations at some height above the ground and internal explosions, in which case the blast waves may be reflected by the internal surfaces of the structure with a wide range of angles (Baker *et al.* [3]).

Reflected wave

Incident wave

P_i

P_r

α_1

2.1 (a). Regular reflection

Explosion source

I

R

Path of triple point

I

R

I

Mach stem

I

R

I

R

I

R

R

I

R

Regular reflection region

Triple point

Mach reflection region

(I = Incident, R = Reflected)
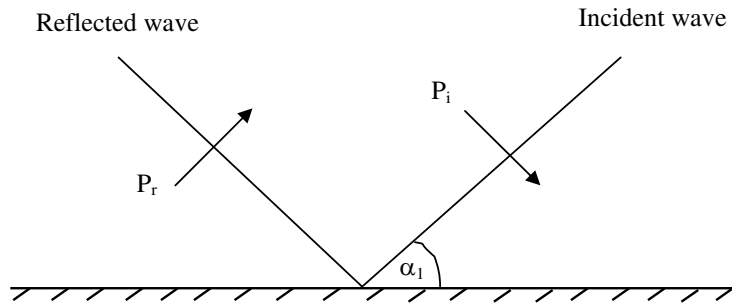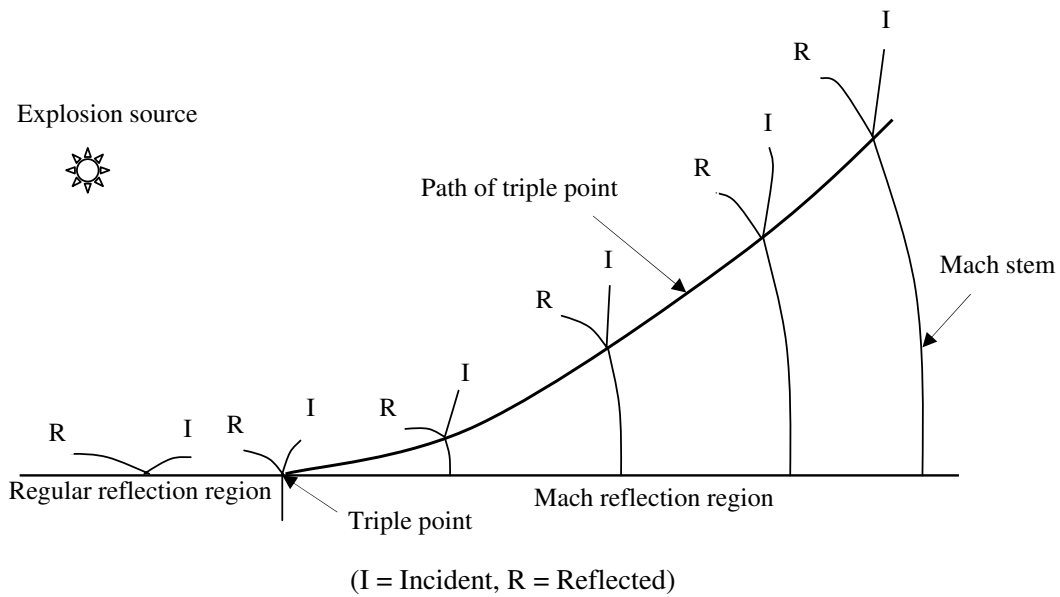
2.1 (b). Mach reflection

Fig. 2.1. Regular and Mach reflection (Baker, [4]).

2.5   Ideal blast wave pressure profile

Regardless the the physical properties of an explosion source, at some point far from the explosion centre all blast waves develop the same pressure profile, shown in Fig. 2.2. At a time t_A, representing the time when a blast wavefront reaches a certain point nearby the charge, the pressure at that location undergoes a step rise above the ambient pressure P_0, reaching its peak value P_{s0}. A rapid decay, usually idealized as exponential, follows, which brings back the pressure to the ambient value at a time $t_A + t_0$. This part of the pressure–time profile is usually called positive phase, since the wavefront pressure remains above the ambient value. A mathematical description of such phase, representing the side– on overpressure P_s
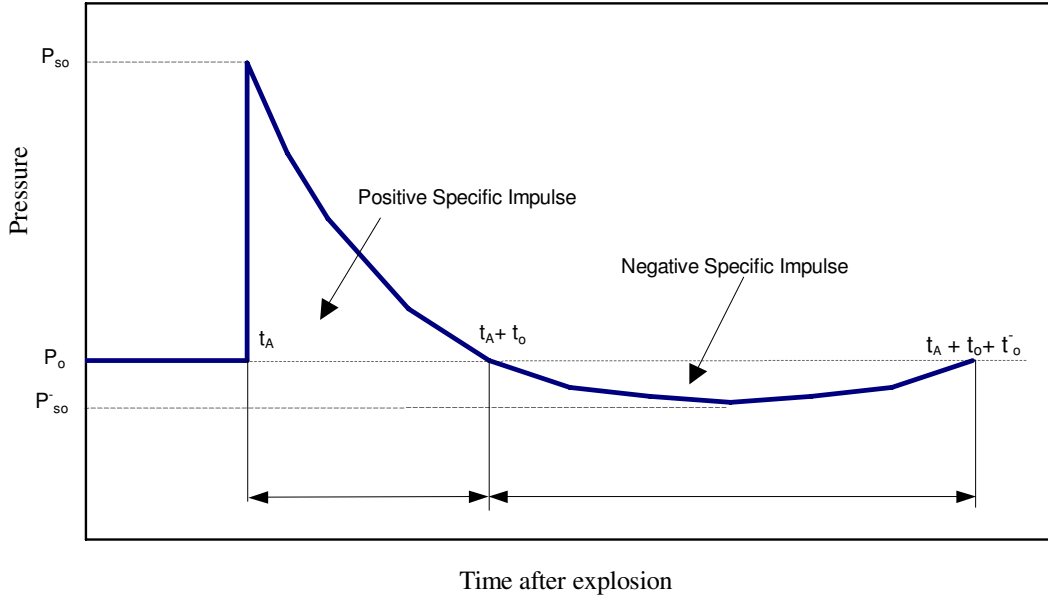
Fig. 2.2. Pressure–time profile of blast wave in free air (TM 5–1300 [6])

as a function of time t and a dimensionless coefficient α, was proposed by Baker [4],

$$P_s(t) = P_{s0} \left(1 - \frac{t}{t_0} \right) e^{-\alpha \frac{t}{t_0}}$$

After $t_A + t_0$, because of the momentum gained by the gas particles, a negative phase of suction takes place, during which the pressure decreases until it reaches a partial vacuum of peak under pressure P_{s0}^{-}, and then returns to P_{s0} at a time $t_A + t_0 + t_0^{-}$. Notoriously, the negative phase last longer than the positive one but is much less intense ($|P_{s0}^{-}| \ll |P_{s0}|$), therefore it is usually neglected. On the contrary, positive phase parameters such as peak overpressure, duration, dynamic pressure, shock front velocity, and wind velocity are essential in order to establish the load acting on the target structure. Simplified pressure–time functions describing the positive phase have been suggested over the years by many authors. Amon them, Newmark [5] proposed a linear equivalent profile, characterized by the same initial peak overpressure P_{s0} but different durations.

2.6   Blast wave front parameters

Analytical expressions of blast wave front parameters have been reported in a number of publications (Liepmann and A.Roshko [7], Brode [8], Baker [4], Smith and

9

Explosive	Mass Specific Energy Q_x (KJ/Kg)	TNT Equivalent Q_x/Q_{TNT}
Amatol 80/20 (80% ammonium nitrate, 20% TNT)	2650	0.586
Compound B (60% RDX, 40% TNT)	5190	1.148
RDX (Cyclonite)	5360	1.185
HMX	5680	1.256
Lead azide	1540	0.340
Mercury fulminate	1790	0.395
Nitroglycerin (liquid)	6700	1.481
PETN	5800	1.282
Pentolite 50/50 (50% PENT, 50% TNT)	5110	1.129
Tetryl	4520	1.000
TNT	4520	1.000
Torpex (42% RDX, 40% TNT, 18% Aluminium)	7540	1.667
Blastin gelatin (91% nitroglycerin, 7.9% nitrocellulose, 0.9% antacid, 0.2% water	4520	1.000
60% Nitroglycerin Dynamite	2710	0.600

Tab. 2.1. TNT equivalent mass: conversion factors for common explosives (Baker [3]).

Hetherington [2]). Brode's [8] numerical analysis of spherical blast waves from an air burst of high explosives led to the following expressions, regarding the velocity of the wave front U_s, the maximum dynamic pressure P_d, and the peak static overpressure P_s

$$U_s = \sqrt{\frac{6P_{s0} + 7P_0}{7P_0}} \cdot a_0 \tag{2.1}$$

$$P_d = \frac{5P_{s0}^2}{2(P_{s0} + 7P_0)} \tag{2.2}$$

$$P_{s0} = -0.019 + \frac{0.975}{Z} + \frac{1.455}{Z^2} + \frac{585}{Z^3}, \qquad 0.1 < P_{s0} < 10 \ (\text{bar}) \tag{2.3}$$

$$P_{s0} = \frac{6.7}{Z^3} + 1, \qquad P_{s0} > 10 \ (\text{bar}) \tag{2.4}$$

P_{s0} being the peak side–on overpressure, P_0 the ambient air pressure in bars and

a_0 the speed of sound in air at ambient pressure. Z is the scaled distance given by

$$Z = \frac{SD}{m^{\frac{1}{3}}} \tag{2.5}$$

where SD id the standoff distance from the charge centre in meters and m is the charge mass in kilograms of TNT.

Since the actual charge needs to be converted in an equivalent mass of TNT, many approaches have been introduced over the years in order to achieve such result. Among them, it is worth recalling the methods adopted in the technical manual TM5–855–1 [9] and by Baker *et al.* [3]. The former is based on two conversion factors, which enable to mach either the peak overpressure or the impulse delivered by the actual explosive and the TNT equivalent. The latter is based on a single conversion factor, equal to the ratio between the mass specific energy of the actual explosive and the mass specific energy of TNT. Ratios for the most common explosives are shown in Tab. 2.1.

2.7 Blast wave scaling laws

Since physical proprieties of explosives and medium the blast waves propagate through affect the blast waves themselves, the necessity of relating different types of explosions to some reference, ideal, cases, arises. Non ideal explosions may be related to reference experiments conducted in ideal conditions by the Hopkinson–Cranz [10, 11] scaling law, commonly known as the cube–root scaling law. This law states that two explosive charges of different sizes, similar geometry, and of the same explosive, detonated in the same atmospheric conditions, yield self–similar blast waves at equal scaled distances (Baker [3]). The scaled distance Z is defined in the Eq. (2.5). The Hopkinson law, applied to the diameters d_1 and d_2 of spherical charges, leads to the following relation,

$$\frac{d_1}{d_2} = \left(\frac{m_1}{m_2}\right)^{\frac{1}{3}} = \frac{SD_1}{SD_2}$$

where SD_1 and SD_2 are the standoff distances at which the two explosives yield the same blast wave.

Scaling law applies to other parameters, such as time t,

$$t_{sc} = \frac{t}{m^{\frac{1}{3}}}$$

where t_{sc} stands for scaled time.

2.8   Blast wave interactions

In order to establish the the blast load acting on a target structure, it is of fundamental importance to understand the interaction phenomena that take place as soon as a blast wave, while propagating outward the explosion source, strikes an object of density higher than that of the medium surrounding the charge. Interaction effects are usually categorized as *diffraction effects* and *drag effects*.

The regular and Mach reflection process described above is referred to infinite reflecting surfaces, which do not allow diffraction to occur. Diffraction effects, in fact, are essentially caused by the finite size of the target compared to the scale of the blast, and consist of how the side–on overpressure evolves and reflects on any target surface. Drag effects, on the other hand, are caused by the drag force due to the dynamic pressure (transient wind) behind the blast wave front. Such pressure is much less intense than the wave front overpressure, but the resulting drag loading last much longer than the diffraction loads. Also, it is worth mentioning that the drag pressure is responsible for carrying the debris away from the explosion site. Both diffraction and drag effects are responsible, in different measure, of the damage undergone by the hit target.

According to Newmark1 [5], depending on the the kind of load the damage is mostly caused by, target structures may be roughly classified as *diffraction–type* or *drag–type*. The former are mainly affected by the wavefront overpressure, and a good example is offered by buildings having sturdy external walls and relatively small venting areas, under a large–scale blast wave, such as multi–storey reinforced concrete buildings undergoing the effects of a big explosive charge externally detonated. If this is the case, the structure is engulfed and crushed by the blast waves, and is also loaded by a drag force tending to move the whole building laterally, which is unlike to happen due to the size of the target. A different scenario, emphasizing drag effects, might be the case of a large–scale blast wave interacting with a small structure, such as a vehicle. Here the target is still engulfed and crushed and, due to its size, any part of the vehicle experiences more or less the same overpressure. The resultant translational force lasts for a short time end it is unlikely to yield remarkable damage, therefore diffraction effects may be neglected. On the opposite, the drag force produced by the dynamic pressure acts sufficiently long to move a such light target, and it is very likely that a substantial part of the resulting damage

is caused by this motion. Other structures undergoing dominant drag effects are electric transmission towers, telephone poles, smoke stacks, truss bridges, etc...

It is finally worth recalling that the detonation of small amounts of explosive might yield blast loads affecting structural elements in different ways, depending on their location with respect to the explosion source.

Fig. 2.3 shows the engulfing and dynamic pressure variation on the structure surfaces at significant times. The blast wave, approaching orthogonally the side facing the charge (Fig. 2.3 (a)), loads the front face with a peak reflected pressure of value P_r, at a time t_2. Consequently, the structure experience a push to the right as diffraction effect. As soon as the wave passes over and round the target, the reflected pressure on the front face decays within a time interval $t_c - t_2$ (Fig. 2.3 (b)), where t_c is given approximately by

$$t_c = \frac{3S}{U_s}$$

S being the smaller of half of the structure breadth or height and U_s being the blast wave front velocity. The front face pressure continues to decay until the stagnation pressure, P_{stag}, equal to the sum of the dynamic pressure P_d and the incident wave overpressure P_s, is reached. At a time t_3, the blast wave reaches the rear face (Fig. 2.3 (c)), and the diffraction is completed with a further, less intense, push of the building to the right. Drag loads also start acting on the front face at the time t_2 (Fig. 2.3 (d)), causing a push on the left side, followed by a suction force on the opposite side as the blast wind reaches the rear face at a time t_3 (Fig. 2.3 (e)). The drag force F_D acting both sides of the target may be expressed in terms of a drag coefficient C_D, the loaded area A, and the peak of dynamic pressure P_d, as $F_D = C_D \cdot A \cdot P_d$.

2.9   External explosions

According to the technical manual TM 5–1300 [6], a blast load from convention explosives acting on a target structure consists of three components, the incident wave overpressure, which is a function of mass and type of explosive as well as the standoff distance, the reflected pressure, due to the interaction of the incident wave with the target surfaces, and the dynamic pressure, caused by the transient wind behind the wave front. All those parameters need to be estimated in order to define an ideal pressure–time profile.

Propagating
blast wave
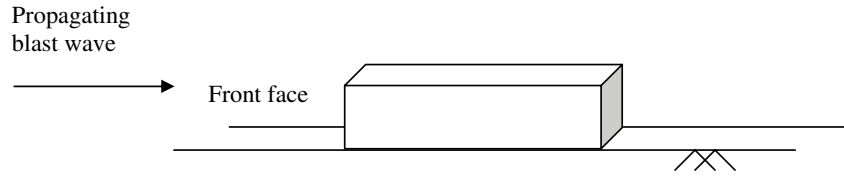
Front face

2.3 (a). Elevation of the structure

$$P_{stag}(t) = P_{so}(t) + P_d(t)$$
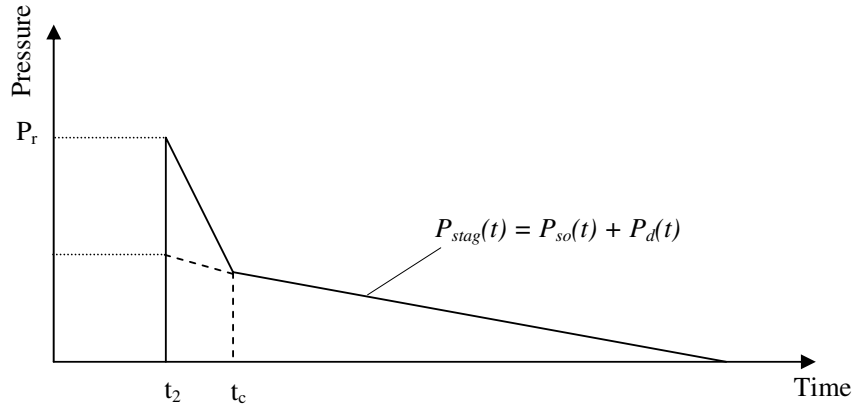
2.3 (b). Diffraction loads (front face)
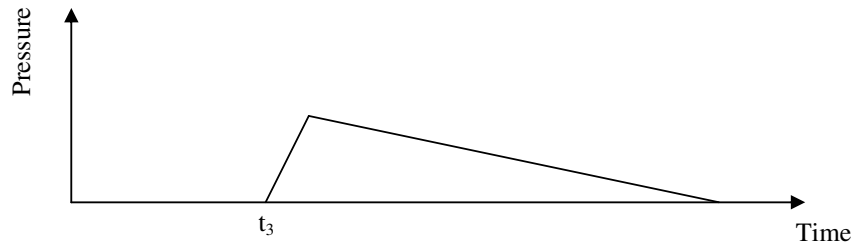
2.3 (c). Diffraction loads (rear face)

$C_D = 1 \sim 1.2$
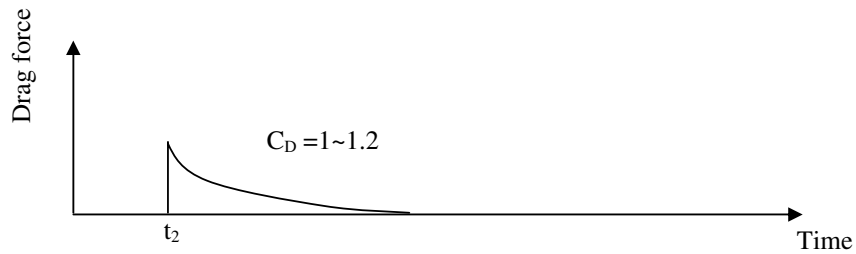
2.3 (d). Drag loads (front face)

$C_D = -0.3$
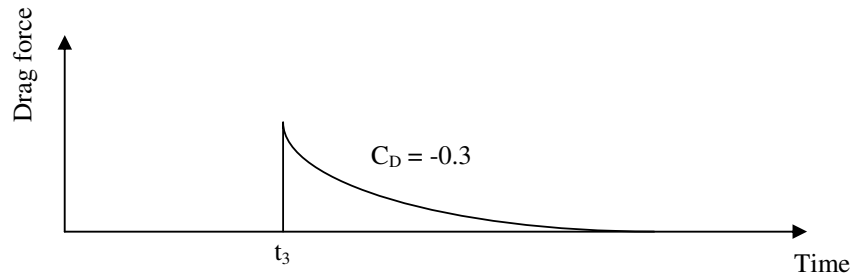
2.3 (e). Drag loads (rear face)

Fig. 2.3. Diffraction and drag effects of blast loads on *diffraction–type* structures (Smith and Hetherington [2]).

14

2.9.1 Peak wave front overpressure

Many expressions have been proposed over the years to predict the peak side–on overpressure P_{s0} of a blast wavefront (Newmark and Hansen [12], Mills [13], Crawford and Karagozian [14]).

In 1961 Newmark and Hansen [12] introduced the side–on overpressure, in bars, yielded by a detonation at the ground surface as a function of the standoff distance SD, between the charge centre and the point of measurements, and the equivalent mass of explosive, m, expressed in tons of TNT,

$$P_{s0} = 6784 \frac{m}{SD^3} + 93 \left(\frac{m}{SD^3} \right)^{\frac{1}{2}}$$

In 1987 Mills [13] proposed the following expression

$$P_{s0} = \frac{1772}{Z^3} - \frac{114}{Z^2} + \frac{108}{Z}$$

where the peak overpressure is expressed in kPa and Z is the scaled distance from the Eq. (2.5).

New equations involving the peak side–on overpressure in psi and the positive phase duration (t_0) in second were presented in 1995 by Crawford and Karagozian [14],

$$\frac{P_{s0}}{P_0} = \frac{40.4\,SD^2 + 810}{\sqrt{(1 + 434\,SD^2)(9.77\,SD^2)(1 - 0.55\,SD^2)}}$$

$$\frac{t_0}{m^{\frac{1}{3}}} = \frac{990 + 4.65 \cdot 10^5\,SD^{10}}{(1 + 125 \cdot 10^3\,SD^3)(1 + 6.1\,SD^6)\sqrt{1 + 0.02\,SD^2}}$$

where m is the charge mass in Kilotons of TNT, P_{s0} is the ambient atmospheric pressure in psi, and SD still stands for standoff distance.

2.9.2 Reflected pressure

Shock parameters of the reflected wave, derived from consideration of conservation of momentum and energy, were reported by Smith and Hetherington [2] in terms of incident wave front parameters. For a zero angle of incidence, the reflected peak pressure P_r was given as a function of incident peak overpressure and dynamic pressure,

$$P_r = 2P_{s0} + (\gamma + 1)P_d \tag{2.6}$$

in which γ is the specific heat ration of the air, idealized as a perfect gas. By substituting the dynamic pressure from the Eqs. (2.2), when γ is set equal to 1.4, the equation above becomes

$$P_r = 2P_{s0}\frac{7P_0 + 4P_{s0}}{7P_0 + P_{s0}} \tag{2.7}$$

If a reflection coefficient is defined as the ratio of the reflected pressure to the incident pressure, Eq. (2.7) predicts that such coefficient lies within the interval [2, 8]. Nevertheless, due to gas dissociation effects at very close range, reflection coefficients of up to 20 have been measured, pointing out the inadequate approximation, nearby the charge, of the air as an ideal gas. An alternative and empirically based expression for P_r was also given by Newmark [15],

$$P_r = P_{s0}(1.5 + 4\log_{10} P_{s0})$$

In case of a lack of accurate predictions, the reflected specific impulse i_r may be estimated by assuming similarities between incident and reflected blast wave pressure–time profiles (Baker [3]),

$$\frac{i_r}{i_s} = \frac{P_r}{P_{s0}}$$

which requires the knowledge of the incident wave specific impulse i_s.

2.9.3 Dynamic pressure

As previously stated, drag–type structures may be severely damage by the transient wind behind the blast wave front. Drag effects are cause by the dynamic pressure, which depends upon the velocity of the shock front, the peak wind velocity, and the density of air behind the shock front (Baker [4], Kinney and Graham [1]). The wave front velocity is calculated as

$$U_s = C_0 M_s$$

where C_0 is the speed of sound in the atmosphere surrounding the charge and M_s is the Mach number corresponding to the peak overpressure of the shock front and specific heat of the air r_h,

$$M_s = \left[1 + \frac{r_h + 1}{2r_h}\frac{P_{s0}}{P_0}\right]^{-\frac{1}{2}}$$

16

The particle velocity is given by

$$u_s = \frac{2}{1 + r_h} \cdot \frac{U_s^2 - C_0^2}{U_s}$$

The technical manual TM 5-1300 introduces the following expressions for the wind speed and the air density behind the shock front (ρ_s),

$$u_s = \frac{C_0 P_{s0}}{r_h P_0} \left[1 + \frac{r_h + 1}{2 r_h} \frac{P_{s0}}{P_0} \right]^{-\frac{1}{2}}$$

$$\rho_s = \rho_0 \frac{(\gamma + 1) P_{s0} + 2\gamma P_0}{(\gamma - 1) P_{s0} + 2\gamma P_0}$$

Recalling the definition of the dynamic pressure as kinetic energy per mass unit, finally we get

$$P_d = \frac{1}{2} \rho_s u_s^2 = \frac{P_{s0}^2}{2\gamma P_0 + (\gamma - 1) P_{s0}}$$

which, for $\gamma = 1.4$, yields

$$P_d = 2.5 \frac{P_{s0}^2}{7 P_0 + P_{s0}}$$

2.9.4 External blast loading

A simple geometry target under the effects of a free air burst or a surface burst (Fig.2.3 (a)) undergoes a resultant translational force equal to the difference between the front face and the rear face loading. The target roof is also subjected to a vertical force, which develops while the shock front passes above the structure. In order to establish such forces, it is necessary to know the pressure–time history acting on the front face, the rear face, and the roof of the target. Moreover, in case the shock waves take a long time to cross the whole structure from the front side to the rear one, the fundamental characteristics of the wave acting on the front and rear faces may be different. If that was the case, a separate pressure–time history for each of the two sides would be needed. As shown in Fig. 2.4 (a), as soon as the the blast wave strikes the front face, that side of the target experiences a pressure rising almost instantaneously up to the value P_r, followed by a decay to a value equal to the sum of the dynamic pressure and the side–on overpressure. The time interval elapsed during that stage of the diffraction process is called clearing time, t_c, and it is established by the following ratio
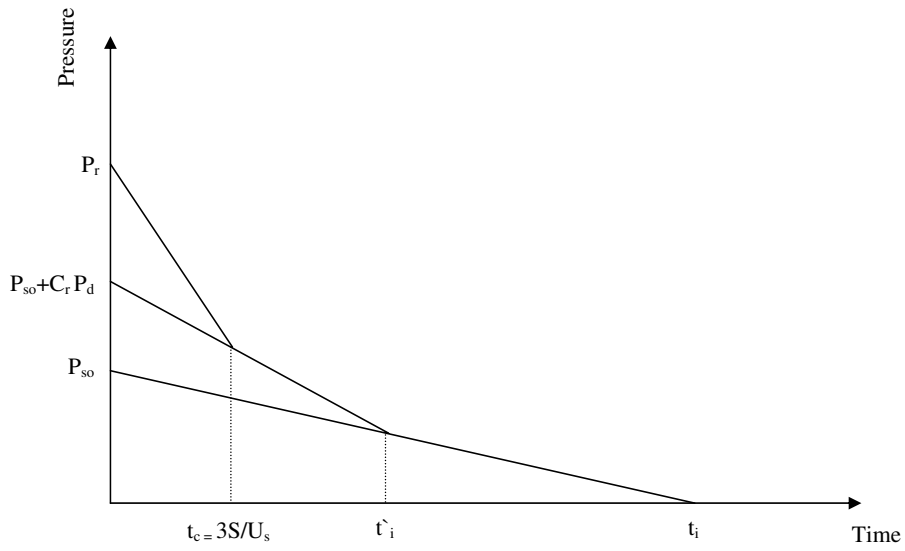
2.4 (a). Resultant pressure on front face

Figure (a) axis labels: Pressure (vertical), Time (horizontal). Marked values: P_r, $P_{so}+C_r P_d$, P_{so}. Horizontal axis marks: $t_{c\,=}\,3S/U_s$, $t\grave{}_i$, t_i.
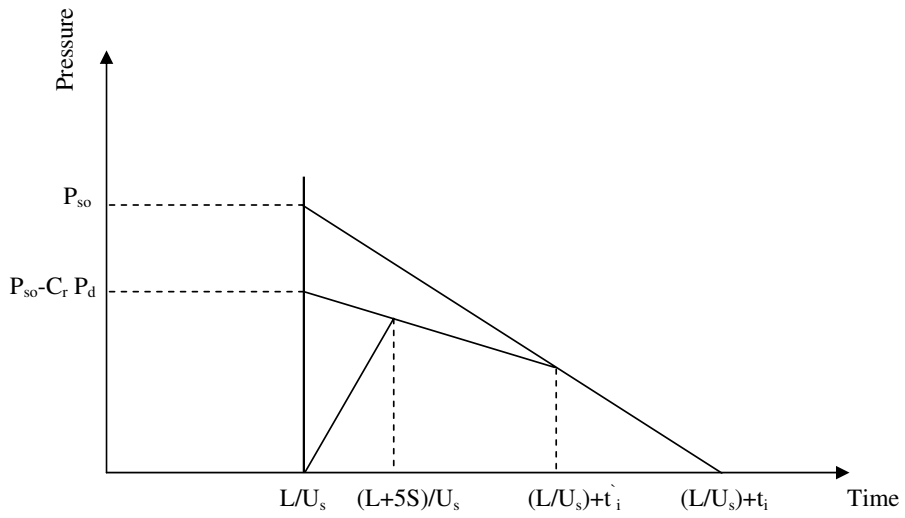
2.4 (b). Resultant pressure on rear face

Figure (b) axis labels: Pressure (vertical), Time (horizontal). Marked values: P_{so}, $P_{so}-C_r P_d$. Horizontal axis marks: L/U_s, $(L+5S)/U_s$, $(L/U_s)+t\grave{}_i$, $(L/U_s)+t_i$.

Fig. 2.4. External blast loading on front and rear sides of a structure (Newmark [15]).

$$t_c = \frac{3S}{U_s}$$

in which U_s, as usual, represents the wave front velocity and S is equal to the smaller of the height of the structures or one–half its width (Smith and Hetherington [2]). After t_c, the resultant pressure is given by

$$P_{front} = P_{s0} + C_f P_d$$

where the front face drag coefficient C_f may be considered equal to 1.2 (TM 5–1300 [6]). The so called *fictitious durations* t'_i and t_i, shown in Fig. 2.4 (a), are helpful for making up the resultant pressure–time profile.

After a time $t_r = L/U_s$, L standing for the length of the structure in the direction of the wave propagation, the shock front reaches the rear side, which experiences a maximum pressure $P_{rear} = P_{s0} - C_r P_d$. According to the technical manual TM 5–1300 [6], the rear face drag coefficient ranges between 0.5 and 0.3. The time t_{rb}, required to reach the maximum pressure on the rear side, is given by the following ratio

$$t_{rb} = \frac{L + 5S}{U_s}$$

with usual meaning of the symbols.

As the shock front passes above the target, the consequent airflow causes suction acting on the roof. The global roof pressure P_{roof} is given by

$$P_{roof} = P_{s0} + C_t P_d$$

in which $C_t P_d$ is the negative drag pressure caused by suction. Newmark and Hansen [12] suggested a roof drag coefficient C_t equal to 0.3–0.5. The pressure–time profile of the roof is usually simplified as triangular shaped, with a peak value P_{s0}, a rising time $t_{roof} = t_{rf} + L/U_s$, and an equivalent impulse duration $t_{ds} = t_{roof} + t_i$.

2.10 Internal explosions

High explosives detonated inside a structure cause two loading phases, both responsible for the possible damage. The first phase is related to reflection and re–reflection of blast waves, and might involve both regular and Mach reflection phenomena. Since the whole process is very difficult to predict in details, very often

some approximations are made, regarding the pressure–time profile and the magnitude of re–reflected waves. The second phase consists of a quasi–static pressure builded up by the gaseous products of detonation, and commonly lasts much longer than the first one. The load undergone by the structure is strongly affected by venting areas, which may allow a significant pressure relief.

2.10.1   Internal loading from shock wave reflection

It is rather straightforward to predict the reflected wave front parameters, by applying the expressions given in § 2.9.2 or the charts reported in a number of references (Smith and Hetherington [2], Baker [3], Mays and Smith [16]). Quantification of re–reflected waves magnitude however is generally much more complicated, since reflections inducing Mach steam waves makes the evaluation of blast loads requiring the use of dedicated programs, such as BLASTIN code [17] and CHAMBER code [18], developed for detonations in box–shaped rooms. Baker *et al.* [3] suggested some simplifications to be made in order to get reasonably accurate results. The firs approximation is to assume triangular blast pulses with abrupt rise for both incident and reflected waves. That assumption leads to the following pressure–time history,

$$P_s(t) = P_{s0}\left(1 - \frac{t}{T_s}\right), \qquad P_r(t) = P_{r0}\left(1 - \frac{t}{T_r}\right)$$

where P_s and P_r are the incident and reflected overpressure, and T_s and T_r are the corresponding pulse durations derived by preserving the proper impulses,

$$T_s(t) = \frac{2i_s}{P_s}, \qquad T_r(t) = \frac{2i_r}{P_r}$$

The wave front parameters may be also assumed from regular reflections, which is most likely to happen for box–shape structures with side length ratios close to unity. A third simplification is to assume that the peak pressure is halved on each reflection, whereas the pulse duration remains constant. Thus, after three reflections, the reflected pressure may be neglected. If the response time of the structure is much longer than the total duration of the blast load, a final approximation can be made. That is to combine all the three pulses into a single one, having a peak pressure equal to sum of the three peaks and a total specific impulse equal to the sum of the three ones. The assumptions made up to this point lead to the simplified pressure–time history shown in Fig. 2.10.2.
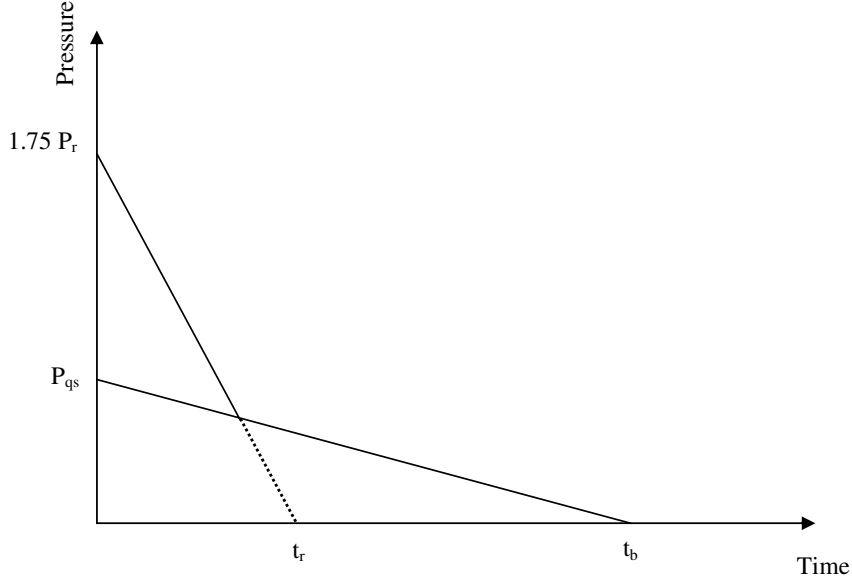
Fig. 2.5. Simplified blast load function caused by multiple reflection of shock waves from internal explosion (Baker [3]).

2.10.2 Internal loading from gas pressure

While the pressure from shock wave multiple reflections decades, the gas pressure develops, and eventually the global pressure settles to a slowly decaying level, which is a function of the energy released by the explosion and the volume and vent area of the structure. Because of the low rate of decaying, the gas pressure is commonly referred to as quasi–static pressure, which usually last much longer than the loading caused by shock wave reflections. The pressure–time history is described by two main parameters, the peak quasi–static pressure, P_{qs}, and the so called blow down time, t_b, at which the pressure reaches the ambient value. An approximate expression for the pressure profile was reported by Baker [3],

$$P(t) = (P_{qs} + P_0)e^{-2.13\bar{\tau}}$$

where P_0 is the ambient pressure and the quantity $\bar{\tau}$ is a dimensionless time for venting, given by

$$\bar{\tau} = \frac{\alpha_e A_{sur} t_b a_0}{V}$$

Here α_e is the ratio of the vent area to wall area, A_{sur} is the total inner surface of the structure, V is the volume, and a_0 is the speed of sound at ambient conditions. The scaled pressure–time history during the gas venting process, integrated over a

21
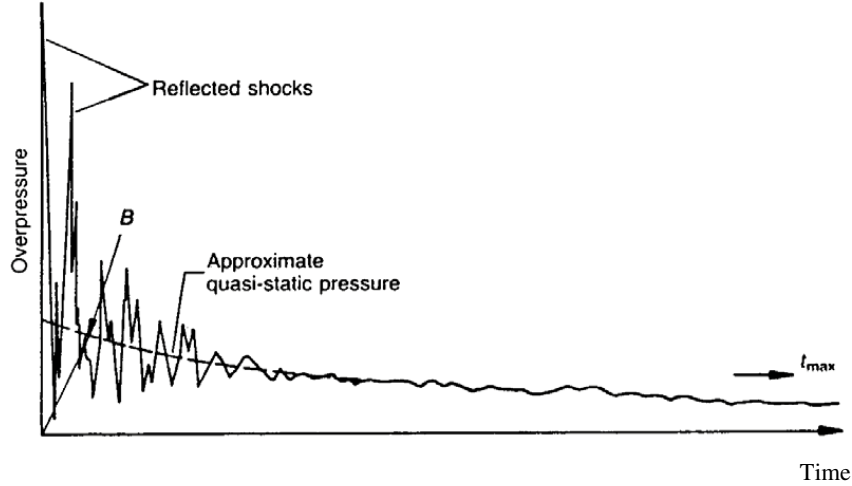
Fig. 2.6. Blast load function induced by gas pressure from internal explosion (Smith and Hetherington [2]).

positive load duration t_0, yield the scaled gas impulse i_g

$$i_g = \int_0^{t_0} (P(t) - P_0)dt = \frac{P_{qs} + P_0}{C}(1 - e^{Ct_0}) - P_0 t_0, \quad C = \frac{2.13\bar{\tau}}{t_b}$$

2.11 Ground shocks

Ground shocks may result from different scenarios. Nuclear devices detonated above the ground may cause significant ground shock levels. Conventional explosives, on the other hand, may produce remarkable effects only if detonated on or below the ground surface, because of the higher lever of coupling between the explosion and the ground. The result is a *direct–induced* ground shock, which involve a direct transmission of explosive energy through the ground. Free air bursts may cause *air–induced* ground shocks, which result when the blast waves compress the ground surface and send a stress pulse into the ground layers underneath the surface. Generally, motion due to air–induced shocks is maximum at the ground surface and attenuates quickly with depth (TM 5-1300 [6]).

The shock waves yielded by detonations near or under the ground surface may be classified as body waves and surface waves. Pressure waves (P–waves) and shear waves (S–waves) are body waves, since they cause particle motions of the ground layers underneath the surface. P–waves are responsible for particle motions parallel to the direction of propagation, which leads to compression or dilatation of the soil, whereas S–waves involve particle motions perpendicular to the direction of

22

propagation and shear stress. Circular particle motions near the surface are typical of surface waves known as Rayleigh waves (R–waves), characterized by a slower rate of decay with respect to body waves. Thus, their effects are dominant in case of surface bursts and for buried explosions at large range. On the contrary, body wave effects are dominant at close range from buried explosives (Smith and Hetherington [2]).

Many formulas are available to predict ground motions caused by direct–induced or air–induced ground shocks. Newmark [15] employed one–dimensional wave propagation theory to obtain vertical and horizontal displacement, velocity, and acceleration due to air–induced ground shocks. The technical manual TM 5–1300 [6] proposed some empirically based formulas to derive the same motion parameters in three different ground media (dry soil, saturated soil, rock), in case of direct–induced shocks.

Chapter 3

Failure Modes, Damage Criteria and Strain Rate Effects

3.1 Blast load induced failure modes

Blast loaded structural members may undergo different failure modes, associated with different types of response. According to Crawford and Karagozian [14], a global structural response is usually caused by out–of–plane, long time lasting loads, and bending and shear stresses are always involved. Thus, a first global failure mode may be reffered to as membrane/bending failure.

Four types of shear induced failure modes such as diagonal tension, diagonal compression, punching shear, and direct shear have been studied by Woodson [20]. Generally, diagonal tension and compression have been noticed in statically loaded reinforced concrete members, whilst punching shear is typically a cause of local failure of flat slabs punched by columns. Unlike the other shear mechanisms, which may usually be neglected, dynamic shear is of primary importance for the response of blast loaded elements, since the shear force caused by the transient short duration overpressure is many times higher than the shear force associated with flexural failure modes. The high shear stresses involved may lead to a global shear failure within a few milliseconds from the shock wave arrival to the member surface facing the detonation, even before any noticeable bending deformations. Experiments involving high speed dynamic behavior of concrete structures subjected to such failure modes have been conducted by Toutlemonde and Boulay [21, 22] and Watson [23].

Close–in explosions may result in localized breaching and spalling, due to local shear or flexural failure. Breaching failure caused by punching effects is typically accompanied by spalling and scabbing of concrete covers as well as low and high–

24
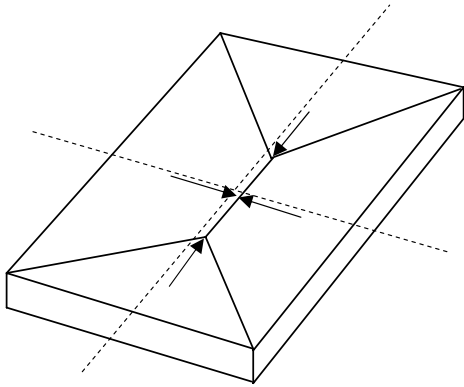
Global bending failure
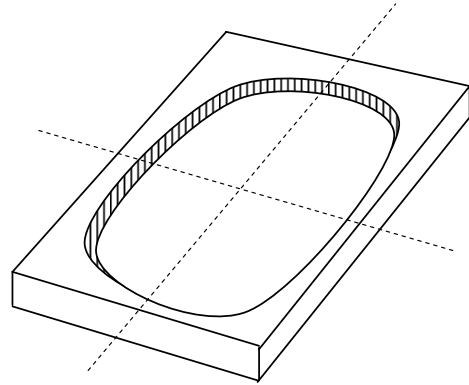
Global shear failure
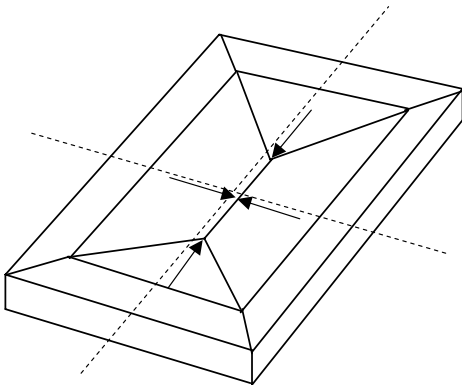
Local bending failure
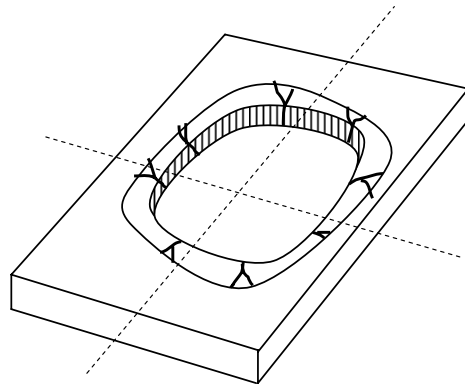
Local shear (breaching) failure

Fig. 3.1. Main failure modes for slabs (Tolba [19])

25

speed fragments. Fig. 3.1 shows the principal failure mechanisms for slabs.

3.2 Damage criteria

There are a number of global damage indices that may be used to express a certain level of structural damage. Among them, support rotations or mid–span deflection have been widely employed. While using a one–degree of freedom model as an approximate design method, Biggs [24] defined a ductility ratio μ as the ratio of the maximum deflexion δ_{max} to the elastic deflection δ_{e},

$$\mu = \frac{\delta_{\mathrm{max}}}{\delta_{\mathrm{e}}}$$

where δ_{e} is established by Biggs as the threshold inflection value between the elastic and the plastic parts of an elastic–perfectly plastic stress strain constitutive law. In general such parameter varies with geometry, material proprieties, reinforcement ratio, etc... It should be noted that, in this context, μ represents a required ductility, which the structural member needs to develop in order to stand a loading condition without failure. It should not be confused with the maximum ductility of that member, defined as an upper bound for the capacity of that particular structural element (TM 5–1300 [6]). Also, the strain rate has to be taken into account while establishing a failure criteria, since it may affect material strength, elastic modulus, strain value at maximum stress and ultimate strain (Scott *et al.* [25]).

3.2.1 Overall and localized damage criteria

Localized damage is often caused by shear failure. It is indeed a property of shear deformations being more localized than flexural ones (it may be worth recalling that a plastic hinge size is about equal to the member depth). As stated above, local failure may be caused by close–in explosion effects, which end up with spalling and breaching. Such effects may be dealt with through different approaches. The 3–D non–linear finite element modeling performed by Bogosian [26] takes into account the strain rate influence on material properties, and accurately predicts the size of breach and the velocity of fragments. Spalling diagrams, on the other hand, have been developed using a considerable amount of experimental data collected from both the US Army tests and from the literature (TM 5–1300 [6]). Three different categories of damage are defined: no damage, spalling, and breaching (Langberg [27]).
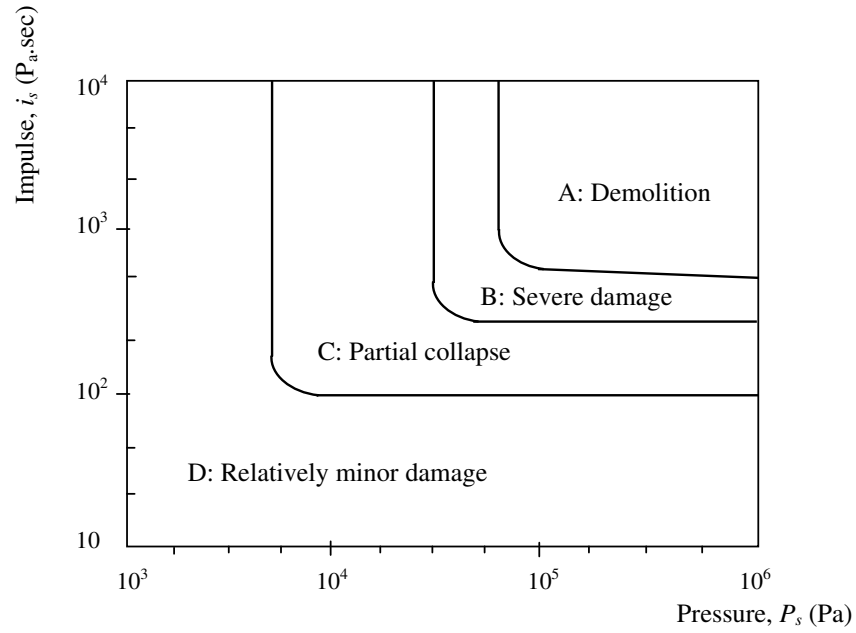
Fig. 3.2. Pressure–Impulse diagram for building damage (Baker *et al.* [3])

3.2.2 Damage level representation via pressure–impulse diagram

Pressure–impulse diagrams, also known as iso–damage curves, have been derived from a study of houses damaged by bombs dropped on the United Kingdom in World War II. The results of such investigations were used as part of the evaluation of safe–stand–off distances for explosive testing in the United Kingdom (Smith and Hetherington [2]). The axes of the curves are simply side–on peak overpressure P_s, and side–on specific impulse i_s, as shown in Fig. 3.2. The level of damage of brick houses is identified among four regions. Region A corresponds to complete demolition and region B refers to damage severe enough to require demolition. Region C impulse causes partial collapse of some structural members, such as roof and walls, and would make the house temporarily uninhabitable. Finally, region D refers to damage not severe enough to render building uninhabitable, but requiring urgent repair. Baker *et al.* [3] reported other P–I diagrams related to human response to blast, where three categories of blast–induced injuries (primary, secondary, and tertiary) are identified.

27

Creep Static Earthquake Hard Impact Blast

10^{-8} 10^{-7} 10^{-6} 10^{-5} 10^{-4} 10^{-3} 10^{-2} 10^{-1} 10^{0} 10^{1} 10^{2} 10^{3} 10^{4}
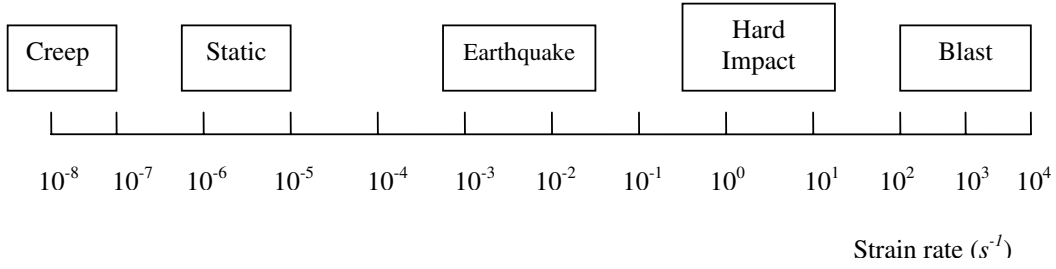
Strain rate (s^{-1})

Fig. 3.3. Magnitude of strain rates expected for various loading conditions (Bischoff and Perry [28])

3.3 Strain rate effects

3.3.1 Theories and tests at high strain rate

Strain rate is defined as the rate of change of strain ε with time t. Since structural members under shock waves from detonations undergo high loading rate and, consequently, high strain rate, it is necessary to consider how the properties of the material they are made of are affected by different strain rates, in order to model the structural behavior and get the system response. Fig. 3.3 shows the expected strain rate ranges for different loading conditions (Bischoff and Perry [28]). Static strain rates lie within the range of $10^{-6} \sim 10^{-5}$ s^{-1}, while blast pressures from high condensed explosives generally involve loads yielding strain rates in the range of $10^{2} \sim 10^{4}$ s^{-1}.

The dynamic properties of building materials have been object of many studies and tests, in order to establish a relationship between strain rate and some material characteristics, such as maximum strength, strain at maximum strength, ultimate strain, and elastic modulus. Murr [30] investigated the metallurgic effects arising when the material microstructure is affected by high strain rate and leading to a sudden change in the deformation mode and mechanical properties. For concrete, Johansson [29] proposed to classify the strain rate effects as viscous or structural effects. Viscous effects are generally believed to be related to the presence of free water within the concrete micropores, and are responsible for a moderate enhancement of the concrete strength when strain rates up to 30 s^{-1} are reached. Above such threshold value structural effects, such as inertia and confinement, are dominant, and cause a dramatic increase of the dynamic strength, which may reach up to four times the static one. According to Bischoff and Perry [28], such phenomenon may be explained as a transition from a creep behavior, which determines failure at low strain rates, to a mechanism of tensile microcracking that occurs under high strain rates. This change in behavior might be caused by the inertia resistance of

28
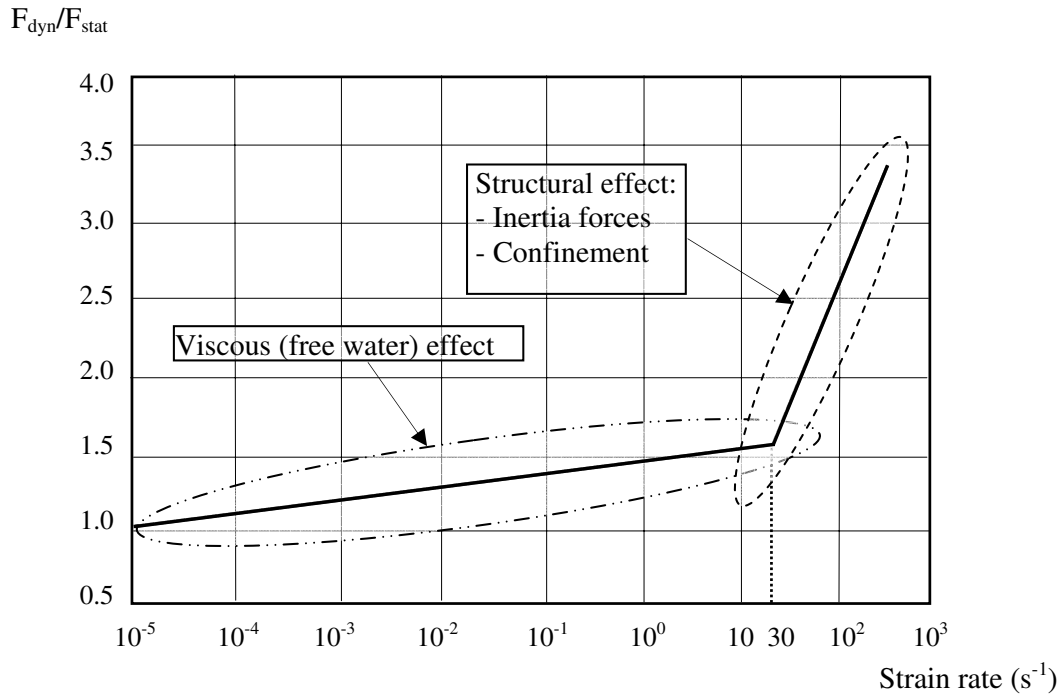
Fig. 3.4. Viscous and structural effects on concrete (Johansson [29])

the material the crack propagates through, and leads to a much higher value of stress, at failure, than that for static loads, because the crack if forced to propagate through regions of grater resistance and the formation of a fracture surface may require a larger amount of microcracking. Fig. 3.4 shows both viscous and structural effects takeing place at different strain rate ranges. The dynamic increase in concrete strength is presented in terms dynamic increase factor (DIF), generally defined as the ratio between dynamic strength, F_{dyn}, and static strength, F_{stat}, of the material under consideration.

Figs. 3.5 and 3.6 show a large amount of data collected since the early fifties from experiments conducted on plain concrete specimens in compression and in tension, under high speed dynamic loads. Bischoff and Perry [28] interpreted the large scatter as a proof that dynamic load tests are much more complicated than static ones, since a lot of parameters might affect the test results, such as specimen dimensions and moisture, uniformity of stress and strain along the specimen length, stress wave propagation effects, maximu aggregate size, water–cament ratio, cement content, cement type and quality, etc...

The following three sections report a brief overview of the tests run over the years on specimens made of plain concrete, reinforcing steel bars, and reinforced concrete. The influence of some parameters on the test results is highlighted.

Fig. 3.5. Strain rate influence on compressive strength of concrete (Bishoff and Perry [28])

30
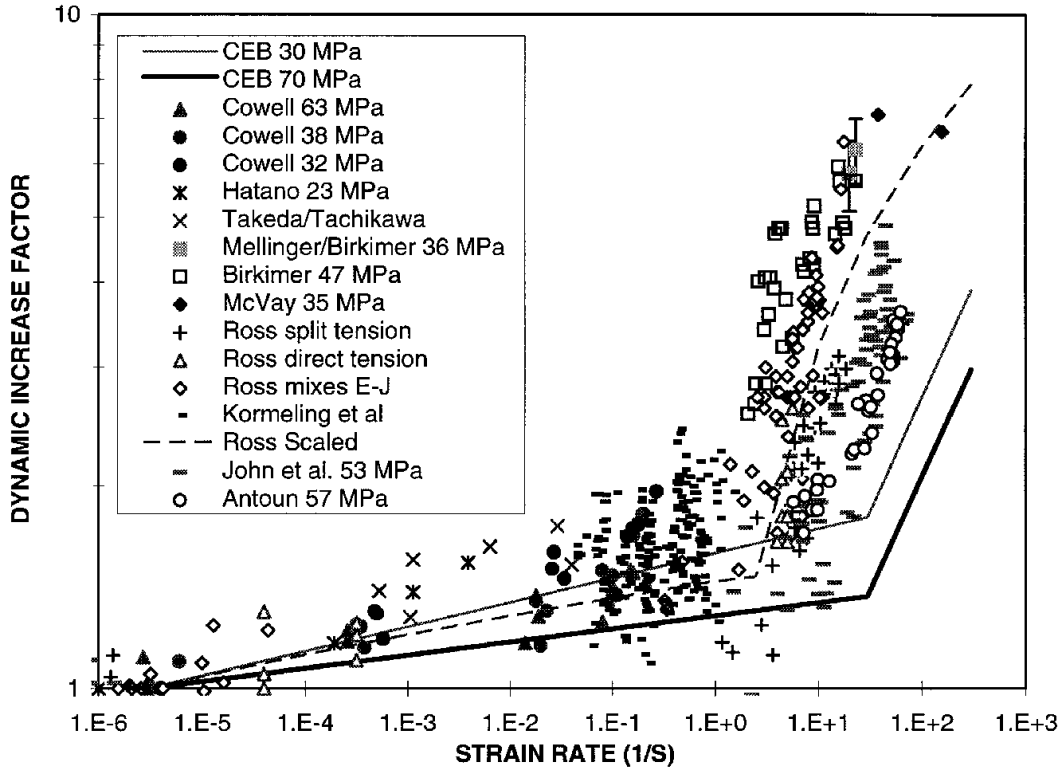
Fig. 3.6. Strain rate influence on tensile strength of concrete (Malvar and Ross [31])

3.3.2 Plain concrete under high strain rate

As a general result of the experiments conducted since 1917 to investigate the relationship between stain rate and compressive strength of plain concrete (see Abrams [32]), we may state that the higher the stain rate, the higher the concrete compressive strength.

Tests run by Watstein [33] in 1953 and by Atchley and Furr [34] in 1967 investigated the influence of the concrete strength on the specimens under high strain rate. Watstein's experimental campaign showed no significant relationship between dynamic increase factor and static concrete strength, since two different concrete batches, with static compressive strength of 17.4 MPa and 45.1 MPa, showed a strength gain under dynamic loads of 84% and 85% respectively. Atchley's campaign however, pointed out that strong concrete seems to be less sensitive to the loading rate than weak concrete.

Sparks and Menzies [35] investigated the effect of aggregate type on strain rate sensitivity. Specimens made of gravel, limestone, and lytag aggregate were tested, and the results appeared to be consistent with Atchley's campaign, since limestone specimens showed an increase in compressive strength of 4%, whereas lytag speci-

31
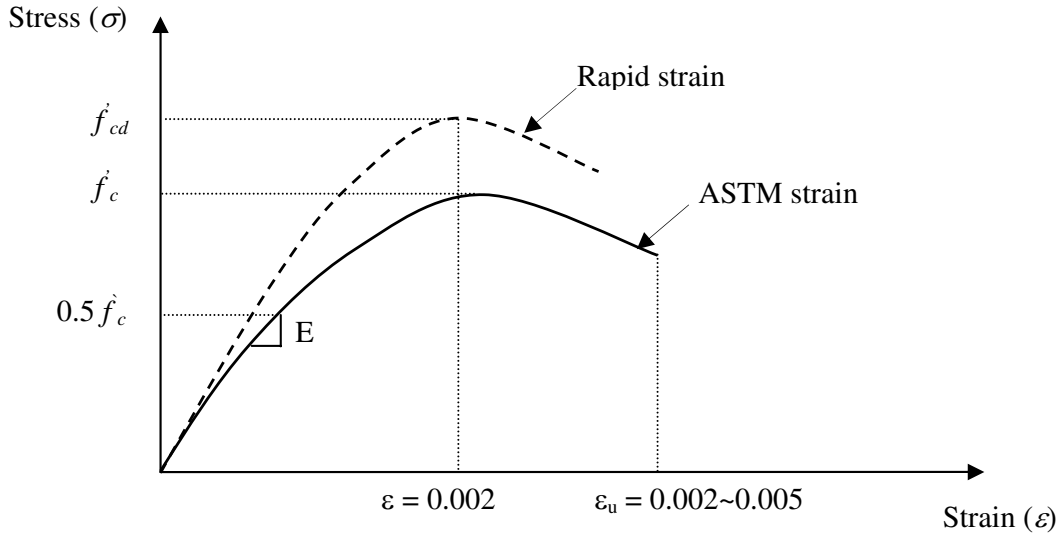
Fig. 3.7. Stress–strain curve of concrete under different strain rates (TM 5–1300 [6])

mens had a 16% of strength increase under the same loading rates.

Curing condition effects were explored by Spooner [36], who tested specimens cured in water and in air. Dynamic tests showed that dry concrete is less sensitive to strain rate.

The whole stress–strain curve was found to be strain rate dependent. Wakabayshi [37] observed that peak stress and initial tangent modulus are both increased under high strain rate. The U.S. Army manual TM 5–1300 [6] presented stress–strain curves yielded by different loading rates (Fig.3.7). It may be noted that up to the 50% of the load, such curves are almost superimposed. Also, the dynamic strength of concrete (f'_{cd}) is about the 25% higher than the static strength (f'_c). Experimental campaigns, conducted by Scott *et al.* [25] on both plain and reinforced concrete specimens, indicated that stress and strain at failure are both increased of 25% in case of high strain rate. Moreover, for any given stress level, the corresponding strain value was found to be decreasing as the strain rate increases; as a consequence, the higher the loading rate, the higher both the secant and the rupture moduli.

Concrete in tension was found to be much more sensitive to the loading rate. Malvar and Ross [31] reported experimental results showing a noticeable increase in concrete tensile strength of more than 600%, whereas compression strength of concrete and steel were increased by 100% and 50% respectively. They also proposed an expression for the dynamic increase factor of concrete in tension,
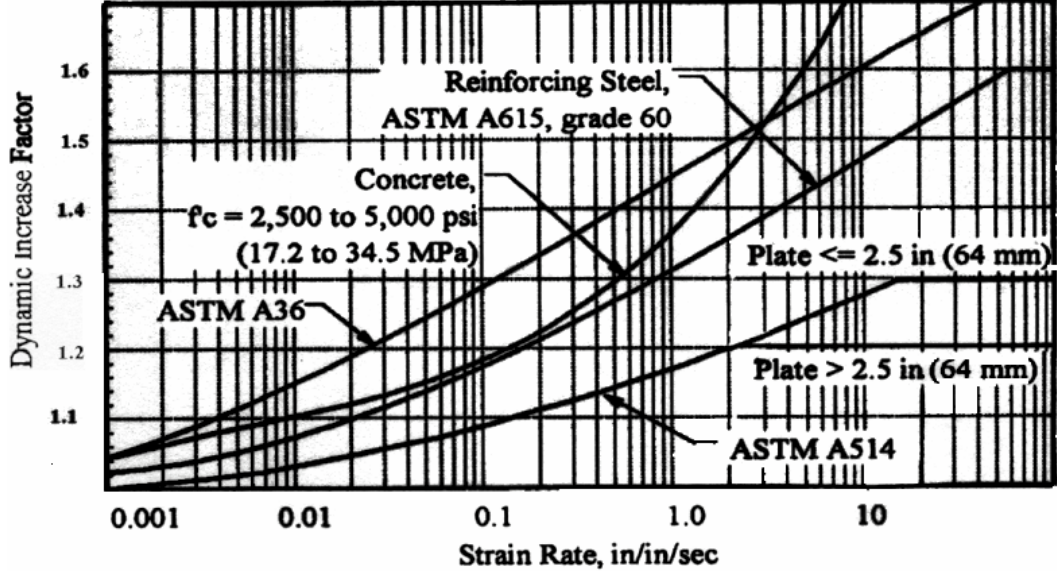
Fig. 3.8. Dynamic strength of materials under different strain rates (TM 5–1300 [6])

$$\text{DIF} = \frac{f_{td}}{f_{ts}} = \left(\frac{\dot{\varepsilon}_c}{\dot{\varepsilon}_{cs}}\right)^{\delta}, \qquad\qquad \dot{\varepsilon}_c \leq 1 \text{ s}^{-1}$$

$$\text{DIF} = \frac{f_{td}}{f_{ts}} = \beta \left(\frac{\dot{\varepsilon}_c}{\dot{\varepsilon}_{cs}}\right)^{\frac{1}{3}}, \qquad\qquad \dot{\varepsilon}_c > 1 \text{ s}^{-1}$$

where f_{td} and f_{ts} represent the dynamic and static tensile strength of concrete, respectively; DIF is the dynamic increase factor; $\dot{\varepsilon}_c$ and $\dot{\varepsilon}_{cs}$ are the current strain rate (up to 10^4 s^{-1}) and the static strain rate ($10^{-5} \sim 10^{-6}$ s^{-1}); $\beta = e^{6\delta-2}$; $\delta = 1/[1 + 8(f'_c/f'_{c0})]$; f'_{c0} is a fraction of concrete strength in compression (10 Mpa).

In general the results seemed in good agreement with what predicted by Atchley and Furr [34], since it was found that the faster the material is strained, the higher strength increase is expected. Also, the higher the static strength, the lower the gain in dynamic strength. Fig. 3.8 illustrates some plots of the dynamic increase factor against the strain rate for reinforcing steel, concrete, and structural steel.

3.3.3 Reinforcing steel under high strain rate

Experiments conducted on steel bars by Norris *et al.* [38], Dowling and Harding [39], Wakabayashi [37], and Keenan [40] all resulted in a remarkable gain of steel strength caused by an increasing loading rate. The greatest strain rate sensitivity was showed by materials of body–centered cubic structure, since the lower yielding

33
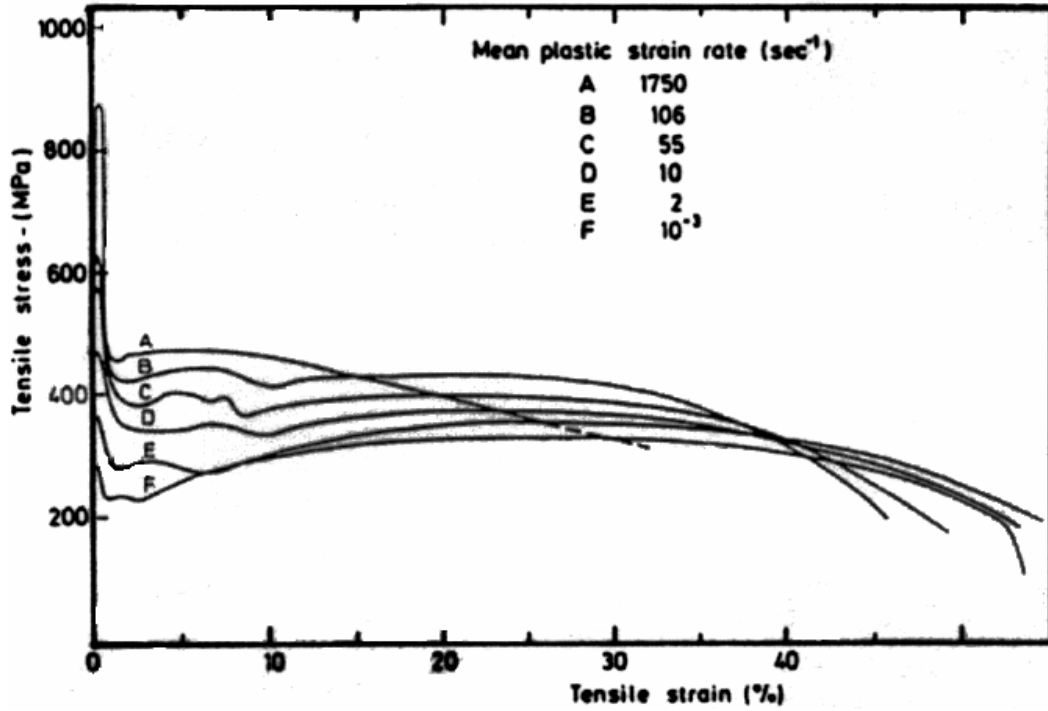
Fig. 3.9. Stress–strain curve of mild steel under different strain rates (Dowling and Harding [39])

tensile strength doubled and the upper one also increased considerably (Dowling and Harding [39]); the ultimate tensile stress gained about the 50% of its static value and the ultimate tensile strain was reduced by an increasing strain rate. Stress–strain curves for mild steel under several strain rates are illustrated in Fig. 3.9.

The tests performed by Wakabayashi [37] apparently showed no effect of strain rate on modulus of elasticity, and a little influence on the ultimate strength and the strain–hardening zone of the constitutive law.

Malvar [41] proposed the following expression, which gives the dynamic increase factor, for both yield and ultimate stress, as a function of ultimate stress f_y and strain rate $\dot{\varepsilon}_s$,

$$\text{DIF} = \left(\frac{\dot{\varepsilon}_s}{10^{-4}} \right)^{\alpha}$$

in which $\alpha = \alpha_{fy} = 0.074 - 0.04(f_y/414)$ for yield stress calculation, and $\alpha = \alpha_{fu} = 0.019 - 0.009(f_y/414)$ in case the ultimate stress is needed.

34

3.3.4 Flexural capacity of reinforced concrete under high strain rate

Since tensile and compressive strength of concrete and reinforcing steel are both increased by high strain rates, the flexural capacity of reinforced concrete members is expected to be increased as well.

Aiming to investigate the elastic behavior of simple members under impulsive loads, Penzien and Hansen [42] found out that the dynamic magnification factor, defined as the ratio of maximum strain produced at a certain point under dynamic loading to strain occurred under equivalent static loads, appeared to assume values within the interval $[1.5, 3]$. Those results pointed out that maximum strains in reinforced concrete elements under impulsive loads may be remarkably larger than those yielded by static loads of equivalent magnitude. Also, the steel sensitivity to strain rate effects was found to be more predictable than the increase in concrete strength. Based on such data, reinforced concrete structures, designed to be impulsive load resistant, were suggested to be under–reinforced.

A possible change in failure mode of reinforced concrete members was discussed by Bertero *et al.* [43] and by Takeda *et al.* [44]. Tests run by Bertero *et al.* [43] showed an increasing stiffness and moment capacity at first yielding of reinforcing steel bars under high strain rate, which might lead to a brittle failure in case of inadequate shear reinforcement. Besides, Takeda *et al.* [44] were able to demonstrate that different failure mechanisms of the same structural element under the same load take place under different strain rates. In particular, reinforced concrete beams were found to undergo a brittle failure under high speed dynamic load, whereas the same specimens failed in a ductile manner when the same load were applied statically.

Experiments conducted by Wakabayshi[37] showed that, under high strain rates, both compressive strength of concrete and tensile strength of steel increased linearly with the logarithm of strain rate. A global enhancement of the load carrying capacity of about 30% was reached.

3.3.5 Summary

As a general rule, the higher the strain rate produced by dynamic loads, the larger the gain in material strength.

Concrete under high strain rate shows a different sensitivity, depending on whether it is in compression or in tension. In fact, the gain in compressive strength

of concrete may range between 25% and 100%, whereas the static tensile strength may by increased by 6 times when a strain rate of 10^3 s^{-1} is applied.

A stronger concrete is less sensitive to strain rate effects. Tests showed an inverse correlation between static strength of concrete and strength growth due to strain rate.

The whole stress–strain curve is strain rate dependent. A high strain rate yield a reduction of strain at maximum stress in compression, and an increase in the secant modulus. Yet, strain rate effects on tangent modulus are negligible.

Reinforced concrete members under high strain rate experience an increase in strength and stiffness, which may lead a shift in flexural mode failure from ductile to brittle.

Chapter 4

Linear Single Degree of Freedom Model

4.1 Introduction

In order to analyze the dynamic response of structures under blast loadings, two main theoretical topics need to be dealt with, the definition of a time–pressure profile acting on the target and the choice of an ideal model representing the actual structure.

The pressure profile yielded by an explosion may be considered either deterministic or aleatory. A random excitation of space structures was considered by Chang [45], whom analyzed a free–free beam with a lumped mass and hysteretically damped; the cross spectral density function of the applied load was a Gaussian stochastic process in time. It was shown that larger uncertainties of random loads decrease the system reliability.

Although uncertainties concerning explosion phenomena make a random model more appropriate, deterministic loadings are still useful to compare results of different models and to get a rapid assessment of structural behaviors. Baker *et al.* [3] suggested two different deterministic expressions to describe the simplified pressure profiles yielded by a detonation or a deflagration. As mentioned in the previous chapter, a detonation involves a pressure–time history characterized by a step rise followed by an exponential decay as well as monotonic pressure–impulse curves, whereas a deflagration causes a wavefront pressure with a finite rise time and non monotonic pressure–impulse curves.

The choice of an adequate expression for a blast load function is not discussed in this chapter. According to Li and Meng [46, 47], a four parameter expression

is assumed, involving the peak overpressure, the loading duration, and two shape parameters. Such formula is intended to describe a general descending pulse load generated by a detonation.

Since the aim of this thesis is to develop simplified methods of analysis for blast design, a single degree of freedom model (SDOF model) is chosen as an approximate technique for the dynamic analysis of a wide range of geometries. A SDOF model was widely employed to predict the structural response of actual structures under blast loads (Bangash [48]; Mays and Smith [16]; Krauthammer [49]). It was considered helpful for the structural design because it allows to easily predict the overall response of a structure. For complex systems, Abrahamson and Lindberg [50] proposed to construct a critical pressure–impulse curve as the envelope of the critical load curves for the structural elements, schematized as SDOF models. However it is well known that such models, since providing information just for one point in the actual system, are limited for identifying complex structural behaviours. In general, structural models like plates and shells are more representative of the structural behaviour and of the state of damage. For a class of problems in which elastic effects are significant, Schleyer and Hsu [51] proposed a structural schema made of two beams and five springs. The maximum deflections calculated by such schema and by an elastic–perfectly plastic SDOF model were compared, and agreed quite well since both methods are based on assumed first mode shapes. The main difference between the two them is that a more accurate transfer from one mode shape to another is implemented in Schleyer's analytical scheme. Thereafter, a SDOF model may be regarded as a first order design method or a first step analytical method, useful when a structure is analyzed starting from simple approaches, as noted by Krauthammer [49].

The simple oscillator presented in this chapter has constant stiffness until failure, which establish an elastic–fragile behaviour typical of those systems where the elastic deformations are dominant, due to a large ratio of initial kinetic energy to maximum elastic strain energy and a high value of the stiffness itself. Any kind of damping is also neglected. Indeed, although all dynamic systems contain damping to some degree, in case of structures with a load–time function described in Eq. (4.1) the damping effect is not significant if some conditions suggested by Biggs [24] are respected; the load duration must be short, as shown in § 4.2.3, and the only output datum of interest is the maximum dynamic response of the structure.

Shear effects on the system response are also neglected. The key parameters to decide when such effects have to be taken into account were established by Li and

Jones [52, 53, 54], who considered transverse shear effects on fully clamped circular plates, 'short' cylindrical shell and fully clamped beams.

The second part of this chapter is focused on the loading shape influence on the structural response, a topic widely surveyed by Youngdahl [55], who examined several kinds of structures with a rigid–plastic stress–strain relation (circular plate, reinforced circular cylindrical shell, free–free beam, circular shell with a ring load), under different load shapes (rectangular, linearly decaying, exponentially decaying, triangular and sinusoidal). He tried to eliminate the dependence of the response from the load shape by introducing two key parameters, the total impulse and the effective load, involving a loading function and two time parameters referring to the beginning and the end of the plastic deformation. A theoretical foundation for Youngdahl's work [55] was given by Li and Meng [47] for a rigid–plastic single degree of freedom model. In successive works Youngdahl [56, 57] considered problems where the load becomes a function both of position and time, or the stress–strain relation is more complex, such as the strain hardening. In this cases the calculation of effective parameters results more complicated. Abrahamson and Lindberg [50] suggested the use of a simple hyperbolic shape for the pressure–impulse diagram, which provided significant discrepancies (20%–40%) with respect to the isodamage curves given by an exponentially and a linearly decaying load acting on a SDOF model. Zhu *et al.* [58] used Youngdahl's work to develop simple characteristic curves for rigid–plastic structural models, as was done by Abrahamson and Lindberg. Lately, a non–load–shape–dependent pressure–impulse diagram was proposed by Li and Meng [46]. In § 4.3.2 the influence of the pulse shape on the dynamic load factor and pressure–impulse diagram is shown, with emphasis placed upon the analysis of the transient response, which represents a major concern in case of blast loads. The knowledge of the transient response of a linear elastic model is primarily important to understand the behavior of a SDOF model with several stress–strain relations, which may be often simplified as linear or piecewise linear. Many problems concerning the response spectrum are highlighted, like the position of the spectrum transition point. A discussion about the formulation of a general expression for the transient response spectrum is reported. An analytical expression of isodamage curves is examined for different pulse shapes, and the validity of the non–load–shape–dependent pressure–impulse diagram proposed in Ref. [46] is discussed.

4.2 Response analysis

When a system configuration can be described by the displacement of a single point, the known principles of structural dynamics allow to convert the actual structures into a SDOF model by using equivalent mass, damping and resistance function.

The pressure profile assumed by Li and Meng [46] for an explosive charge, is a generalized form of the Friedlander equation [2]:

$$
F(t) = \begin{cases} F_{\max} \left(1 - \lambda \dfrac{t}{t_d} \right) \exp \left(-\gamma \dfrac{t}{t_d} \right) & \text{for} \quad 0 \leq t \leq t_d \\[3mm] 0 & \text{for} \quad t > t_d \end{cases} \tag{4.1}
$$

where:

- t is the time in seconds;

- $F_{\max}$ is the peak load value, in kN (if the load is a force) or in kN/m^2 (if it is a pressure);

- t_d is the duration of the loading positive phase. Since the negative phase can be neglected to evaluate the effect of an explosion, t_d represent the total duration of loading;

- λ and γ are shape parameters.

The load described from Eq. (4.1) acts on the structure with an impulse as follows:

$$
I = \int_0^{t_d} F(t)dt = F_{\max} \, t_d \, \psi(\lambda, \gamma), \quad \psi(\lambda, \gamma) = \frac{(\gamma - \lambda)\left(1 - e^{-\gamma}\right) + \lambda \gamma e^{-\gamma}}{\gamma^2} \tag{4.2}
$$

The effects on a linear spring–mass system loaded by a pulse load with $\lambda \in [0, 1]$ and $\gamma \in [0, 10]$ have been studied; these ranges are suitable to describe a pulse load from detonations that are characterized by a step rise and a following decay, with a fixed magnitude at $t = t_d$.

By applying D'Alembert's principle, the motion equation results:

$$
m\ddot{y} + ky = F(t) \qquad 0 \leq t \leq t_d \qquad \text{(forced vibrations)} \tag{4.3a}
$$

$$
m\ddot{y} + ky = 0 \qquad t > t_d \qquad \text{(free vibrations)} \tag{4.3b}
$$

with initial conditions:

$$i.c. \begin{cases} y\,(t=0) = 0 \\ \dot{y}\,(t=0) = 0 \end{cases} \tag{4.4}$$

where m and k are, respectively, the equivalent mass and stiffness and y is the mass displacement. To represent the system response, the following symbols are adopted:

- $\omega = \sqrt{k/m}$ is the natural frequency of the structure;

- $\tau = \omega t$ is the dimensionless time variable;

- $\tau_d = \omega t_d$ is the dimensionless loading duration;

- $t_{\max}$ is a point in the time domain corresponding to a relative maximum point of the displacement function;

- $\tau_{\max} = \omega t_{\max}$ is a dimensionless time value corresponding to a relative maximum displacement;

- $y_{\mathrm{st}} = F_{\max}/k$ is the static displacement;

- $y_f(t)$ represents the displacement function for forced vibrations;

- $y_l(t)$ is the displacement function for free vibrations;

- $DLF_f(\tau) = y_f/y_{\mathrm{st}}$ is the Dynamic Load Factor of forced vibrations;

- $DLF_l(\tau) = y_l/y_{\mathrm{st}}$ is the Dynamic Load Factor of free vibrations.

In order to calculate the solution of the motion equation during the forced vibrations, the general integral of the Eq. (4.3a) can be established by solving the Duhamel's integral applied to the assigned force. According to Biggs [24], we have

$$y_f(t) = \int_0^t \frac{F(t')}{\sqrt{mk}} \sin\left(\frac{t-t'}{\sqrt{m/k}}\right)\,dt' = \frac{F_{\max}}{\sqrt{mk}} \int_0^t f(t') \sin\omega(t-t')\,dt'$$

where $f(t')$ represents the load function from Eq. (4.1) normalized with respect to the peak value $F_{\max}$.

By defining

$$f_1(\lambda,\gamma,t_d) = 1 - \frac{2\lambda\gamma}{\gamma^2 + (\omega t_d)^2}, \qquad f_2(\lambda,\gamma,t_d) = \lambda + \gamma f_1(\lambda,\gamma,t_d) \tag{4.5}$$

we get:

$$DLF_f(\tau) = \frac{\tau_d^2}{\gamma^2 + \tau_d^2} \left\{ f_2 \frac{\sin\tau}{\tau_d} - f_1 \cos\tau + \left(f_1 - \lambda\frac{\tau}{\tau_d}\right) \exp\left(-\gamma\frac{\tau}{\tau_d}\right) \right\} \tag{4.6}$$

41

From Eqs. (4.3b) and (4.6), the solution of the motion equation during the free vibrations can be obtained by imposing the continuity of the Dynamic Load Factor and its first derivative at $\tau = \tau_d$:

$$
\begin{cases}
DLF_l(\tau) = \dfrac{y_l(\tau)}{y_{\text{st}}} = \text{A}\cos\tau + \text{B}\sin\tau \\[2mm]
\text{A} = \dfrac{\tau_d^2}{\gamma^2 + \tau_d^2}\left\{-f_1 + e^{-\gamma}\left[(f_1 - \lambda)\cos\tau_d + \dfrac{f_2 - \lambda\gamma}{\tau_d}\sin\tau_d\right]\right\} \\[3mm]
\text{B} = \dfrac{\tau_d^2}{\gamma^2 + \tau_d^2}\left\{\dfrac{f_2}{\tau_d} + e^{-\gamma}\left[(f_1 - \lambda)\sin\tau_d - \dfrac{f_2 - \lambda\gamma}{\tau_d}\cos\tau_d\right]\right\}
\end{cases}
\tag{4.7}
$$

4.2.1   Stationary points of the displacement function

According to Campidelli and Viola [59], during the free vibration phase the time values when a relative maximum displacement is reached are established as follows:

$$
\tau_{\max} = n\pi + \arctan\left(\frac{\text{B}}{\text{A}}\right), \quad n \in \mathbb{N}
\tag{4.8}
$$

During the forced vibration phase, $\tau_{\max}$ is defined by equating to zero the first derivative of the displacement function which describes the forced vibrations:

$$
\frac{dy_f}{dt}(t_{\max}) = \frac{d}{dt}\left\{f_2\frac{\sin\omega t}{\omega t_d} - f_1\cos\omega t + \left(f_1 - \lambda\frac{t}{t_d}\right)\exp\left(-\gamma\frac{t}{t_d}\right)\right\}\bigg|_{t=t_{\max}} = 0
$$

By defining a new variable $\vartheta = 1/\tau_d$, we obtain:

$$
\varphi(\vartheta, \tau_{\max}) = f_1\sin\tau_{\max} + f_2\vartheta\cos\tau_{\max} - [f_2 - \lambda\gamma\vartheta\tau_{\max}]\exp(-\gamma\vartheta\tau_{\max}) = 0 \quad (4.9)
$$

Eq. (4.9) represents an implicit function $\tau_{\max}(\vartheta)$, which can be simply calculated when $\vartheta \to 0$ (or $\tau_d \to +\infty$); in fact, from Eq. (4.1) we have:

$$
\lim_{\tau_d \to +\infty} F(\tau) = \lim_{\tau_d \to +\infty} F_{\max}\left(1 - \lambda\frac{\tau}{\tau_d}\right)\exp\left(-\gamma\frac{\tau}{\tau_d}\right) = F_{\max}
\tag{4.10}
$$

When $\tau_d \to \infty$, Eq. (4.10) shows that the system is excited by a rectangular load (step rise, constant magnitude, step decay) with infinite duration for all the finite values of λ and γ. Therefore, the time values when a relative maximum displacement is reached can be deduced using the corresponding solution coming from a spring–mass system under a rectangular pressure profile:

$$
\tau_{\max}(\tau_d \to +\infty) = \tau_{\max}(\vartheta \to 0) = n\pi, \quad n \in \mathbb{N}_0, \quad \forall(\lambda, \gamma) \in \mathbb{R}^2
\tag{4.11}
$$

The first derivative of $\tau_{\max}(\vartheta)$ can be calculated. Since this function is implicitly defined by zeros of $\varphi(\vartheta, \tau_{\max})$, the first derivative $D\tau_{\max}/D\vartheta$ can be obtained by

equating to zero the total derivative of $\varphi(\vartheta, \tau_{\max})$:

$$\frac{D\varphi}{D\vartheta}(\vartheta, \tau_{\max}) = \left(\frac{\partial \varphi}{\partial \vartheta} + \frac{\partial \varphi}{\partial \tau_{\max}}\frac{D\tau_{\max}}{D\vartheta}\right)(\vartheta, \tau_{\max}) = 0$$

$$\frac{D\tau_{\max}}{D\vartheta}(\vartheta, \tau_{\max}) = -\frac{\dfrac{\partial \varphi}{\partial \vartheta}(\vartheta, \tau_{\max})}{\dfrac{\partial \varphi}{\partial \tau_{\max}}(\vartheta, \tau_{\max})}$$

It should be noted that $D\tau_{\max}/D\vartheta$ depends on the value of its primitive function $\tau_{\max}(\vartheta)$. Setting $\tau_{\max}^{(k)} = D^k\tau_{\max}/D\vartheta^k$ and proceeding with implicit derivation with respect to the ϑ variable, the nth derivative can be calculated:

$$\tau_{\max}^{(1)}(\vartheta, \tau_{\max}) = -\frac{\dfrac{\partial \varphi}{\partial \vartheta}(\vartheta, \tau_{\max})}{\dfrac{\partial \varphi}{\partial \tau_{\max}}(\vartheta, \tau_{\max})}$$

$$\tau_{\max}^{(2)}(\vartheta, \tau_{\max}) = \frac{\partial \tau_{\max}^{(1)}}{\partial \vartheta} + \frac{\partial \tau_{\max}^{(1)}}{\partial \tau_{\max}}\tau_{\max}^{(1)} = \left(\frac{\partial}{\partial \vartheta} + \tau_{\max}^{(1)}\frac{\partial}{\partial \tau_{\max}}\right)\tau_{\max}^{(1)}$$

$$\vdots$$

$$\tau_{\max}^{(n)}(\vartheta, \tau_{\max}) = \frac{\partial \tau_{\max}^{(n-1)}}{\partial \vartheta} + \frac{\partial \tau_{\max}^{(n-1)}}{\partial \tau_{\max}}\tau_{\max}^{(1)} = \left(\frac{\partial}{\partial \vartheta} + \tau_{\max}^{(1)}\frac{\partial}{\partial \tau_{\max}}\right)\tau_{\max}^{(n-1)}$$

The above derivatives have $\tau_{\max}(\vartheta)$ as argument and thus, if the value of this function is known when $\vartheta \to 0$, a Maclaurin series expansion of the unknown function can be obtained in a neighborhood of the chosen point $\vartheta_0 = 0$ or, from another point of view, in a neighborhood of $\mathbf{x}_0 = (\vartheta_0, \tau_{\max}(\vartheta_0)) = (0, n\pi)$:

$$\tau_{\max}(\vartheta) = \underbrace{\tau_{\max}(0)}_{n\pi} + \tau_{\max}^{(1)}\Big|_{\mathbf{x}_0}\vartheta + \frac{\tau_{\max}^{(2)}}{2!}\Big|_{\mathbf{x}_0}\vartheta^2 + \ldots + \frac{\tau_{\max}^{(n)}}{n!}\Big|_{\mathbf{x}_0}\vartheta^n$$

$$= n\pi + \sum_{k=1}^{n}\frac{\tau_{\max}^{(k)}}{k!}\Big|_{\mathbf{x}_0}\vartheta^k$$

Remembering that $\vartheta = 1/\tau_d$, we can write:

$$\tau_{\max}(\tau_d) = n\pi + \sum_{k=1}^{n}\frac{\tau_{\max}^{(k)}}{k!}\Big|_{\mathbf{x}_0}\left(\frac{1}{\tau_d}\right)^k \tag{4.12}$$

By truncating the series expansion at the fourth term, a good approximation of the time values corresponding to the maximum displacements can be obtained, for each value of λ and γ. In fact, for each set of constants $(n_0, n_1, n_2, n_3, n_4) \in \mathbb{N}_0^5$, from Eq. (4.12) we obtain:

43

$$\tau_{\max}(\tau_d) = n_0\pi + (\lambda + \gamma)\left(\frac{1}{\cos n_1\pi} - 1\right)\left(\frac{1}{\tau_d}\right) - \frac{n_2\pi\gamma(2\lambda + \gamma)}{\cos n_2\pi}\left(\frac{1}{\tau_d}\right)^2 +$$

$$+ \left[\left(2\lambda\gamma^2 + 3\lambda^2\gamma + \frac{2}{3}\gamma^3 - \frac{\lambda^3}{3}\right)\left(\frac{1}{\cos n_3\pi} - 1\right) + \right.$$

$$\left. + \frac{(n_3\pi)^2\left(\frac{3}{2}\lambda\gamma^2 + \frac{\gamma^3}{2}\right)}{\cos n_3\pi}\right]\left(\frac{1}{\tau_d}\right)^3 +$$

$$+ \frac{n_4\pi\gamma}{6}\left[\left(24\lambda\gamma^2 + 21\lambda^2\gamma + 6\gamma^3\right)\left(2 - \frac{1}{\cos n_4\pi}\right) - \right.$$

$$\left. - \frac{21\lambda^2\gamma + (n_4\pi)^2(4\lambda\gamma^2 - \gamma^3)}{\cos n_4\pi}\right]\left(\frac{1}{\tau_d}\right)^4 \quad (4.13)$$
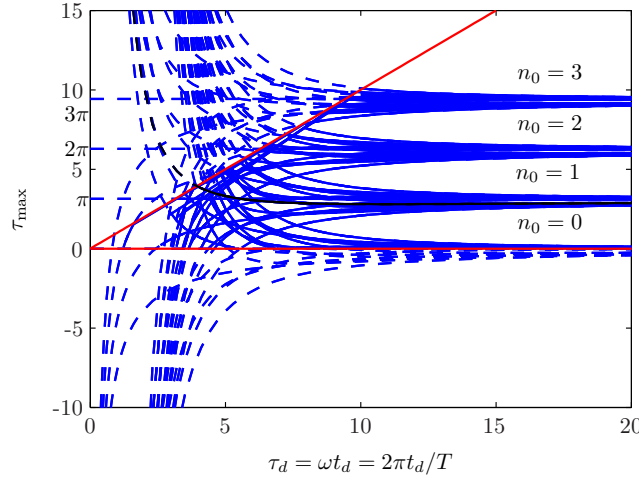
Fig. 4.1. Exponentially decaying load ($\lambda = 1, \gamma = 2.8$): times of local maximum displacement against load duration, during the forced vibrations phase. Solid lines identify the parts of the charts in time range $(0, \tau_d)$.

Eq. (4.13) is shown in Fig. 4.1, when $\lambda = 1$, $\gamma = 2.8$ and natural constants have the following values:

$$n_0 = 0, 1, 2, 3 \quad n_1 = 0, 1, 2, 3 \quad n_2 = 0, 1 \quad n_3 = 0, 1 \quad n_4 = 0, 1$$

Since the set of constants $(n_0, n_1, n_2, n_3, n_4)$ corresponding to the absolute maximum displacement can not be calculated in closed form, in order to build the response spectrum it is necessary to analyze the influence of the natural constants on the dynamic load factor.

44
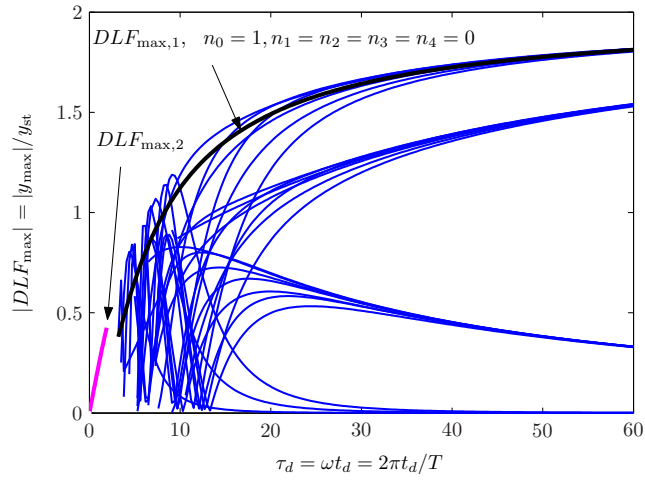
Fig. 4.2. Exponentially decaying load ($\lambda = 1, \gamma = 2.8$): displacements by 28 different sets of constants $(n_0, \ldots, n_4)$.
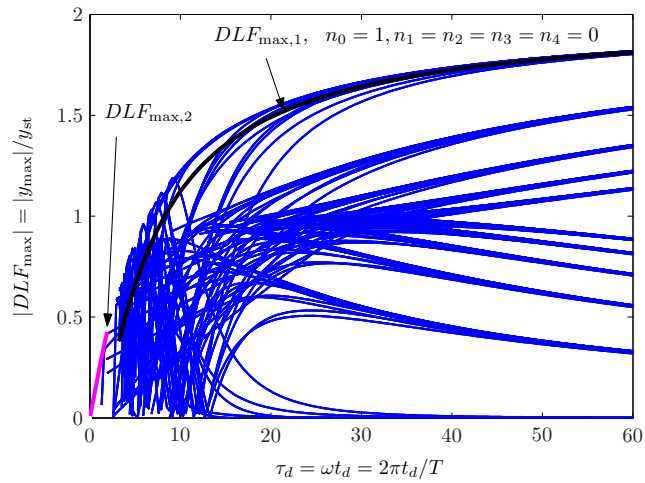
Fig. 4.3. Exponentially decaying load ($\lambda = 1, \gamma = 2.8$): displacements by 396 different sets of constants $(n_0, \ldots, n_4)$.

4.2.2 Response spectrum

The response spectrum can be obtained from the solutions of the motion equation for both motion phases, that is the forced vibration phase and the free vibration one. A first empirical assessment for the transient response spectrum can be obtained by building the envelope function generated by enveloping the displacement functions, which are evaluated at $\tau_{\max}$ for several values of $n_0, n_1, \ldots, n_4$. So, when forced vibrations occur, we get:

$$|DLF_{\max,1}(\tau_d)| =$$

$$= \frac{\tau_d^2}{\gamma^2 + \tau_d^2} \left| f_2 \frac{\sin \tau_{\max}}{\tau_d} - f_1 \cos \tau_{\max} + \left(f_1 - \lambda \frac{\tau_{\max}}{\tau_d} \right) \exp \left(-\gamma \frac{\tau_{\max}}{\tau_d} \right) \right| \quad (4.14)$$

with $\tau_{\max}$ from Eq. (4.13). And for free vibrations we have:

$$\begin{cases} |DLF_{\max,2}(\tau_d)| = \sqrt{A^2 + B^2} \\ A = \frac{\tau_d^2}{\gamma^2 + \tau_d^2} \left\{ -f_1 + e^{-\gamma} \left[(f_1 - \lambda) \cos \tau_d + \frac{f_2 - \lambda\gamma}{\tau_d} \sin \tau_d \right] \right\} \\ B = \frac{\tau_d^2}{\gamma^2 + \tau_d^2} \left\{ \frac{f_2}{\tau_d} + e^{-\gamma} \left[(f_1 - \lambda) \sin \tau_d - \frac{f_2 - \lambda\gamma}{\tau_d} \cos \tau_d \right] \right\} \end{cases} \quad (4.15)$$

where $DLF_{\max,1}$ e $DLF_{\max,2}$ denote the relative maximum values of dynamic load factor for forced and free vibrations, respectively.

For low values of the load duration, the spectrum is determined by free vibrations (Eq. (4.15)). For high values of τ_d instead, the spectrum is determined by solution (4.14), with $(n_0, \ldots, n_4) = (1, 0, 0, 0, 0)$. Finally, for intermediate values of the load duration, the response can only be obtained varying the values $(n_0, \ldots, n_4)$ and choosing, for each value of τ_d, the maximum displacement. In Figs. 4.2 and 4.3 the $DLF - \tau_d$ charts are presented to show the influence of $n_0, \ldots, n_4$ on the response spectrum. The charts are obtained from all the combinations of the following values of natural constants:
for Fig. 4.2,

$$n_0 = 0, 1, 2, 3 \quad n_1 = 0 \quad n_2 = 0, 1, \ldots, 6 \quad n_3 = 0 \quad n_4 = 0$$

for Fig. 4.3,

$$n_0 = 0, \ldots, 10 \quad n_1 = 0, \ldots, 5 \quad n_2 = 0, \ldots, 5 \quad n_3 = 0 \quad n_4 = 0$$

By enveloping a larger number of displacement functions, obtained with wider ranges of natural constants, we get the curves in Figs. 4.4 and 4.5.
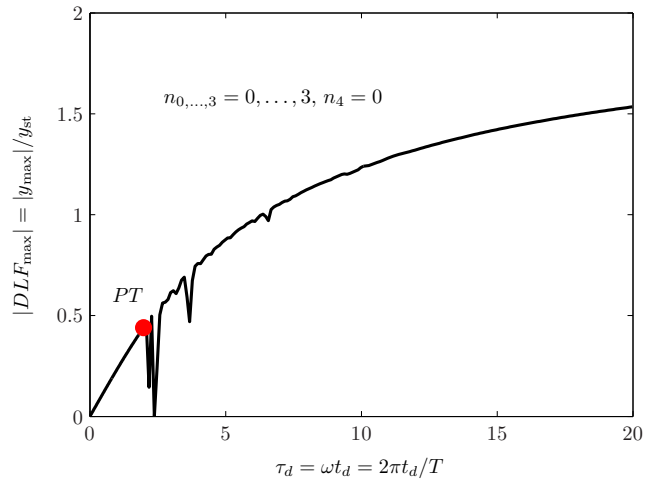
Fig. 4.4. Envelope function, by enveloping 256 different displacement functions ($\lambda = 1, \gamma = 2.8$).
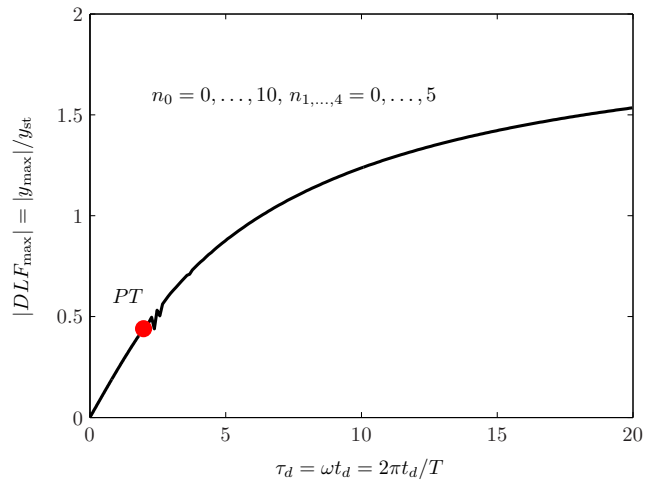
Fig. 4.5. Envelope function, by enveloping 14256 different displacement functions, ($\lambda = 1, \gamma = 2.8$).

As can be seen in these figures, a descending pulse load originates a concave downward spectrum of displacements, without changes of curvature sign. Numerical results show narrower zones where the curvature sign changes as the amount of sets of constants used to calculate the spectrum is increased.

In the present paper, the negative sign of the second spectrum derivative is assumed as a hypothesis, and will be called *concavity spectrum hypothesis* or, more shortly, *concavity hypothesis*. Based on this hypothesis, a smoothing algorithm is introduced to adjust the ordinates of those points where the concavity hypothesis is not respected. The algorithm allows a lowering of the computational cost, because it allows to calculate the response spectrum by using a smaller amount of sets of constants $(n_0, \ldots, n_4)$. Results produced by the smoothing algorithm are shown in Figs. 4.6 and 4.7. This way, it is possible to eliminate all the changes of curvature in the envelope function.

4.2.3 Approximate expression of the transient response spectrum
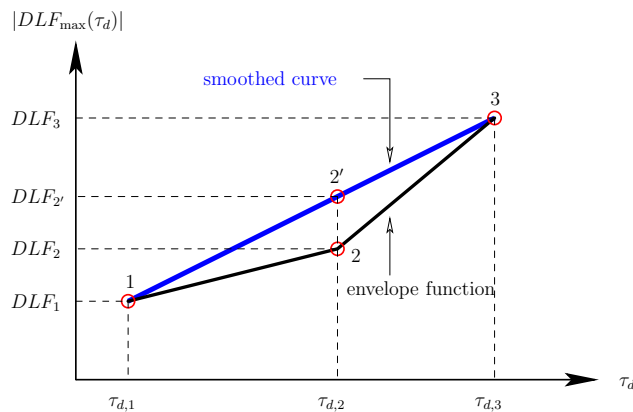
Fig. 4.6. Smoothing of response spectrum: the point 2 ordinate is replaced by the point 2' one, calculated by linear interpolation between points 2 and 3.

The research of an analytical expression for the response spectrum requires the solution of three problems: the choice of the spectrum domain, the demonstration of the spectrum concavity and the definition of the spectrum transition time.

The choice of the spectrum domain depends on the range in which the natural period of vibration of the loaded structure lies, as well as on the positive phase duration of the blast load. For civil structures, the fundamental period of vibration T can be assumed in the interval $[0.1, 20]$ s. For the loading duration of a detonation, Smith and Hetherington [2] suggest $t_d \in [10^{-1}, 10]$ ms, as it is also prescribed in Eurocode 1 [60], which predicts a loading time lower than 10 ms. In case of

deflagration, Eurocode 1 suggests a loading time of 100 ms, but in literature various pressure profiles are presented whose positive phase achieves 300 ms [61]. On that account the spectrum domain can be established in the following range

$$\tau_d = 2\pi \frac{t_d}{T} \in [10^{-5}\pi, 6\pi] \approx [10^{-5}, 20]$$

The concavity hypothesis, which is the basis of the smoothing algorithm introduced in sec. 4.2.2, can be rigorously demonstrated only for rectangular or triangular load shapes, but it is assumed true for each descending pulse load.

The third problem mentioned above concerns the definition of the spectrum transition time $\tau_{d,0}$ which corresponds with the abscissa of the transition point (PT). The first part of the spectrum, near the axis origin $(\tau_d \leq \tau_{d,0})$, is generated by free vibrations, and the second one is generated by forced vibrations $(\tau_d > \tau_{d,0})$. For rectangular or triangular pulse shapes, $\tau_{d,0}$ can be analytically established; for each other load shape $\tau_{d,0}$ is assumed coincident with the upper boundary of existence for the first solution of Eq. (4.8). When $n = 1$ and $\tau_d > \tau_{d,0}$, Eq. (4.8) predicts $\tau_{\max} < \tau_d$, but when this condition occurs, the motion is forced and Eq. (4.8) does not work. So, $\tau_{d,0}$ is given by:

$$\pi + \arctan\left(B/A\right)\big|_{\tau_d=\tau_{d,0}} = \tau_{d,0}$$
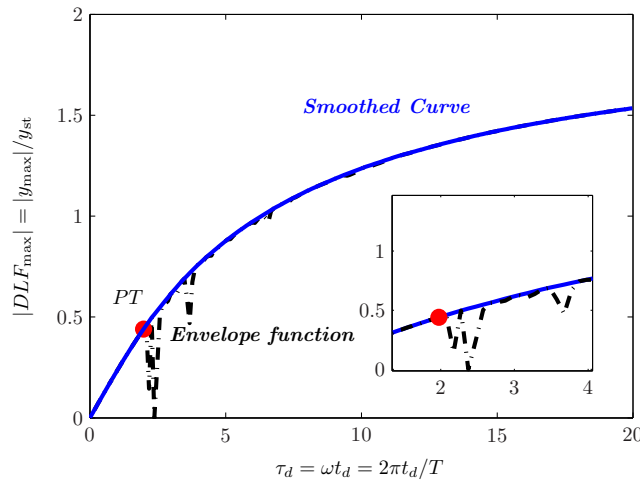
Fig. 4.7. Envelope function (dash–dot line) and smoothed curve (continuous line).

When $\tau_d > \tau_{d,0}$, an analytical expression for the response curve can be calculated by the least squares method [62], with a polynomial regression on spectrum points. The spectrum shape suggests the use of regression functions as follows:

$$S_r(\tau_d) = a_r \left[2^r - \left(\frac{1}{\tau_d + 0.5}\right)^r\right], \quad r \in \mathbb{N}, \quad a_r \in \mathbb{R} \tag{4.16}$$

By adding the first g functions given from Eq. (4.16), we get an expression $S(\tau_d)$ for the fitted curve, depending on unknown parameters a_r of the analytical model:

$$S(\tau_d) = a_0 - \sum_{r=1}^{g} \frac{a_r}{(\tau_d + 0.5)^r} \qquad (4.17)$$

In order to join the two curves described from Eqs. (4.15) and (4.17), which both represent the system response corresponding to the transition point, the same values of the two functions and their derivatives must be set when $\tau_d = \tau_{d,0}$. After fixing the following positions

$$X = (\tau_d + 0.5)^{-1} \qquad b_0 = a_0, \; b_r = -a_r \; \forall r > 0$$

$$X_0 = (\tau_{d,0} + 0.5)^{-1} \qquad S_0 = S(\tau_{d,0}) \qquad S_0' = S'(\tau_{d,0}) = \tan \alpha_0$$

and when the axis origin is translated into $PT \equiv (\tau_{d,0}; S(\tau_{d,0}))$

$$\overline{X} = X - X_0, \quad \overline{S} = S - S_0$$

we can write:

$$\overline{S} = \sum_{r=0}^{g} b_r \overline{X}^r \qquad (4.18)$$

where b_r are the new unknown parameters that have to be estimated. Then, by fixing the ordinate of the spectrum and the slope of his tangent line at $\tau_d = \tau_{d,0}$, we get:

$$\bar{S}(0) = \sum_{r=0}^{g} b_r \bar{X}^r \bigg|_{\bar{X}=0} = b_0 = 0 \qquad (4.19)$$

and also

$$\frac{d\bar{S}}{d\tau_d}\bigg|_{\tau_d=\tau_{d,0}} = \tan \alpha_0 \quad \Rightarrow \quad b_1 = -(\tau_{d,0} + 0.5)^2 \tan \alpha_0 \qquad (4.20)$$

The overdetermined system (4.18) becomes:

$$S - S_0 + (\tau_{d,0} + 0.5)^2 \tan \alpha_0 = \sum_{r=2}^{g} b_r (X - X_0)^r \qquad (4.21)$$

When the system (4.21) is solved, the expression of the transient response spectrum is given by:

$$S(\tau_d) = S(\tau_{d,0}) - (\tau_{d,0} + 0.5)^2 \tan \alpha_0 \left(\frac{1}{\tau_d + 0.5} - \frac{1}{\tau_{d,0} + 0.5} \right) +$$
$$+ \sum_{r=2}^{g} b_r \left(\frac{1}{\tau_d + 0.5} - \frac{1}{\tau_{d,0} + 0.5} \right)^r, \quad \forall \tau_d > \tau_{d,0} \qquad (4.22)$$

If τ_d and the constants $n_{0,1,\dots,4}$ have the following values:

- $\tau_d = \tau_{d,0}, \tau_{d,0} + 0.1, \tau_{d,0} + 0.2, \ldots, 20$

- $n_{0,1,2,3} = 0, 1, 2, 3$

- $n_4 = 0$

we get the fitted curve shown in Figs. 4.8 and 4.9. The regression parameters are presented in Tab. 4.1.
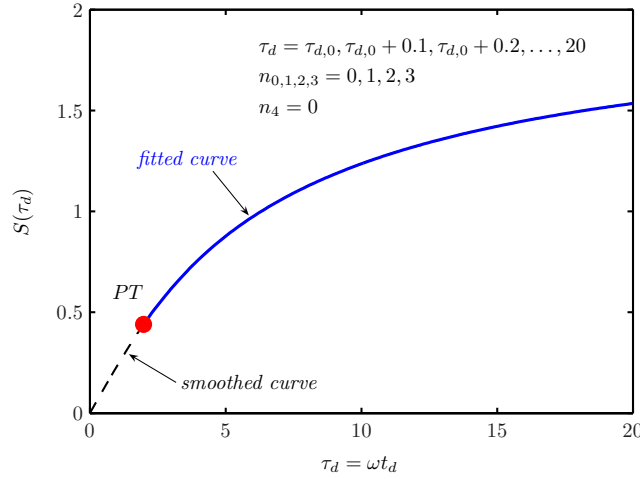
Fig. 4.8. Regression function of response spectrum ($\lambda = 1$, $\gamma = 2.8$).
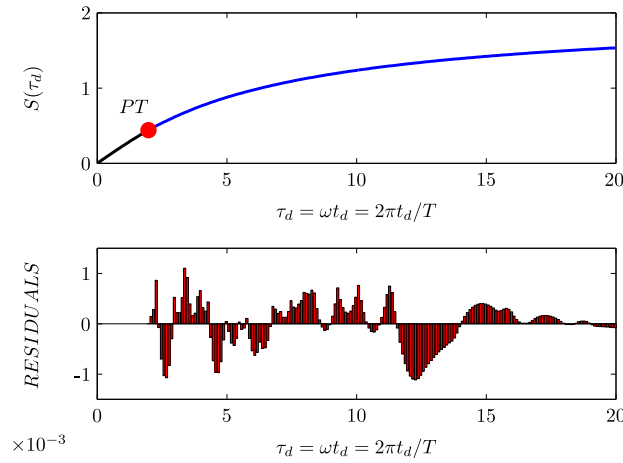
Fig. 4.9. Residuals distribution ($\lambda = 1$, $\gamma = 2.8$).

4.2.4   Influence of computation parameters on response spectrum

The coefficients b_r in Eq. (4.22), obtained by solving the system (4.21), are strongly influenced by the following computation parameters:

$\tau_d = [\tau_{d,0}, \tau_{d,0} + 0.1, \tau_{d,0} + 0.2, \ldots, 20]$, $n_{0,1,2,3} = 0, 1, 2, 3$, $n_4 = 0$	
r	b_r
0	0.0000
1	$-1.1933e + 000$
2	$1.4487e + 000$
3	$-1.0797e + 001$
4	$-5.8500e + 000$
5	$4.6883e + 001$
6	$1.8058e + 002$

Tab. 4.1. Response spectrum ($\lambda = 1$, $\gamma = 2.8$): coefficients of the regression polynomial of 6th degree.

1. the values assigned to $(n_0, n_1, n_2, n_3, n_4)$ which give a numerical assessment of Eqs. (4.13) and (4.14), and thus decide the ordinates of the envelope function;

2. the choice of points in the spectrum domain, which have a great influence on the polynomial regression;

3. the choice of the regression functions to model the response $S(\tau_d)$ and apply the least squares method.

Fig. 4.10 shows a possible convergence of the coefficients b_r as the amount of computed sets of constants $n_{0,\ldots,4}$ is increased, as well as the variation of the spectrum chart. But these results are not definitive and can only show a trend of the response depending on the set $(n_0, \ldots, n_4)$. Therefore, to improve the knowledge about the existing relation between $n_{0,\ldots,4}$ and the response curve, it could be necessary to use statistical techniques like design of experiment (robust design) and response surfaces.

In order to choose the points within the transient spectrum domain $[\tau_{d,0}, 20]$, an evident convergence of b_r can be noted as the mesh approaches zero, if a uniform domain partition is considered, as shown in Fig. 4.11.

Finally, a regression function for the response curve must satisfy some fundamental requirements.

Firstly, the quality of the fit is acceptable when the standardized residuals are normal and (approximately) independently distributed with a zero mean and with $[-1.96, 1.96]$ as confidence interval, with about 95% of confidence level (Fig. 4.9).

Secondly, under ideal circumstances, a plot of the residuals must show no geometric regularity, as it verified. It is worth noting that expression in Eq. (4.22) has these features.
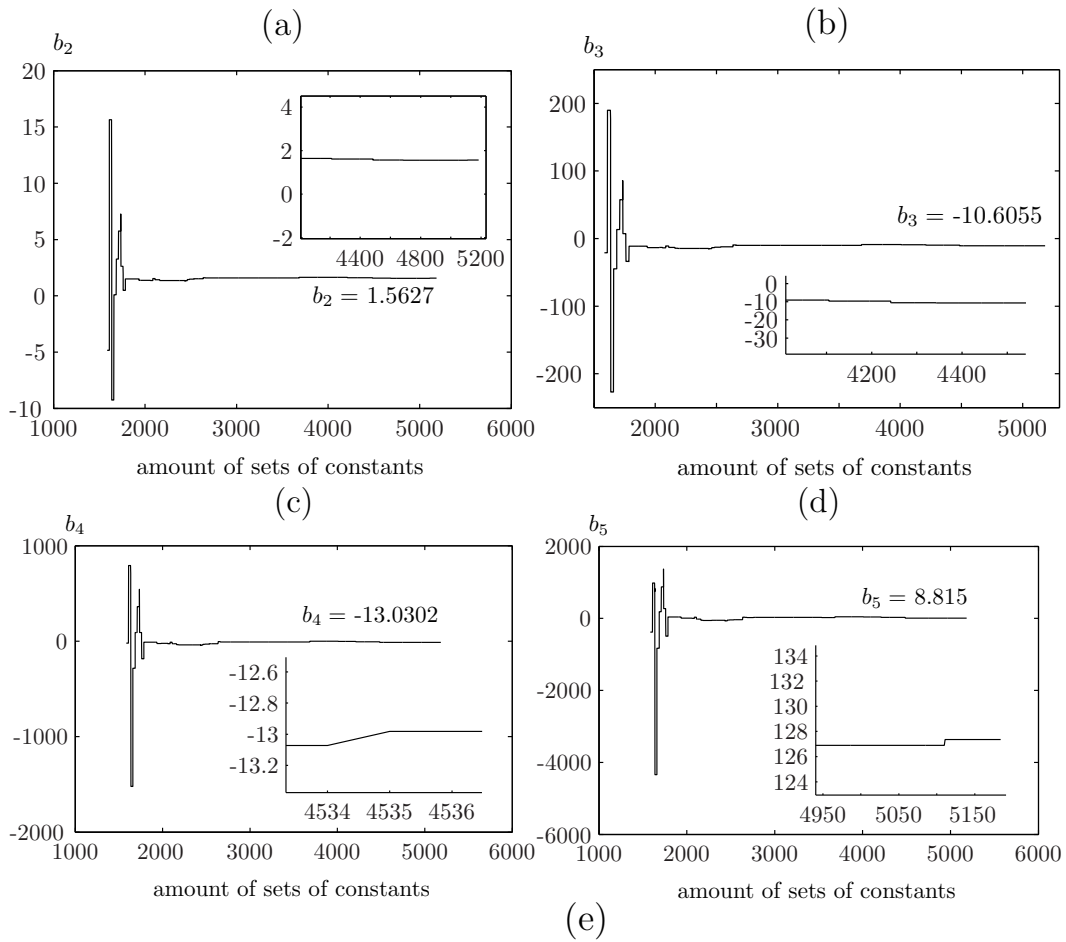
Fig. 4.10. Influence of the amount of computed sets of constants on the regression function $S(\tau_d)$: (a) variation of b_2, (b) variation of b_3, (c) variation of b_4, (d) variation of b_5, (e) variation of spectrum chart.

53

In order to define the degree of the polynomial $S(\tau_d)$, it has to be noted that, as the degree is increased, we get a badly conditioned system solving the least squares problem. Moreover, with a 6th degree polynomial, the residuals values obtained are very low and decreasing while the amount of sets $n_{0,\dots,4}$ used to make the envelope–function increases. In fact, when the argument $\overline{X}$ of the rth power in $S(\tau_d)$ is less than the unity, the influence of b_r decreases as r goes up. This condition is always verified when $\tau_{d,0} > 0.5$ (Fig. 4.12), as it happens when $\lambda \in [0,1]$ and $\gamma \in [0,10]$.
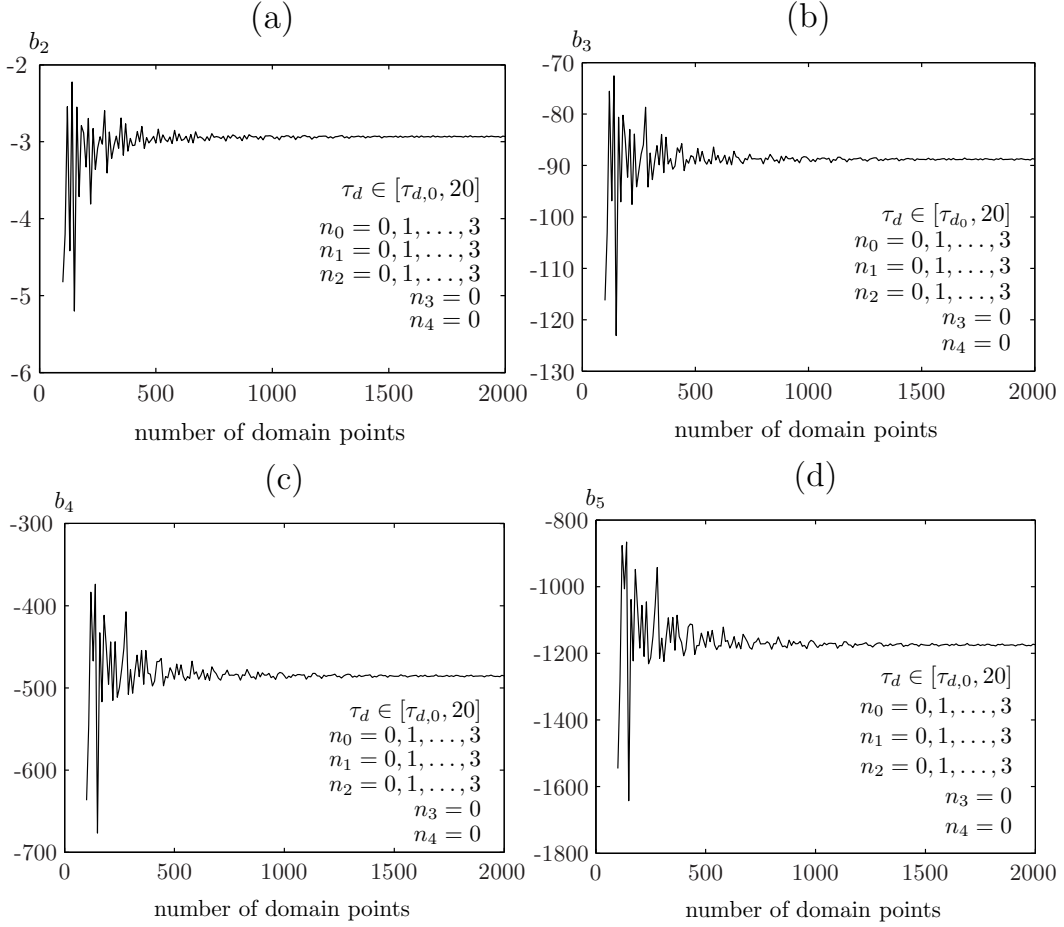
Fig. 4.11. Convergence of b_k varying the partition of the spectrum domain when $\lambda = 1$ and $\gamma = 2.8$: (a) convergence of b_2, (b) convergence of b_3, (c) convergence of b_4, (d) convergence of b_5.

4.3   Structural damage and p–i diagram

Let us suppose y_c to be a critical displacement corresponding to structural failure. If the resistance function of the spring is linear until failure (elastic–fragile
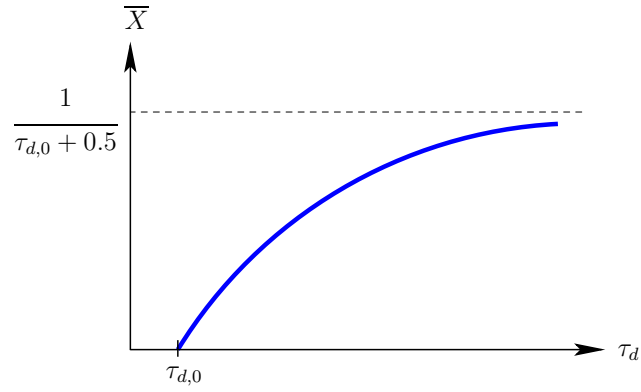
Fig. 4.12. Argument of rth power in spectrum expression against load duration.
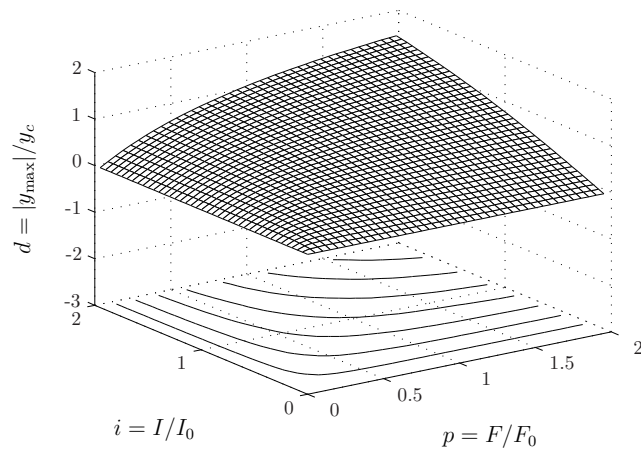
Fig. 4.13. Damage function ($\lambda = 1$, $\gamma = 2.8$); under the surface some level curves given by $d=cost$ are reported.

behavior), the damage level can be defined by the following ratio:

$$d = \frac{|y_{\max}|}{y_c} \qquad (4.23)$$

where $|y_{\max}|$ is the absolute maximum displacement. It should be noted that a "real damage" of the system occurs only when $d = 1$. When $d < 1$ the elastic deformation is recovered by the spring, and so d^{-1} can be regarded as a safety factor against the failure. In order to represent the damage level it is convenient to define the following dimensionless pressure and impulse:

$$p = \frac{F_{\max}}{F_0} \qquad (4.24a)$$

$$i = \frac{I}{I_0} \qquad (4.24b)$$

where $0.5\, F_0 = 0.5\, y_c k$ is the magnitude of the step load that produces the specified critical displacement y_c and $I_0 = y_c\sqrt{mk}$ is the ideal impulse that produces the same displacement.
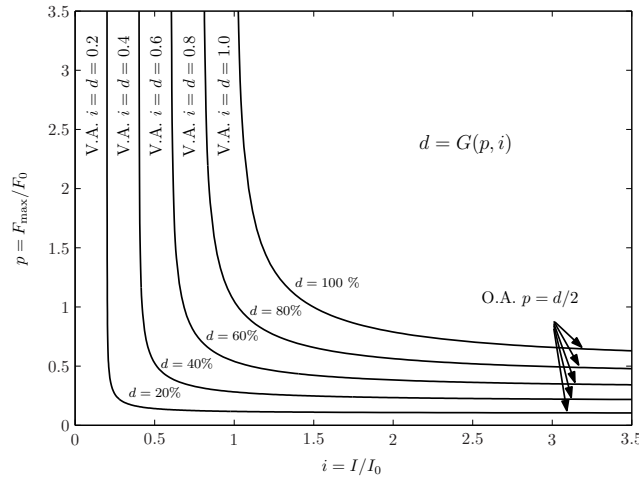
Fig. 4.14. Isodamage curves corresponding to 5 different damage levels ($\lambda = 1$, $\gamma = 2.8$).

Once the analytical expression of $S(\tau_d)$ is known from Eqs. (4.15) and (4.22), and remembering the definition of $DLF_{\max}$ and the impulse expression from Eq. (4.2), the structural damage level can be shown as a function with four variables:

$$d = G(p, i, \lambda, \gamma) = p \cdot S(\tau_d), \quad \tau_d = \frac{i}{p}\, \psi(\lambda, \gamma)^{-1} \qquad (4.25)$$

Fig. 4.13 shows the surface given from Eq. (4.25), generated by an exponentially decaying load ($\lambda = 1$, $\gamma = 8$). The level curves of this surface, where the G function takes on given constant values, are the well known isodamage curves, which

56

represent the set of the points in the pressure–impulse space that correspond to all the different loads, of fixed pulse shape, which produce a damage level equal to d. The isodamage curves, given implicitly from Eq. $G(p, i, \lambda, \gamma) = const.$, can be represented in explicit form as parametric curves with respect to the parameter τ_d (Fig. 4.14):

$$p = \frac{d}{S(\tau_d)}, \quad i = p \cdot \tau_d \cdot \psi(\lambda, \gamma) \tag{4.26}$$

4.3.1 Response limits
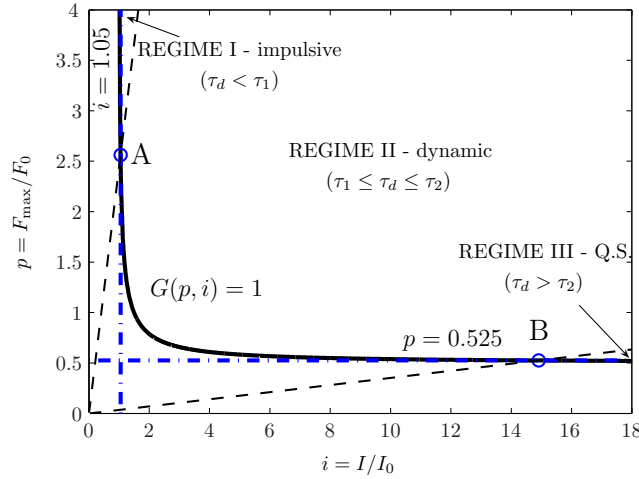
Fig. 4.15. Response regimes ($\lambda = 1$, $\gamma = 2.8$): impulsive, dynamic (A–B portion), quasi–static.

Generally a p-i diagram is not a monotonically decreasing function. This is not the case, for example, when the loading pressure profile has a finite rise time, or when the negative loading phase can not be neglected, as shown by Baker *et al.* [3]. When the loading pressure profile is monotonically decreasing, i.e. when $\lambda \in [0, 1]$ and $\gamma \in [0, 10]$, the isodamage curves are monotonically decreasing and they have vertical and horizontal asymptotes. These asymptotes can be established via an energy criterion. The energy balance for the spring–mass system at a generic time is given by

$$W_e = \Phi + T \tag{4.27a}$$

$$\int_0^t F(t') \, \dot{y}(t') \, dt' = \frac{1}{2} \, k y^2(t) + \frac{1}{2} \, m \dot{y}^2(t) \tag{4.27b}$$

in which W_e represents the work done by external load, T is the kinetic energy of the system and Φ is the elastic strain energy of the spring.

57

For an impulsive load, the equation of the impulsive asymptote is deduced from Eq. (4.27):

$$|T(0)| = |\Phi_{\text{max}}|$$

$$\frac{I^2}{2m} = \frac{1}{2} k y_{\text{max}}^2(t)$$

$$i = \frac{I}{I_0} = d \tag{4.28}$$

On the other hand, for a quasi–static load (step rise, constant magnitude, step decaying), the equation of the quasi–static asymptote can be obtained as follows:

$$\int_0^{t_{\text{max}}} F \, \dot{y}(t) \, dt = \frac{1}{2} k y^2(t_{\text{max}}) + \frac{1}{2} m \dot{y}^2(t_{\text{max}})$$

$$F y_{\text{max}} = \frac{1}{2} k y_{\text{max}}^2, \quad y_{\text{max}} = y(t_{\text{max}})$$

$$p = \frac{F}{F_0} = \frac{d}{2} \tag{4.29}$$

Generally, all charts relative to a given pulse shape can be conventionally divided into three regions, depending on the ratio of load duration to fundamental period of the structures:

$$\frac{t_d}{T} = \frac{\tau_d}{2\pi} \tag{4.30}$$

For low values of τ_d, a p-i curve collapses into its vertical asymptote, and the response is similar to that one of a system excited by an impulsive load. This regime is called impulsive (I). For high values of τ_d the diagram collapse into its horizontal asymptote, like a system excited by a quasi–static load, corresponding to a quasi–static regime (III). Finally, for intermediate values of this ratio, the system response can be calculated only with a rigorous dynamic analysis; it corresponds to the dynamic regime (II). Points A and B on the $p - i$ curve, corresponding to a transition from a kind of regime to another, have been established by Li and Meng with a 5% relative accuracy about the values of the horizontal and vertical asymptotes, as shown in Fig. 4.15.

4.3.2 Pulse shape effects on the system response

The influence of the pulse shape on the structural response is shown in Figs. 4.16, 4.17, 4.18 and 4.19. When λ and γ increase, the response spectrum moves down progressively and slowly approaches the horizontal asymptote ($DLF = 2$). The isodamage curves move away from the origin and their length in dynamic regime increases.
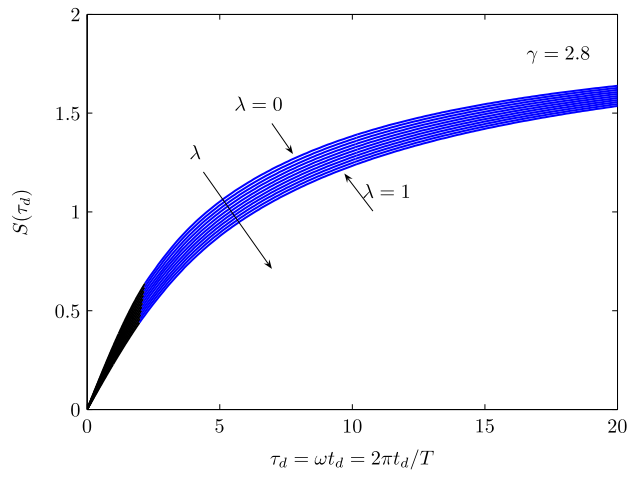
Fig. 4.16. Influence of load shape on response spectrum; $\gamma = 2.8$, $\lambda = 0, 0.1, 0.2, \ldots, 1$.
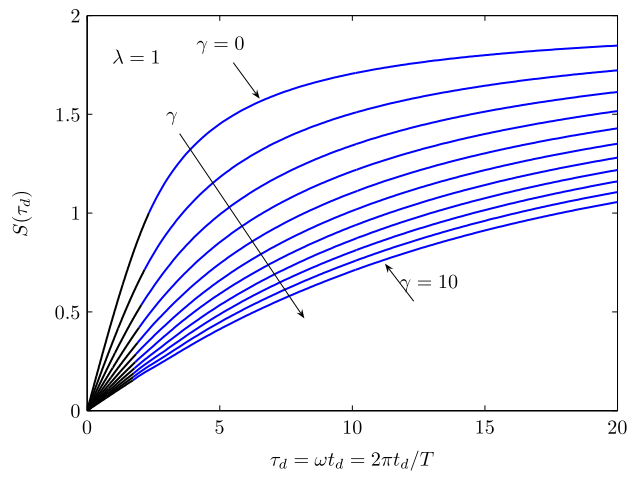
Fig. 4.17. Influence of load shape on response spectrum; $\lambda = 1$, $\gamma = 0, 1, 2, \ldots, 10$.
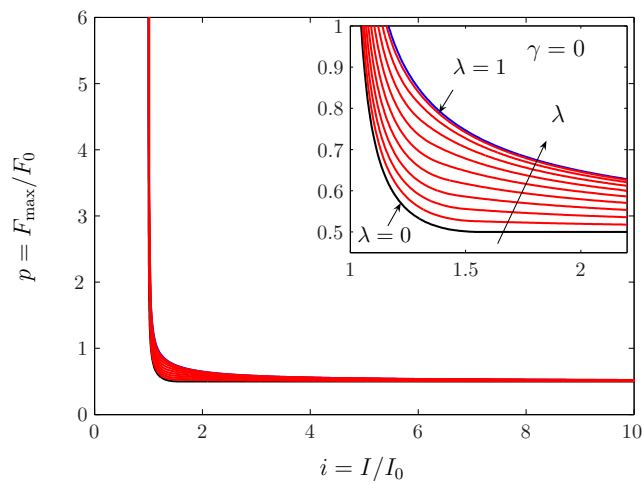
Fig. 4.18. Influence of load shape on p-i diagrams; $\lambda = 0, 0.1, 0.2, \ldots, 1$, $\gamma = 0$, $d = 1$.

59
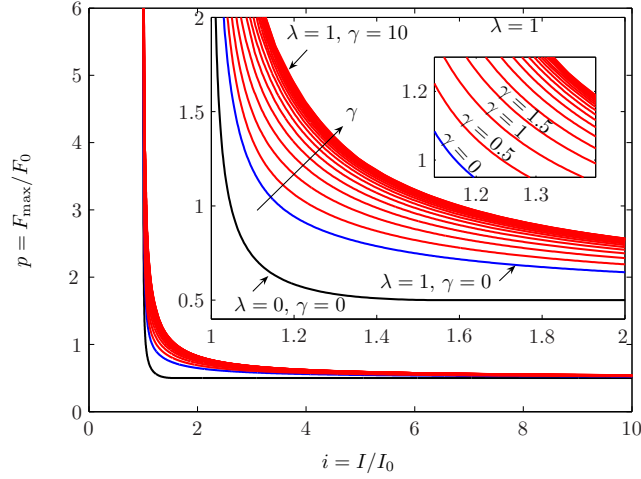
Fig. 4.19. Influence of load shape on p-i diagrams; $\gamma = 0, 0.5, 1.0, \ldots, 10$, $\lambda = 1$, $d = 1$.

4.3.3 Regression model for isodamage curves
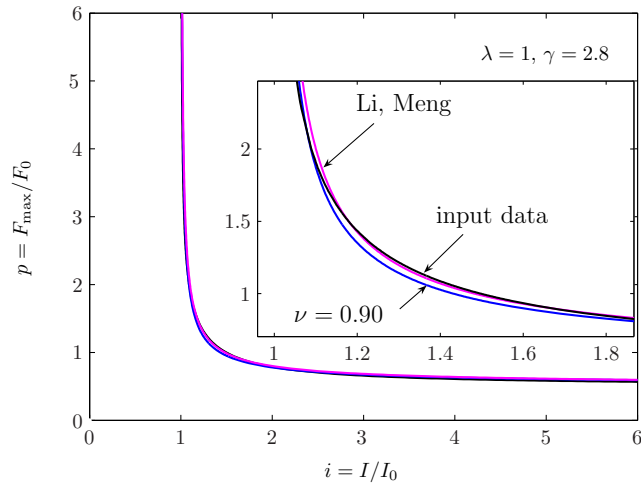
Fig. 4.20. Simplified p–i diagram; $\lambda = 1$, $\gamma = 2.8$, $d = 1$.

When the response spectrum is known, the consequent expression derived for p–i diagrams is rather complex. In fact, from Eqs. (4.15), (4.22) and (4.26), we get:

$$\begin{cases} p = \dfrac{d}{\sqrt{\mathrm{A}^2 + \mathrm{B}^2}} & \text{for } \tau_d \leq \tau_{d,0} \\ i = p\,\tau_d\,\psi(\lambda, \gamma) \end{cases} \qquad (4.31)$$
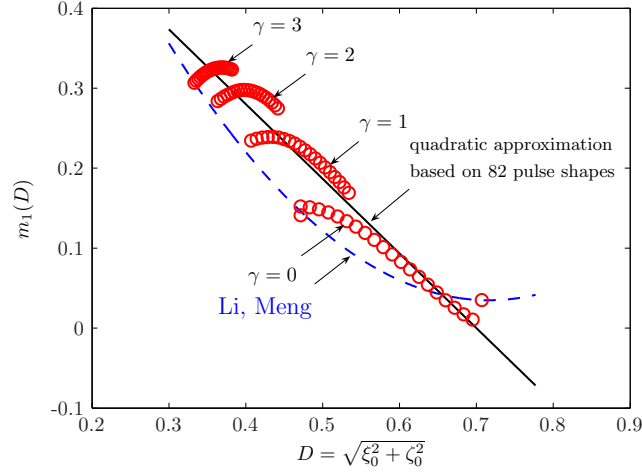
Fig. 4.21. Quadratic approximation for m_1; ($\lambda = 1$, $\gamma = 2.8$, $d = 1$).
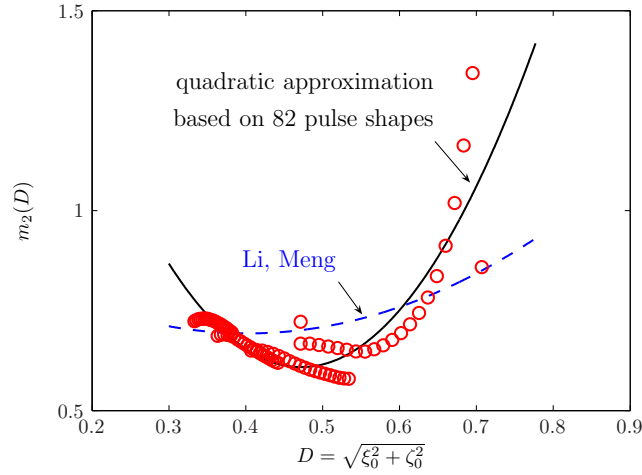
Fig. 4.22. Quadratic approximation for m_2; ($\lambda = 1$, $\gamma = 2.8$, $d = 1$).

$$
\begin{cases}
p = \dfrac{d}{\left(S_0 + \sum\limits_{r=1}^{g} b_r \left(\dfrac{1}{\tau_d + 0.5} - \dfrac{1}{\tau_{d,0} + 0.5} \right) \right)^r} & \text{for } \tau_d > \tau_{d,0} \\[4ex]
i = p\, \tau_d\, \psi(\lambda, \gamma)
\end{cases} \qquad (4.32)
$$

In order to find a simplified representation, the curve shape suggests the use of hyperbolic regression functions, like those proposed by Li and Meng:

$$
p = \frac{1}{2} + \frac{m_1}{(i-1)^{m_2}} \qquad (4.33)
$$

61

ν	Q
-0.95	0.3016
-0.94	0.3015
-0.93	0.3015
-0.92	0.3014
-0.91	0.3014
-0.90	**0.3014**
-0.89	0.3014
-0.88	0.3014
-0.87	0.3015
-0.86	0.3015
-0.85	0.3016

Tab. 4.2. Simplified p–i curves: local minimum of sum of squared deviations; $\lambda = 1$, $\gamma = 2.8$, $d = 1$.

which can be linearized as follow:

$$Y = \bar{m}_1 + m_2 X, \quad \begin{cases} X = -\ln(i-1) \\ Y = \ln(p - 0.5) \\ \bar{m}_1 = \ln(m_1) \end{cases} \tag{4.34}$$

where m_1 and m_2 are unknown parameters that are to be estimated. In order to avoid an excessive discrepancy between regression functions and input data, caused by the asymptotic behavior, it is covenient to assign at the jth input point a weight w_j depending on the chart slope at the same point:

$$w_j = \left(\max \left\{ \left| \frac{dp}{di} \right|_{(i_j, p_j)}, \left| \frac{di}{dp} \right|_{(i_j, p_j)} \right\} \right)^{\nu} \tag{4.35}$$

in which the power ν is chosen by minimizing the sum of squared residuals (Q^2), considering the deviations η_j on both X and Y directions:

$$Q = \sqrt{\sum_j \eta_j^2}, \quad \eta_j = \min \left\{ |Y_j - (\bar{m}_1 + m_2 X_j)|, \left| X_j - \frac{Y_j - \bar{m}_1}{m_2} \right| \right\} \tag{4.36}$$

When the pressure profile is exponentially decaying ($\lambda = 1, \gamma = 2.8$), with $\nu = 0.90$ we obtain a minimum local point of Q, as shown in Tabs. 4.2 and 4.3.

By following the same procedure for other load shapes, we get the values of $m_{1,2}$ in Tab. 4.4. Certainly, even these results are strongly influenced by the choices of the spectrum domain and sets $n_0, n_1, \ldots, n_4$. Similar problems occur when a relationship has to be estimated between $m_{1,2}$ and the load shape, represented by its centroid. From Eq. (4.1), and introducing the following change of variables

$$\xi = \frac{t}{t_d}$$

62

	$\nu = -0.90$			Li and Meng, 2002	
m_1	m_2	Q	m_1	m_2	Q
0.305	0.693	0.301	0.300	0.700	0.301

Tab. 4.3. Regression parameters of p-i diagram; $\lambda = 1$, $\gamma = 2.8$, $d = 1$.

the loading function, normalized with respect to his maximum value, becomes:

$$f(\xi) = \begin{cases} (1 - \lambda\,\xi)\exp(-\gamma\xi) & \text{for } 0 \le \xi \le 1 \\ 0 & \text{for } \xi > 1 \end{cases} \tag{4.37}$$

The centroid position is given by

$$\xi_0 = \frac{\int\limits_0^1 \xi f(\xi)d\xi}{\int\limits_0^1 f(\xi)d\xi}, \qquad \zeta_0 = \frac{\int\limits_0^1 f^2(\xi)d\xi}{2\int\limits_0^1 f(\xi)d\xi} \tag{4.38a}$$

$$D = \sqrt{\xi_0^2 + \zeta_0^2} \tag{4.38b}$$

By using the quadratic approximation proposed by Li and Meng [46]

$$\begin{aligned} m_1(D) &= \beta_{0,1} + \beta_{1,1}D + \beta_{2,1}D^2 \\ m_2(D) &= \beta_{0,2} + \beta_{1,2}D + \beta_{2,2}D^2 \end{aligned} \tag{4.39}$$

and from results in Tab. 4.4, we get the $\beta_{i,j}$ values which, as suggested by Florek and Benaroya [63], are very different from the values determined by only three load shapes:

$\beta_{0,1} = 0.654$	$\beta_{1,1} = -0.936$	$\beta_{2,1} = 0.002$
$\beta_{0,2} = 2.553$	$\beta_{1,2} = -8.237$	$\beta_{2,2} = 8.721$

Charts of $m_1(D)$ ed $m_2(D)$ are shown in Figs. 4.21 and 4.22. A clear relationship can be observed only when one of the shape parameters, λ or γ, is fixed. Therefore, for further research of a simplified expression for p-i diagrams, it could be necessary to establish a relation between $m_{1,2}$ and the load shape in which λ and γ are partially uncoupled:

$$m_i = f_i(\lambda) + g_i(\gamma) + h_i(\lambda, \gamma), \quad i = 1, 2$$

Similar problems occur while investigating the influence of the load shape on the response limits. Even in this case, the quadratic approximation proposed by Li
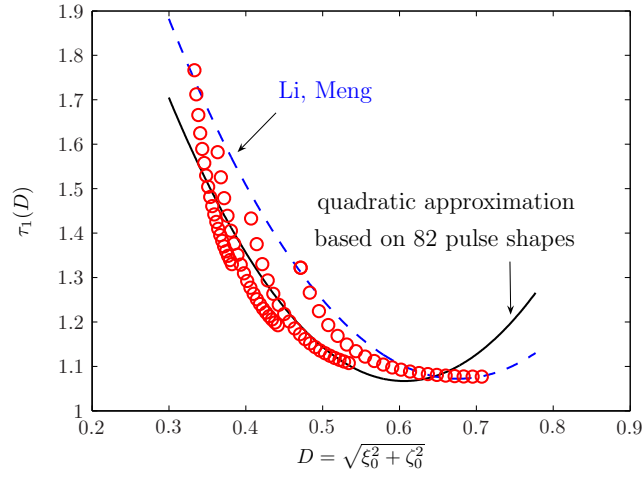
Fig. 4.23. Quadratic approximation for τ_1; ($\lambda = 1$, $\gamma = 2.8$, $d = 1$).
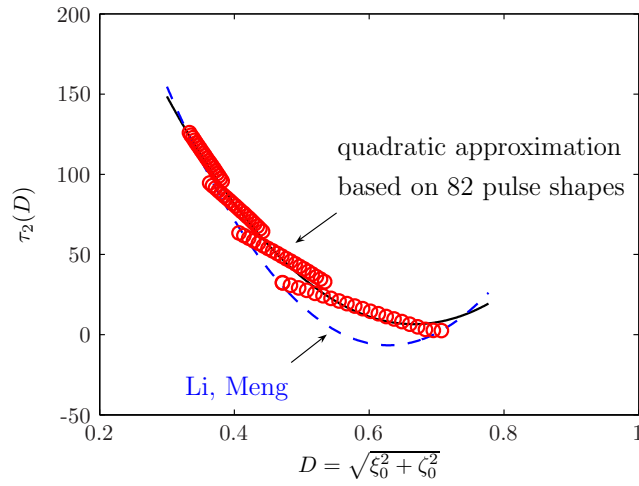
Fig. 4.24. Quadratic approximation for τ_2; ($\lambda = 1$, $\gamma = 2.8$, $d = 1$).
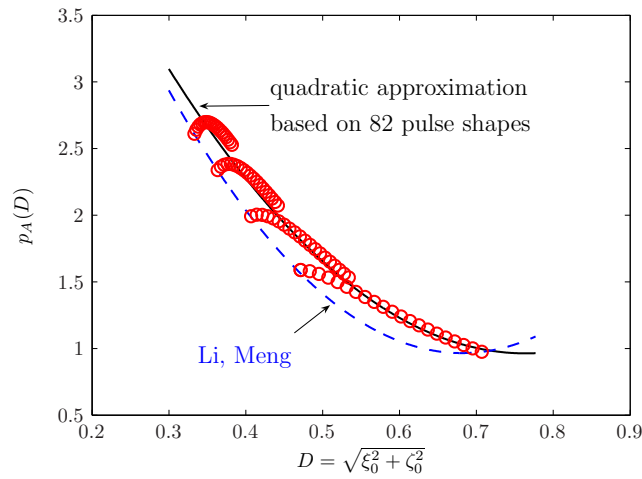
Fig. 4.25. Quadratic approximation for p_A; ($\lambda = 1$, $\gamma = 2.8$, $d = 1$).
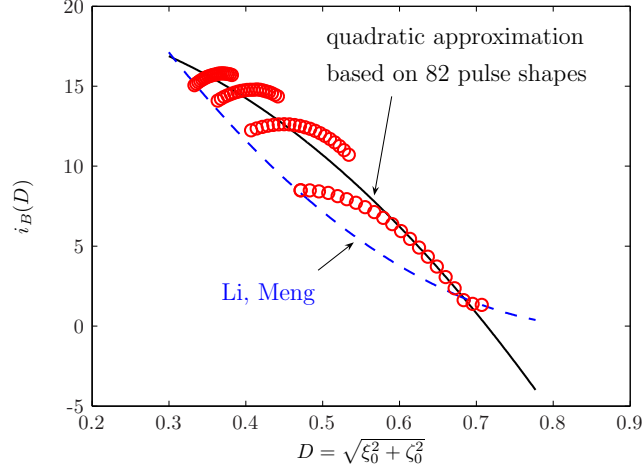
Fig. 4.26. Quadratic approximation for i_B; ($\lambda = 1$, $\gamma = 2.8$, $d = 1$).

and Meng (Eq. (4.40)) produces different results if it is applied to the wide range of load shapes in Tab. 4.4, and all observations made for $m_{1,2}(D)$ functions about the accuracy of the employed method are still valid.

$$
\begin{aligned}
\tau_1(D) &= \beta_{0,\tau_1} &+& \beta_{1,\tau_1}D &+& \beta_{2,\tau_1}D^2 \\
\tau_2(D) &= \beta_{0,\tau_2} &+& \beta_{1,\tau_2}D &+& \beta_{2,\tau_2}D^2 \\
p_A(D) &= \beta_{0,p_A} &+& \beta_{1,p_A}D &+& \beta_{2,p_A}D^2 \\
i_B(D) &= \beta_{0,i_B} &+& \beta_{1,i_B}D &+& \beta_{2,i_B}D^2
\end{aligned}
\tag{4.40}
$$

The regression curves of these functions are represented in Figs. 4.23, 4.24, 4.25 and 4.26, which are defined using the following β–values:

β_{0,τ_1}	$=$	3.566	β_{1,τ_1}	$=$	-8.247	β_{2,τ_1}	$=$	6.803
β_{0,τ_2}	$=$	475.734	β_{1,τ_2}	$=$	-1407.286	β_{2,τ_2}	$=$	1055.256
β_{0,p_A}	$=$	6.745	β_{1,p_A}	$=$	-15.133	β_{2,p_A}	$=$	9.901
β_{0,i_B}	$=$	19.156	β_{1,i_B}	$=$	6.332	β_{2,i_B}	$=$	-46.496

4.3.4 Effective pressure–impulse diagram

In the following the effective impulse is defined in a different way with respect to that shown in Ref. [46]:

$$
i_e = 1 + \frac{(i-1)^{m_2}}{m_1}
\tag{4.41}
$$

and the same definition is used for the effective pressure

$$
p_e = p
\tag{4.42}
$$
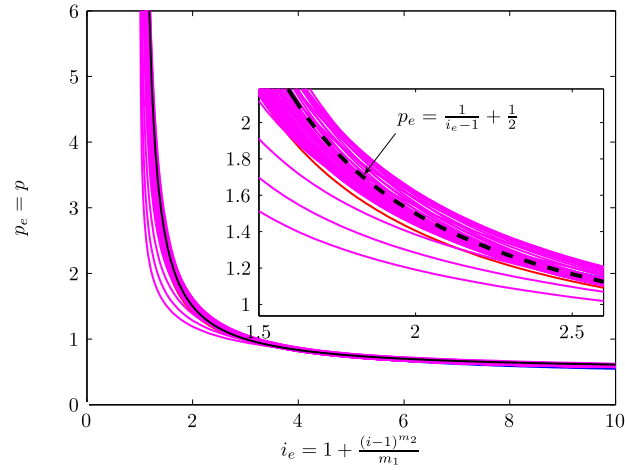
Fig. 4.27. Unique $p_e - i_e$ diagram, compared with charts of load profiles given by $\lambda = 0.05, 1.05, \ldots, 1$, $\gamma = 0.001, 1.001, 2.001, 3.001$; $d = 1$.

Substituting Eq. (4.41) and Eq. (4.42) into Eq. (4.33), we obtain a $p_e - i_e$ curve for a 100% damage level which is shifted towards the p direction by 0.5 with respect to that proposed by Li and Meng:

$$p_e = \frac{1}{i_e - 1} + \frac{1}{2} \tag{4.43}$$

With the values in Tab. 4.4 and from Eqs. (4.41) and (4.42) we can represent the isodamage curves in the $p_e - i_e$ space for different pulse shapes, in order to compare them with the hyperbole described from Eq. (4.43). The charts in Fig. 4.27, related to 82 different pulse shapes, show a maximum discrepancy of 0.488 (24.05%), corresponding to the abscissa $i_e = 1.24$ and a Q value of about 2.49. Therefore, the isodamage curves in $p_e - i_e$ space do not collapse into an unique hyperbolic curve.

λ	γ	m_1	m_2	τ_1	τ_2	p_A	i_B
0.00	0.000	0.035	0.859	1.077	2.5	0.98	1.32
1.00	0.000	0.141	0.722	1.322	32.3	1.59	8.49
0.05	0.001	0.011	1.344	1.077	2.7	1.00	1.39
0.05	1.001	0.169	0.580	1.107	33.0	1.53	10.72
0.05	2.001	0.275	0.620	1.193	64.4	2.07	14.36
0.05	3.001	0.323	0.695	1.330	95.8	2.53	15.70
0.10	0.001	0.017	1.163	1.077	3.3	1.03	1.63
0.10	1.001	0.176	0.580	1.111	34.6	1.56	11.00
0.10	2.001	0.279	0.623	1.199	66.0	2.10	14.46
0.10	3.001	0.324	0.699	1.339	97.4	2.55	15.74
0.15	0.001	0.026	1.019	1.078	4.9	1.05	2.37
$\vdots$	$\vdots$	$\vdots$	$\vdots$	$\vdots$	$\vdots$	$\vdots$	$\vdots$

λ	γ	m_1	m_2	τ_1	τ_2	p_A	i_B
0.15	1.001	0.183	0.582	1.115	36.2	1.59	11.26
0.15	2.001	0.282	0.626	1.206	67.6	2.12	14.55
0.15	3.001	0.325	0.703	1.349	99.0	2.57	15.76
0.20	0.001	0.035	0.912	1.079	6.5	1.08	3.07
0.20	1.001	0.189	0.585	1.119	37.8	1.62	11.49
0.20	2.001	0.285	0.630	1.213	69.2	2.15	14.62
0.20	3.001	0.325	0.706	1.359	100.6	2.59	15.78
0.25	0.001	0.045	0.836	1.081	8.1	1.11	3.73
0.25	1.001	0.195	0.588	1.124	39.4	1.65	11.70
0.25	2.001	0.288	0.635	1.221	70.8	2.18	14.68
0.25	3.001	0.326	0.710	1.370	102.2	2.60	15.80
0.30	0.001	0.054	0.783	1.083	9.7	1.14	4.34
0.30	1.001	0.201	0.592	1.130	41.0	1.68	11.89
0.30	2.001	0.291	0.639	1.230	72.4	2.20	14.73
0.30	3.001	0.326	0.713	1.382	103.8	2.62	15.80
0.35	0.001	0.064	0.744	1.085	11.3	1.17	4.91
0.35	1.001	0.207	0.595	1.136	42.6	1.71	12.06
0.35	2.001	0.293	0.644	1.240	74.0	2.23	14.77
0.35	3.001	0.326	0.716	1.395	105.4	2.64	15.80
0.40	0.001	0.073	0.716	1.089	13.0	1.21	5.46
0.40	1.001	0.212	0.599	1.143	44.2	1.75	12.21
0.40	2.001	0.295	0.648	1.251	75.6	2.25	14.80
0.40	3.001	0.326	0.719	1.410	107.0	2.65	15.79
0.45	0.001	0.083	0.694	1.093	14.6	1.24	5.94
0.45	1.001	0.218	0.603	1.152	45.8	1.78	12.33
0.45	2.001	0.296	0.653	1.264	77.0	2.27	14.77
0.45	3.001	0.325	0.721	1.425	108.4	2.66	15.74
0.50	0.001	0.092	0.677	1.098	16.2	1.28	6.38
0.50	1.001	0.222	0.607	1.161	47.4	1.81	12.44
0.50	2.001	0.297	0.658	1.277	78.6	2.30	14.77
0.50	3.001	0.325	0.724	1.442	110.0	2.68	15.72
0.55	0.001	0.101	0.663	1.104	17.8	1.31	6.77
0.55	1.001	0.227	0.612	1.172	49.0	1.84	12.52
0.55	2.001	0.298	0.663	1.292	80.2	2.32	14.76
0.55	3.001	0.324	0.726	1.461	111.6	2.68	15.69
0.60	0.001	0.110	0.653	1.112	19.4	1.35	7.13
0.60	1.001	0.231	0.618	1.185	50.6	1.87	12.58
0.60	2.001	0.298	0.668	1.310	81.8	2.34	14.74
0.60	3.001	0.323	0.727	1.481	113.2	2.69	15.65
0.65	0.001	0.119	0.648	1.122	21.0	1.39	7.44
0.65	1.001	0.234	0.624	1.201	52.2	1.90	12.61
0.65	2.001	0.298	0.673	1.329	83.4	2.35	14.70
$\vdots$	$\vdots$	$\vdots$	$\vdots$	$\vdots$	$\vdots$	$\vdots$	$\vdots$

λ	γ	m_1	m_2	τ_1	τ_2	p_A	i_B
0.65	3.001	0.321	0.729	1.504	114.8	2.70	15.60
0.70	0.001	0.127	0.648	1.134	22.6	1.43	7.71
0.70	1.001	0.236	0.630	1.218	53.8	1.93	12.62
0.70	2.001	0.297	0.678	1.351	85.0	2.37	14.65
0.70	3.001	0.320	0.730	1.529	116.4	2.70	15.55
0.75	0.001	0.134	0.652	1.149	24.2	1.46	7.94
0.75	1.001	0.238	0.636	1.239	55.4	1.95	12.62
0.75	2.001	0.296	0.684	1.376	86.6	2.38	14.59
0.75	3.001	0.318	0.730	1.558	118.0	2.70	15.48
0.80	0.001	0.140	0.656	1.168	25.8	1.50	8.13
0.80	1.001	0.239	0.642	1.264	57.0	1.98	12.59
0.80	2.001	0.294	0.687	1.405	88.2	2.38	14.51
0.80	3.001	0.316	0.730	1.589	119.6	2.69	15.41
0.85	0.001	0.145	0.660	1.193	27.6	1.53	8.33
0.85	1.001	0.239	0.647	1.293	58.6	1.99	12.53
0.85	2.001	0.292	0.690	1.439	89.8	2.38	14.43
0.85	3.001	0.314	0.730	1.625	121.2	2.68	15.34
0.90	0.001	0.149	0.664	1.224	29.2	1.56	8.43
0.90	1.001	0.238	0.650	1.330	60.2	2.00	12.46
0.90	2.001	0.289	0.691	1.479	91.4	2.38	14.33
0.90	3.001	0.312	0.729	1.666	122.8	2.66	15.25
0.95	0.001	0.151	0.667	1.266	30.8	1.58	8.49
0.95	1.001	0.237	0.651	1.375	61.8	2.00	12.36
0.95	2.001	0.287	0.690	1.526	93.0	2.36	14.22
0.95	3.001	0.310	0.726	1.713	124.4	2.64	15.16
1.00	0.001	0.152	0.668	1.322	32.4	1.59	8.50
1.00	1.001	0.234	0.650	1.433	63.4	1.99	12.24
1.00	2.001	0.284	0.687	1.582	94.6	2.34	14.09
1.00	3.001	0.307	0.724	1.767	126.0	2.61	15.06

Tab. 4.4: Parameters of $p-i$ regression functions and response limits ($\varepsilon = 5\%$) corresponding to different pulse shapes.

4.4 Model validation by genetic algorithms

Since the accuracy estimation of the model presented in this chapter is an open problem, the results so far shown need to be discussed. The optimization problem of finding the response of a spring–mass system may be dealt with by applying many different optimization algorithms [64, 65, 66], such as gradient descent method, Nelder-Mead method, subgradient method, simplex method, ellipsoid method, bundle methods, Newton's method, genetic algorithms (g.a.), evolution strategies.

In the following subsections, the comparison between the response spectrum obtained by the current analytical model and the one obtained by applying genetic algorithms is shown . It proves that, as far as the pulse shapes taken into account are concerned, the current model is capable to calculate the system response with a good accuracy in spite of a very low computational effort.

4.4.1 Genetic algorithm overview

A genetic algorithm is a method for solving both constrained and unconstrained optimization problems that is based on natural selection, the process that drives biological evolution. A genetic algorithm repeatedly modifies a population of individual solutions. At each step, a genetic algorithm selects individuals at random from the current population to be parents and uses them to produce the children for the next generation. After successive generations, the population "evolves" toward an optimal solution. This method is suitable to solve a variety of optimization problems that are not well suited for standard optimization algorithms, including problems in which the objective function is discontinuous, non differentiable, stochastic, or highly nonlinear.

The genetic algorithm uses three main types of rules at each step to create the next generation from the current population. *Selection rules* select individuals, called parents, that contribute to the population at the next generation. *Crossover rules* combine two parents to form children for the next generation. *Mutation rules* apply random changes to individual parents to form children.

4.4.2 Terminology

The *fitness function* is the function which needs to be optimized. For standard optimization algorithms, this is known as the objective function. Usually, genetic algorithms try to find the minimum of the fitness function.

An *individual* is any point to which the fitness function can be applied. The value of the fitness function for an individual is its score. An individual is sometimes referred to as a *genome* and the vector entries of an individual as *genes*.

A *population* is an array of individuals. The same individual can appear more than once in the population. At each iteration, a genetic algorithm performs a series of computations on the current population to produce a new population. Each successive population is called a new *generation*.

Diversity refers to the average distance between individuals in a population. A population has high diversity if the average distance is large; otherwise it has

low diversity. Diversity is essential to a genetic algorithm because it enables the algorithm to search a larger region of the space.

The *fitness value* of an individual is the value of the fitness function for that individual. Since by default a g.a. finds the minimum of the fitness function, the *best* fitness value for a population is the smallest fitness value for any individual in the population.

To create the next generation, a genetic algorithm selects certain individuals in the current population, called *parents*, and uses them to create individuals in the next generation, called *children* or *offspring*. Typically, the algorithm is more likely to select parents that have better fitness values.

4.4.3 Genetic algorithm outline

The path followed by a genetic algorithm can be summarizer in the following steps:

- a random initial population is created;

- a sequence of new populations is created. At each step, the individuals in the current generation are used to create the next population. To create the new population, the algorithm performs the following steps:

  - scores each member of the current population by computing its fitness value;

  - scales the raw fitness scores to convert them into a more usable range of values;

  - selects members, called parents, based on their fitness values;

  - some of the individuals in the current population that have lower fitness are chosen as *elite*. These elite individuals are passed to the next population;

  - offspring is produced, either by making random changes to a single parent (*mutation*) or by combining the vector entries of a pair of parents (*crossover*);

  - the current population is replaced with the children to form the next generation;

- the algorithm stops when one of the stopping criteria is met.

70

4.4.4 Fitness scaling

Fitness scaling converts the raw fitness scores that are returned by the fitness function to values in a range that is suitable for the selection function. The selection function uses the scaled fitness values to select the parents of the next generation. The selection function assigns a higher probability of selection to individuals with higher scaled values. The range of the scaled values affects the performance of the genetic algorithm. If the scaled values vary too widely, the individuals with the highest scaled values reproduce too rapidly, taking over the population gene pool too quickly, and preventing the genetic algorithm from searching other areas of the solution space. On the other hand, if the scaled values vary only a little, all individuals have approximately the same chance of reproduction and the search will progress very slowly.

A very common fitness scaling method, called *rank scaling*, scales the raw scores based on the rank of each individual instead of its score. The rank of an individual is its position in the sorted scores: the rank of the most fit individual is 1, the next most fit is 2, and so on. The rank scaling function assigns scaled values so that the scaled value of an individual with rank n is proportional to $1/\sqrt{n}$, n being the number of individual of the current population, and the sum of the scaled values over the entire population equals the number of parents needed to create the next generation. Rank fitness scaling removes the effect of the spread of the raw scores.

Other quite common scaling methods are [67]:

- *proportional scaling*. Proportional scaling makes the scaled value of an individual proportional to its raw fitness score;

- *top scaling*. Top scaling scales the top individuals equally. A fraction of the population size, which represents those individuals that belong to the top of the current population, needs to be specified;

- *shift linear scaling*. Shift linear scaling scales the raw scores so that the expectation of the fittest individual is equal to a constant multiplied by the average score.

4.4.5 Selection function

The selection function chooses parents for the next generation based on their scaled values from the fitness scaling function. An individual can be selected more

than once as a parent, in which case it contributes its genes to more than one child. Common selection techniques are [67, 68]:

- *stochastic uniform selection function.*The default selection function lays out a line in which each parent corresponds to a section of the line of length proportional to its scaled value. The algorithm moves along the line in steps of equal size. At each step, the algorithm allocates a parent from the section it lands on. The first step is a uniform random number less than the step size;

- *remainder selection.* Remainder selection assigns parents deterministically from the integer part of each individual's scaled value and then uses roulette selection on the remaining fractional part. After parents have been assigned according to the integer parts of the scaled values, the rest of the parents are chosen stochastically. The probability that a parent is chosen in this step is proportional to the fractional part of its scaled value;

- *uniform selection.* Uniform selection chooses parents using the expectations and number of parents. This technique is useful for debugging and testing, but is not a very effective search strategy;

- *roulette selection.* Roulette selection chooses parents by simulating a roulette wheel, in which the area of the section of the wheel corresponding to an individual is proportional to the individual's expectation. The algorithm uses a random number to select one of the sections with a probability equal to its area;

- *tournament selection.* Tournament selection chooses each parent by choosing tournament size players at random and then choosing the best individual out of that set to be a parent.

4.4.6 Reproduction

The method of reproduction specify how the genetic algorithm creates children for the next generation. In order to set up e reproduction method, two input data are needed: the number of *elite elements* that are guaranteed to survive to the next generation and the *crossover fraction*, which specifies the fraction of the next generation, other than elite children, that are produced by crossover. The other individuals, which complete the next generation, are produced by mutation.

Crossover methods

Crossover method specify how the genetic algorithm combines two individuals, or parents, to form a crossover child for the next generation. The most common methods are [67]:

- *scattered crossover*. This method creates a random binary vector and selects the genes where the vector is a 1 from the first parent, and the genes where the vector is a 0 from the second parent, and combines the genes to form the child. For example, if `p1` and `p2` are the parents

$$p1 = [a\ b\ c\ d\ e\ f\ g\ h]$$
$$p2 = [1\ 2\ 3\ 4\ 5\ 6\ 7\ 8]$$

and the binary vector is `[1 1 0 0 1 0 0 0]`, the method returns the following child:

$$child1 = [a\ b\ 3\ 4\ e\ 6\ 7\ 8];$$

- *single point crossover*. A random integer n between 1 and the *number of variables* is chosen. Then:

    - vector entries numbered less than or equal to n are selected from the first parent;
    - vector entries numbered greater than n are selected from the second parent;
    - concatenates these entries to form a child vector;

For example, if `p1` and `p2` are still the same parents above and the crossover point is 3, the crossover function returns the following child:

$$child1 = [a\ b\ c\ 4\ 5\ 6\ 7\ 8];$$

- *two point crossover*. Two random integers m and n are chosen between 1 and the *number of variables*. The crossover function selects:

    - vector entries numbered less than or equal to m from the first parent;
    - vector entries numbered from $m + 1$ to n, inclusive, from the second parent;

- vector entries numbered greater than n from the first parent.

The algorithm then concatenates these genes to form a single gene. For example, if `p1` and `p2` are the parents above and the crossover points are 3 and 6, the function returns the following child:

$$\text{child1 = [a b c 4 5 6 g h];}$$

- *intermediate crossover.* Children are created by taking a weighted average of the parents. Weights may be specified by a single parameter, *ratio.* The function creates the child from `parent1` and `parent2` using the following formula:

$$\text{child = parent1 + rand * ratio * (parent2 - parent1).}$$

If all the entries of ratio lie in the range $[0, 1]$, the children produced are within the hypercube defined by placing the parents at opposite vertices. If ratio is not in that range, the children might lie outside the hypercube. If ratio is a scalar, then all the children lie on the line between the parents;

- *heuristic crossover.* It returns a child that lies on the line containing the two parents, a small distance away from the parent with the better fitness value in the direction away from the parent with the worse fitness value. How far the child is from the better parent may be specified by the parameter *ratio.* If `parent1` and `parent2` are the parents, and `parent1` has the better fitness value, the function returns the child:

$$\text{child = parent2 + ratio * (parent1 - parent2);}$$

- *arithmetic crossover.* It creates children that are the weighted arithmetic mean of two parents. Children are always feasible with respect to linear constraints and bounds.

Mutation

Mutation options specify how the genetic algorithm makes small random changes in the individuals in the population to create mutation offspring. Mutation provides genetic diversity and enable the genetic algorithm to search a broader space. The most common mutation functions are the following:

- *gaussian mutation.* This function adds a random number taken from a Gaussian distribution with mean 0 to each entry of the parent vector. The variance

of this distribution is determined by the parameters *scale* and *shrink*, and by the *initial range* of the population. The initial variation is given by the scale factor multiplied by the length of the initial range. The Shrink parameter controls how the variance shrinks as generations go by. If initial range is a 2-by-1 vector, the variance at the qth generation, $\mathtt{var_q}$, is given by the recursive formula

$$\mathtt{var_q} = \mathtt{var_{q\text{-}1}} \left(1 - \mathtt{shrink} \cdot \frac{\mathtt{q}}{\mathtt{generations}} \right);$$

- *uniform mutation.* This is a two-step process. First, the algorithm selects a fraction of the vector entries of an individual for mutation, where each entry has a probability rate of being mutated. In the second step, the algorithm replaces each selected entry by a random number selected uniformly from the range for that entry;

- *adaptive feasible mutation.* Directions are randomly generated, adaptive with respect to the last successful or unsuccessful generation. The feasible region is bounded by the constraints and inequality constraints. A step length is chosen along each direction so that linear constraints and bounds are satisfied.

4.4.7 Stopping criteria

The stopping criteria determine what causes the algorithm to terminate. Usual criteria are [67]:

- *generations.* The maximum number of iterations the genetic algorithm will perform needs to be specified;

- *time limit.* The maximum time in seconds the genetic algorithm runs before stopping is specified;

- *fitness limit.* The algorithm stops if the best fitness value is less than or equal to the value of fitness limit;

- *stall generations.* The algorithm stops if the weighted average change in the fitness function value over stall generations is less than the *function tolerance*;

- *stall time limit.* The algorithm stops if there is no improvement in the best fitness value for an interval of time in seconds specified by stall time;

- *function tolerance.* The algorithm runs until the cumulative change in the fitness function value over stall generations is less than function tolerance.
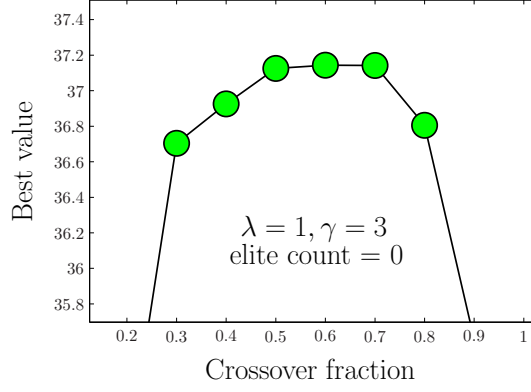
Fig. 4.28. Best fitness value against crossover fraction, in absence of elite individuals.
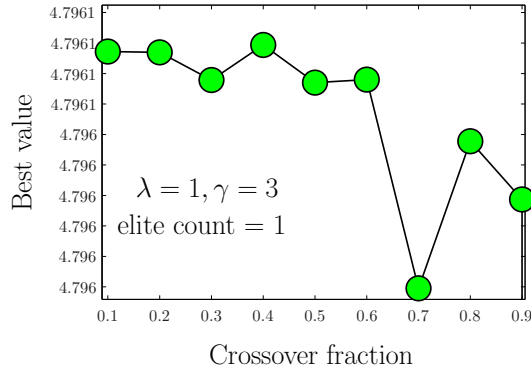
Fig. 4.29. Best fitness value against crossover fraction, in case of 1 elite element.

4.4.8 Response spectra and genetic algorithms

In order to get the response spectrum by applying genetic algorithms, the following procedure is repeated for several values of the loading time τ_d. Any individual is a real number within the interval $[0, \tau_d]$, and the population size n is chosen according to the formula

$$n = [\tau_d] + 4$$

where $[\tau_d]$ represents the integer part of τ_d.

The first population is made of individuals τ_i randomly chosen within the domain $[0, \tau_d]$, according to the standard uniform distribution $U(0, 1)$:

$$\tau_i = \theta \cdot \tau_d, \quad \theta \sim U(0, 1), \quad i = 1, \ldots, n$$

The fitness function is given by the modulus of the dynamic load factor multiplied by -1 $(-|DLF(\tau)|)$, and the fitness values are scaled according to their rank (*rank scaling*). If $\{\tau_i\}_{i=1}^{n} = (\tau_1, \tau_2, \ldots, \tau_n)$ is the vector of individuals in ascending
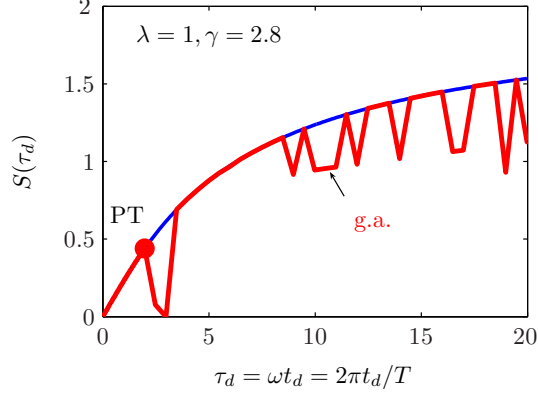
Fig. 4.30. Comparison of response spectra, from g.a. (red line) and from analytical model (blue line). No elite elements, crossover fraction 80%, $\lambda = 1$, $\gamma = 2.8$.

order of fitness values, the ith scaled fitness value FV_i is calculated according to the rank i of the ith element:

$$FV_i = n \cdot \frac{1/\sqrt{i}}{\sum_{i=1}^{n} 1/\sqrt{i}}$$

which leads to the following vector

$$\left(FV_1, FV_1 + FV_2, \ldots, \sum_{q=1}^{i} FV_q, \ldots, \sum_{q=1}^{n} FV_q \right)$$

For any iteration, the vector below is generated via standard uniform distribution:

$$(\theta_1, \theta_2, \ldots, \theta_i, \ldots, \theta_N), \quad \theta_i = n \cdot \tilde{\theta}_i, \quad \tilde{\theta}_i \sim U(0,1)$$

and some individuals are selected to create the parent vector $(P_1, P_2, \ldots, P_i, \ldots, P_n)$ of the next generation applying the following rule:

$$P_i = \begin{cases} \tau_1 & \text{if} \quad \theta_i \leq FV_1 \\ \tau_r & \text{if} \quad \sum_{q=1}^{r-1} FV_q < \theta_i \leq \sum_{q=1}^{r} FV_q, \quad \forall r > 1 \end{cases}$$

As far as the reproduction of the current generation is concerned, Campidelli *et al.* [69] showed that, for exponentially decaying loadings, the best g.a. performance is reached when the number of elite elements is equal to 1 and the crossover fraction is within the range 20%-40%, as shown in Figs. 4.28, 4.29, 4.30, and 4.31. A scattered crossover was chosen to combine the parents of the current generation,
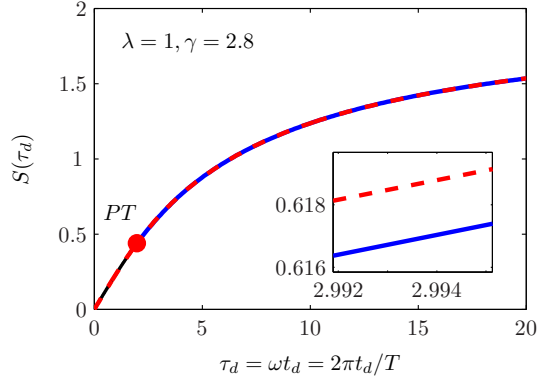
Fig. 4.31. Comparison of response spectra, from g.a. (dashed line) and from analytical model (solid line). One elite element, crossover fraction 20%, $\lambda = 1$, $\gamma = 2.8$.
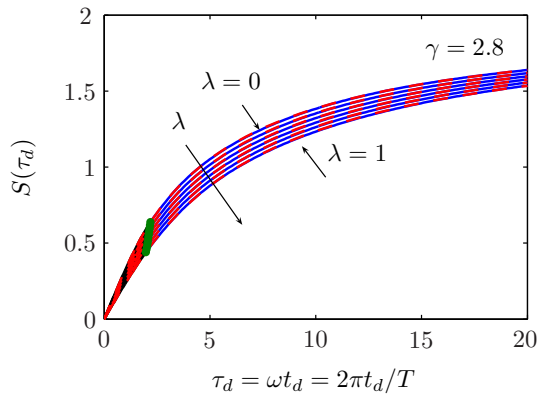
Fig. 4.32. Comparison of response spectra, from g.a. (red line) and from analytical model (blue line). One elite element, crossover fraction 20%, $\lambda = 0, 0.2., \ldots, 1$, $\gamma = 2.8$.

and an adaptive feasible mutation was chosen to create the mutant offspring. Some suitable stopping criteria were a maximum number of generation equal to 100, a stall generation number equal to 50, and a fitness function tolerance equal to 10^{-6}.

In Figs. 4.32 and 4.33 the response spectra calculated by the analytical model described in this chapter and the ones from genetic algorithms are compared. Several loading shapes are taken into account, and the difference between the ordinates of the two kind of charts is always smaller than 0.5%, which suggests that, despite the low computational effort, the proposed method produces accurate response curves.
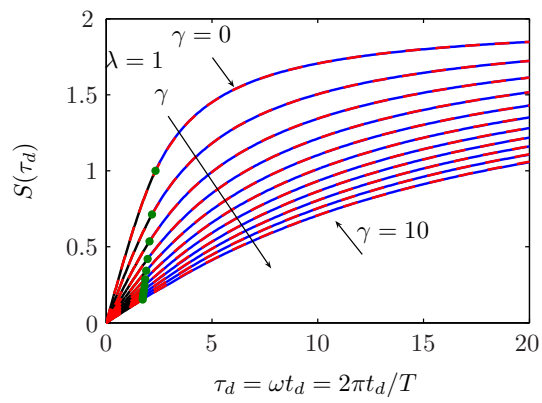
Fig. 4.33. Comparison of response spectra, from g.a. (red line) and from analytical model (blue line). One elite element, crossover fraction 20%, $\lambda = 1$, $\gamma = 0, 1, \ldots, 10$

79

Chapter 5

Non Linear Single Degree of Freedom Model

5.1   Introduction

The linear oscillator described in the previous chapter is of any use for dynamic analysis only when elastic deformations are dominant. Such linear model, obviously, is not capable to capture the actual behavior a structure which undergoes large plastic deformations due to material nonlinearity. Also, as stated in § 3.3, structural members under shock waves from detonations undergo high loading rate and, consequently, high strain rate, which affects the material constitutive laws. Hence the necessity to develop a strain rate dependent numerical model.

The non linear oscillator described in the present chapter is intended to be a simple, low time consuming, design tool, able to predict the overall response of a single structural member under dynamic loadings from high condensed explosive detonations. It may provide displacement, velocity, and acceleration dependent springs and dampers, without any restriction concerning the constitutive laws and the load–time function. Some applications of this model may concern seismic design, since many kinds of dampers, such as hysteretic, fluid viscous, dual phase, etc..., may be modeled. Nonetheless, those applications are beyond the scope of this dissertation and will not be discussed.

The task of modeling a non linear and strain rate dependent material, such as reinforced concrete, is accomplished by takeing into account a non linear, displacement and velocity dependent, spring. A constant damping ratio $\zeta = 5\%$ is also considered. A piecewise linear approximation is performed for any input function, such as the spring constitutive relationship and the loading function. Such
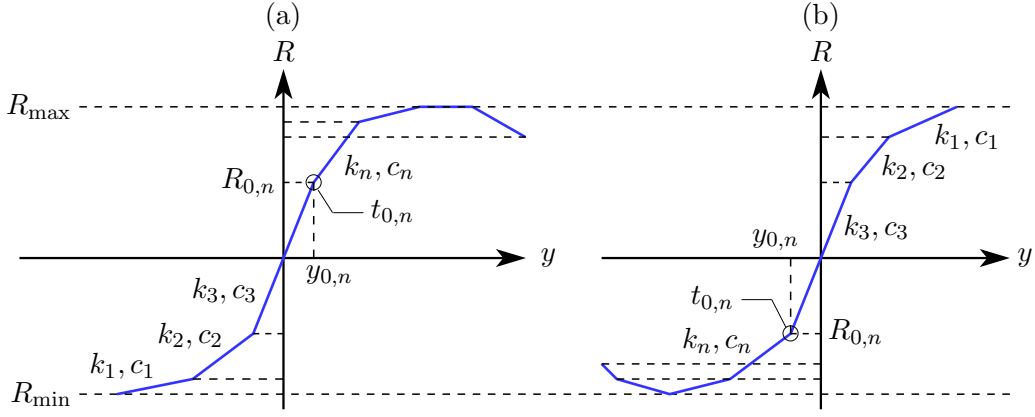
Fig. 5.1. Multi–linear resistance–displacement diagram. The branch (a) defines any possible spring configuration in case of a monotonically increasing displacement function, while the branch (b) is related to a monotonically decreasing displacement function.

approximation reduces the system equation of motion to a well known second order differential equation with constant coefficients, which are related to the stiffness and damping values. The motion equation is solved within any subinterval of the time domain in which stiffness and damping are constant. The limits of any subinterval are given by the times at which a stiffness or a damping update is accomplished, and are found to be roots of non linear equations involving trigonometric and exponential functions. In order to find those roots the Newton–Raphson method is applied, in such a way that enables the error range to be established "a priori". Any possible drawback of this method is carefully avoided, and a quadratic speed of convergence is always ensured. The full time history of the system is obtained by imposing continuity conditions of displacement and velocity functions at any break point of the time domain.

5.2   Piecewise linear oscillator

Besides its mass m, a non linear one degree of freedom model is entirely defined by a resistance function, $R(y)$, and a damping function, $\mathcal{D}(\dot{y})$. The former function describes the resistance of a spring caused by a mass displacement y, while the latter describes the force developed by a damper as a function of a mass velocity $\dot{y}$. If the resistance function chart is subdivided in a number of subintervals, each of them with constant spring stiffness k_n and damping coefficient c_n (Fig. 5.1), for the nth segment of such multi–linear chart the resistance and damping functions become:
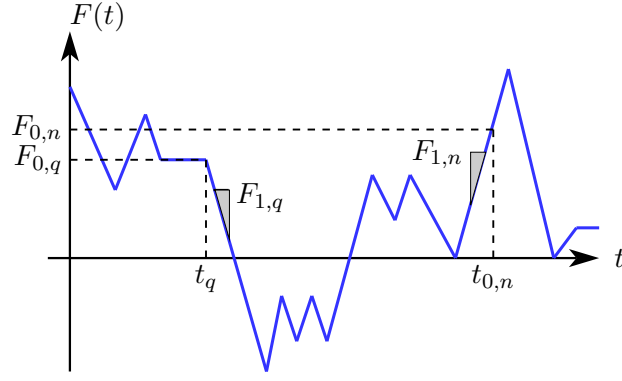
Fig. 5.2. Piecewise linear excitation.

$$R(t) = R_n(t) = R_{0,n} + k_n(y(t) - y(t_{0,n})), \quad R_{0,n} = R(t_{0,n}), \quad n = 1, 2, \ldots \quad (5.1)$$

$$\mathcal{D}(t) = \mathcal{D}_n(t) = \mathcal{D}_{0,n} + c_n(\dot{y}(t) - \dot{y}(t_{0,n})), \quad \mathcal{D}_{0,n} = \mathcal{D}(t_{0,n}), \quad n = 1, 2, \ldots \quad (5.2)$$

where $t_{0,n}$ is the time when the nth segment of the $R - y$ chart is reached.

A piecewise linear excitation $F(t)$ of such system is shown in Fig. 5.2. Any qth segment of the load function may be described by two parameters, $F_{0,q}$ and $F_{1,q}$, which determine the external force value and its variation at any time $t \in [t_q, t_{q+1}]$:

$$F(t) = F_q(t) = F_{0,q} + F_{1,q}(t - t_q), \quad \forall t \in [t_q, t_{q+1}], \quad q = 1, 2, \ldots \quad (5.3)$$

As long as the dynamic equilibrium of this system is considered, for any $t \in [t_{0,n}, t_q]$, $t_{0,n} \leq t_q$, we may write:

$$m\ddot{y} + \mathcal{D}(\dot{y}) + R(y) = F_{0,n} + F_{1,n}(t - t_{0,n}), \quad y = y(t), \quad \dot{y} = \frac{dy}{dt}, \quad \ddot{y} = \frac{d^2y}{dt^2} \quad (5.4)$$

whit initial conditions $y(t_{0,n}) = y_{0,n}$ and $\dot{y}(t_{0,n}) = \dot{y}_{0,n}$.

Introducing the new variable $\tau = t - t_{0,n}$ and taking into account the Eqs. (5.1) and (5.2), the Eq. (5.4) becomes:

$$m\ddot{y}_n(\tau) + \mathcal{D}_{0,n} + c_n(\dot{y}_n(\tau) - \dot{y}_n(0)) + R_{0,n} + k_n(y_n(\tau) - y_n(0)) = F_{0,n} + F_{1,n}\,\tau \quad (5.5)$$

where $y_n(\tau)$, $\dot{y}_n(\tau)$, and $\ddot{y}_n(\tau)$ are respectively the displacement, the velocity, and the acceleration functions associated to the nth segment of the $R - y$ diagram, while $F_{0,n}$ and $F_{1,n}$ describe the external excitation acting when $t \in [t_{0,n}, t_q]$, $t_{0,n} \leq t_q$.

The new initial conditions are $y_n(0) = y_{0,n}$ and $\dot{y}_n(0) = \dot{y}_{0,n}$. Introducing the new variable

$$\mathbf{F}_{0,n} = -(F_{0,n} - R_{0,n} - \mathcal{D}_{0,n} + c_n \dot{y}_{0,n}) \tag{5.6}$$

after some rearrangements the Eq. (5.5) becomes:

$$\ddot{y}_n + \frac{c}{m}\dot{y}_n + \frac{k_n}{m}y_n = \frac{1}{m}(F_{0,n} - R_{0,n} - \mathcal{D}_{0,n} + k_n y_{0,n} + c_n \dot{y}_{0,n} + F_{1,n}\,\tau)$$

$$\ddot{y}_n + \frac{c}{m}\dot{y}_n + \frac{k_n}{m}y_n = \frac{1}{m}(-\mathbf{F}_{0,n} + k_n y_{0,n} + F_{1,n}\,\tau) \tag{5.7a}$$

$$\ddot{y}_n + 2\zeta_n\omega_n\dot{y}_n + \omega_n^2 y_n = \frac{1}{m}(-\mathbf{F}_{0,n} + k_n y_{0,n} + F_{1,n}\,\tau) \tag{5.7b}$$

where $\zeta_n = c_n/(2\omega_n m)$ is the damping ratio and $\omega_n = \sqrt{k_n/m}$ is the circular frequency of the oscillator.

As well known, a general solution of the Eq. (5.7b) is nothing but the sum of a general solution y_h of the associated homogeneous equation, and a particular solution y_p of the nonhomogeneous equation:

$$y_n(\tau) = y_{h,n}(\tau) + y_{p,n}(\tau) \tag{5.8}$$

The associated homogeneous equation is defined as it follows:

$$\ddot{y}_{h,n} + 2\zeta_n\omega_n\dot{y}_{h,n} + \omega_n^2 y_{h,n} = 0 \tag{5.9}$$

Assuming $y_{h,n}(\tau) = e^{-\Lambda\tau}$ as a solution of the Eq. (5.9), we get:

$$e^{-\Lambda\tau}\left(\Lambda^2 - 2\zeta_n\omega_n\Lambda + \omega_n^2\right) = 0 \quad \Rightarrow \quad \Lambda^2 - 2\zeta_n\omega_n\Lambda + \omega_n^2 = 0$$

$$\Lambda = \zeta_n\omega_n \pm \sqrt{(\zeta_n\omega_n)^2 - \omega_n^2}$$

$$\Lambda = \zeta_n\omega_n \pm i\omega_n\sqrt{1 - \zeta_n^2} = \zeta_n\omega_n \pm i\omega_{d,n}, \quad \omega_{d,n} = \omega_n\sqrt{1 - \zeta_n^2} \tag{5.10}$$

where "i" represents the imaginary unit. Recalling $\zeta_n = c/(2\omega_n m)$, when $\zeta_n = 1$ the corresponding damping coefficient achieves its critical value $c_{c,n}$

$$c_{c,n} = c_n|_{\zeta_n=1} = (2\zeta_n\omega_n m)|_{\zeta_n=1} = 2\omega_n m$$

83

which leads to another definition of the nth damping ratio

$$\zeta_n = \frac{c_n}{c_{c,n}} \tag{5.11}$$

From the Eq. (5.10), the solution of the Eq. (5.9) may be written as

$$y_{h,n}(\tau) = e^{-\zeta_n \omega_n \tau} \left[C_1 e^{-i\omega_{d,n}\tau} + C_2 e^{+i\omega_{d,n}\tau} \right] \tag{5.12}$$

or, in another form:

$$y_{h,n}(\tau) = \exp\left(-\frac{c_n}{2m}\tau \right) \left[C_1 e^{-i\omega_n \sqrt{1-\zeta_n^2}\tau} + C_2 e^{+i\omega_n \sqrt{1-\zeta_n^2}\tau} \right] \tag{5.13}$$

where C_1 and C_2 depend on the initial conditions.

The Eq. (5.13) can be developed in different manners, depending on if the quantities ω_n and $(1 - \zeta_n^2)^{1/2}$ are real numbers or not . This also depends on the stiffness sign (negative, zero, or positive) and the damping coefficient value ($|\zeta_n| < 1$, $|\zeta_n| = 1$, and $|\zeta_n| > 1$).

Since the external excitation is linear, a particular solutions of the Eq. (5.7b) may be supposed to have the form:

$$y_{p,n}(\tau) = C_3 \tau + C_4 \tag{5.14}$$

Substituting the Eq. (5.14) into the Eq. (5.7b), we get

$$2\zeta_n \omega_n C_3 + \omega_n^2 (C_3 \tau + C_4) = \frac{1}{m} \left[-\mathbf{F}_{0,n} + k_n y_{0,n} + F_{1,n}\ \tau \right]$$

which implies:

$$\begin{cases} 2\zeta_n\omega_n C_3 + \omega_n^2 C_4 = \dfrac{1}{m}\left(-\mathbf{F}_{0,n} + k_n y_{0,n}\right) \\[2mm] \omega_n^2 C_3 = \dfrac{F_{1,n}}{m} \end{cases}$$

$$\begin{cases} C_3 = \dfrac{F_{1,n}}{k_n} \\[2mm] 2\zeta_n\omega_n \dfrac{F_{1,n}}{k_n} + \omega_n^2 C_4 = \dfrac{1}{m}\left(-\mathbf{F}_{0,n} + k_n y_{0,n}\right) \end{cases}$$

$$\begin{cases} C_3 = \dfrac{F_{1,n}}{k_n} \\[2mm] C_4 = \dfrac{1}{\omega_n^2}\left[-\dfrac{\mathbf{F}_{0,n}}{m} + \omega_n^2 y_{0_n} - 2\zeta_n\omega_n\dfrac{F_{1,n}}{k_n}\right] \end{cases}$$

$$\begin{cases} C_3 = \dfrac{F_{1,n}}{k_n} \\[2mm] C_4 = y_{0,n} - \dfrac{\mathbf{F}_{0,n}}{k_n} - 2\zeta_n\dfrac{F_{1,n}}{\omega_n k_n} \end{cases} \tag{5.15}$$

By substituting the constants C_3 and C_4 into the Eq. (5.14), we get the expression of aparticular solution of the motion equation:

$$y_{p,n}(\tau) = \frac{F_{1,n}}{k_n}\tau + y_{0,n} - \frac{\mathbf{F}_{0,n}}{k_n} - 2\zeta_n\frac{F_{1,n}}{\omega_n k_n} \tag{5.16}$$

It should be noted that the Eqs. (5.12) and (5.16) does not apply to some cases, when $\zeta_n = 0$ or $k_n = 0$. In these cases, since the structure of the differential equation (5.7a) changes, a new solution needs to be found.

5.3 Equation of motion of a linear oscillator under linear excitation

5.3.1 Underdamped system with negative stiffness

The damping ratio and the spring constant lie within the following intervals

$$|\zeta_n| \in [0,1), \quad k_n \in (-\infty, 0)$$

Let us define

$$\Omega_n = -\mathrm{i}\omega_n \tag{5.17}$$

Since $k_n < 0$, the equation above becomes:

$$\Omega_n = -\mathrm{i}\sqrt{\frac{k_n}{m}} = -\mathrm{i}\sqrt{\frac{-|k_n|}{m}} = -\mathrm{i}^2\sqrt{\frac{|k_n|}{m}} = \sqrt{\frac{|k_n|}{m}}$$

By substituting the definition (5.17) into the Eq. (5.13), we may write

$$y_{h,n}(\tau) = \exp\left(-\frac{c_n}{2m}\tau\right)\left[C_1 e^{+\Omega_n\sqrt{1-\zeta_n^2}\tau} + C_2 e^{-\Omega_n\sqrt{1-\zeta_n^2}\tau}\right]$$

where all the quantities are real numbers. Finally, from the equation above and from the Eq. (5.16), we get the displacement function for an under dumped system whit a negative stiffness:

$$y_n(\tau) = e^{-\zeta_n\omega_n\tau}\left[C_1 e^{+\Omega_{d,n}\tau} + C_2 e^{-\Omega_{d,n}\tau}\right] +$$

$$+ \frac{F_{1,n}}{k_n}\tau + y_{0,n} - \frac{\mathbf{F}_{0,n}}{k_n} - 2\zeta_n\frac{F_{1,n}}{\omega_n k_n}, \quad \Omega_{d,n} = \Omega_n\sqrt{1-\zeta_n^2} \tag{5.18}$$

while the velocity is

$$\dot{y}_n(\tau) = e^{-\zeta_n\omega_n\tau}\left[(\Omega_{d,n} - \zeta_n\omega_n)C_1 e^{+\Omega_{d,n}\tau} - (\Omega_{d,n} + \zeta_n\omega_n)C_2 e^{-\Omega_{d,n}\tau}\right] + \frac{F_{1,n}}{k_n} \tag{5.19}$$

and the acceleration is

$$\ddot{y}_n(\tau) = e^{-\zeta_n\omega_n\tau}\left[(\Omega_{d,n} - \zeta_n\omega_n)^2 C_1 e^{+\Omega_{d,n}\tau} + (\Omega_{d,n} + \zeta_n\omega_n)^2 C_2 e^{-\Omega_{d,n}\tau}\right] \tag{5.20}$$

The constants C_1 and C_2 can be derived by applying the initial conditions:

$$y_n(0) = y_{0,n} \quad \Rightarrow \quad C_1 + C_2 + y_{0,n} - \frac{\mathbf{F}_{0,n}}{k_n} - 2\zeta_n\frac{F_{1,n}}{\omega_n k_n} = y_{0,n}$$

$$C_2 = \frac{1}{k_n}\left(\mathbf{F}_{0,n} + \frac{2\zeta_n}{\omega_n}F_{1,n}\right) - C_1 \tag{*}$$

$$\dot{y}_n(0) = \dot{y}_{0,n} \quad \Rightarrow \quad C_1(\Omega_{d,n} - \zeta_n\omega_n) - C_2(\Omega_{d,n} + \zeta_n\omega_n) + \frac{F_{1,n}}{k_n} = \dot{y}_{0,n} \tag{**}$$

By substituting the Eq. (*) into the Eq. (**), we get the first constant

$$C_1(\Omega_{d,n} - \zeta_n\omega_n) - \left[\frac{1}{k_n}\left(\mathbf{F}_{0,n} + \frac{2\zeta_n}{\omega_n}F_{1,n}\right) - C_1\right](\Omega_{d,n} + \zeta_n\omega_n) + \frac{F_{1,n}}{k_n} = \dot{y}_{0,n}$$

$$+ 2\Omega_{d,n}C_1 - \left(\mathbf{F}_{0,n} + \frac{2\zeta_n}{\omega_n}F_{1,n}\right)\frac{\Omega_{d,n} + \zeta_n\omega_n}{k_n} + \frac{F_{1,n}}{k_n} = \dot{y}_{0,n}$$

$$C_1 = \frac{1}{2\Omega_{d,n}}\left[\left(\mathbf{F}_{0,n} + \frac{2\zeta_n}{\omega_n}F_{1,n}\right)\frac{\Omega_{d,n} + \zeta_n\omega_n}{k_n} - \frac{F_{1,n}}{k_n} + \dot{y}_{0,n}\right] \tag{5.21}$$

and by substituting the Eq. (5.21) into the Eq. ($*$) we get the second constant

$$C_2 = \frac{1}{k_n}\left(\mathbf{F}_{0,n} + \frac{2\zeta_n}{\omega_n}F_{1,n}\right)\left(1 - \frac{\Omega_{d,n} + \zeta_n\omega_n}{2\Omega_{d,n}}\right) - \frac{1}{2\Omega_{d,n}}\left(\dot{y}_{0,n} - \frac{F_{1,n}}{k_n}\right)$$

$$C_2 = \frac{1}{2\Omega_{d,n}}\left[\left(\mathbf{F}_{0,n} + \frac{2\zeta_n}{\omega_n}F_{1,n}\right)\frac{\Omega_{d,n} - \zeta_n\omega_n}{k_n} + \frac{F_{1,n}}{k_n} - \dot{y}_{0,n}\right] \tag{5.22}$$

Therefore:

$$y_n(\tau) = \frac{1}{2\Omega_{d,n}}\left[\left(\mathbf{F}_{0,n} + \frac{2\zeta_n}{\omega_n}F_{1,n}\right)\frac{\Omega_{d,n} + \zeta_n\omega_n}{k_n} - \frac{F_{1,n}}{k_n} + \dot{y}_{0,n}\right]e^{+(\Omega_{d,n} - \zeta_n\omega_n)\tau} +$$

$$\frac{1}{2\Omega_{d,n}}\left[\left(\mathbf{F}_{0,n} + \frac{2\zeta_n}{\omega_n}F_{1,n}\right)\frac{\Omega_{d,n} - \zeta_n\omega_n}{k_n} + \frac{F_{1,n}}{k_n} - \dot{y}_{0,n}\right]e^{-(\Omega_{d,n} + \zeta_n\omega_n)\tau} +$$

$$+ \frac{F_{1,n}}{k_n}\tau + y_{0,n} - \frac{\mathbf{F}_{0,n}}{k_n} - 2\zeta_n\frac{F_{1,n}}{\omega_n k_n} \tag{5.23}$$

$$\dot{y}_n(\tau) = +\frac{\Omega_{d,n} - \zeta_n\omega_n}{2\Omega_{d,n}}e^{+(\Omega_{d,n} - \zeta_n\omega_n)\tau}.$$

$$\cdot\left[\left(\mathbf{F}_{0,n} + \frac{2\zeta_n}{\omega_n}F_{1,n}\right)\frac{\Omega_{d,n} + \zeta_n\omega_n}{k_n} - \frac{F_{1,n}}{k_n} + \dot{y}_{0,n}\right] -$$

$$- \frac{\Omega_{d,n} + \zeta_n\omega_n}{2\Omega_{d,n}}e^{-(\Omega_{d,n} + \zeta_n\omega_n)\tau}.$$

$$\cdot\left[\left(\mathbf{F}_{0,n} + \frac{2\zeta_n}{\omega_n}F_{1,n}\right)\frac{\Omega_{d,n} - \zeta_n\omega_n}{k_n} + \frac{F_{1,n}}{k_n} - \dot{y}_{0,n}\right] + \frac{F_{1,n}}{k_n} \tag{5.24}$$

$$\ddot{y}_n(\tau) = -2\zeta_n \omega_n \dot{y}(\tau) - \omega_n^2 \left(y(\tau) - y_{0,n} + \frac{\mathbf{F}_{0,n}}{k_n} - \frac{F_{1,n}}{k_n} \tau \right)$$

$$\ddot{y}_n(\tau) = +\frac{(\Omega_{d,n} - \zeta_n \omega_n)^2}{2\Omega_{d,n}} e^{+(\Omega_{d,n} - \zeta_n \omega_n)\tau}.$$
$$\cdot \left[\left(\mathbf{F}_{0,n} + \frac{2\zeta_n}{\omega_n} F_{1,n} \right) \frac{\Omega_{d,n} + \zeta_n \omega_n}{k_n} - \frac{F_{1,n}}{k_n} + \dot{y}_{0,n} \right] +$$
$$+\frac{(\Omega_{d,n} + \zeta_n \omega_n)^2}{2\Omega_{d,n}} e^{-(\Omega_{d,n} + \zeta_n \omega_n)\tau}.$$
$$\cdot \left[\left(\mathbf{F}_{0,n} + \frac{2\zeta_n}{\omega_n} F_{1,n} \right) \frac{\Omega_{d,n} - \zeta_n \omega_n}{k_n} + \frac{F_{1,n}}{k_n} - \dot{y}_{0,n} \right] \qquad (5.25)$$

If $\zeta_n = 0$, we get the solutions for an undamped oscillator:

$$y_n(\tau) = +\frac{1}{2} \left[\frac{\mathbf{F}_{0,n}}{k_n} + \frac{1}{\Omega_n} \left(\dot{y}_{0,n} - \frac{F_{1,n}}{k_n} \right) \right] e^{+\Omega_n \tau} +$$
$$+\frac{1}{2} \left[\frac{\mathbf{F}_{0,n}}{k_n} - \frac{1}{\Omega_n} \left(\dot{y}_{0,n} - \frac{F_{1,n}}{k_n} \right) \right] e^{-\Omega_n \tau} +$$
$$+\frac{F_{1,n}}{k_n} \tau + y_{0,n} - \frac{\mathbf{F}_{0,n}}{k_n} \qquad (5.26)$$

$$\dot{y}_n(\tau) = +\frac{1}{2} \left(\frac{\mathbf{F}_{0,n}}{k_n} \Omega_n + \dot{y}_{0,n} - \frac{F_{1,n}}{k_n} \right) e^{+\Omega_n \tau} -$$
$$-\frac{1}{2} \left(\frac{\mathbf{F}_{0,n}}{k_n} \Omega_n - \dot{y}_{0,n} + \frac{F_{1,n}}{k_n} \right) e^{-\Omega_n \tau} + \frac{F_{1,n}}{k_n} \qquad (5.27)$$

$$\ddot{y}_n(\tau) = -\omega_n^2 \left(y(\tau) - y_{0,n} + \frac{\mathbf{F}_{0,n}}{k_n} - \frac{F_{1,n}}{k_n} \tau \right)$$

$$\ddot{y}_n(\tau) = \frac{\Omega_n}{2} \left[\left(\frac{\mathbf{F}_{0,n}}{k_n} \Omega_n + \dot{y}_{0,n} - \frac{F_{1,n}}{k_n} \right) e^{+\Omega_n \tau} + \left(\frac{\mathbf{F}_{0,n}}{k_n} \Omega_n - \dot{y}_{0,n} + \frac{F_{1,n}}{k_n} \right) e^{-\Omega_n \tau} \right]$$
$$(5.28)$$

Overdamped system with positive stiffness

In this case we have $|\zeta_n| > 1$ and $k_n \in (0, \infty)$. Nothing changes with respect to the case above, and it may be noted that $\Omega_{d,n}$ is still a real number. Recalling the Eqs. (5.17) and (5.18), $\Omega_{d,n}$ becomes:

$$\Omega_{d,n} = \Omega_n \sqrt{1 - \zeta_n^2} = -\mathrm{i}\omega_n\, \mathrm{i}\sqrt{\zeta_n^2 - 1} = -\mathrm{i}^2 \omega_n \sqrt{\zeta_n^2 - 1} = \omega_n \sqrt{\zeta_n^2 - 1} \in \mathbb{R}$$

5.3.2 Damped system with no stiffness

The damping coefficient and the spring constant satisfy the following conditions

$$c_n \neq 0, \quad k_n = 0$$

The equation of motion (5.7a) becomes:

$$\ddot{y}_n + \frac{c_n}{m}\, \dot{y}_n = \frac{1}{m}\, (-\mathbf{F}_{0,n} + F_{1,n}\, \tau) \tag{5.29}$$

Whether an exponential solution $y(\tau) = e^{\Lambda\tau}$ is supposed, the characteristic equation is:

$$\Lambda^3 \left(\Lambda + \frac{c_n}{m} \right) = 0$$

which has solutions $\Lambda = 0$, with algebraic multiplicity 3, and $\Lambda = -c_n/m$. The corresponding displacement function is

$$y_n(\tau) = C_0 + C_1\tau + C_2\tau^2 + C_3 e^{-\frac{c_n}{m}\tau} \tag{5.30}$$

By substituting the Eq. (5.30) into the Eq. (5.29), we get

$$2C_2 + \frac{c_n}{m}\, (C_1 + 2C_2\tau) = \frac{-\mathbf{F}_{0,n} + F_{1,n}\tau}{m}$$

$$\begin{cases} 2C_2 + \dfrac{c_n}{m} C_1 = -\dfrac{\mathbf{F}_{0,n}}{m} \\[2mm] \dfrac{2c_n}{m} C_2 = \dfrac{F_{1,n}}{m} \end{cases} \Rightarrow \begin{cases} 2\dfrac{F_{1,n}}{2c_n} + \dfrac{c_n}{m} C_1 = -\dfrac{\mathbf{F}_{0,n}}{m} \\[2mm] C_2 = \dfrac{F_{1,n}}{2c_n} \end{cases}$$

$$\begin{cases} C_1 = \dfrac{m}{c_n}\left(-\dfrac{\mathbf{F}_{0,n}}{m} - \dfrac{F_{1,n}}{c_n}\right) \\[4mm] C_2 = \dfrac{F_{1,n}}{2c_n} \end{cases} \Rightarrow \begin{cases} C_1 = -\left(\dfrac{\mathbf{F}_{0,n}}{c_n} + \dfrac{m}{c_n^2}\,F_{1,n}\right) \\[4mm] C_2 = \dfrac{F_{1,n}}{2c_n} \end{cases} \tag{5.31}$$

Taking into account the Eq.(5.31), by imposing the initial conditions we get

$$\begin{cases} y(0) = y_{0,n} \\[2mm] \dot{y}(0) = \dot{y}_{0,n} \end{cases} \Rightarrow \begin{cases} C_0 + C_3 = y_{0,n} \\[4mm] -\dfrac{\mathbf{F}_{0,n}}{c_n} - \dfrac{m}{c_n^2}\,F_{1,n} - \dfrac{c_n}{m}\,C_3 = \dot{y}_{0,n} \end{cases}$$

$$C_0 = y_{0,n} + \frac{m}{c_n}\left(\dot{y}_{0,n} + \frac{\mathbf{F}_{0,n}}{c_n} + \frac{m}{c_n^2}\,F_{1,n}\right), \qquad C_3 = -\frac{m}{c_n}\left(\dot{y}_{0,n} + \frac{\mathbf{F}_{0,n}}{c_n} + \frac{m}{c_n^2}\,F_{1,n}\right) \tag{5.32}$$

Therefore:

$$y_n(\tau) = y_{0,n} + \frac{m}{c_n}\left(\dot{y}_{0,n} + \frac{\mathbf{F}_{0,n}}{c_n} + \frac{m}{c_n^2}\,F_{1,n}\right) - \left(\frac{\mathbf{F}_{0,n}}{c_n} + \frac{m}{c_n^2}\,F_{1,n}\right)\tau +$$
$$+ \frac{F_{1,n}}{2c_n}\,\tau^2 - \frac{m}{c_n}\left(\dot{y}_{0,n} + \frac{\mathbf{F}_{0,n}}{c_n} + \frac{m}{c_n^2}\,F_{1,n}\right)e^{-\frac{c_n}{m}\tau} \tag{5.33}$$

$$\dot{y}_n(\tau) = -\left(\frac{\mathbf{F}_{0,n}}{c_n} + \frac{m}{c_n^2}\,F_{1,n}\right) + \frac{F_{1,n}}{c_n}\,\tau + \left(\dot{y}_{0,n} + \frac{\mathbf{F}_{0,n}}{c_n} + \frac{m}{c_n^2}\,F_{1,n}\right)e^{-\frac{c_n}{m}\tau} \tag{5.34}$$

$$\ddot{y}_n(\tau) = \frac{1}{m}\left(-c_n\dot{y}(\tau) + -\mathbf{F}_{0,n} + F_{1,n}\,\tau\right)$$

$$\ddot{y}_n(\tau) = \frac{F_{1,n}}{c_n} - \left(\frac{c_n}{m}\,\dot{y}_{0,n} + \frac{\mathbf{F}_{0,n}}{m} + \frac{F_{1,n}}{c_n}\right)e^{-\frac{c_n}{m}\tau} \tag{5.35}$$

5.3.3 Undamped system with no stiffness

The damping coefficient and the spring constant both vanish. The equation of motion (5.7a) becomes:

$$\ddot{y}_n = \frac{1}{m}(-\mathbf{F}_{0,n} + F_{1,n}\,\tau) \tag{5.36}$$

By direct integration and applying the initial conditions we get

$$\dot{y}_n(\tau) = C_1 + \frac{1}{m}\left(-\mathbf{F}_{0,n}\,\tau + F_{1,n}\frac{\tau^2}{2}\right)$$

$$\dot{y}_n(0) = \dot{y}_{0,n} \quad \Rightarrow \quad C_1 = \dot{y}_{0,n}$$

$$y_n(\tau) = C_0 + \dot{y}_{0,n}\tau + \frac{1}{m}\left(-\mathbf{F}_{0,n}\frac{\tau^2}{2} + F_{1,n}\frac{\tau^3}{6}\right)$$

$$y_n(0) = y_{0,n} \quad \Rightarrow \quad C_0 = y_{0,n}$$

Therefore:

$$y_n(\tau) = y_{0,n} + \dot{y}_{0,n}\,\tau - \frac{\mathbf{F}_{0,n}}{2m}\tau^2 + \frac{F_{1,n}}{6m}\tau^3 \tag{5.37}$$

$$\dot{y}_n(\tau) = \dot{y}_{0,n} - \frac{\mathbf{F}_{0,n}}{m}\tau + \frac{F_{1,n}}{2m}\tau^2 \tag{5.38}$$

$$\ddot{y}_n(\tau) = -\frac{\mathbf{F}_{0,n}}{m} + \frac{F_{1,n}}{m}\tau \tag{5.39}$$

5.3.4 Underdamped system with positive stiffness

The damping ratio and the spring constant satisfy the following conditions:

$$|\zeta_n| \in [0, 1), \quad k_n \in (0, \infty)$$

Under this hypotheses, ω_n is a real number. Recalling the Euler formula $e^{ix} = \cos(x) + i\sin(x)$, form the Eqs. (5.13) and (5.16) we get the displacement function for an under dumped system whit a positive stiffness:

$$y_n(\tau) = e^{-\zeta_n \omega_n \tau}\left[A\cos(\omega_{d,n}\tau) + B\sin(\omega_{d,n}\tau)\right] +$$

$$+ \frac{F_{1,n}}{k_n}\tau + y_{0,n} - \frac{\mathbf{F}_{0,n}}{k_n} - 2\zeta_n\frac{F_{1,n}}{\omega_n k_n} \tag{5.40}$$

while the velocity is

$$\dot{y}_n(\tau) = + e^{-\zeta_n \omega_n \tau} \cdot \underbrace{(-\zeta_n\omega_n A + \omega_{d,n}B)}_{\bar{A}}\cos(\omega_{d,n}\tau) -$$

$$- e^{-\zeta_n \omega_n \tau} \cdot \underbrace{(\omega_{d,n}A + \zeta_n\omega_n B)}_{\bar{B}}\sin(\omega_{d,n}\tau) + \frac{F_{1,n}}{k_n} \tag{5.41}$$

and the acceleration is

$$\ddot{y}_n(\tau) = e^{-\zeta_n \omega_n \tau}\left[\underbrace{-(\zeta_n\omega_n\bar{A} + \omega_{d,n}\bar{B})}_{\bar{\bar{A}}}\cos(\omega_{d,n}\tau) + \underbrace{(-\omega_{d,n}\bar{A} + \zeta_n\omega_n\bar{B})}_{\bar{\bar{B}}}\sin(\omega_{d,n}\tau)\right] \tag{5.42}$$

Applying the initial conditions, the constants $A, \bar{A}, \bar{\bar{A}}, B, \bar{B}, \bar{\bar{B}}$ may be derived:

$$y_n(0) = y_{0,n} \; \Rightarrow \; A + y_{0,n} - \frac{\mathbf{F}_{0,n}}{k_n} - 2\zeta_n\frac{F_{1,n}}{\omega_n k_n} = y_{0,n} \; \Rightarrow \; A = \frac{\mathbf{F}_{0,n}}{k_n} + 2\zeta_n\frac{F_{1,n}}{\omega_n k_n}$$

$$\dot{y}_n(0) = \dot{y}_{0,n} \quad \Rightarrow \quad \frac{F_{1,n}}{k_n} - \zeta_n\omega_n A + \omega_{d,n}B = \dot{y}_{0,n}$$

$$\frac{F_{1,n}}{k_n} - \zeta_n\omega_n\left(\frac{\mathbf{F}_{0,n}}{k_n} + 2\zeta_n\frac{F_{1,n}}{\omega_n k_n}\right) + \omega_{d,n}B = \dot{y}_{0,n}$$

$$B = \frac{1}{\omega_{d,n}}\left[\dot{y}_{0,n} + \frac{\mathbf{F}_{0,n}}{k_n}\zeta_n\omega_n + \frac{F_{1,n}}{k_n}(2\zeta_n^2 - 1)\right]$$

$$\bar{A} = \dot{y}_{0,n} - \frac{F_{1,n}}{k_n}$$

$$\bar{B} = \omega_{d,n} \left(\frac{\mathbf{F}_{0,n}}{k_n} + 2\zeta_n \frac{F_{1,n}}{\omega_n k_n} \right) + \frac{\zeta_n \omega_n}{\omega_{d,n}} \left(\dot{y}_{0,n} + \frac{\mathbf{F}_{0,n}}{k_n} \zeta_n \omega_n + \frac{F_{1,n}}{k_n} (2\zeta_n^2 - 1) \right)$$

$$\bar{B} = \frac{\mathbf{F}_{0,n}}{k_n} \left(\omega_{d,n} + \frac{\zeta_n^2 \omega_n^2}{\omega_{d,n}} \right) + \frac{F_{1,n}}{k_n} \left(\frac{2\zeta_n \omega_{d,n}}{\omega_n} + \frac{\zeta_n \omega_n}{\omega_{d,n}} (2\zeta_n^2 - 1) \right) + \frac{\zeta_n \omega_n}{\omega_{d,n}} \dot{y}_{0,n}$$

$$\bar{B} = \frac{\mathbf{F}_{0,n}}{k_n} \frac{\omega_{d,n}^2 + \zeta_n^2 \omega_n^2}{\omega_{d,n}} + \frac{F_{1,n}}{k_n} \frac{2\zeta_n \omega_{d,n} \sqrt{1 - \zeta_n^2} + \zeta_n \omega_n (2\zeta_n^2 - 1)}{\omega_{d,n}} + \frac{\zeta_n \omega_n}{\omega_{d,n}} \dot{y}_{0,n}$$

$$\bar{B} = \frac{\mathbf{F}_{0,n}}{k_n} \frac{\omega_n^2 (1 - \zeta_n^2 + \zeta_n^2)}{\omega_n \sqrt{1 - \zeta_n^2}} + \frac{F_{1,n}}{k_n} \frac{2\zeta_n \omega_n (1 - \zeta_n^2) + \zeta_n \omega_n (2\zeta_n^2 - 1)}{\omega_n \sqrt{1 - \zeta_n^2}} + \frac{\zeta_n \omega_n \dot{y}_{0,n}}{\omega_n \sqrt{1 - \zeta_n^2}}$$

$$\bar{B} = \frac{\mathbf{F}_{0,n}}{k_n} \frac{\omega_n}{\sqrt{1 - \zeta_n^2}} + \frac{F_{1,n}}{k_n} \frac{\zeta_n}{\sqrt{1 - \zeta_n^2}} + \frac{\zeta_n}{\sqrt{1 - \zeta_n^2}} \dot{y}_{0,n}$$

$$\bar{B} = \frac{\zeta_n}{\sqrt{1 - \zeta_n^2}} \left(\frac{\mathbf{F}_{0,n}}{k_n} \frac{\omega_n}{\zeta_n} + \frac{F_{1,n}}{k_n} + \dot{y}_{0,n} \right)$$

$$\bar{\bar{A}} = -\zeta_n \omega_n \left(\dot{y}_{0,n} - \frac{F_{1,n}}{k_n} \right) - \frac{\zeta_n \omega_{d,n}}{\sqrt{1 - \zeta_n^2}} \left(\frac{\mathbf{F}_{0,n}}{k_n} \frac{\omega_n}{\zeta_n} + \frac{F_{1,n}}{k_n} + \dot{y}_{0,n} \right)$$

$$\bar{\bar{A}} = -\zeta_n \omega_n \left(\dot{y}_{0,n} - \frac{F_{1,n}}{k_n} + \frac{\mathbf{F}_{0,n}}{k_n} \frac{\omega_n}{\zeta_n} + \frac{F_{1,n}}{k_n} + \dot{y}_{0,n} \right) = - \left(2\zeta_n \omega_n \dot{y}_{0,n} + \frac{\mathbf{F}_{0,n}}{m} \right)$$

$$\bar{\bar{B}} = -\omega_{d,n} \left(\dot{y}_{0,n} - \frac{F_{1,n}}{k_n} \right) + \frac{\zeta_n^2 \omega_n}{\sqrt{1 - \zeta_n^2}} \left(\frac{\mathbf{F}_{0,n}}{k_n} \frac{\omega_n}{\zeta_n} + \frac{F_{1,n}}{k_n} + \dot{y}_{0,n} \right)$$

$$\bar{\bar{B}} = +\omega_{d,n} \left(-\dot{y}_{0,n} + \frac{F_{1,n}}{k_n} + \frac{\zeta_n^2}{1 - \zeta_n^2} \left(\frac{\mathbf{F}_{0,n}}{k_n} \frac{\omega_n}{\zeta_n} + \frac{F_{1,n}}{k_n} + \dot{y}_{0,n} \right) \right)$$

$$\bar{\bar{B}} = +\omega_{d,n} \left(\dot{y}_{0,n} \left(\frac{\zeta_n^2}{1 - \zeta_n^2} - 1 \right) + \frac{F_{1,n}}{k_n} \left(\frac{\zeta_n^2}{1 - \zeta_n^2} + 1 \right) + \frac{\mathbf{F}_{0,n}}{k_n} \frac{\zeta_n \omega_n}{1 - \zeta_n^2} \right)$$

$$\bar{\bar{B}} = +\omega_{d,n} \left(\frac{2\zeta_n^2 - 1}{1 - \zeta_n^2} \dot{y}_{0,n} + \frac{F_{1,n}}{k_n} \frac{1}{1 - \zeta_n^2} + \frac{\mathbf{F}_{0,n}}{k_n} \frac{\zeta_n \omega_n}{1 - \zeta_n^2} \right)$$

$$\bar{\bar{B}} = +\frac{\omega_n}{\sqrt{1 - \zeta_n^2}} \left(\frac{\mathbf{F}_{0,n}}{k_n} \zeta_n \omega_n + \frac{F_{1,n}}{k_n} + \dot{y}_{0,n} (2\zeta_n^2 - 1) \right)$$

Therefore:

$$
\begin{aligned}
y_n(\tau) = \ e^{-\zeta_n\omega_n\tau} & \left\{ \left[\frac{\mathbf{F}_{0,n}}{k_n} + 2\zeta_n\frac{F_{1,n}}{\omega_n k_n} \right] \cos\omega_{d,n}\tau + \right. \\
& \left. \frac{1}{\omega_{d,n}} \left[\dot{y}_{0,n} + \frac{\mathbf{F}_{0,n}}{k_n}\zeta_n\omega_n + \frac{F_{1,n}}{k_n}(2\zeta_n^2 - 1) \right] \sin\omega_{d,n}\tau \right\} + \\
& + \frac{F_{1,n}}{k_n}\tau + y_{0,n} - \frac{\mathbf{F}_{0,n}}{k_n} - 2\zeta_n\frac{F_{1,n}}{\omega_n k_n} \quad (5.43)
\end{aligned}
$$

$$
\begin{aligned}
\dot{y}_n(\tau) = \ e^{-\zeta_n\omega_n\tau} & \left[\left(\dot{y}_{0,n} - \frac{F_{1,n}}{k_n} \right) \cos(\omega_{d,n}\tau) - \right. \\
& \left. - \frac{\zeta_n}{\sqrt{1-\zeta_n^2}} \left(\frac{\mathbf{F}_{0,n}}{k_n}\frac{\omega_n}{\zeta_n} + \frac{F_{1,n}}{k_n} + \dot{y}_{0,n} \right) \sin(\omega_{d,n}\tau) \right] + \frac{F_{1,n}}{k_n} \quad (5.44)
\end{aligned}
$$

$$
\ddot{y}_n(\tau) = -2\zeta_n\omega_n\dot{y}(\tau) - \omega_n^2 \left(y(\tau) - y_{0,n} + \frac{\mathbf{F}_{0,n}}{k_n} - \frac{F_{1,n}}{k_n}\tau \right)
$$

$$
\begin{aligned}
\ddot{y}_n(\tau) = \ e^{-\zeta_n\omega_n\tau} & \left[- \left(2\zeta_n\omega_n\dot{y}_{0,n} + \frac{\mathbf{F}_{0,n}}{m} \right) \cos(\omega_{d,n}\tau) + \right. \\
& \left. + \frac{\omega_n}{\sqrt{1-\zeta_n^2}} \left(\frac{\mathbf{F}_{0,n}}{k_n}\zeta_n\omega_n + \frac{F_{1,n}}{k_n} + \dot{y}_{0,n}(2\zeta_n^2 - 1) \right) \sin(\omega_{d,n}\tau) \right] \\
& \quad (5.45)
\end{aligned}
$$

If $\zeta_n = 0$, the solutions for an undamped system may be derived:

$$
y_n(\tau) = \frac{\mathbf{F}_{0,n}}{k_n}\cos\omega_n\tau + \frac{1}{\omega_n}\left(\dot{y}_{0,n} - \frac{F_{1,n}}{k_n} \right)\sin\omega_n\tau + \frac{F_{1,n}}{k_n}\tau + y_{0,n} - \frac{\mathbf{F}_{0,n}}{k_n} \quad (5.46)
$$

$$
\dot{y}_n(\tau) = \left(\dot{y}_{0,n} - \frac{F_{1,n}}{k_n} \right)\cos(\omega_n\tau) - \left(\frac{\mathbf{F}_{0,n}}{k_n}\omega_n \right)\sin(\omega_n\tau) + \frac{F_{1,n}}{k_n} \quad (5.47)
$$

94

$$\ddot{y}_n(\tau) = -\omega_n^2 \left(y(\tau) - y_{0,n} + \frac{\mathbf{F}_{0,n}}{k_n} - \frac{F_{1,n}}{k_n}\tau \right)$$

$$\ddot{y}_n(\tau) = -\frac{\mathbf{F}_{0,n}}{m}\cos(\omega_n\tau) + \omega_n\left(\frac{F_{1,n}}{k_n} - \dot{y}_{0,n}\right)\sin(\omega_n\tau) \tag{5.48}$$

Overdamped system with negative stiffness

The damping ratio and the spring constant satisfy the conditions $|\zeta_n| > 1$ and $k_n \in (-\infty, 0)$. Nothing changes with respect to the case above, except the definition of $\omega_{d,n}$:

$$\omega_{d,n} = |\omega_n\sqrt{1-\zeta_n^2}| = |\omega_n|\sqrt{\zeta_n^2 - 1}$$

5.3.5   Critically damped system with nonzero stiffness

The damping ratio and the spring constant satisfy the conditions $|\zeta_n| = 1$ and $k_n \neq 0$. Since the system is critically damped, the roots of the Eq. (5.10) become $\Lambda = \zeta_n\omega_n$, with algebraic multiplicity 2. The corresponding displacement function which solves the equation of motion (5.7b) is

$$y_n(\tau) = (C_0 + C_1\tau)e^{-\zeta_n\omega_n\tau} + y_{p,n}(\tau) \tag{5.49}$$

where $y_{p,n}(\tau)$ is from Eq. (5.16):

$$y_{p,n}(\tau) = \frac{F_{1,n}}{k_n}\tau + y_{0,n} - \frac{\mathbf{F}_{0,n}}{k_n} - 2\zeta_n\frac{F_{1,n}}{\omega_n k_n}$$

It should be noted that $\zeta_n\omega_n = c_n/(2m) \in \mathbb{R}, \forall c_n \in \mathbb{R}, \forall m > 0$. Also, $|\zeta_n| = 1 \Leftrightarrow c_n = \pm 2|\omega_n|m$.

The velocity expression is

$$\dot{y}_n(\tau) = [-\zeta_n\omega_n C_0 + (1 - \zeta_n\omega_n\tau)C_1]e^{-\zeta_n\omega_n\tau} + \frac{F_{1,n}}{k_n} \tag{5.50}$$

By imposing the initial conditions we get

$$y_n(0) = y_{0,n} \implies C_0 + y_{0,n} - \frac{\mathbf{F}_{0,n}}{k_n} - 2\zeta_n\frac{F_{1,n}}{\omega_n k_n} = y_{0,n} \implies C_0 = \frac{\mathbf{F}_{0,n}}{k_n} + 2\zeta_n\frac{F_{1,n}}{\omega_n k_n}$$

$$\dot{y}_n(0) = \dot{y}_{0,n} \ \Rightarrow \ -\zeta_n\omega_n \, C_0 + C_1 + \frac{F_{1,n}}{k_n} = \dot{y}_{0,n}$$

$$-\zeta_n\omega_n \left(\frac{\mathbf{F}_{0,n}}{k_n} + 2\zeta_n \frac{F_{1,n}}{\omega_n k_n} \right) + C_1 + \frac{F_{1,n}}{k_n} = \dot{y}_{0,n}$$

$$C_1 = \frac{\mathbf{F}_{0,n}}{k_n} \zeta_n\omega_n + \frac{F_{1,n}}{k_n} (2\zeta_n^2 - 1) + \dot{y}_{0,n}$$

Therefore:

$$y_n(\tau) = \left[\frac{\mathbf{F}_{0,n}}{k_n} + 2\zeta_n \frac{F_{1,n}}{\omega_n k_n} + \left(\frac{\mathbf{F}_{0,n}}{k_n} \zeta_n\omega_n + \frac{F_{1,n}}{k_n} (2\zeta_n^2 - 1) + \dot{y}_{0,n} \right) \tau \right] e^{-\zeta_n\omega_n\tau} +$$

$$+ \frac{F_{1,n}}{k_n} \tau + y_{0,n} - \frac{\mathbf{F}_{0,n}}{k_n} - 2\zeta_n \frac{F_{1,n}}{\omega_n k_n} \tag{5.51}$$

$$\dot{y}_n(\tau) = \left[\dot{y}_{0,n} - \frac{F_{1,n}}{k_n} - \zeta_n\omega_n \left(\frac{\mathbf{F}_{0,n}}{k_n} \zeta_n\omega_n + \frac{F_{1,n}}{k_n} (2\zeta_n^2 - 1) + \dot{y}_{0,n} \right) \tau \right] e^{-\zeta_n\omega_n\tau} +$$

$$+ \frac{F_{1,n}}{k_n} \tag{5.52}$$

$$\ddot{y}_n(\tau) = -2\zeta_n\omega_n \dot{y}(\tau) - \omega_n^2 \left(y(\tau) - y_{0,n} + \frac{\mathbf{F}_{0,n}}{k_n} - \frac{F_{1,n}}{k_n} \tau \right)$$

$$\ddot{y}_n(\tau) = - \left[\dot{y}_{0,n} - \frac{F_{1,n}}{k_n} + \left(\frac{\mathbf{F}_{0,n}}{k_n} \zeta_n\omega_n + \frac{F_{1,n}}{k_n} (2\zeta_n^2 - 1) + \dot{y}_{0,n} \right) (1 - \zeta_n\omega_n\tau) \right] \cdot$$

$$\cdot \zeta_n\omega_n \, e^{-\zeta_n\omega_n\tau} \tag{5.53}$$

5.3.6 Rigid system

In this particular case, at some point $k_n \rightarrow \pm\infty$, and the velocity drops to zero instantaneously. The system configuration in the $R - y$ space undergoes a jump

from the point $(y_{0,n}; R_{0,n})$ to the point $(y_{0,n}; R_n(\tau_0 + d\tau))$, where $R_n(\tau_0 + d\tau)$ is established as it follows

$$R_n(\tau_0 + d\tau) = \min\{F_{0,n}, R_{0,n+1}\}, \qquad \text{if } k_n \to +\infty \ (R \text{ is increasing})$$
$$R_n(\tau_0 + d\tau) = \max\{F_{0,n}, R_{0,n+1}\}, \qquad \text{if } k_n \to -\infty \ (R \text{ is decreasing}) \qquad (5.54)$$

5.4 Stiffness update of a displacement dependent spring

At each time, the spring configuration is described by the resistance–displacement diagram, where the spring resistance is plotted against the mass displacement. As shown in Fig. 5.1, a multi–linear $R - y$ diagram is defined by two branches. One of them defines the spring behavior when $\dot{y} > 0$ or $\dot{y} = 0 \ \wedge \ \dot{R} \to +\infty$, while the other one defines the spring behavior when $\dot{y} < 0$ or $\dot{y} = 0 \ \wedge \ \dot{R} \to -\infty$. Now let $y_{0,n}$, $\dot{y}_{0,n}$, and $R_{0,n}$ be a set of initial conditions of the nth segment of the $R - y$ diagram at $t = t_{0,n}$. In order to update the stiffness of the SDOF model, first of all it is necessary to find, whether it exists, the first time $t_{v,n} > t_{0,n}$ when the velocity sign changes. In case $t_{v,n}$ there exists and it is $t_{v,n} < t_{0,n+1}$, at that time the spring configuration undergoes a jump from one branch of the $R - y$ diagram to another. As a consequence, the stiffness must be updated to the value which defines the new branch at $R_{v,n} = R_n(t_{v,n})$.

If $t_{v,n}$ does not exist or $t_{v,n} > t_{0,n+1}$, a stiffness update is needed when the resistance value $R_{0,n+1}$ is reached. In case $R_{0,n+1}$ is never reached, a stiffness change never occurs. The problem of finding the times corresponding to a stiffness update is completely defined by the following equations,

$$\dot{y}(t_{v,n}) = v(t_{v,n}) = 0, \quad \text{or} \quad v_n(\tau_{v,n}) = 0, \quad \tau_{v,n} = t_{v,n} - t_{0,n} \qquad (5.55)$$

$$R(t_{0,n+1}) = R_{0,n+1}, \quad \text{or} \quad R_n(\Delta t_n) = R_{0,n+1}, \quad \Delta t_n = t_{0,n+1} - t_{0,n} \qquad (5.56)$$

where $t_{v,n}$ and $t_{0,n+1}$ are two possible breaking point candidate for a stiffness update. By recalling $R_n(\tau) = R_{0,n} + k_n[y_n(\tau) - y_{0,n}]$, the Eq. (5.56) may be written as

$$R_{0,n} + k_n[y_n(\Delta t_n) - y_{0,n}] = R_{0,n+1}$$

$$y_n(\Delta t_n) = y_{0,n} + \frac{R_{0,n+1} - R_{0,n}}{k_n} = y_{0,n} + \frac{\Delta R_n}{k_n}$$

$$\hat{y}_n(\Delta t_n) = y_n(\Delta t_n) - \left(y_{0,n} + \frac{\Delta R_n}{k_n}\right) = 0, \quad \Delta t_n = t_{0,n+1} - t_{0,n} \quad (5.57)$$

Therefore, the procedure for finding the stiffness update times $t_{v,n}$ and $t_{0,n+1}$ is accomplished by finding the roots of the functions v_n and $\hat{y}_n$, which are solutions of the Eqs. (5.55) and (5.57). In the following sections, the problem of finding the solutions of such equations is dealt with, for any real value of the stiffness and damping coefficients.

5.4.1 Underdamped system with negative stiffness

In order to find the solutions of the Eq. (5.55), an analysis of its derivatives is needed. Recalling the Eqs. (5.23), (5.24), and (5.25), we have

$$y_n(\tau) = e^{-\zeta_n \omega_n \tau} \left(A_1 e^{+\Omega_{d,n}\tau} + A_2 e^{-\Omega_{d,n}\tau}\right) + A_3 \tau + A_4 \quad (5.58)$$

$$A_1 = \frac{1}{2\Omega_{d,n}}\left[\left(\mathbf{F}_{0,n} + \frac{2\zeta_n}{\omega_n}F_{1,n}\right)\frac{\Omega_{d,n} + \zeta_n\omega_n}{k_n} - \frac{F_{1,n}}{k_n} + \dot{y}_{0,n}\right]$$

$$A_2 = \frac{1}{2\Omega_{d,n}}\left[\left(\mathbf{F}_{0,n} + \frac{2\zeta_n}{\omega_n}F_{1,n}\right)\frac{\Omega_{d,n} - \zeta_n\omega_n}{k_n} + \frac{F_{1,n}}{k_n} - \dot{y}_{0,n}\right]$$

$$A_3 = \frac{F_{1,n}}{k_n}$$

$$A_4 = y_{0,n} - \frac{\mathbf{F}_{0,n}}{k_n} - 2\zeta_n\frac{F_{1,n}}{\omega_n k_n}$$

$$v_n(\tau) = e^{-\zeta_n \omega_n \tau} \left(B_1 e^{+\Omega_{d,n}\tau} + B_2 e^{-\Omega_{d,n}\tau}\right) + A_3 \quad (5.59)$$

$$B_1 = +(\Omega_{d,n} - \zeta_n\omega_n)A_1$$

$$B_2 = -(\Omega_{d,n} + \zeta_n\omega_n)A_2,$$

$$a_n(\tau) = e^{-\zeta_n\omega_n\tau}\left(C_1 e^{+\Omega_{d,n}\tau} + C_2 e^{-\Omega_{d,n}\tau}\right) \tag{5.60}$$
$$C_1 = (\Omega_{d,n} - \zeta_n\omega_n)^2 A_1$$
$$C_2 = (\Omega_{d,n} + \zeta_n\omega_n)^2 A_2.$$

$$j_n(\tau) = e^{-\zeta_n\omega_n\tau}\left(D_1 e^{+\Omega_{d,n}\tau} + D_2 e^{-\Omega_{d,n}\tau}\right) \tag{5.61}$$
$$D_1 = +(\Omega_{d,n} - \zeta_n\omega_n)^3 A_1$$
$$D_2 = -(\Omega_{d,n} + \zeta_n\omega_n)^3 A_2$$

where $v_n = \dot{y}_n$, $a_n = \ddot{y}_n$, and $j_n = \dddot{y}_n$. Remembering that $\omega_n^2 = k_n/m$, $\zeta_n = c_n/(2\omega_n m)$, $\Omega_n = (|k_n|/m)^{1/2}$, and $\Omega_{d,n} = \Omega_n(1-\zeta_n^2)^{1/2}$, we get

$$\zeta_n\omega_n = \frac{c_n}{2m} \tag{5.62}$$

$$\Omega_{d,n} = \sqrt{\frac{|k_n|}{m}}\sqrt{1 - \frac{c_n^2}{4\omega_n^2 m^2}} = \sqrt{\frac{|k_n|}{m}}\sqrt{1 + \frac{c_n^2}{4|k_n|m}} = \sqrt{\frac{|k_n|}{m} + \left(\frac{c_n}{2m}\right)^2} \tag{5.63}$$

Thus, an analysis of the exponent signs of the Eqs. (5.59) and (5.60) gives

$$\Omega_{d,n} - \zeta_n\omega_n = 0 \quad \Rightarrow \quad \sqrt{\frac{|k_n|}{m} + \left(\frac{c_n}{2m}\right)^2} - \frac{c_n}{2m} = 0 \quad \Rightarrow \quad \frac{c_n}{2m} = \sqrt{\frac{|k_n|}{m} + \left(\frac{c_n}{2m}\right)^2}$$
$$\left(\frac{c_n}{2m}\right)^2 = \frac{|k_n|}{m} + \left(\frac{c_n}{2m}\right)^2 \quad \Rightarrow \quad k_n = 0,$$

and since $k_n < 0$, the expression $\Omega_{d,n} - \zeta_n\omega_n$ is of constant sign. Also, by evaluating that expression when $c_n = 0$, we get

$$\Omega_{d,n} - \zeta_n\omega_n = \sqrt{\frac{|k_n|}{m}} > 0, \quad \text{which implies}$$

$$\Omega_{d,n} - \zeta_n\omega_n > 0, \ \forall\,|\zeta_n| \in [0,1)\ \forall k_n \in (-\infty, 0) \tag{5.64}$$

Even the second exponent $-(\Omega_{d,n} + \zeta_n\omega_n)$ vanish only when $k_n = 0$. Also, when $\zeta_n = 0$ we get

$$-(\Omega_{d,n} + \zeta_n\omega_n) = -\sqrt{\frac{|k_n|}{m}} < 0, \quad \text{which implies}$$

$$-(\Omega_{d,n} + \zeta_n\omega_n) < 0, \ \forall \, |\zeta_n| \in [0,1) \ \forall k_n \in (-\infty, 0) \tag{5.65}$$

When $\tau \to \pm\infty$, from the Eqs. (5.59), (5.64), and (5.65) we obtain

$$\lim_{\tau \to +\infty} v_n(\tau) = \begin{cases} A_3, \ A_1 = 0 \\ \text{sgn}(A_1) \cdot \infty, \ A_1 \neq 0 \end{cases}$$
$$\lim_{\tau \to -\infty} v_n(\tau) = \begin{cases} A_3, \ A_2 = 0 \\ -\text{sgn}(A_2) \cdot \infty, \ A_2 \neq 0 \end{cases} \tag{5.66}$$

and when $\tau = 0$ we get $v_n(0) = B_1 + B_2 + A_3$. The stationary points of v_n are the solutions of the equation $a_n(\tau_{a,n}) = 0$, that is

$$e^{-\zeta_n\omega_n\tau_{a,n}} \left(C_1 e^{+\Omega_{d,n}\tau_{a,n}} + C_2 e^{-\Omega_{d,n}\tau_{a,n}} \right) = 0 \quad \Rightarrow \quad C_1 e^{+\Omega_{d,n}\tau_{a,n}} + C_2 e^{-\Omega_{d,n}\tau_{a,n}} = 0$$

$$C_1 e^{+\Omega_{d,n}\tau_{a,n}} = -C_2 e^{-\Omega_{d,n}\tau_{a,n}} \quad \Rightarrow \quad e^{+2\Omega_{d,n}\tau_{a,n}} = -\frac{C_2}{C_1}$$

$$\tau_{a,n} = \frac{1}{2\Omega_{d,n}} \ln\left(-\frac{C_2}{C_1}\right), \quad \frac{C_2}{C_1} < 0 \tag{5.67}$$

Recalling the Eq. (5.61), the jerk function j_n vanishes if and only if there exists $\tau_{j,n} \in \mathbb{R}$ such that $j_n(\tau_{j,n}) = 0$, that is

$$e^{-\zeta_n\omega_n\tau_{j,n}} \left(D_1 e^{+\Omega_{d,n}\tau_{j,n}} + D_2 e^{-\Omega_{d,n}\tau_{j,n}} \right) = 0 \quad \Rightarrow \quad D_1 e^{+\Omega_{d,n}\tau_{j,n}} + D_2 e^{-\Omega_{d,n}\tau_{j,n}} = 0$$

$$D_1 e^{+\Omega_{d,n}\tau_{j,n}} = -D_2 e^{-\Omega_{d,n}\tau_{j,n}} \quad \Rightarrow \quad e^{+2\Omega_{d,n}\tau_{j,n}} = -\frac{D_2}{D_1}$$

$$\tau_{j,n} = \frac{1}{2\Omega_{d,n}} \ln\left(-\frac{D_2}{D_1}\right), \quad \frac{D_2}{D_1} < 0 \tag{5.68}$$

By comparing the Eqs. (5.67) and (5.68), we have

$$\tau_{j,n} = \frac{1}{2\Omega_{d,n}} \ln\left[-\frac{C_2}{C_1}\left(-\frac{\Omega_{d,n} + \zeta_n\omega_n}{\Omega_{d,n} - \zeta_n\omega_n}\right)\right] = \tau_{a,n} + \frac{1}{2\Omega_{d,n}} \ln\left(-\frac{\Omega_{d,n} + \zeta_n\omega_n}{\Omega_{d,n} - \zeta_n\omega_n}\right) \tag{5.69}$$

5.3 (a).

5.3 (b).

5.3 (c).

5.3 (d).

5.3 (e).

5.3 (f).

5.3 (g).

5.3 (h).

5.3 (i).

5.3 (j).
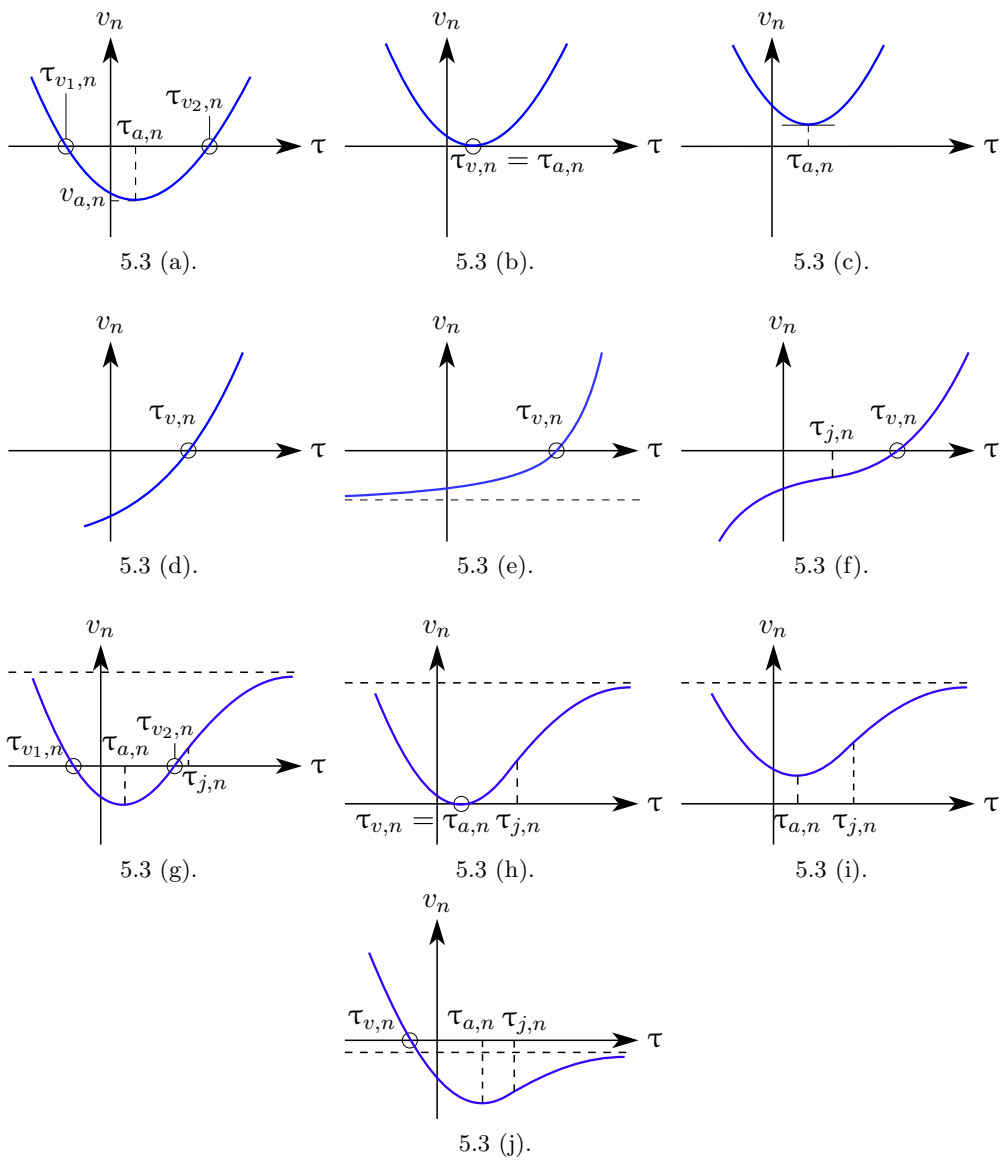
Fig. 5.3. Exponential velocity function roots of a linear oscillator under linear excitation.

The Eqs. (5.67) and (5.69) apply only when both C_1 and C_2 do not vanish, which means $A_1 \neq 0$ and $A_2 \neq 0$. If $A_1 = A_2 = 0, \Rightarrow a_n(\tau_{a,n}) = j_n(\tau_{j,n}) = 0 \; \forall \, \tau_{a,n}, \tau_{j,n} \in \mathbb{R}$. If $A_1 = 0$ and $A_2 \neq 0$ or $A_1 \neq 0$ and $A_2 = 0, \Rightarrow \tau_{a,n}, \tau_{j,n} \notin \mathbb{R}$. If $A_1 \neq 0$ and $A_2 \neq 0$, from Eqs. (5.64) and (5.65) we know that $-(\Omega_{d,n} + \zeta_n \omega_n)/(\Omega_{d,n} - \zeta_n \omega_n) < 0$, which implies that $\tau_{a,n}$ and $\tau_{j,n}$ can not be both real. If $\tau_{j,n} \in \mathbb{R}$, $\tau_{a,n} \notin \mathbb{R}$ and the sign of a_n never changes. On the other hand, if $\tau_{j,n} \notin \mathbb{R}$ and $\tau_{a,n} \in \mathbb{R}$, $v_n(\tau)$ has a unique stationary point $(\tau_{a,n})$, and the curvature sign is constant on the entire domain.

In order to find the roots of v_n, by recalling the Eqs. (5.59), (5.64), (5.65), (5.66), (5.67), (5.69), and the relationship between $A_{1,2}$, $B_{1,2}$, $C_{1,2}$, $D_{1,2}$, we may conclude that

1. $A_1 = A_2 = 0. \Rightarrow v_n(\tau) = A_3 \Rightarrow$ either $A_3 = 0$ and $v_n(\tau) = 0 \; \forall \tau \in \mathbb{R}$, or $A_3 \neq 0$ and v_n does not have any real root;

2. $A_1 \neq 0, A_2 = 0. \Rightarrow \tau_{a,n}, \tau_{j,n} \notin \mathbb{R}$, therefore a_n and j_n never vanish. Also,

   1. $A_1 A_3 < 0. \Rightarrow v_n$ has one real root (Fig. 5.3 (e)),

   $$\tau_{v,n} = \frac{1}{\Omega_{d,n} - \zeta_n \omega_n} \ln\left(-\frac{A_3}{B_1}\right)$$

   2. $A_1 A_3 \geq 0. \Rightarrow v_n$ does not have any real root;

3. $A_1 = 0, A_2 \neq 0. \Rightarrow \tau_{a,n}, \tau_{j,n} \notin \mathbb{R}$;

   1. $A_2 A_3 > 0. \Rightarrow v_n$ has one real root (Fig. 5.3 (e)),

   $$\tau_{v,n} = -\frac{1}{\Omega_{d,n} + \zeta_n \omega_n} \ln\left(-\frac{A_3}{B_2}\right)$$

   2. $A_2 A_3 \leq 0. \Rightarrow v_n$ does not have any real root;

4. $A_1 A_2 > 0. \Rightarrow \tau_{a,n} \notin \mathbb{R}$ and $\tau_{j,n} \in \mathbb{R}$, and v_n has one real root. The Newton–Raphson algorithm converges to the root if $\alpha_0 = \tau_{j,n}$ (*Lemma* B.3, Fig. 5.3 (f));

5. $A_1 A_2 < 0. \Rightarrow \tau_{a,n} \in \mathbb{R}$ and $\tau_{j,n} \notin \mathbb{R}$. This time the sign of $A_1 v_{a,n} = A_1 v_n(\tau_{a,n})$ needs to be checked out;

   1. $A_1 v_{a,n} < 0. \Rightarrow v_n$ has two real roots, $\tau_{v_1,n} < \tau_{a,n}$ and $\tau_{v_2,n} > \tau_{a,n}$ (Fig. 5.3 (a));

102

2. $A_1 v_{a,n} = 0. \Rightarrow \tau_{v,n} = \tau_{a,n}$ is the unique real root (Fig. 5.3 (b));

3. $A_1 v_{a,n} > 0. \Rightarrow v_n$ does not have any real root (Fig. 5.3 (c)).

Whether $A_1 v_{a,j} < 0$, *Lemma* B.4 shows that the Newton–Raphson method converges to a root for any choice of the initial guess α_0; when $\alpha_0 < \tau_{a,n}$ the method converges to the root $\tau_{v_1,n}$, and when $\alpha_0 > \tau_{a,n}$ the method converges toward $\tau_{v_2,n}$.

The roots of interest lie in $[0, \Delta t_n]$, and in case of multiple roots the least one is needed. If there are no roots within such interval, either the next step $R_{0,n+1}$ of the $R - y$ diagram is reached without any change of the velocity sign, or $y_n(\tau) = A_4 = $ const. and $R_{0,n+1}$ is never reached. Anyway, if $y_n(\tau) \neq$ const., the Eq. (5.57) needs to be solved, in order to get Δt_n. From the Eqs. (5.57) and (5.58), we have

$$\hat{y}_n(\Delta t_n) = e^{-\zeta_n \omega_n \Delta t_n} \left(A_1 e^{+\Omega_{d,n} \Delta t_n} + A_2 e^{-\Omega_{d,n} \Delta t_n} \right) + A_3 \Delta t_n + \hat{A}_4 = 0 \quad (5.70)$$

$$\hat{A}_4 = A_4 - \left(y_{0,n} + \frac{\Delta R_n}{k_n} \right)$$

and the solutions of the Eq. (5.70) depend on the constants $A_1, A_2, A_3, \hat{A}_4$. In the following analysis, δt_n represents the time when a stiffness update is actually accomplished.

1. $A_1 = A_2 = A_3 = \hat{A}_4 = 0. \Rightarrow$ In this case $\hat{y}_n(\Delta t_n) = 0 \ \forall \Delta t_n \in \mathbb{R}$, and the system keeps the same configuration as long as the external excitation does not change;

2. $A_1 = A_2 = 0. \Rightarrow$ From the Eq. (5.70) we get $A_3 \Delta t_n + \hat{A}_4 = 0$. Thus, either $A_3 \neq 0$ and $\Delta t_n = -\hat{A}_4/A_3$, or $A_3 = 0$ and we get the previous case;

3. $A_1 \neq 0, A_2 = 0. \Rightarrow a_n$ and j_n never vanish. Also,

$$\lim_{\tau \to +\infty} \hat{y}_n(\tau) = \lim_{\tau \to +\infty} \left(A_1 e^{(\Omega_{d,n} - \zeta_n \omega_n)\tau} + A_3 \tau + \hat{A}_4 \right) = \text{sgn}(A_1) \cdot \infty \quad (5.71a)$$

$$\lim_{\tau \to -\infty} \hat{y}_n(\tau) = \begin{cases} \hat{A}_4, \ A_3 = 0 \\ -\text{sgn}(A_3) \cdot \infty, \ A_3 \neq 0 \end{cases} \quad (5.71b)$$

1. $A_1 A_3 < 0. \Rightarrow v_n$ has a single root $\tau_{v,n}$.

    1. $A_1 y_n(\tau_{v,n}) < 0. \Rightarrow \hat{y}_n$ has two real roots, $\Delta t_{1,n}$ and $\Delta t_{2,n}$, which may be found by choosing $\alpha_0 < \tau_{v,n}$ and $\alpha_0 > \tau_{v,n}$ respectively

(*Lemma* B.4). The time δt_n when the stiffness is updated corresponds to the minimum positive value among $\Delta t_{1,n}$, $\tau_{v,n}$, and $\Delta t_{2,n}$ (Fig. 5.4 (a));

2. $A_1 y_n(\tau_{v,n}) = 0. \Rightarrow \hat{y}_n$ has one real root $\Delta t_n = \tau_{v,n} = \delta t_n$, which corresponds to a jump of the spring configuration from a branch of the $R - y$ diagram to another (Fig. 5.4 (b));

3. $A_1 y_n(\tau_{v,n}) > 0. \Rightarrow \hat{y}_n$ has no real roots, and at $\delta t_n = \tau_{v,n}$ there is a jump of the spring configuration from a branch of the $R - y$ diagram to another (Fig. 5.4 (c));

2. $A_1 A_3 \geq 0. \Rightarrow v_n$ does not have any root.

   1. $A_3 \neq 0. \Rightarrow$ Since $\hat{y}_n$ is strictly monotone, from the Eq. (5.71) we know that there exists a unique root $\Delta t_n = \delta t_n$, shown in Fig. 5.4 (d). This root can be calculated for any choice of $\alpha_0 \in \mathbb{R}$ (*Lemma* B.2);

   2. $A_3 = 0, \ A_1 \hat{A}_4 < 0. \Rightarrow \hat{y}_n$ has one real root

$$\Delta t_n = \delta t_n = \frac{1}{\Omega_{d,n} - \zeta_n \omega_n} \ln \left(-\frac{\hat{A}_4}{A_1} \right)$$

   3. $A_3 = 0, \ A_1 \hat{A}_4 \geq 0. \Rightarrow \hat{y}_n$ does not have any real root.

4. $A_1 = 0, A_2 \neq 0. \Rightarrow a_n$ and j_n never vanish. Also,

$$\lim_{\tau \to -\infty} \hat{y}_n(\tau) = \lim_{\tau \to -\infty} \left(A_2 e^{-(\Omega_{d,n} + \zeta_n \omega_n)\tau} + A_3 \tau + \hat{A}_4 \right) = \text{sgn}(A_2) \cdot \infty \quad (5.72\text{a})$$

$$\lim_{\tau \to +\infty} \hat{y}_n(\tau) = \begin{cases} \hat{A}_4, \ A_3 = 0 \\ \text{sgn}(A_3) \cdot \infty, \ A_3 \neq 0 \end{cases} \quad (5.72\text{b})$$

   1. $A_2 A_3 > 0. \Rightarrow v_n$ has a single root $\tau_{v,n}$.

      1. $A_2 y_n(\tau_{v,n}) < 0. \Rightarrow \hat{y}_n$ has two real roots, $\Delta t_{1,n}$ and $\Delta t_{2,n}$, which may be found by choosing $\alpha_0 < \tau_{v,n}$ and $\alpha_0 > \tau_{v,n}$ respectively (*Lemma* B.4). The time δt_n when the stiffness is updated corresponds to the minimum positive value among $\Delta t_{1,n}$, $\tau_{v,n}$, and $\Delta t_{2,n}$ (Fig. 5.4 (a));

      2. $A_2 y_n(\tau_{v,n}) = 0. \Rightarrow \hat{y}_n$ has one real root $\Delta t_n = \tau_{v,n} = \delta t_n$, which corresponds to a jump of the spring–mass system from a branch of the $R - y$ diagram to another (Fig. 5.4 (b));

      3. $A_2 y_n(\tau_{v,n}) > 0. \Rightarrow \hat{y}_n$ has no real roots, and at $\delta t_n = \tau_{v,n}$ there is a jump of the spring–mass system from a branch of the $R - y$ diagram to another (Fig. 5.4 (c));

2. $A_2 A_3 \leq 0. \Rightarrow v_n$ does not have any root;

    1. $A_3 \neq 0. \Rightarrow$ Since $\hat{y}_n$ is strictly monotone, from the Eq. (5.72) we know that there exists a unique root $\Delta t_n = \delta t_n$, as shown in Fig. 5.4 (d). This root may be calculated for any choice of $\alpha_0 \in \mathbb{R}$ (*Lemma* B.2);

    2. $A_3 = 0, \; A_2 \hat{A}_4 < 0. \Rightarrow \hat{y}_n$ has one real root

$$\Delta t_n = \delta t_n = -\frac{1}{\Omega_{d,n} + \zeta_n \omega_n} \ln\left(-\frac{\hat{A}_4}{A_2}\right)$$

    3. $A_3 = 0, \; A_2 \hat{A}_4 \geq 0. \Rightarrow \hat{y}_n$ does not have any real root (Fig. 5.4 (f));

5. $A_1 A_2 > 0. \Rightarrow v_n$ has one real root $\tau_{v,n}$, a_n never vanish, and j_n has one real root $\tau_{j,n}$. Also,

$$\lim_{\tau \to +\infty} \hat{y}_n(\tau) = \text{sgn}(A_1) \cdot \infty, \quad \lim_{\tau \to -\infty} \hat{y}_n(\tau) = \text{sgn}(A_2) \cdot \infty \qquad (5.73)$$

    1. $A_3 = \hat{A}_4 = 0. \Rightarrow \hat{y}_n$ has no real roots, and at $\delta t_n = \tau_{v,n}$ there is a branch jump of the system configuration;

    2. $\forall A_3, \hat{A}_4.$

        1. $A_1 \, y_n(\tau_{v,n}) < 0. \Rightarrow \hat{y}_n$ has two real roots, $\Delta t_{1,n}$ and $\Delta t_{2,n}$, which may be found by choosing $\alpha_0 < \tau_{v,n}$ and $\alpha_0 > \tau_{v,n}$ respectively (*Lemma* B.4). The time δt_n when the stiffness is updated corresponds to the minimum positive value among $\Delta t_{1,n}$, $\tau_{v,n}$, and $\Delta t_{2,n}$ (Fig. 5.4 (a));

        2. $A_1 \, y_n(\tau_{v,n}) = 0. \Rightarrow \hat{y}_n$ has one real root $\Delta t_n = \tau_{v,n} = \delta t_n$, which corresponds to a jump of the spring configuration from a branch of the $R - y$ diagram to another (Fig. 5.4 (b));

        3. $A_1 \, y_n(\tau_{v,n}) > 0. \Rightarrow \hat{y}_n$ has no real roots, and at $\delta t_n = \tau_{v,n}$ there is a jump of the spring configuration from a branch of the $R - y$ diagram to another (Fig. 5.4 (c));

6. $A_1 A_2 < 0. \Rightarrow a_n$ has one real root $\tau_{a,n}$, and j_n does not have any root;

    1. $A_3 = \hat{A}_4 = 0. \Rightarrow \hat{y}_n$ has one real root,

$$\Delta t_n = \frac{1}{2\Omega_{d,n}} \ln\left(-\frac{A_2}{A_1}\right)$$

and again, δt_n is chosen between Δt_n and $\tau_{v,n}$, whether it exists;

2. $\forall A_3, \hat{A}_4$.

    1. $A_1 v_{a,n} < 0. \Rightarrow v_n$ has two real roots, $\tau_{v_1,n} < \tau_{a,n} < \tau_{v_2,n}$.

        1. $\hat{y}(\tau_{v_1,n})\,\hat{y}(\tau_{v_2,n}) < 0. \Rightarrow \hat{y}_n$ has 3 real roots $\Delta t_{1,n} < \Delta t_{2,n} < \Delta t_{3,n}$ (Fig. 5.5 (a)), which may be found by *Lemma* B.1. Indeed, $\Delta t_{1,n}$, $\Delta t_{2,n}$, and $\Delta t_{3,n}$ may be calculated by choosing $\alpha_0 < \tau_{v_1,n}$, $\alpha_0 = \tau_{a,n}$, and $\alpha_0 > \tau_{v_2,n}$ respectively. The time δt_n when the stiffness is updated corresponds to the minimum positive value among $\Delta t_{1,n}$, $\tau_{v_1,n}$, $\Delta t_{2,n}$, $\tau_{v_2,n}$, and $\Delta t_{3,n}$;

        2. $\hat{y}(\tau_{v_1,n})\,\hat{y}(\tau_{v_2,n}) = 0. \Rightarrow \hat{y}_n$ has 2 real roots $\Delta t_{1,n} < \Delta t_{2,n}$ (Fig. 5.5 (b)), which may be found by *Lemma* B.1. Indeed, if $\hat{y}(\tau_{v_1,n}) = 0$, $\Delta t_1 = \tau_{v_1,n}$ and Δt_2 may be found by choosing $\alpha_0 > \tau_{v_2,n}$. If $\hat{y}(\tau_{v_2,n}) = 0$, Δt_1 may be found by choosing $\alpha_0 < \tau_{v_1,n}$ and $\Delta t_2 = \tau_{v_2,n}$;

        3. $\hat{y}(\tau_{v_1,n})\,\hat{y}(\tau_{v_2,n}) > 0. \Rightarrow \hat{y}_n$ has 1 real root Δt_n (Fig. 5.5 (c)), which may be found by *Lemma* B.1. In case of $A_2\hat{y}(\tau_{v_1,n}) < 0$, $\alpha_0 < \tau_{v_1,n}$ is needed, and whether $A_1\hat{y}(\tau_{v_2,n}) < 0$, $\alpha_0 > \tau_{v_2,n}$ should be chosen;

    2. $A_1 v_{a,n} = 0. \Rightarrow v_n$ and a_n have the same root $\tau_{a,n}$, which means that $\hat{y}_n$ has a stationary point of inflexion at that time (Fig. 5.5 (d)). j_n never vanishes.

        1. $\hat{y}(\tau_{a,n})\,j_{a,n} < 0. \Rightarrow \Delta t_n$ may be found by *Lemma* B.1, by choosing $\alpha_0 > \tau_{a,n}$;

        2. $\hat{y}(\tau_{a,n})\,j_{a,n} = 0. \Rightarrow \Delta t_n = \tau_{a,n}$;

        3. $\hat{y}(\tau_{a,n})\,j_{a,n} > 0. \Rightarrow \Delta t_n$ may be found by *Lemma* B.1, by choosing $\alpha_0 < \tau_{a,n}$;

    Again, δt_n is the minimum positive value between $\tau_{v,n}$ and Δt_n;

    3. $A_1 v_{a,n} > 0. \Rightarrow v_n$ does not have any root and a_n vanish at $\tau_{a,n}$, which means $\hat{y}_n$ has a non stationary point of inflexion at that time (Fig. 5.5 (e)). From *Lemma* B.3, $\hat{y}_n$ has one real root, which may be found by choosing $\alpha_0 = \tau_{a,n}$.
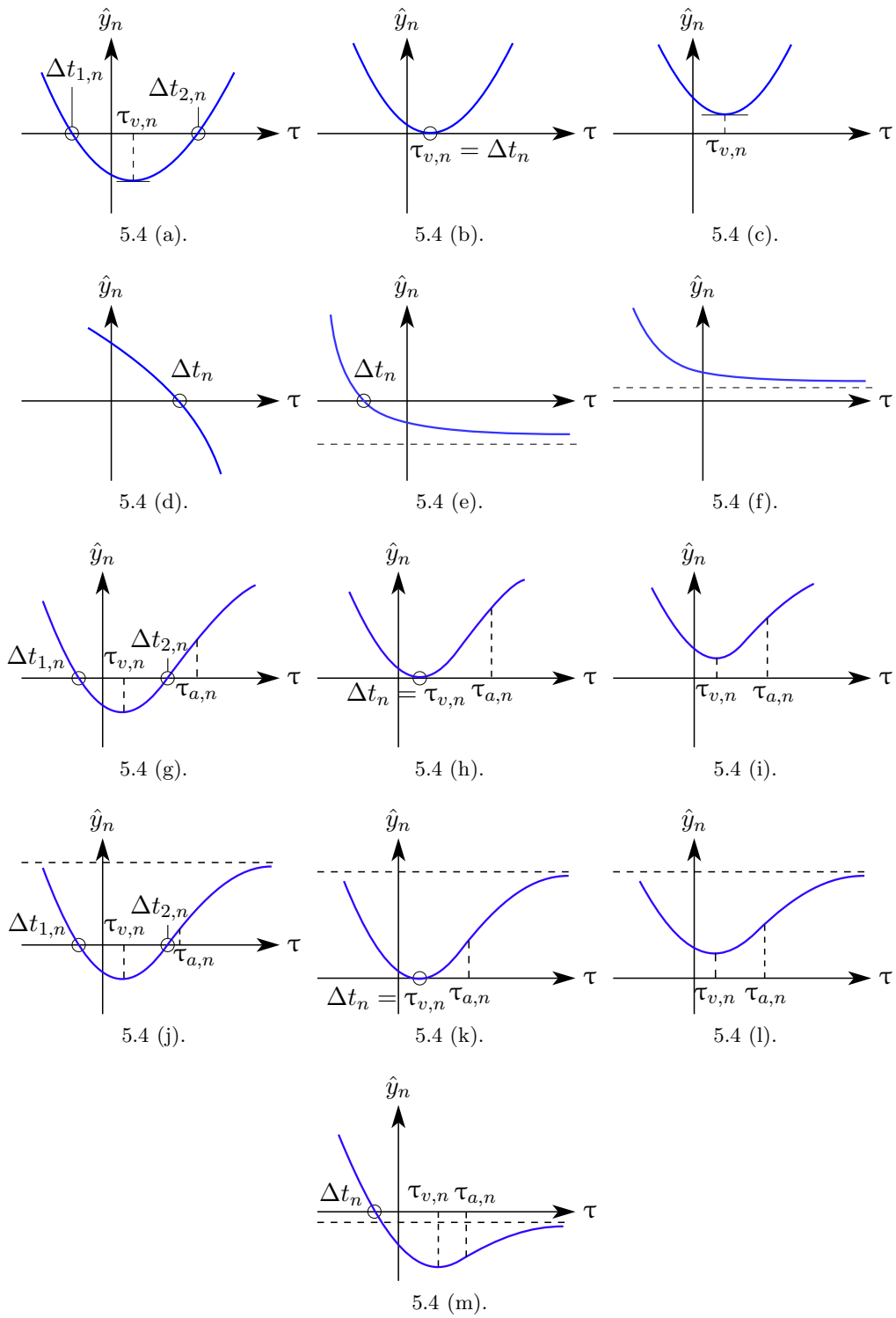
Fig. 5.4. Exponential displacement function roots of a linear oscillator under linear excitation.

5.5 (a).

5.5 (b).

5.5 (c).

5.5 (d).

5.5 (e).
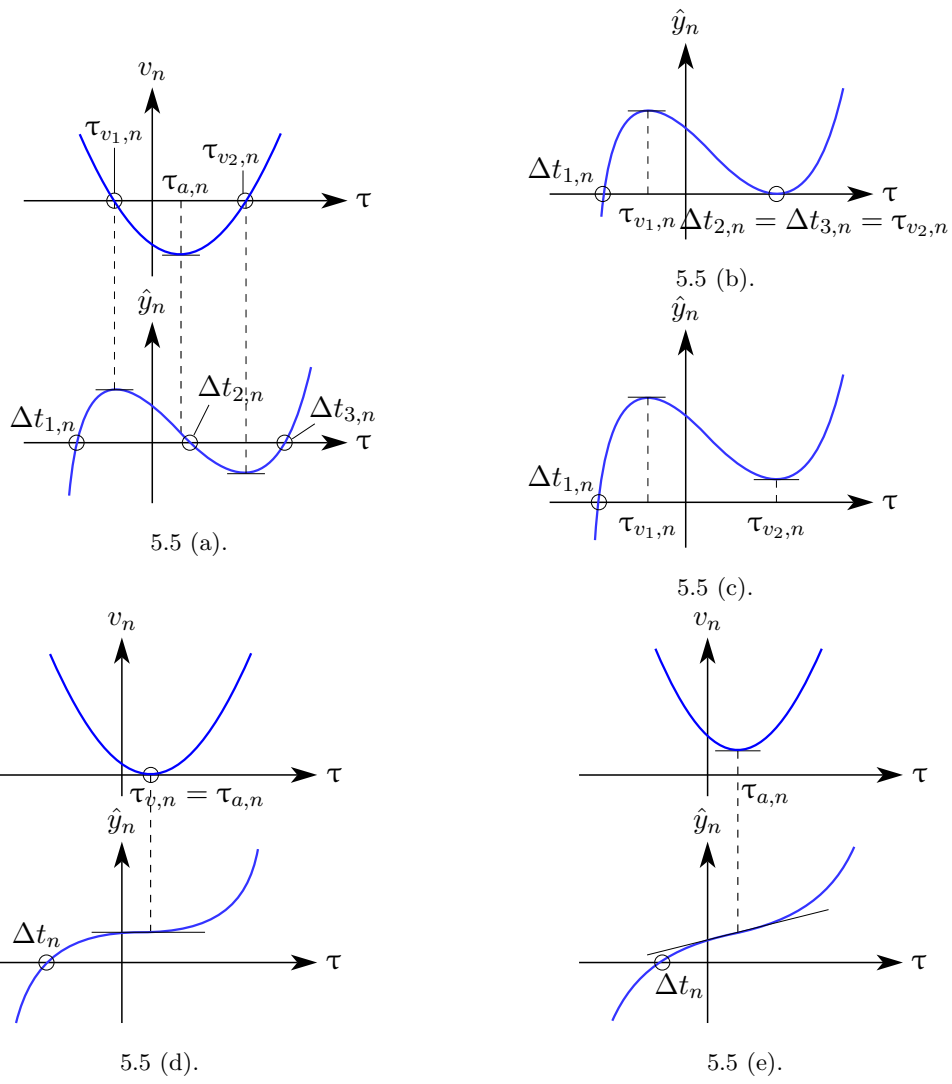
Fig. 5.5. Exponential displacement function roots of a linear oscillator under linear excitation.

Overdamped system with positive stiffness

This time we have

$$\Omega_{d,n} = \omega_n \sqrt{\zeta_n^2 - 1} = \sqrt{\frac{k_n}{m}} \sqrt{\frac{c_n^2}{4\omega_n^2 m^2} - 1} = \sqrt{\frac{k_n}{m}} \sqrt{\frac{c_n^2}{4k_n m} - 1} = \sqrt{\left(\frac{c_n}{2m}\right)^2 - \frac{k_n}{m}}$$
(5.74)

An analysis of the exponent signs in the Eqs. (5.59) and (5.60) gives

$$\Omega_{d,n} - \zeta_n \omega_n = 0 \ \Rightarrow \ \sqrt{\left(\frac{c_n}{2m}\right)^2 - \frac{k_n}{m}} - \frac{c_n}{2m} = 0 \ \Rightarrow \ \frac{c_n}{2m} = \sqrt{\left(\frac{c_n}{2m}\right)^2 - \frac{k_n}{m}}$$

$$\left(\frac{c_n}{2m}\right)^2 = \left(\frac{c_n}{2m}\right)^2 - \frac{k_n}{m} \ \Rightarrow \ k_n = 0$$

and since $k_n > 0$, the expression $\Omega_{d,n} - \zeta_n \omega_n$ is of constant sign. Also, by evaluating that expression when $\zeta_n = 2$ and $c_n = 4\sqrt{k_n m}$, we get

$$\Omega_{d,n} - \zeta_n \omega_n = \sqrt{\left(\frac{4\sqrt{k_n m}}{2m}\right)^2 - \frac{k_n}{m}} - 2\omega_n = \sqrt{4\frac{k_n}{m} - \frac{k_n}{m}} - 2\omega_n = (\sqrt{3} - 2)\omega_n < 0$$

which implies

$$\Omega_{d,n} - \zeta_n \omega_n < 0, \ \forall \, |\zeta_n| > 1 \ \forall k_n \in (0, \infty) \tag{5.75}$$

Even the second exponent $-(\Omega_{d,n} + \zeta_n \omega_n)$ vanish only when $k_n = 0$. Also, when $\zeta_n = 2$ we get

$$-(\Omega_{d,n} + \zeta_n \omega_n) = -(\sqrt{3} + 2)\omega_n < 0, \quad \text{which implies}$$

$$-(\Omega_{d,n} + \zeta_n \omega_n) < 0, \ \forall \, |\zeta_n| > 1 \ \forall k_n \in (0, \infty) \tag{5.76}$$

When $\tau \to \pm\infty$, from the Eqs. (5.59), (5.75), and (5.76) we obtain

$$\lim_{\tau \to +\infty} v_n(\tau) = \lim_{\tau \to +\infty} \left(B_1 e^{(\Omega_{d,n} - \zeta_n \omega_n)\tau} + B_2 e^{-(\Omega_{d,n} + \zeta_n \omega_n)\tau} + A_3 \right) = A_3$$

$$\lim_{\tau \to -\infty} v_n(\tau) = \lim_{\tau \to -\infty} \left(B_1 e^{(\Omega_{d,n} - \zeta_n \omega_n)\tau} + B_2 e^{-(\Omega_{d,n} + \zeta_n \omega_n)\tau} + A_3 \right) =$$

$$= \begin{cases} A_3, \ A_1 = A_2 = 0 \\ -\operatorname{sgn}(A_1) \cdot \infty, \ A_1 \neq 0, \ A_2 = 0 \\ -\operatorname{sgn}(A_2) \cdot \infty, \ A_2 \neq 0 \end{cases} \tag{5.77}$$

The Eqs. (5.67) and (5.69) apply only when both C_1 and C_2 do not vanish, which means $A_1 A_2 \neq 0$. If that is the case, from the Eqs. (5.75) and (5.76) we know that $-(\Omega_{d,n} + \zeta_n \omega_n)/(\Omega_{d,n} - \zeta_n \omega_n) > 0$, which implies that $\tau_{a,n}$ and $\tau_{j,n}$ are distinct and either both real or both complex.

In order to find the roots of v_n, by recalling the Eqs. (5.59), (5.66), (5.67), (5.69), (5.75), (5.76), and the relationship between $A_{1,2}$, $B_{1,2}$, $C_{1,2}$, $D_{1,2}$, we may conclude that

1. $A_1 = A_2 = 0. \Rightarrow v_n(\tau) = A_3 \Rightarrow$ either $A_3 = 0$ and $v_n(\tau) = 0 \ \forall \tau \in \mathbb{R}$, or $A_3 \neq 0$ and v_n does not have any real root;

2. $A_1 \neq 0, A_2 = 0. \Rightarrow, \tau_{a,n}, \tau_{j,n} \notin \mathbb{R}$, therefore a_n and j_n never vanish. Also,

   1. $A_1 A_3 \leq 0. \Rightarrow v_n$ does not have any real root;
   2. $A_1 A_3 > 0. \Rightarrow v_n$ has one real root (Fig. 5.3 (e)),

$$\tau_{v,n} = \frac{1}{\Omega_{d,n} - \zeta_n \omega_n} \ln \left(-\frac{A_3}{B_1} \right)$$

3. $A_1 = 0, A_2 \neq 0. \Rightarrow \tau_{a,n}, \tau_{j,n} \notin \mathbb{R}$;

   1. $A_2 A_3 \leq 0. \Rightarrow v_n$ does not have any real root;
   2. $A_2 A_3 > 0. \Rightarrow v_n$ has one real root (Fig. 5.3 (e)),

$$\tau_{v,n} = -\frac{1}{\Omega_{d,n} + \zeta_n \omega_n} \ln \left(-\frac{A_3}{B_2} \right)$$

4. $A_1 A_2 > 0. \Rightarrow \tau_{a,n}, \tau_{j,n} \notin \mathbb{R}$. Also, $\lim_{\tau \to +\infty} v_n(\tau) = A_3$ and $\lim_{\tau \to -\infty} v_n(\tau) = -\operatorname{sgn}(A_1) \cdot \infty$.

   1. $A_1 A_3 \leq 0. \Rightarrow v_n$ does not have any real root;

110

2. $A_1 A_3 > 0. \Rightarrow$ The Newton–Raphson algorithm converges to the unique root $\tau_{v,n}\ \forall \alpha_0 \in \mathbb{R}$ (*Lemma* B.2, Fig. 5.3 (e));

5. $A_1 A_2 < 0. \Rightarrow \tau_{a,n}, \tau_{j,n} \in \mathbb{R}$. Since $\Omega_{d,n} > 0$ and $-(\Omega_{d,n} + \zeta_n \omega_n)/(\Omega_{d,n} - \zeta_n \omega_n) > 1$, from the Eq. (5.69) we get $\tau_{j,n} > \tau_{a,n}$.

   1. $A_1 A_3 \leq 0. \Rightarrow v_n$ has a unique root $\tau_{v,n}$ (Fig. 5.3 (j)), which may be found from $\alpha_0 < \tau_{a,n}$ (*Lemma* B.1);

   2. $A_1 A_3 > 0.$

      1. $A_1 v_{a,n} < 0. \Rightarrow v_n$ has two real roots, $\tau_{v_1,n} < \tau_{a,n}$ and $\tau_{v_2,n} > \tau_{a,n}$ (Fig. 5.3 (g)). The former may be found from $\alpha_0 < \tau_{a,n}$, while the latter is from $\alpha_0 = \tau_{j,n}$ (*Lemma* B.1);

      2. $A_1 v_{a,n} = 0. \Rightarrow \tau_{v,n} = \tau_{a,n}$ is the unique real root (Fig. 5.3 (h));

      3. $A_1 v_{a,n} > 0. \Rightarrow v_n$ does not have any real root (Fig. 5.3 (i)).

As far as the solutions of the Eq. (5.70) is concerned, we have

1. $A_1 = A_2 = A_3 = \hat{A}_4 = 0. \Rightarrow$ In this case $\hat{y}_n(\Delta t_n) = 0\ \forall \Delta t_n \in \mathbb{R}$, and the system keeps the same configuration as long as the external excitation does not change;

2. $A_1 = A_2 = 0. \Rightarrow$ From the Eq. (5.70) we get $A_3 \Delta t_n + \hat{A}_4 = 0$. Thus, either $A_3 \neq 0$ and $\Delta t_n = -\hat{A}_4/A_3$, or $A_3 = 0$ and we get the previous case;

3. $A_1 \neq 0, A_2 = 0. \Rightarrow a_n$ and j_n never vanish. Also,

$$\lim_{\tau \to +\infty} \hat{y}_n(\tau) = \begin{cases} \hat{A}_4, & A_3 = 0 \\ \mathrm{sgn}(A_3) \cdot \infty, & A_3 \neq 0 \end{cases} \tag{5.78a}$$

$$\lim_{\tau \to -\infty} \hat{y}_n(\tau) = \mathrm{sgn}(A_1) \cdot \infty \tag{5.78b}$$

   1. $A_1 A_3 \leq 0. \Rightarrow v_n$ does not have any root.

      1. $A_3 \neq 0. \Rightarrow$ Since $\hat{y}_n$ is strictly monotone, from the Eq. (5.78) we know that there exists a unique root $\Delta t_n = \delta t_n$, shown in Fig. 5.4 (d). This root can be calculated for any choice of $\alpha_0 \in \mathbb{R}$ (*Lemma* B.2);

      2. $A_3 = 0,\ A_1 \hat{A}_4 < 0. \Rightarrow \hat{y}_n$ has one real root

$$\Delta t_n = \delta t_n = \frac{1}{\Omega_{d,n} - \zeta_n \omega_n} \ln\left(-\frac{\hat{A}_4}{A_1}\right)$$

111

3. $A_3 = 0$, $A_1 \hat{A}_4 \geq 0$. $\Rightarrow \hat{y}_n$ does not have any real root;

2. $A_1 A_3 > 0$. $\Rightarrow v_n$ has a single root $\tau_{v,n}$.

    1. $A_1 y_n(\tau_{v,n}) < 0$. $\Rightarrow \hat{y}_n$ has two real roots, $\Delta t_{1,n}$ and $\Delta t_{2,n}$, which can be found by choosing $\alpha_0 < \tau_{v,n}$ and $\alpha_0 > \tau_{v,n}$ respectively (*Lemma* B.4). The time δt_n when the stiffness is updated corresponds to the minimum positive value among $\Delta t_{1,n}$, $\tau_{v,n}$, and $\Delta t_{2,n}$ (Fig. 5.4 (a));

    2. $A_1 y_n(\tau_{v,n}) = 0$. $\Rightarrow \hat{y}_n$ has one real root $\Delta t_n = \tau_{v,n} = \delta t_n$, which corresponds to a jump of the spring configuration from a branch of the $R - y$ diagram to another (Fig. 5.4 (b));

    3. $A_1 y_n(\tau_{v,n}) > 0$. $\Rightarrow \hat{y}_n$ has no real roots, and at $\delta t_n = \tau_{v,n}$ there is a jump of the spring configuration from a branch of the $R - y$ diagram to another (Fig. 5.4 (c));

4. $A_1 = 0, A_2 \neq 0$. $\Rightarrow a_n$ and j_n never vanish. Also,

$$\lim_{\tau \to -\infty} \hat{y}_n(\tau) = \lim_{\tau \to -\infty} \left(A_2 e^{-(\Omega_{d,n} + \zeta_n \omega_n)\tau} + A_3 \tau + \hat{A}_4 \right) = \text{sgn}(A_2) \cdot \infty \quad (5.79a)$$

$$\lim_{\tau \to +\infty} \hat{y}_n(\tau) = \begin{cases} \hat{A}_4, & A_3 = 0 \\ \text{sgn}(A_3) \cdot \infty, & A_3 \neq 0 \end{cases} \quad (5.79b)$$

1. $A_2 A_3 \leq 0$. $\Rightarrow v_n$ does not have any root;

    1. $A_3 \neq 0$. $\Rightarrow$ Since $\hat{y}_n$ is strictly monotone, from the Eq. (5.79) we know that there exists a unique root $\Delta t_n = \delta t_n$, as shown in Fig. 5.4 (d). This root may be calculated for any choice of $\alpha_0 \in \mathbb{R}$ (*Lemma* B.2);

    2. $A_3 = 0$, $A_2 \hat{A}_4 < 0$. $\Rightarrow \hat{y}_n$ has one real root

$$\Delta t_n = \delta t_n = -\frac{1}{\Omega_{d,n} + \zeta_n \omega_n} \ln \left(-\frac{\hat{A}_4}{A_2} \right)$$

    3. $A_3 = 0$, $A_2 \hat{A}_4 \geq 0$. $\Rightarrow \hat{y}_n$ does not have any real root;

2. $A_2 A_3 > 0$. $\Rightarrow v_n$ has a single root $\tau_{v,n}$.

    1. $A_2 y_n(\tau_{v,n}) < 0$. $\Rightarrow \hat{y}_n$ has two real roots, $\Delta t_{1,n}$ and $\Delta t_{2,n}$, which may be found by choosing $\alpha_0 < \tau_{v,n}$ and $\alpha_0 > \tau_{v,n}$ respectively (*Lemma* B.4). The time δt_n when the stiffness is updated corresponds to the minimum positive value among $\Delta t_{1,n}$, $\tau_{v,n}$, and $\Delta t_{2,n}$ (Fig. 5.4 (a));

2. $A_2 \, y_n(\tau_{v,n}) = 0. \Rightarrow \hat{y}_n$ has one real root $\Delta t_n = \tau_{v,n} = \delta t_n$, which corresponds to a jump of the spring–mass system from a branch of the $R - y$ diagram to another (Fig. 5.4 (b));

3. $A_2 \, y_n(\tau_{v,n}) > 0. \Rightarrow \hat{y}_n$ has no real roots, and at $\delta t_n = \tau_{v,n}$ there is a jump of the spring–mass system from a branch of the $R - y$ diagram to another (Fig. 5.4 (c));

5. $A_1 A_2 > 0. \Rightarrow a_n(\tau)$ and $j_n(\tau)$ never vanish. Also,

$$\lim_{\tau \to +\infty} \hat{y}_n(\tau) = \begin{cases} \hat{A}_4, & A_3 = 0 \\ \text{sgn}(A_3) \cdot \infty, & A_3 \neq 0 \end{cases} \qquad \lim_{\tau \to -\infty} \hat{y}_n(\tau) = \text{sgn}(A_2) \cdot \infty$$

(5.80)

1. $A_1 A_3 \leq 0. \Rightarrow v_n(\tau) \neq 0 \forall \tau \in \mathbb{R}$ and $A_2 A_3 \leq 0$.

   1. $A_2 A_3 < 0. \Rightarrow$ From the Eq. (5.80), $\hat{y}_n$ has one real root (Fig. 5.4 (d)), which may be found $\forall \alpha_0 \in \mathbb{R}$ (*Lemma* B.1);

   2. $A_2 A_3 = 0. \Rightarrow A_3 = 0$;

      1. $A_2 \hat{A}_4 < 0. \Rightarrow \hat{y}_n$ has one real root Δt_n (Fig. 5.4 (e)), which might come from any $\alpha_0 \in \mathbb{R}$ (*Lemma* B.1);

      2. $A_2 \hat{A}_4 \geq 0. \Rightarrow \hat{A}_4 = 0.$ $\hat{y}_n$ does not have real roots (Fig. 5.4 (f));

2. $A_1 A_3 > 0. \Rightarrow \exists! \; \tau_{v,n} \in \mathbb{R}$, and $A_2 A_3 > 0$.

   1. $A_2 \, y_n(\tau_{v,n}) < 0. \Rightarrow \hat{y}_n$ has two real roots, $\Delta t_{1,n}$ and $\Delta t_{2,n}$, which may be found by choosing $\alpha_0 < \tau_{v,n}$ and $\alpha_0 > \tau_{v,n}$ respectively (*Lemma* B.4). The time δt_n when the stiffness is updated corresponds to the minimum positive value among $\Delta t_{1,n}$, $\tau_{v,n}$, and $\Delta t_{2,n}$ (Fig. 5.4 (a));

   2. $A_2 \, y_n(\tau_{v,n}) = 0. \Rightarrow \hat{y}_n$ has one real root $\Delta t_n = \tau_{v,n} = \delta t_n$, which corresponds to a jump of the spring configuration from a branch of the $R - y$ diagram to another (Fig. 5.4 (b));

   3. $A_2 \, y_n(\tau_{v,n}) > 0. \Rightarrow \hat{y}_n$ has no real roots, and at $\delta t_n = \tau_{v,n}$ there is a jump of the spring configuration from a branch of the $R - y$ diagram to another (Fig. 5.4 (c));

6. $A_1 A_2 < 0. \Rightarrow a_n$ has one real root $\tau_{a,n}$, and j_n has one real root $\tau_{j,n} > \tau_{a,n}$. The Eq. (5.80) still holds.

   1. $A_1 A_3 \leq 0. \Rightarrow A_2 A_3 \geq 0$ and $v_n(\tau)$ has a unique root $\tau_{v,n} < \tau_{a,n}$;

1. $A_3 \neq 0$.

   1. $A_2 \hat{y}_{v,n} < 0$. $\Rightarrow \hat{y}_n$ has two real roots, $\Delta t_{1,n}$ and $\Delta t_{2,n}$, which may be found by choosing $\alpha_0 < \tau_{v,n}$ and $\alpha_0 > \tau_{v,n}$ respectively (*Lemma* B.4). The time δt_n when the stiffness is updated corresponds to the minimum positive value among $\Delta t_{1,n}$, $\tau_{v,n}$, and $\Delta t_{2,n}$ (Fig. 5.4 (g));

   2. $A_2 \hat{y}_{v,n} = 0$. $\Rightarrow \hat{y}_n$ has one real root $\Delta t_n = \tau_{v,n} = \delta t_n$, which corresponds to a jump of the spring configuration from a branch of the $R - y$ diagram to another (Fig. 5.4 (h));

   3. $A_2 \hat{y}_{v,n} > 0$. $\Rightarrow \hat{y}_n$ has no real roots, and at $\delta t_n = \tau_{v,n}$ there is a jump of the spring configuration from a branch of the $R - y$ diagram to another (Fig. 5.4 (i));

2. $A_3 = 0$.

   1. $A_2 A_4 < 0$. $\Rightarrow \exists! \, \Delta t_n$ which may be found from $\alpha_0 < \tau_{v,n}$ (Fig. 5.4 (m)). δt_n is the minimum positive value between Δt_n and $\tau_{v,n}$;

   2. $A_2 A_4 = 0$. $\Rightarrow A_4 = 0$ and $\Delta t_n = \dfrac{1}{2\Omega_{d,n}} \ln\left(-\dfrac{A_2}{A_1}\right)$. δt_n is the minimum positive value between Δt_n and $\tau_{v,n}$;

   3. $A_2 A_4 > 0$.

      - $A_2 \hat{y}_{v,n} < 0$. $\Rightarrow \hat{y}_n$ has two real roots, $\Delta t_{1,n}$ and $\Delta t_{2,n}$, which may be found by choosing $\alpha_0 < \tau_{v,n}$ and $\alpha_0 > \tau_{v,n}$ respectively (*Lemma* B.4). The time δt_n when the stiffness is updated corresponds to the minimum positive value among $\Delta t_{1,n}$, $\tau_{v,n}$, and $\Delta t_{2,n}$ (Fig. 5.4 (j));

      - $A_2 \hat{y}_{v,n} = 0$. $\Rightarrow \hat{y}_n$ has one real root $\Delta t_n = \tau_{v,n} = \delta t_n$, which corresponds to a jump of the spring configuration from a branch of the $R - y$ diagram to another (Fig. 5.4 (k));

      - $A_2 \hat{y}_{v,n} > 0$. $\Rightarrow \hat{y}_n$ has no real roots, and at $\delta t_n = \tau_{v,n}$ there is a jump of the spring configuration from a branch of the $R - y$ diagram to another (Fig. 5.4 (l));

2. $A_1 A_3 > 0$.

   1. $A_1 v_{a,n} < 0$. $\Rightarrow v_n$ has two real roots, $\tau_{v_1,n} < \tau_{a,n} < \tau_{v_2,n}$.

      1. $\hat{y}(\tau_{v_1,n}) \, \hat{y}(\tau_{v_2,n}) < 0$. $\Rightarrow \hat{y}_n$ has 3 real roots $\Delta t_{1,n} < \Delta t_{2,n} < \Delta t_{3,n}$ (Fig. 5.5 (a)), which may be found by *Lemma* B.1. Indeed, $\Delta t_{1,n}$, $\Delta t_{2,n}$, and $\Delta t_{3,n}$ may be calculated by choosing $\alpha_0 < \tau_{v_1,n}$,

$\alpha_0 = \tau_{a,n}$, and $\alpha_0 > \tau_{v_2,n}$ respectively. The time δt_n when the stiffness is updated corresponds to the minimum positive value among $\Delta t_{1,n}$, $\tau_{v_1,n}$, $\Delta t_{2,n}$, $\tau_{v_2,n}$, and $\Delta t_{3,n}$;

2. $\hat{y}(\tau_{v_1,n})\,\hat{y}(\tau_{v_2,n}) = 0.$ $\Rightarrow$ The function $\hat{y}_n$ has two real roots $\Delta t_{1,n} < \Delta t_{2,n}$ (Fig. 5.5 (b)), which may be found by *Lemma* B.1. Indeed, if $\hat{y}(\tau_{v_1,n}) = 0$, $\Delta t_1 = \tau_{v_1,n}$ and Δt_2 may be found by choosing $\alpha_0 > \tau_{v_2,n}$. If $\hat{y}(\tau_{v_2,n}) = 0$, Δt_1 may be found by choosing $\alpha_0 < \tau_{v_1,n}$ and $\Delta t_2 = \tau_{v_2,n}$;

3. $\hat{y}(\tau_{v_1,n})\,\hat{y}(\tau_{v_2,n}) > 0.$ $\Rightarrow$ $\hat{y}_n$ has 1 real root Δt_n (Fig. 5.5 (c)), which may be found by *Lemma* B.1. In case of $A_2 \cdot \hat{y}(\tau_{v_1,n}) < 0$, $\alpha_0 < \tau_{v_1,n}$ is needed, and whether $A_3 \cdot \hat{y}(\tau_{v_2,n}) < 0$, $\alpha_0 > \tau_{v_2,n}$ should be chosen;

2. $A_1\,v_{a,n} = 0.$ $\Rightarrow$ v_n and a_n has the same root $\tau_{a,n}$, which means that $\hat{y}_n$ has a stationary point of inflexion at that time (Fig. 5.5 (d));

1. $\hat{y}(\tau_{a,n})\,j_{a,n} < 0.$ $\Rightarrow$ Δt_n may be found by *Lemma* B.1, by choosing $\alpha_0 > \tau_{a,n}$;

2. $\hat{y}(\tau_{a,n})\,j_{a,n} = 0.$ $\Rightarrow$ $\Delta t_n = \tau_{a,n}$;

3. $\hat{y}(\tau_{a,n})\,j_{a,n} > 0.$ $\Rightarrow$ Δt_n may be found by *Lemma* B.1, by choosing $\alpha_0 < \tau_{a,n}$.

δt_n is the minimum positive value between $\tau_{v,n}$ and Δt_n;

3. $A_1\,v_{a,n} > 0.$ $\Rightarrow$ v_n does not have any root and a_n vanish at $\tau_{a,n}$, which means $\hat{y}_n$ has a non stationary point of inflexion at that time (Fig. 5.5 (e)). From *Lemma* B.3, $\hat{y}_n$ has one real root, which may be found by choosing $\alpha_0 = \tau_{a,n}$.

5.4.2 Damped system with no stiffness

From the Eqs. (5.33), (5.34), and (5.35) we get

$$y_n(\tau) = y_{0,n} + C_1\tau + C_2\tau^2 + C_3\left(e^{-\frac{c_n}{m}\tau} - 1\right) \tag{5.81}$$

$$C_1 = -\left(\frac{\mathbf{F}_{0,n}}{c_n} + \frac{m}{c_n^2}F_{1,n}\right)$$

$$C_2 = \frac{F_{1,n}}{2c_n}$$

$$C_3 = -\frac{m}{c_n}\left(\dot{y}_{0,n} + \frac{\mathbf{F}_{0,n}}{c_n} + \frac{m}{c_n^2}F_{1,n}\right)$$

$$v_n(\tau) = C_1 + 2C_2\tau - \frac{c_n}{m}C_3 e^{-\frac{c_n}{m}\tau} \tag{5.82}$$

$$a_n(\tau) = 2C_2 + \left(\frac{c_n}{m}\right)^2 C_3 e^{-\frac{c_n}{m}\tau} \tag{5.83}$$

$$j_n(\tau) = -\left(\frac{c_n}{m}\right)^3 C_3 e^{-\frac{c_n}{m}\tau} \tag{5.84}$$

Also, from the Eqs. (5.57) and (5.81), we get

$$\hat{y}_n(\tau) = y_n(\tau) - \left(y_{0,n} + \frac{\Delta R_n}{k_n}\right) = C_0 + C_1\tau + C_2\tau^2 + C_3 e^{-\frac{c_n}{m}\tau} \tag{5.85}$$

$$C_0 = -\left(C_3 + \frac{\Delta R_n}{k_n}\right)$$

It is worth noting the behavior of $\hat{y}_n(\tau)$, $v_n(\tau)$, and $a_n(\tau)$ when $\tau \to \pm\infty$,

$$\lim_{\tau\to+\infty}\hat{y}_n(\tau) \stackrel{c_n\geq 0}{=} \begin{cases} C_0, & C_1 = C_2 = 0 \\ \text{sgn}(C_1)\cdot\infty, & C_1 \neq 0,\ C_2 = 0 \\ \text{sgn}(C_2)\cdot\infty, & C_2 \neq 0 \end{cases} \tag{5.86}$$

$$\lim_{\tau\to-\infty}\hat{y}_n(\tau) \stackrel{c_n\geq 0}{=} \begin{cases} C_0, & C_1 = C_2 = C_3 = 0 \\ -\text{sgn}(C_1)\cdot\infty, & C_1 \neq 0,\ C_2 = C_3 = 0 \\ +\text{sgn}(C_2)\cdot\infty, & C_2 \neq 0,\ C_3 = 0 \\ +\text{sgn}(C_3)\cdot\infty, & C_3 \neq 0 \end{cases} \tag{5.87}$$

116

$$\lim_{\tau \to +\infty} \hat{y}_n(\tau) \overset{c_n \leq 0}{=} \begin{cases} C_0, & C_1 = C_2 = C_3 = 0 \\ + \operatorname{sgn}(C_1) \cdot \infty, & C_1 \neq 0, \ C_2 = C_3 = 0 \\ + \operatorname{sgn}(C_2) \cdot \infty, & C_2 \neq 0, \ C_3 = 0 \\ + \operatorname{sgn}(C_3) \cdot \infty, & C_3 \neq 0 \end{cases} \tag{5.88}$$

$$\lim_{\tau \to -\infty} \hat{y}_n(\tau) \overset{c_n \leq 0}{=} \begin{cases} C_0, & C_1 = C_2 = 0 \\ - \operatorname{sgn}(C_1) \cdot \infty, & C_1 \neq 0, \ C_2 = 0 \\ + \operatorname{sgn}(C_2) \cdot \infty, & C_2 \neq 0 \end{cases} \tag{5.89}$$

$$\lim_{\tau \to +\infty} v_n(\tau) = \lim_{\tau \to +\infty} \left(C_1 + 2C_2\tau - \frac{c_n}{m} C_3 e^{-\frac{c_n}{m}\tau} \right) \overset{c_n \geq 0}{=} \begin{cases} C_1, & C_2 = 0 \\ \operatorname{sgn}(C_2) \cdot \infty, & C_2 \neq 0 \end{cases} \tag{5.90}$$

$$\lim_{\tau \to -\infty} v_n(\tau) \overset{c_n \geq 0}{=} \begin{cases} C_1, & C_2 = C_3 = 0 \\ - \operatorname{sgn}(C_2) \cdot \infty, & C_2 \neq 0, \ C_3 = 0 \\ - \operatorname{sgn}(C_3) \cdot \infty, & C_3 \neq 0 \end{cases} \tag{5.91}$$

$$\lim_{\tau \to +\infty} v_n(\tau) \overset{c_n \leq 0}{=} \begin{cases} C_1, & C_2 = C_3 = 0 \\ + \operatorname{sgn}(C_2) \cdot \infty, & C_2 \neq 0, \ C_3 = 0 \\ + \operatorname{sgn}(C_3) \cdot \infty, & C_3 \neq 0 \end{cases} \tag{5.92}$$

$$\lim_{\tau \to -\infty} v_n(\tau) \overset{c_n \leq 0}{=} \begin{cases} C_1, & C_2 = 0 \\ - \operatorname{sgn}(C_2) \cdot \infty, & C_2 \neq 0 \end{cases} \tag{5.93}$$

$$\lim_{\tau \to +\infty} a_n(\tau) = \lim_{\tau \to +\infty} \left[2C_2 + \left(\frac{c_n}{m} \right)^2 C_3 e^{-\frac{c_n}{m}\tau} \right] \overset{c_n \geq 0}{=} 2C_2 \tag{5.94}$$

$$\lim_{\tau \to -\infty} a_n(\tau) \overset{c_n \geq 0}{=} \begin{cases} 2C_2, & C_3 = 0 \\ \operatorname{sgn}(C_3) \cdot \infty, & C_3 \neq 0 \end{cases} \tag{5.95}$$

$$\lim_{\tau \to +\infty} a_n(\tau) \overset{c_n \leq 0}{=} \begin{cases} 2C_2, & C_3 = 0 \\ \operatorname{sgn}(C_3) \cdot \infty, & C_3 \neq 0 \end{cases} \tag{5.96}$$

$$\lim_{\tau \to -\infty} a_n(\tau) \overset{c_n \leq 0}{=} 2C_2 \tag{5.97}$$

As long as $C_3 \neq 0$, $j_n(\tau)$ never vanishes and $a_n(\tau)$ is strictly monotone. The acceleration roots are,

1. $C_2 = C_3 = 0. \Rightarrow a_n = 0 \ \forall \tau \in \mathbb{R}$;

2. $C_2 \neq 0, C_3 = 0 \ \lor \ C_2 = 0, C_3 \neq 0. \Rightarrow a_n \neq 0 \ \forall \tau \in \mathbb{R}$;

3. $C_2 C_3 < 0. \Rightarrow a_n$ has one root,

$$\tau_{a,n} = -\frac{m}{c_n} \ln \left[-2 \left(\frac{m}{c_n} \right)^2 \frac{C_2}{C_3} \right]$$

4. $C_2 C_3 > 0. \Rightarrow a_n$ does not have any real root.

In order to find the roots of $v_n(\tau)$, by recalling the Eqs. (5.82) and (5.90)–(5.97), we may conclude what follows,

1. $C_3 = 0$.

$$v_n(\tau_{v,n}) = 0 \ \Rightarrow \ C_1 + 2 C_2 \tau_{v,n} = 0 \ \Rightarrow \ \begin{cases} \tau_{v,n} = -\dfrac{C_1}{2 C_2}, \ C_2 \neq 0 \\[2mm] \nexists \tau_{v,n} \in \mathbb{R}, \ C_1 \neq 0, \ C_2 = 0 \\[2mm] \forall \tau_{v,n} \in \mathbb{R}, \ C_1 = C_2 = 0 \end{cases}$$

2. $C_1 = C_2 = 0, \ C_3 \neq 0. \Rightarrow v_n(\tau) \neq 0 \ \forall \tau \in \mathbb{R}$;

3. $C_1 \neq 0, \ C_2 = 0, \ C_3 \neq 0. \Rightarrow a_n$ never vanishes, hence v_n is strictly monotone on $\mathbb{R}$.

   1. $c_n > 0. \Rightarrow \lim_{\tau \to +\infty} v_n(\tau) = C_1$ and $\lim_{\tau \to -\infty} v_n(\tau) = -\mathrm{sgn}(C_3) \cdot \infty$

      1. $C_1 C_3 < 0. \Rightarrow v_n$ does not have any root;
      2. $C_1 C_3 > 0. \Rightarrow v_n$ has one root $\tau_{v,n}$, as shown in Fig. 5.3 (e),

      $$\tau_{v,n} = -\frac{m}{c} \ln \left(\frac{m}{c} \frac{C_1}{C_3} \right)$$

   2. $c_n < 0. \Rightarrow \lim_{\tau \to +\infty} v_n(\tau) = \mathrm{sgn}(C_3) \cdot \infty$ and $\lim_{\tau \to -\infty} v_n(\tau) = C_1$

      1. $C_1 C_3 < 0. \Rightarrow v_n$ has one root $\tau_{v,n}$ (*Lemma* B.2, Fig. 5.3 (e));
      2. $C_1 C_3 > 0. \Rightarrow v_n$ does not have any root;

4. $C_2 \neq 0, \ C_3 \neq 0$.

If $c_n > 0$ we get,

$$\lim_{\tau \to +\infty} a_n(\tau) = 2C_2$$

$$\lim_{\tau \to -\infty} a_n(\tau) = \text{sgn}(C_3) \cdot \infty$$

$$\lim_{\tau \to +\infty} v_n(\tau) = \text{sgn}(C_2) \cdot \infty$$

$$\lim_{\tau \to -\infty} v_n(\tau) = -\text{sgn}(C_3) \cdot \infty$$

If $c_n < 0$ we have,

$$\lim_{\tau \to +\infty} a_n(\tau) = \text{sgn}(C_3) \cdot \infty$$

$$\lim_{\tau \to -\infty} a_n(\tau) = 2C_2$$

$$\lim_{\tau \to +\infty} v_n(\tau) = \text{sgn}(C_3) \cdot \infty$$

$$\lim_{\tau \to -\infty} v_n(\tau) = -\text{sgn}(C_2) \cdot \infty$$

1. $C_2C_3 < 0. \Rightarrow a_n$ has one root $\tau_{a,n}$ (*Lemma* B.2);

    1. $C_3v_{a,n}c_n < 0. \Rightarrow v_n$ has two roots, $\tau_{v1,n}$ and $\tau_{v2,n}$, which may be found by *Lemma* B.4 choosing $\alpha_0 < \tau_{a,n}$ and $\alpha_0 > \tau_{a,n}$ respectively (Fig. 5.3 (a));

    2. $C_3v_{a,n}c_n = 0. \Rightarrow v_n$ has a unique root $\tau_{v,n} = \tau_{a,n}$ (Fig. 5.3 (b));

    3. $C_3v_{a,n}c_n > 0. \Rightarrow v_n$ does not have any real root (Fig. 5.3 (c));;

2. $C_2C_3 > 0. \Rightarrow a_n$ has no roots and v_n is strictly monotone. If $c_n < 0$, $\lim_{\tau \to +\infty} v_n(\tau) = \text{sgn}(C_3) \cdot \infty$ and $\lim_{\tau \to -\infty} v_n(\tau) = -\text{sgn}(C_2) \cdot \infty$. If $c_n > 0$, the limit values above have opposite sign. Both ways, v_n has one root $\tau_{v,n}$, which may be found $\forall \alpha_0 \in \mathbb{R}$ (*Lemma* B.2, Fig. 5.3 (d));

In order to find the roots of $\hat{y}_n$, by recalling the Eq. (5.85) and (5.86)–(5.89), what follows may be stated,

1. $C_3 = 0$.

    1. $C_2 \neq 0$.
    $$\Delta t_{1:2,n} = -\frac{C_1 \pm \sqrt{C_1^2 - 4C_0C_2}}{2C_2}$$

    2. $C_1 \neq 0, C_2 = 0. \Rightarrow \Delta t_n = -C_0/C_1$;

    3. $C_1 = C_2 = 0. \Rightarrow$ It is either $C_0 = 0$ and $\hat{y}(\tau) = 0 \forall \tau \in \mathbb{R}$, or $C_0 \neq 0$ and $\hat{y}(\tau) \neq 0 \forall \tau \in \mathbb{R}$. both ways, the system configuration does not change;

119

2. $C_1 = C_2 = 0, C_3 \neq 0$. Either $C_0/C_3 \geq 0$ and $\hat{y}_n$ does not have real roots, or $C_0/C_3 < 0$ and $\hat{y}_n$ has one real root, that is

$$C_0 + C_3 e^{-\frac{c_n}{m}\Delta t_n} = 0 \;\Rightarrow\; \Delta t_n = -\frac{m}{c_n} \ln\left(-\frac{C_0}{C_3}\right), \quad \frac{C_0}{C_3} < 0$$

3. $C_1 \neq 0, C_2 = 0, C_3 \neq 0. \Rightarrow a_n$ never vanishes and v_n is strictly monotone on $\mathbb{R}$. Also, when $c_n > 0$, $\lim_{\tau \to +\infty} \hat{y} = \text{sgn}(C_1) \cdot \infty$ and $\lim_{\tau \to -\infty} \hat{y} = \text{sgn}(C_3) \cdot \infty$. When $c_n < 0$, $\lim_{\tau \to +\infty} \hat{y} = \text{sgn}(C_3) \cdot \infty$ and $\lim_{\tau \to -\infty} \hat{y} = -\text{sgn}(C_1) \cdot \infty$.

1. $C_1 C_3 c_n < 0. \Rightarrow$ From the previous analysis we know that v_n has no roots. Therefore, $\hat{y}_n$ is strictly monotone and has one root Δt_n, as shown in Fig. 5.4 (d). Such root may be found by *Lemma* B.2, $\forall \alpha_0 \in \mathbb{R}$;

2. $C_1 C_3 c_n > 0. \Rightarrow v_n$ is strictly monotone and vanishes at $\tau_{v,n}$. Let $\hat{y}_{v,n} = \hat{y}(\tau_{v,n})$;

   1. $C_3 \hat{y}_{v,n} < 0. \Rightarrow \hat{y}_n$ has two roots, $\Delta t_{1,n}$ and $\Delta t_{2,n}$ (Fig. 5.4 (a)). Such roots may be found by *Lemma* B.4, by choosing $\alpha_0 < \tau_{v,n}$ and $\alpha_0 > \tau_{v,n}$ respectively;

   2. $C_3 \hat{y}_{v,n} = 0. \Rightarrow \hat{y}_n$ has one root $\Delta t_n = \tau_{v,n}$ (Fig. 5.4 (b));

   3. $C_3 \hat{y}_{v,n} > 0. \Rightarrow \hat{y}_n$ does not have any real root (Fig. 5.4 (c));

4. $C_2 C_3 < 0$. When $c_n > 0$, $\lim_{\tau \to +\infty} \hat{y}_n(\tau) = \text{sgn}(C_2) \cdot \infty$ and $\lim_{\tau \to -\infty} \hat{y}_n(\tau) = \text{sgn}(C_3) \cdot \infty$. When $c_n < 0$, the limit values above are switched;

1. $C_3 v_{a,n} c_n < 0. \Rightarrow a_n$ has a unique root $\tau_{a,n}$, and v_n has two roots, $\tau_{v_1,n}$ and $\tau_{v_2,n}$. Let $\hat{y}_{v_1,n} = \hat{y}(\tau_{v_1,n})$ and $\hat{y}_{v_2,n} = \hat{y}(\tau_{v_2,n})$.

   1. $\hat{y}_{v_1,n} \hat{y}_{v_2,n} < 0. \Rightarrow \hat{y}_n$ has 3 roots, $\Delta t_{1,n}$, $\Delta t_{2,n}$, and $\Delta t_{3,n}$ (Fig. 5.5 (a)), which may be found by applying *Lemma* B.4, by choosing $\alpha_0 < \tau_{v_1,n}$, $\alpha_0 = \tau_{a,n}$, and $\alpha_0 > \tau_{v_2,n}$ respectively;

   2. $\hat{y}_{v_1,n} \hat{y}_{v_2,n} = 0. \Rightarrow \hat{y}_n$ has 2 real roots (Fig. 5.5 (b)).

      1. $\hat{y}_{v_1,n} = 0. \Rightarrow \Delta t_1 = \tau_{v_1,n}$ and, from *Lemma* B.1, Δt_2 may be found by choosing $\alpha_0 > \tau_{v_2,n}$;

      2. $\hat{y}_{v_2,n} = 0. \Rightarrow \Delta t_2 = \tau_{v_2,n}$ and, from *Lemma* B.1, Δt_1 may be found by choosing $\alpha_0 < \tau_{v_1,n}$;

      3. $\hat{y}_{v_1,n} \hat{y}_{v_2,n} > 0. \Rightarrow$ From *Lemma* B.1, the unique root Δt_n may be found by choosing the initial guess α_0 properly (Fig. 5.5 (c));

         1. $c_n > 0, C_3 \hat{y}_{v_1,n} < 0. \Rightarrow \Delta t_n$ may be found from $\alpha_0 < \tau_{v_1,n}$;

2. $c_n > 0, C_3\hat{y}_{v_1,n} > 0. \Rightarrow \Delta t_n$ may be found from $\alpha_0 > \tau_{v_2,n}$;

3. $c_n < 0, C_2\hat{y}_{v_1,n} < 0. \Rightarrow \Delta t_n$ may be found from $\alpha_0 < \tau_{v_1,n}$;

4. $c_n < 0, C_2\hat{y}_{v_1,n} > 0. \Rightarrow \Delta t_n$ may be found from $\alpha_0 > \tau_{v_2,n}$;

2. $C_3 v_{a,n} c_n = 0. \Rightarrow v_n$ and a_n have the same root $\tau_{v,n} = \tau_{a,n}$. $\hat{y}_n$ has one root either (Fig. 5.5 (d)), which may be found by *Lemma* B.1;

  1. $\hat{y}_{a,n} j_{a,n} < 0. \Rightarrow \Delta t_n$ may be found from $\alpha_0 > \tau_{a,n}$;

  2. $\hat{y}_{a,n} j_{a,n} = 0. \Rightarrow \Delta t_n = \tau_{a,n}$;

  3. $\hat{y}_{a,n} j_{a,n} > 0. \Rightarrow \Delta t_n$ may be get from $\alpha_0 < \tau_{a,n}$;

3. $C_3 v_{a,n} c_n > 0. \Rightarrow v_n$ has no roots and $\hat{y}_n$ has a unique root Δt_n, as shown in (Fig. 5.5 (e)). Such root may be found by *Lemma* B.3, setting $\alpha_0 = \tau_{a,n}$;

5. $C_2 C_3 > 0. \Rightarrow v_n$ has one root $\tau_{v,n}$ and a_n has no roots. Also,when $c_n > 0$, $\lim_{\tau \to +\infty} \hat{y}_n(\tau) = \text{sgn}(C_2) \cdot \infty$ and $\lim_{\tau \to -\infty} \hat{y}_n(\tau) = \text{sgn}(C_3) \cdot \infty$. When $c_n < 0$, the above limit values are switched.

  1. $C_2 \hat{y}_{v,n} < 0. \Rightarrow \hat{y}_n$ has two roots, $\Delta t_{1,n}$ and $\Delta t_{2,n}$, as shown in Fig. 5.4 (a). Such roots may be found by *Lemma* B.4;

  2. $C_2 \hat{y}_{v,n} = 0. \Rightarrow \hat{y}_n$ has one root $\Delta t_n = \tau_{v,n}$ (Fig. 5.4 (b));

  3. $C_2 \hat{y}_{v,n} > 0. \Rightarrow \hat{y}_n$ does not have any real root (Fig. 5.4 (c)).

In order to get the actual time δt_n when the spring stiffness does change, in case of multiple solutions $\tau_{v_q,n}$ and $\Delta t_{q,n}$, $q = 1, 2, \ldots$, the minimum positive one, whether it exist, is needed.

5.4.3 Undamped system with no stiffness

From Eqs. (5.37), (5.38), and (5.57) we get

$$y_n(\tau) = A_0 + A_1\tau + A_2\tau^2 + A_3\tau^3 \tag{5.98}$$

$$A_0 = y_{0,n}, \quad A_1 = \dot{y}_{0,n}, \quad A_2 = -\frac{\mathbf{F}_{0,n}}{2m}, \quad A_3 = \frac{F_{1,n}}{6m}$$

$$\hat{y}_n(\tau) = \hat{a}_0 + A_1\tau + A_2\tau^2 + A_3\tau^3, \quad \hat{a}_0 = A_0 - \left(y_{0,n} + \frac{\Delta R_n}{k_n}\right) \tag{5.99}$$
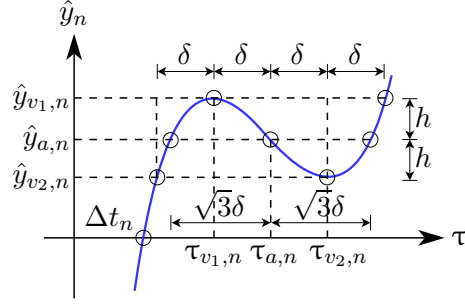
Fig. 5.6. Cubic displacement function roots of a linear oscillator under linear excitation.

$$v_n(\tau) = A_1 + 2A_2\tau + 3A_3\tau^2 \tag{5.100}$$

$$a_n(\tau) = 2A_2 + 6A_3\tau \tag{5.101}$$

$$j_n(\tau) = 6A_3 \tag{5.102}$$

Since the Eq. (5.100) is quadratic, the roots of v_n are

$$\tau_{v,n} = \begin{cases} -\dfrac{A_2 \pm \sqrt{A_2^2 - 3A_1 A_3}}{3A_3}, & A_3 \neq 0 \\[2ex] -\dfrac{A_1}{2A_2}, & A_2 \neq 0, \ A_3 = 0 \\[2ex] \nexists \tau \in \mathbb{R}, & A_1 \neq 0, \ A_2 = A_3 = 0 \\[1ex] \forall \tau \in \mathbb{R}, & A_1 = A_2 = A_3 = 0 \end{cases} \tag{5.103}$$

As far as the roots of the Eq. (5.99) are concerned, according to Nickalls [70] the following quantities may be defined (Fig. 5.6),

$$\tau_{a,n} = -\frac{A_2}{3A_3}, \quad \hat{y}_{a,n} = \frac{2}{27}\frac{A_2^3}{A_3^2} - \frac{A_1 A_2}{3A_3} + \hat{a}_0 \tag{5.104}$$

$$\delta^2 = \frac{A_2^2 - 3A_1 A_3}{9A_3^2}, \quad h = 2A_3\delta^3$$

where $(\tau_{a,n}, \hat{y}_{a,n})$ are the coordinates of the inflexion point of the cubic function $\hat{y}_n(\tau)$, $\delta = \tau_{v2,n} - \tau_{a,n} = \tau_{a,n} - \tau_{v1,n}$ is the distance along the τ axis between the inflexion point and the stationary points, and $h = \hat{y}_{v2,n} - \hat{y}_{a,n} = \hat{y}_{a,n} - \hat{y}_{v1,n}$ is the projection of the same distance on the $\hat{y}_n$ axis.

122

In case of $A_3 = 0$, the Eq. (5.99) becomes quadratic, and the roots of $\hat{y}_n$ are

$$
\Delta t_n = \begin{cases}
-\dfrac{A_1 \pm \sqrt{A_1^2 - 4\hat{a}_0 A_2}}{2A_2}, & A_2 \neq 0 \\[2ex]
-\dfrac{\hat{a}_0}{A_1}, & A_1 \neq 0, \ A_2 = 0 \\[2ex]
\nexists \tau \in \mathbb{R}, & \hat{a}_0 \neq 0, \ A_1 = A_2 = 0 \\[2ex]
\forall \tau \in \mathbb{R}, & \hat{a}_0 = A_1 = A_2 = 0
\end{cases} \tag{5.105}
$$

In case of $A_3 \neq 0$, since the coefficients $A_0, \ldots, A_3$ are all real and because of the intermediate value theorem, $\hat{y}_n$ has at least one real root. In general, the number of the real roots and their algebraic multiplicity depends on the sign of the discriminant $\hat{y}_{a,n}^2 - h^2$. A total number of three cases may be considered.

Positive discriminant $\circ$ $\hat{y}_{a,n}^2 - h^2 > 0$

Under these circumstances there are one real root and two complex conjugate roots,

$$
w_1 = \sqrt[3]{\frac{1}{2A_3}\left(-\hat{y}_{a,n} - \sqrt{\hat{y}_{a,n}^2 - h^2}\right)}, \quad w_2 = \sqrt[3]{\frac{1}{2A_3}\left(-\hat{y}_{a,n} + \sqrt{\hat{y}_{a,n}^2 - h^2}\right)}
$$

$$
\Delta t_{1,n} = \tau_{a,n} + w_1 + w_2 \tag{5.106}
$$

$$
\Delta t_{2:3,n} = \tau_{a,n} - w_1 \left(\frac{1}{2} \pm \frac{\sqrt{3}}{2}i\right) - w_2 \left(\frac{1}{2} \mp \frac{\sqrt{3}}{2}i\right) \tag{5.107}
$$

Zero discriminant $\circ$ $\hat{y}_{a,n}^2 - h^2 = 0$

When the discriminant vanishes, we get

$$
\delta = \sqrt[3]{\frac{\hat{y}_{a,n}}{2A_3}}
$$

$$
\Delta t_{1:2,n} = \tau_{a,n} + \delta \quad \text{(algebraic multiplicity 2)} \tag{5.108}
$$

$$
\Delta t_{3,n} = \tau_{a,n} - 2\delta. \tag{5.109}
$$

Whether $\hat{y}_{a,n} = h = 0$, then $\delta = 0$ and there are three equal roots at $\tau = \tau_{a,n}$.

Negative discriminant $\circ \; \hat{y}_{a,n}^2 - h^2 < 0$

As long as the discriminant becomes negative, $\hat{y}_n$ has three distinct real roots,

$$\varsigma = \frac{1}{3} \arccos\left(-\frac{\hat{y}_{a,n}}{h}\right)$$

$$\Delta t_{1,n} = \tau_{a,n} + 2\delta \cos \varsigma \tag{5.110}$$

$$\Delta t_{2,n} = \tau_{a,n} + 2\delta \cos\left(\varsigma + \frac{2}{3}\pi\right) \tag{5.111}$$

$$\Delta t_{2,n} = \tau_{a,n} + 2\delta \cos\left(\varsigma + \frac{4}{3}\pi\right) \tag{5.112}$$

Again, in case of multiple solutions $\tau_{v_q,n}$ and $\Delta t_{q,n}$, $q = 1, 2, \ldots$, the minimum positive one is needed, in order to get the time δt_n when a stiffness update is actually accomplished.

5.4.4 Underdamped system with positive stiffness – overdamped system with negative stiffness

From the Eqs. (5.43), (5.44), and (5.45) we have

$$y_n(\tau) = e^{-\zeta_n \omega_n \tau}\left(A_1 \cos(\omega_{d,n}\tau) + A_2 \sin(\omega_{d,n}\tau)\right) + A_3\tau + A_4 \tag{5.113}$$

$$A_1 = \frac{\mathbf{F}_{0,n}}{k_n} + 2\zeta_n \frac{F_{1,n}}{\omega_n k_n}$$

$$A_2 = \frac{1}{\omega_{d,n}}\left[\dot{y}_{0,n} + \frac{\mathbf{F}_{0,n}}{k_n}\zeta_n\omega_n + \frac{F_{1,n}}{k_n}(2\zeta_n^2 - 1)\right]$$

$$A_3 = \frac{F_{1,n}}{k_n}$$

$$A_4 = y_{0,n} - \frac{\mathbf{F}_{0,n}}{k_n} - 2\zeta_n \frac{F_{1,n}}{\omega_n k_n}$$

$$\tag{5.114}$$

$$v_n(\tau) = e^{-\zeta_n \omega_n \tau}\left(B_1 \cos(\omega_{d,n}\tau) + B_2 \sin(\omega_{d,n}\tau)\right) + A_3 \tag{5.115}$$

$$B_1 = -\zeta_n\omega_n A_1 + \omega_{d,n} A_2$$

$$B_2 = -\zeta_n\omega_n A_2 - \omega_{d,n} A_1$$

$$a_n(\tau) = e^{-\zeta_n \omega_n \tau} \left(C_1 \cos(\omega_{d,n}\tau) + C_2 \sin(\omega_{d,n}\tau) \right) \tag{5.116}$$

$$C_1 = -\zeta_n \omega_n B_1 + \omega_{d,n} B_2$$

$$C_2 = -\zeta_n \omega_n B_2 - \omega_{d,n} B_1$$

$$j_n(\tau) = e^{-\zeta_n \omega_n \tau} \left(D_1 \cos(\omega_{d,n}\tau) + D_2 \sin(\omega_{d,n}\tau) \right) \tag{5.117}$$

$$D_1 = -\zeta_n \omega_n C_1 + \omega_{d,n} C_2$$

$$D_2 = -\zeta_n \omega_n C_2 - \omega_{d,n} C_1$$

Also, from the Eq. (5.57) we get

$$\hat{y}_n(\tau) = e^{-\zeta_n \omega_n \tau} \left(A_1 \cos(\omega_{d,n}\tau) + A_2 \sin(\omega_{d,n}\tau) \right) + A_3 \tau + \hat{A}_4 \tag{5.118}$$

$$\hat{A}_4 = A_4 - \left(y_{0,n} + \frac{\Delta R_n}{k_n} \right) \tag{5.119}$$

The roots of $j_n(\tau)$ depend on the values of D_1 and D_2,

1. $D_1 = D_2 = 0. \Rightarrow j_n(\tau) = 0 \; \forall \tau \in \mathbb{R}$;

2. $D_1 \neq 0, D_2 = 0. \Rightarrow \cos(\omega_n \tau_{j,n}) = 0 \;\Rightarrow\; \tau_{j,n} = \dfrac{\pi}{\omega_{d,n}} \left(q + \dfrac{1}{2} \right), \; q \in \mathbb{Z}_0$;

3. $D_1 = 0, D_2 \neq 0. \Rightarrow \sin(\omega_n \tau_{j,n}) = 0 \;\Rightarrow\; \tau_{j,n} = \dfrac{q\pi}{\omega_{d,n}}, \; q \in \mathbb{Z}_0$;

4. $D_1 \neq 0, D_2 \neq 0. \;\Rightarrow\;$ If $\cos(\omega_n \tau_{j,n}) = 0 \;\Rightarrow\; \sin(\omega_n \tau_{j,n}) = \pm 1 \;\Rightarrow\; D_2 = 0$. Therefore $\cos(\omega_n \tau_{j,n}) \neq 0$, and $D_1 + D_2 \tan(\omega_{d,n}\tau_{j,n}) = 0$, which implies

$$\tau_{j,n} = \frac{1}{\omega_{d,n}} \left(\arctan\left(-\frac{D_1}{D_2} \right) + q\pi \right), \; q \in \mathbb{Z}_0$$

The first q positive roots are put in the following order,

$$0 < \tau_{j+1,n} < \tau_{j+2,n} < \cdots < \tau_{j+q,n}$$

while the negatives are

$$0 > \tau_{j-1,n} > \tau_{j-2,n} > \cdots > \tau_{j-q,n}.$$

The roots of $a_n(\tau)$ depend on the values of C_1 and C_2,

1. $C_1 = C_2 = 0. \Rightarrow a_n(\tau) = 0 \ \forall \tau \in \mathbb{R}$;

2. $C_1 \neq 0, C_2 = 0. \Rightarrow \cos(\omega_n \tau_{a,n}) = 0 \Rightarrow \tau_{a,n} = \dfrac{\pi}{\omega_{d,n}}\left(q + \dfrac{1}{2}\right), \ q \in \mathbb{Z}_0$;

3. $C_1 = 0, C_2 \neq 0. \Rightarrow \sin(\omega_n \tau_{a,n}) = 0 \Rightarrow \tau_{a,n} = \dfrac{q\pi}{\omega_{d,n}}, \ q \in \mathbb{Z}_0$;

4. $C_1 \neq 0, C_2 \neq 0. \Rightarrow$ If $\cos(\omega_n \tau_{a,n}) = 0 \Rightarrow \sin(\omega_n \tau_{a,n}) = \pm 1 \Rightarrow C_2 = 0.$
   Therefore $\cos(\omega_n \tau_{a,n}) \neq 0$, and $C_1 + C_2 \tan(\omega_{d,n} \tau_{a,n}) = 0$, which implies

$$\tau_{a,n} = \frac{1}{\omega_{d,n}}\left(\arctan\left(-\frac{C_1}{C_2}\right) + q\pi\right), \ q \in \mathbb{Z}_0$$

Again, the roots are put in the following order,

$$\tau_{a-q,n} < \tau_{a-q+1,n} < \cdots < \tau_{a-1,n} < 0 < \tau_{a+1,n} < \tau_{a+2,n} < \cdots < \tau_{a+q,n}$$

As far as the velocity is concerned, it may be noted that such function is nothing but a sine or cosine function with an exponentially decreasing amplitude. Also, it is translated along the v axis by a quantity A_3. When $A_3 = 0$, it is straight forward to find the roots of $v_n(\tau)$. Indeed,

$$A_3 = 0 \quad \Rightarrow \quad v_n(\tau_{v,n}) = 0 \quad \Leftrightarrow \quad B_1 \cos(\omega_{d,n} \tau_{v,n}) + B_2 \sin(\omega_{d,n} \tau_{v,n}) = 0$$

1. $B_1 = B_2 = 0. \Rightarrow v_n(\tau) = 0 \ \forall \ \tau \in \mathbb{R}$;

2. $B_1 \neq 0, B_2 = 0. \Rightarrow \cos(\omega_{d,n} \tau_{v,n}) = 0 \Rightarrow \omega_{d,n} \tau_{v,n} = \left(q + \dfrac{1}{2}\right)\pi, \ q \in \mathbb{Z}_0$

$$\tau_{v,n} = \frac{\pi}{\omega_{d,n}}\left(q + \frac{1}{2}\right), \ q \in \mathbb{Z}_0$$

3. $B_1 = 0, B_2 \neq 0. \Rightarrow \sin(\omega_{d,n} \tau_{v,n}) = 0 \Rightarrow \omega_{d,n} \tau_{v,n} = q\pi \Rightarrow \tau_{v,n} = \dfrac{q\pi}{\omega_{d,n}}, \ q \in \mathbb{Z}_0$;

4. $B_1 \neq 0, B_2 \neq 0. \Rightarrow \cos(\omega_{d,n} \tau_{v,n}) \neq 0 \Rightarrow B_1 + B_2 \tan(\omega_{d,n} \tau_{v,n}) = 0$

$$\tau_{v,n} = -\frac{1}{\omega_{d,n}}\left(\arctan\left(\frac{B_1}{B_2}\right) + q\pi\right), \ q \in \mathbb{Z}_0$$

126

When $A_3 \neq 0$, it is useful to rewrite v_n as it follows

$$v_n(\tau) = e^{-\zeta_n \omega_n \tau} B \cos(\omega_{d,n} \tau + \phi_v) + A_3 \qquad (5.120)$$

where $B = \sqrt{B_1^2 + B_2^2}$ and ϕ_v is the phase angle given in §C. Now let us consider the case $\zeta_n \neq 0$, and let the time τ_n^* be defined as it follows,

$$\tau_n^* = \begin{cases} -\dfrac{1}{\zeta_n \omega_n} \ln \left| \dfrac{A_3}{B_2} \right|, & C_1 \neq 0, C_2 = 0 \\[3mm] -\dfrac{1}{\zeta_n \omega_n} \ln \left| \dfrac{A_3}{B_1} \right|, & C_1 = 0, C_2 \neq 0 \\[3mm] -\dfrac{1}{\zeta_n \omega_n} \ln \left| \dfrac{A_3}{B \sqrt{1 - \zeta_n^2}} \right|, & C_1 C_2 \neq 0 \end{cases} \qquad (5.121)$$

It might be shown that, depending on the sign of c_n, before or after τ_n^* the function $v_n(\tau)$ can not have any real root ($c_n < 0$ or $c_n > 0$ respectively), because the function sign is constant. For example, if $c_n < 0$, $C_1 \neq 0$ and $C_2 = 0$, recalling the roots of the acceleration function, we have

$$\tau_{a,n} = \frac{\pi}{\omega_{d,n}} \left(q + \frac{1}{2} \right)$$

$$|v_n(\tau_{a,n}) - A_3| = e^{-\zeta_n \omega_n \tau_{a,n}} |B_1 \cos(\omega_{d,n} \tau_{a,n}) + B_2 \sin(\omega_{d,n} \tau_{a,n})| = |B_2| e^{-\zeta_n \omega_n \tau_{a,n}}$$

If $\tau_{a,n} \leq \tau_n^*$, we get

$$\tau_{a,n} \leq \tau_n^* \Leftrightarrow \tau_{a,n} \leq -\frac{1}{\zeta_n \omega_n} \ln \left| \frac{A_3}{B_2} \right| \Leftrightarrow -\zeta_n \omega_n \tau_{a,n} \leq \ln \left| \frac{A_3}{B_2} \right| \Leftrightarrow \exp(-\zeta_n \omega_n \tau_{a,n}) \leq \left| \frac{A_3}{B_2} \right| \Leftrightarrow$$

$$\Leftrightarrow |B_2| \exp(-\zeta_n \omega_n \tau_{a,n}) \leq |A_3| \Leftrightarrow |v_n(\tau_{a,n}) - A_3| \leq |A_3| \Leftrightarrow -|A_3| \leq v_n(\tau_{a,n}) - A_3 \leq |A_3|$$

$$A_3 < 0 \Rightarrow |A_3| = -A_3 \Rightarrow 2A_3 \leq v_n(\tau_{a,n}) \leq 0$$
$$A_3 > 0 \Rightarrow |A_3| = +A_3 \Rightarrow 0 \leq v_n(\tau_{a,n}) \leq 2A_3$$

The equations above show that $\tau_{a,n} = \tau_n^*$ implies $v_n(\tau_{a,n}) = 0$, and $\tau_{a,n} < \tau_n^*$ implies $\mathrm{sgn}(v_n(\tau_{a,n})) = \mathrm{sgn}(A_3) = \pm 1$. Then, taking into account the proprieties of the function (5.120), we may state that $\mathrm{sgn}(v_n(\tau)) = \mathrm{sgn}(A_3)$, $\forall \tau < \tau_n^*$.

127

5.7 (a).

5.7 (b).

5.7 (c).

5.7 (d).

5.7 (e).

5.7 (f).

5.7 (g).
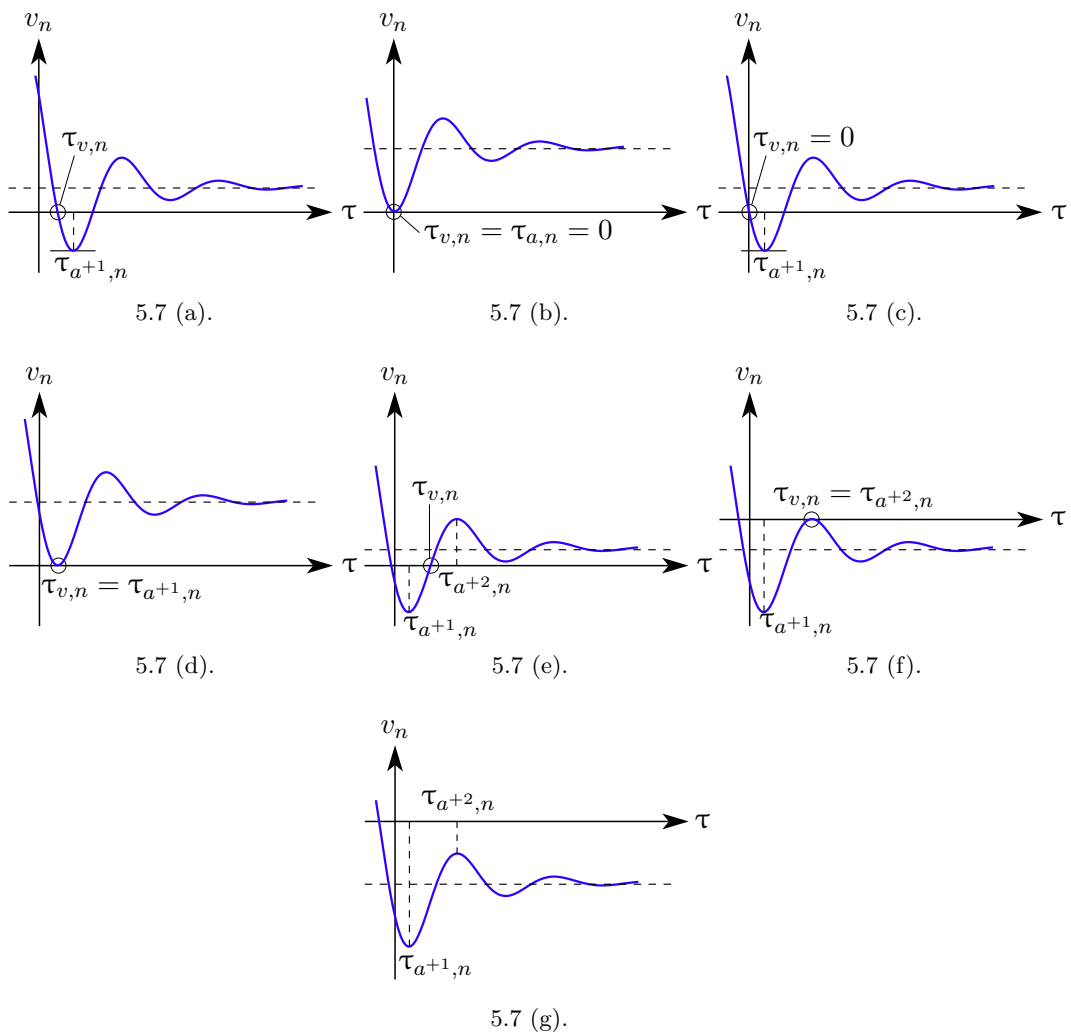
Fig. 5.7. Sinusoidal velocity function roots of a linear oscillator with positive damping coefficient.

128

When $\tau_n^* > 0$, by using the notations $v_{0,n} = v_n(0)$, $v_{a+1,n} = v_n(\tau_{a+1,n})$, $v_{a+2,n} = v_n(\tau_{a+2,n})$, and $a_{0,n} = a_n(0)$, we may find the roots of v_n in case of $c_n > 0$,

1. $B_1 = B_2 = 0. \Rightarrow v_n(\tau) = A_3$. Thus, if $A_3 = 0$, $v_n(\tau) = 0 \ \forall \tau \in \mathbb{R}$, and if $A_3 \neq 0$, v_n does not have any real root.

2. $B_1^2 + B_2^2 > 0$.

    1. $v_{0,n} v_{a+1,n} < 0. \Rightarrow \tau_{v,n} \in (0, \tau_{a+1,n})$, and it may be calculated via Newton–Raphson method (*Lemma* B.1). If $\tau_{j+1,n} < \tau_{a+1,n}$, a good initial guess is $\alpha_0 = \tau_{j+1,n}$, otherwise it is $\alpha_0 = \tau_{j-1,n}$ (Fig. 5.7 (a));

    2. $v_{0,n} v_{a+1,n} \geq 0$.

        1. $v_{a+1,n} = 0. \Rightarrow \tau_{v,n} = \tau_{a+1,n}$, and there is no jump of the system configuration from a branch of the $R-y$ diagram to another (Fig. 5.7 (d));

        2. $v_{a+1,n} \neq 0. \Rightarrow$ If $v_{0,n} = 0$, then $\tau_{v,n} = 0$, and it is either $a_{0,n} = 0$ (Fig. 5.7 (b)) or $a_{0,n} \neq 0$ (Fig. 5.7 (c)). In the latter case, at $\tau_{v,n} = 0$ there is a jump of the system configuration from a branch of the $R-y$ diagram the other one. The first positive root $\tau_{v+1,n}$ is needed;

            1. $v_{a+1,n} v_{a+2,n} < 0. \Rightarrow \tau_{v+1,n} \in (\tau_{a+1,n}, \tau_{a+2,n})$, and this root can be found by choosing an appropriate value for α_0 (*Lemma* B.1, Fig. 5.7 (e)),

                - $\tau_{j+1,n} > \tau_{a+1,n}. \Rightarrow \alpha_0 = \tau_{j+1,n}$;
                - $\tau_{j+1,n} < \tau_{a+1,n}. \Rightarrow \alpha_0 = \tau_{j+2,n}$;

            2. $v_{a+1,n} v_{a+2,n} = 0. \Rightarrow v_{a+2,n} = 0 \Rightarrow \tau_{v+1,n} = \tau_{a+2,n}$, and there is not any jump of the spring configuration (Fig. 5.7 (f));

            3. $v_{a+1,n} v_{a+2,n} > 0. \Rightarrow v_n$ has no positive roots (Fig. 5.7 (g)).

When $\zeta_n = 0$, the roots of v_n may be found in a closed form,

$$v_n(\tau_{v,n}) = B\cos(\omega_n \tau_{v,n} + \phi_v) + A_3 = 0 \quad \Rightarrow \quad \cos(\omega_n \tau_{v,n} + \phi_v) = -\frac{A_3}{B}$$

$$\tau_{v,n} = \frac{1}{\omega_n}\left[2q\pi \pm \arccos\left(-\frac{A_3}{B}\right) - \phi_v\right], \ q \in \mathbb{Z}_0 \tag{5.122}$$

When $c_n < 0$, it is useful to find the stationary point $\tau_{a_q,n} \geq \tau_n^*$ closest to τ_n^*, which is implicitly defined by the following equation

$$q = \lfloor q^* \rfloor + 1, \ \tau_{a_{q^*},n} = \tau_n^*,$$

129

5.8 (a).

5.8 (b).

5.8 (c).

5.8 (d).

5.8 (e).

5.8 (f).

5.8 (g).

5.8 (h).

5.8 (i).
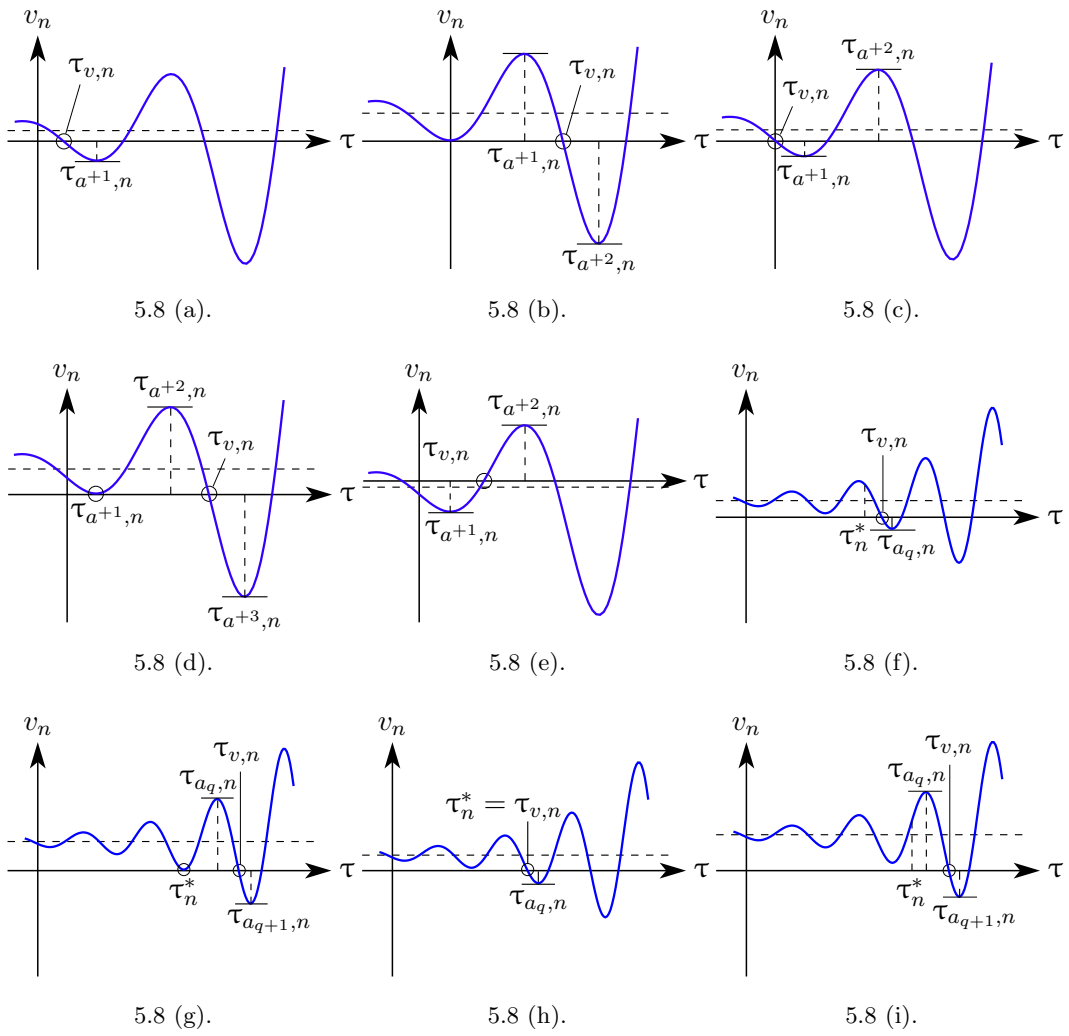
Fig. 5.8. Sinusoidal velocity function roots of a linear oscillator with negative damping coefficient.

where $\lfloor q^* \rfloor$ is the largest integer less than or equal to q^*. In order to obtain an explicit value of q^*, the equation above needs to be solved for the three following cases,

1. $C_1 \neq 0, C_2 = 0$.

$$\tau_{a_{q^*},n} = \frac{\pi}{\omega_{d,n}} \left(q^* + \frac{1}{2} \right) = \tau_n^* \;\Rightarrow\; q^* = \frac{\omega_{d,n}}{\pi} \tau_n^* - \frac{1}{2}$$

2. $C_1 = 0, C_2 \neq 0$.

$$\tau_{a_{q^*},n} = \frac{q^* \pi}{\omega_{d,n}} = \tau_n^* \;\Rightarrow\; q^* = \frac{\omega_{d,n}}{\pi} \tau_n^*$$

3. $C_1 C_2 \neq 0$.

$$\tau_{a_{q^*},n} = \frac{1}{\omega_{d,n}} \left(\arctan\left(-\frac{C_1}{C_2} \right) + q^* \pi \right) = \tau_n^* \;\Rightarrow\; q^* = \frac{\omega_{d,n}}{\pi} \tau_n^* + \frac{1}{\pi} \arctan\left(\frac{C_1}{C_2} \right)$$

Also, it is useful to know the largest value of $\tau_{j_q,n} \leq \tilde{\tau}$, $\forall \tilde{\tau} > 0$, which is implicitly defined by the following equation

$$q = \lfloor \tilde{q} \rfloor, \;\; \tau_{a_{\tilde{q}},n} = \tilde{\tau},$$

where $\lfloor \tilde{q} \rfloor$ is the largest integer less than or equal to $\tilde{q}$. Explicit values of $\tilde{q}$ are,

1. $D_1 \neq 0, D_2 = 0$.

$$\tau_{j_{\tilde{q}},n} = \frac{\pi}{\omega_{d,n}} \left(\tilde{q} + \frac{1}{2} \right) = \tilde{\tau} \;\Rightarrow\; \tilde{q} = \frac{\omega_{d,n}}{\pi} \tilde{\tau} - \frac{1}{2}$$

2. $D_1 = 0, D_2 \neq 0$.

$$\tau_{j_{\tilde{q}},n} = \frac{\tilde{q} \pi}{\omega_{d,n}} = \tilde{\tau} \;\Rightarrow\; \tilde{q} = \frac{\omega_{d,n}}{\pi} \tilde{\tau}$$

3. $D_1 D_2 \neq 0$.

$$\tau_{j_{\tilde{q}},n} = \frac{1}{\omega_{d,n}} \left(\arctan\left(-\frac{D_1}{D_2} \right) + \tilde{q} \pi \right) = \tilde{\tau} \;\Rightarrow\; \tilde{q} = \frac{\omega_{d,n}}{\pi} \tilde{\tau} + \frac{1}{\pi} \arctan\left(\frac{D_1}{D_2} \right)$$

By using the notations $v_n^* = v_n(\tau_n^*)$, $v_{a_q,n} = v_n(\tau_{a_q,n})$, and $a_n^* = a_n(\tau_n^*)$, the roots of v_n are the following,

131

1. $\tau_n^* \leq 0$.

   1. $v_{0,n}v_{a+1,n} < 0. \Rightarrow \tau_{v,n} \in (\tau_{0,n}, \tau_{a+1,n})$ (Fig. 5.8 (a)), and it may be calculated by the Newton–Raphson method, with $\alpha_0 = \tau_{j_q,n}$, $q = \lfloor \tilde{q}(\tilde{\tau}) \rfloor$ and $\tilde{\tau} = \tau_{a+1,n}$ (*Lemma* B.1);

   2. $v_{0,n}v_{a+1,n} = 0. \Rightarrow$ Since $\tau_n^* \leq 0$, must be $v_{0,n} = 0$ and $\tau_{v,n} = 0$. The first positive root is $\tau_{v+1,n} \in (\tau_{a+1,n}, \tau_{a+2,n})$, and it may be found by choosing $\alpha_0 = \tau_{j_q,n}$, $q = \lfloor \tilde{q}(\tilde{\tau} = \tau_{a+2,n}) \rfloor$;

      1. $a_{0,n} = 0. \Rightarrow$ At $\tau = 0$ there is not any jump of the system configuration from a branch of the $R - y$ diagram to another (Fig. 5.8 (b));

      2. $a_{0,n} \neq 0. \Rightarrow$ At $\tau = 0$ there is a jump of the system configuration from a branch of the $R - y$ diagram to another (Fig. 5.8 (c));

   3. $v_{0,n}v_{a+1,n} > 0. \Rightarrow \tau_{v,n} \in (\tau_{a+1,n}, \tau_{a+2,n})$, and it may be found by choosing $\alpha_0 = \tau_{j_q,n}$, $q = \lfloor \tilde{q}(\tilde{\tau} = \tau_{a+2,n}) \rfloor$ (Fig. 5.8 (e));

2. $\tau_n^* > 0. \Rightarrow \tau_{a_q,n}$ is needed, where $q = \lceil q^* \rceil$;

   1. $v_n^* v_{a_q,n} < 0. \Rightarrow \tau_{v,n} \in (\tau_n^*, \tau_{a_q,n})$ (Fig. 5.8 (f)), and it may be calculated by the Newton–Raphson method, with $\alpha_0 = \tau_{j_\epsilon,n}$, $\epsilon = \lfloor \tilde{\epsilon}(\tilde{\tau}) \rfloor$ and $\tilde{\tau} = \tau_{a_q,n}$ (*Lemma* B.1);

   2. $v_n^* v_{a_q,n} = 0. \Rightarrow v_n^* = 0$ and $\tau_{v,n} = \tau_n^*$;

      1. $a_n^* = 0. \Rightarrow$ There is not any jump of the system configuration from a branch of the $R - y$ diagram to another (Fig. 5.8 (g));

      2. $a_n^* \neq 0. \Rightarrow$ There is a jump of the system configuration from a branch of the $R - y$ diagram to another at $\tau = \tau_n^*$ (Fig. 5.8 (h));

   3. $v_n^* v_{a_q,n} > 0. \Rightarrow \tau_{v,n} \in (\tau_{a_q,n}, \tau_{a_{q+1},n})$, and it may be found by choosing $\alpha_0 = \tau_{j_\epsilon,n}$, $\epsilon = \lfloor \tilde{\epsilon}(\tilde{\tau} = \tau_{a_{q+1},n}) \rfloor$ (*Lemma* B.1, Fig. 5.8 (i)).

Referring to the Eqs. (5.129) and (5.118), we may rewrite the periodic part of $\hat{y}_n$ and the acceleration as it follows,

$$\tilde{y}_n(\tau) = Ae^{-\zeta_n \omega_n \tau} \cos(\omega_{d,n} \tau + \phi_y) \tag{5.123}$$

$$a_n(\tau) = Ce^{-\zeta_n \omega_n \tau} \cos(\omega_{d,n} \tau + \phi_a) \tag{5.124}$$

where the vibration amplitudes (A, C) and the phase angles (ϕ_y, ϕ_a) are given in § C. By comparing the two equations above, we get the phase shift $\Delta\phi_n$ between $\tilde{y}_n$ and a_n, which is related to the distance $\Delta\tau_n$ between the roots of such functions,

$$\Delta\phi_n = \phi_a - \phi_y, \quad \Delta\tau_n = -\frac{\Delta\phi_n}{\omega_d} \tag{5.125}$$

From the Eq. (5.118), we get the equation which defines the roots of $\hat{y}_n$,

$$\hat{y}_n(\Delta t_n) = e^{-\zeta_n \omega_n \Delta t_n} \left(A_1 \cos(\omega_{d,n}\Delta t_n) + A_2 \sin(\omega_{d,n}\Delta t_n) \right) + A_3 \Delta t_n + \hat{A}_4 = 0 \tag{5.126}$$

Let $\tau_{v+1,n}$ be the first positive root of $v_n(\tau)$, and $\hat{y}_{v+1,n} = \hat{y}_n(\tau_{v+1,n})$. Then,

1. $A_1 = A_2 = A_3 = \hat{A}_4 = 0. \Rightarrow y_n(\Delta t_n) = 0, \ \forall \Delta t_n \in \mathbb{R}$;

2. $A_1 = A_2 = A_3 = 0, \hat{A}_4 \neq 0. \Rightarrow y_n(\Delta t_n) \neq 0, \ \forall \Delta t_n \in \mathbb{R}$;

3. $A_1 = A_2 = 0, A_3 \neq 0. \Rightarrow \Delta t = -\dfrac{\hat{A}_4}{A_3}$;

4. $A_1^2 + A_2^2 \neq 0, A_3 = \hat{A}_4 = 0.$

    1. $A_1 \neq 0, A_2 = 0. \Rightarrow \cos(\omega_{d,n}\Delta t_n) = 0 \ \Rightarrow \ \omega_{d,n}\Delta t_n = \left(q + \dfrac{1}{2} \right) \pi, \ q \in \mathbb{Z}_0$

    $$\Delta t_n = \frac{\pi}{\omega_{d,n}} \left(q + \frac{1}{2} \right), \ q \in \mathbb{Z}_0$$

    2. $A_1 = 0, A_2 \neq 0. \Rightarrow \sin(\omega_{d,n}\Delta t_n) = 0 \ \Rightarrow \ \omega_{d,n}\Delta t_n = q\pi \ \Rightarrow \ \Delta t_n = \dfrac{q\pi}{\omega_{d,n}}, \ q \in \mathbb{Z}_0$;

    3. $A_1 \neq 0, A_2 \neq 0. \Rightarrow \cos(\omega_{d,n}\Delta t_n) \neq 0 \ \Rightarrow \ A_1 + A_2 \tan(\omega_{d,n}\Delta t_n) = 0$

    $$\Delta t_n = -\frac{1}{\omega_{d,n}} \left(\arctan\left(\frac{A_1}{A_2} \right) + q\pi \right), \ q \in \mathbb{Z}_0$$

5. $A_1^2 + A_2^2 \neq 0, A_3 = 0, \hat{A}_4 \neq 0. \Rightarrow$ In this case, $\hat{y}_n$ is nothing but a sine or cosine function with an exponentially varying amplitude (unless $\zeta_n = 0$), translate in the $\hat{y}_n$ direction by the quantity $\hat{A}_4$. The roots of such function may be found by following the procedure used for the velocity analysis above, taking care of the appropriate substitutions. For instance, $B_1 \to A_1, B_2 \to A_2, A_3 \to \hat{A}_4, \tau_{j_q,n} \to \tau_{a_q,n}, \tau_{a_q,n} \to \tau_{v_q,n}$, etc. . . ;

133

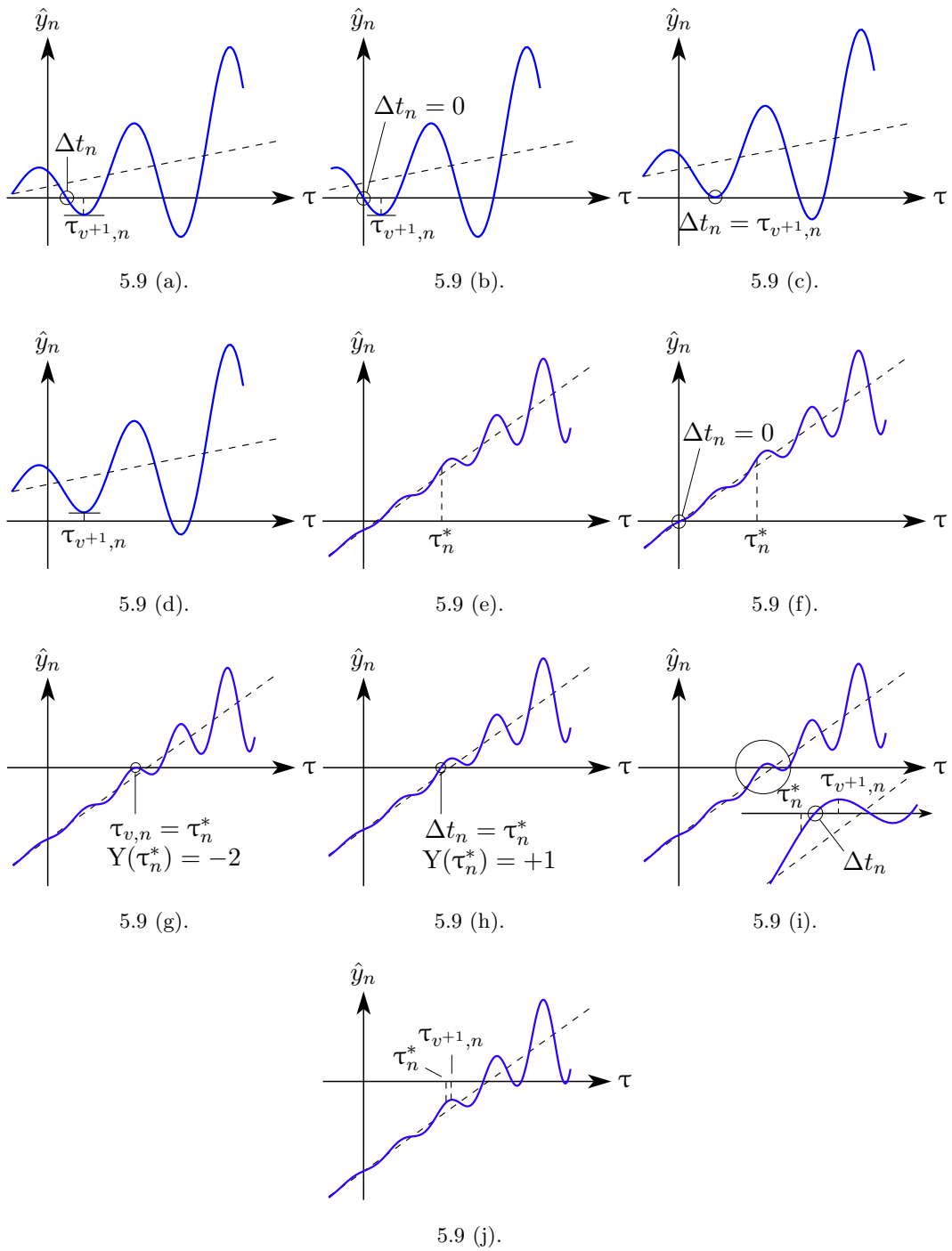Fig. 5.9. Sinusoidal displacement function roots of a linear oscillator with negative damping coefficient.

134

5.10 (a).

5.10 (b).

5.10 (c).

5.10 (d).

5.10 (e).

5.10 (f).

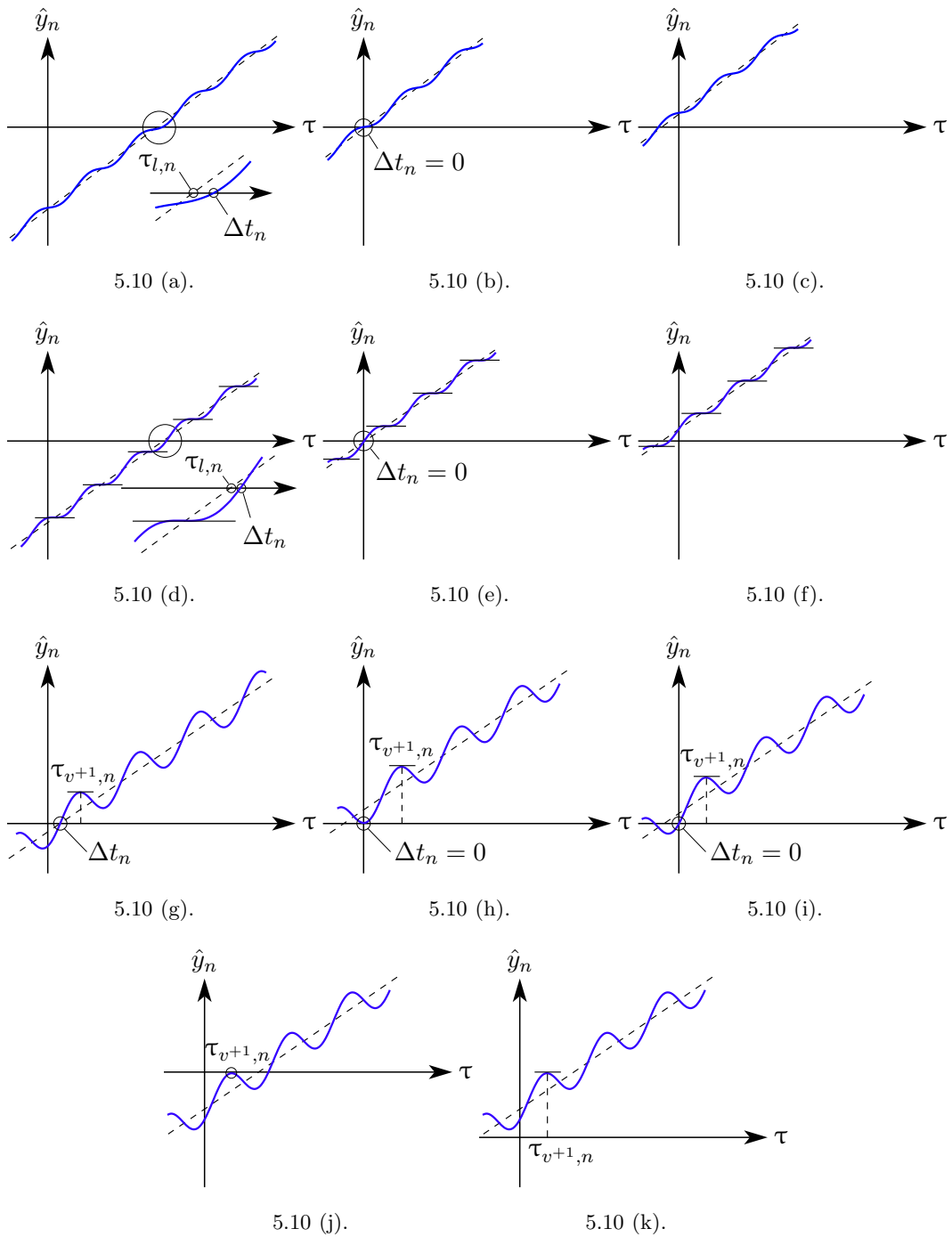5.10 (g).

5.10 (h).

5.10 (i).

5.10 (j).

5.10 (k).

Fig. 5.10. Sinusoidal displacement function roots of a linear oscillator with zero damping coefficient.

6. $A_1^2 + A_2^2 \neq 0$.

Whether $\hat{y}_n(t_{0,n}) = $ constant, the system stands still until the first derivative of the external excitation undergoes any change. If $\hat{y}_n$ has an extremum at $t = t_{0,n}$, at that time the system configuration undergoes a branch jump. Otherwise, $\hat{y}_n$ being monotonic, the following analysis may be carried out.

1. $c_n < 0$.

   1. $\tau_n^* \leq 0$.

      - $\hat{y}_{0,n}\hat{y}_{v+1,n} < 0. \Rightarrow \Delta t_n \in (\tau_{0,n}, \tau_{v+1,n}) \rightarrow \alpha_0 = \tau_{a_{\bar{q}},n}$, where $\tau_{a_{\bar{q}},n}$ is the largest acceleration root less than or equal to $\tau_{v+1,n}$, as shown below in case of $c_n > 0$ and $\tau_n^* > 0$ (Fig. 5.9 (a));

      - $\hat{y}_{0,n}\hat{y}_{v+1,n} = 0$.

        - $\hat{y}_{0,n} = 0. \Rightarrow \Delta t_n = 0$ (Fig. 5.9 (b));

        - $\hat{y}_{0,n} \neq 0. \Rightarrow$ At $\Delta t_n = \tau_{v+1,n}$ there is a branch jump of the system configuration (Fig. 5.9 (c));

      - $\hat{y}_{0,n}\hat{y}_{v+1,n} > 0. \Rightarrow$ At $\tau_{v+1,n}$ there is a branch jump of the system configuration (Fig. 5.9 (d));

   2. $\tau_n^* > 0$.

      1. $\hat{y}_{0,n}\hat{y}_n^* < 0. \Rightarrow$ The largest root $\tau_{\tilde{y}^*,n}$ of $\tilde{y}_n$ such that $\tau_{\tilde{y}^*,n} < \tau_n^*$ is needed, as well as the largest acceleration root $\tau_{a^*,n} < \tau_n^*$;

         - $\hat{y}_n(\tau_{\tilde{y}^*,n})\hat{y}_n^* < 0$.

           - $\tau_{a^*,n} > \tau_{\tilde{y}^*,n}$.

             $\hat{y}_n(\tau_{\tilde{y}^*,n})\hat{y}_n(\tau_{a^*,n}) < 0. \Rightarrow \Delta t_n \in (\tau_{\tilde{y}^*,n}, \tau_{a^*,n})$, and it may be found by choosing $\alpha_0 = \tau_{\tilde{y}^*,n}$ if $|v_n(\tau_{\tilde{y}^*,n})| > |v_n(\tau_{a^*,n})|$, or $\alpha_0 = \tau_{a^*,n}$ if $|v_n(\tau_{\tilde{y}^*,n})| < |v_n(\tau_{a^*,n})|$;

             $\hat{y}_n(\tau_{\tilde{y}^*,n})\hat{y}_n(\tau_{a^*,n}) = 0. \Rightarrow \Delta t_n = \tau_{a^*,n}$;

             $\hat{y}_n(\tau_{\tilde{y}^*,n})\hat{y}_n(\tau_{a^*,n}) > 0. \Rightarrow \Delta t_n \in (\tau_{a^*,n}, \tau_n^*)$, and it may be found by choosing $\alpha_0 = \tau_{a^*,n}$ if $|v_n(\tau_{a^*,n})| > |v_n(\tau_n^*)|$, and $\alpha_0 = \tau_n^*$ if $|v_n(\tau_{a^*,n})| < |v_n(\tau_n^*)|$;

           - $\tau_{a^*,n} \leq \tau_{\tilde{y}^*,n}. \Rightarrow \Delta t_n \in (\tau_{\tilde{y}^*,n}, \tau_n^*)$, and it may be found by choosing $\alpha_0 = \tau_{\tilde{y}^*,n}$ if $|v_n(\tau_{\tilde{y}^*,n})| > |v_n(\tau_n^*)|$, or $\alpha_0 = \tau_n^*$ if $|v_n(\tau_{\tilde{y}^*,n})| < |v_n(\tau_n^*)|$;

         - $\hat{y}_n(\tau_{\tilde{y}^*,n})\hat{y}_n^* = 0$.

           - $\hat{y}_n^* = 0. \Rightarrow \Delta t_n = \tau_n^*$;

- $\hat{y}_n^* \neq 0. \Rightarrow \Delta t_n = \tau_{\tilde{y}^*,n}$;

- $\hat{y}_n(\tau_{\tilde{y}^*,n})\hat{y}_n^* > 0$. The root Δt_n may be found in a neighborhood of $\tau_{l,n}$, exactly the same way followed in case of $c_n > 0$ and $\tau_n^* \leq 0$ (Fig. 5.9 (e));

2. $\hat{y}_{0,n}\hat{y}_n^* = 0$.
   - $\hat{y}_{0,n} = 0. \Rightarrow \Delta t_n = 0$ (Fig. 5.9 (f));
   - $\hat{y}_{0,n} \neq 0. \Rightarrow \Delta t_n = \tau_n^*$;
     - τ_n^* is an extremum of $\hat{y}_n \Rightarrow$ at τ_n^* there is a branch jump of the system configuration (Fig. 5.9 (g));
     - $\hat{y}_n$ is monotonic in a neighborhood of $\tau_n^* \Rightarrow \Delta t_n = \tau_n^*$ (Fig. 5.9 (h));

3. $\hat{y}_{0,n}\hat{y}_n^* > 0. \Rightarrow$ There are no roots before τ_n^*;
   - $\hat{y}_{0,n}\hat{y}_{v+1,n} < 0. \Rightarrow \Delta t_n \in (\tau_n^*, \tau_{v+1,n}) \rightarrow \alpha_0 = \tau_{a_{\bar{q}},n}$, where $\bar{q}$ is from the case $c_n > 0$ below (Fig. 5.9 (i));
   - $\hat{y}_{0,n}\hat{y}_{v+1,n} = 0. \Rightarrow \Delta t_n = \tau_{v+1,n}$;
   - $\hat{y}_{0,n}\hat{y}_{v+1,n} > 0. \Rightarrow$ If $\tau_{v+1,n} \neq \tau_n^*$, at $\tau_{v+1,n}$ there is a branch jump (Fig. 5.9 (j)), otherwise τ_n^* is a stationary point of inflexion;

2. $c_n = 0. \Rightarrow$ As shown in § C, when the damping coefficient vanishes, each root of $\tilde{y}_n(\tau)$ is also a root of $a_n(\tau)$. This is due to a phase shift $\Delta\phi = \pi$, and implies that *Lemma* B.1 applies within the interval $[\tau_{\tilde{y}_q,n}, \tau_{\tilde{y}_{q+1},n}]$, whose boundaries are the roots of $\tilde{y}_n$ closest to $\tau_{l,n}$, as shown below for the case $c_n > 0$;

1. $|A_3/B| > 1. \Rightarrow v_n(\tau) \neq 0 \ \forall\tau \in \mathbb{R}$;
   1. $y_{0,n}A_3 < 0. \Rightarrow \Delta t_n$ may be found by choosing $\alpha_0 = \tau_{\tilde{y}_q,n}$ if $|v_{\tilde{y}_q,n}| > |v_{\tilde{y}_{q+1},n}|$, and $\alpha_0 = \tau_{\tilde{y}_{q+1},n}$ otherwise (*Lemma* B.1, Fig. 5.10 (a));
   2. $y_{0,n}A_3 = 0. \Rightarrow y_{0,n} = 0 \Rightarrow \Delta t_n = 0$ (Fig. 5.10 (b));
   3. $y_{0,n}A_3 > 0. \Rightarrow \tilde{y}_n$ does not have any positive root (Fig. 5.10 (c));

2. $|A_3/B| = 1. \Rightarrow$ Each stationary point of $\hat{y}_n$ is also an inflexion point;
   1. $y_{0,n}A_3 < 0. \Rightarrow \Delta t_n$ may be found by choosing $\alpha_0 = \tau_{\tilde{y}_q,n}$ if $|v_{\tilde{y}_q,n}| > |v_{\tilde{y}_{q+1},n}|$, and $\alpha_0 = \tau_{\tilde{y}_{q+1},n}$ otherwise (*Lemma* B.1, Fig. 5.10 (d));
   2. $y_{0,n}A_3 = 0. \Rightarrow y_{0,n} = 0 \Rightarrow \Delta t_n = 0$ (Fig. 5.10 (e));

3. $y_{0,n} A_3 > 0. \Rightarrow \tilde{y}_n$ does not have any positive root (Fig. 5.10 (f));

3. $|A_3/B| < 1.$

    1. $y_{0,n} y_{v+1,n} < 0. \Rightarrow \Delta t_n$ may be found by choosing $\alpha_0 = \tau_{a_{\bar{q}},n}$, where $\bar{q}$ is from the case $c_n > 0$ and $\tau_n^* > 0$ below (Fig. 5.10 (g));

    2. $y_{0,n} y_{v+1,n} = 0.$

       - $y_{0,n} = 0.$

          - $\tau_{0,n}$ is an extremum of $\hat{y}_n \Rightarrow$ at $\tau_{0,n}$ there is a branch jump of the system configuration (Fig. 5.10 (h));

          - $\hat{y}_n$ is monotonic in a neighborhood of $\tau_{0,n} \Rightarrow$ since $v_{0,n} \neq 0$, it is $\Delta t_n = 0$ (Fig. 5.10 (i));

       - $y_{0,n} \neq 0. \Rightarrow$ At $\delta t_n = \tau_{v+1,n}$ there is a branch jump of the system configuration (Fig. 5.10 (j));

    3. $y_{0,n} y_{v+1,n} > 0.$ At $\delta t_n = \tau_{v+1,n}$ there is a branch jump of the system configuration (Fig. 5.10 (k));

3. $c_n > 0.$

    1. $\tau_n^* \leq 0. \Rightarrow A_3 \neq 0, v_n(\tau) \neq 0 \ \forall \tau > 0$, and the root Δt_n, whether it exists, is close to $\tau_{l,n} = -\dfrac{\hat{A}_4}{A_3}$.

        1. $\hat{y}_{0,n} A_3 < 0. \Rightarrow$ There exists Δt_n close to $\tau_{l,n}$. In order to find such root, it is useful to know the largest value of $\tau_{\tilde{y}_q,n} \leq \tau_{l,n}$, which represents the root of the periodic part of $\hat{y}_n$ less than or equal to $\tau_{l,n}$ (Fig. 5.11 (a)), and the largest acceleration root $\tau_{a_q,n} \leq \tau_{l,n}$;

       - $A_1 \neq 0, A_2 = 0.$

$$q = \left\lfloor \left| \frac{\omega_{d,n}}{\pi} \tau_{l,n} - \frac{1}{2} \right| \right\rfloor$$

       - $A_1 = 0, A_2 \neq 0.$

$$q = \left\lfloor \left| \frac{\omega_{d,n}}{\pi} \tau_{l,n} \right| \right\rfloor$$

       - $A_1 A_2 \neq 0.$

$$q = \left\lfloor \left| \frac{\omega_{d,n}}{\pi} \tau_{l,n} + \frac{1}{\pi} \arctan\left(\frac{A_1}{A_2} \right) \right| \right\rfloor$$

138

$$
\tau_{\tilde{y}_q,n} = \begin{cases} \dfrac{\pi}{\omega_{d,n}}\left(q + \dfrac{1}{2}\right), & A_1 \neq 0, A_2 = 0 \\[4mm] \dfrac{q\pi}{\omega_{d,n}}, & A_1 = 0, A_2 \neq 0 \\[4mm] \dfrac{1}{\omega_{d,n}}\left(\arctan\left(-\dfrac{A_1}{A_2}\right) + q\pi\right), & A_1 A_2 \neq 0 \end{cases}
$$

$$
\tau_{a_q,n} = \begin{cases} \dfrac{\pi}{\omega_{d,n}}\left(q + \dfrac{1}{2}\right), & C_1 \neq 0, C_2 = 0 \\[4mm] \dfrac{q\pi}{\omega_{d,n}}, & C_1 = 0, C_2 \neq 0 \\[4mm] \dfrac{1}{\omega_{d,n}}\left(\arctan\left(-\dfrac{C_1}{C_2}\right) + q\pi\right), & C_1 C_2 \neq 0 \end{cases}
$$

Also the first positive root of $\tilde{y}_n$ is needed,

$$
\tau_{\tilde{y}+1,n} = \begin{cases} \dfrac{\pi}{2\omega_{d,n}}, & A_1 \neq 0, A_2 = 0 \\[4mm] \dfrac{\pi}{\omega_{d,n}}, & A_1 = 0, A_2 \neq 0 \\[4mm] \dfrac{1}{\omega_{d,n}}\arctan\left(-\dfrac{A_1}{A_2}\right), & A_1 A_2 < 0 \\[4mm] \dfrac{1}{\omega_{d,n}}\left(\arctan\left(-\dfrac{A_1}{A_2}\right) + \pi\right), & A_1 A_2 > 0 \end{cases}
$$

- $\hat{y}_{0,n}\hat{y}_{\tilde{y}+1,n} < 0$.

  - $\tau_{a+1,n} < \tau_{\tilde{y}+1,n}$.

    $\hat{y}_{0,n}\hat{y}_{a+1,n} < 0. \Rightarrow \Delta t_n \in (0, \tau_{a+1,n})$, and it may be found by choosing $\alpha_0 = 0$ if $|v_{0,n}| > |v_n(\tau_{a+1,n})|$, or $\alpha_0 = \tau_{a+1,n}$ if $|v_{0,n}| < |v_n(\tau_{a+1,n})|$;

    $\hat{y}_{0,n}\hat{y}_{a+1,n} = 0. \Rightarrow \Delta t_n = \tau_{a+1,n}$;

    $\hat{y}_{0,n}\hat{y}_{a+1,n} > 0. \Rightarrow \Delta t_n \in (\tau_{a+1,n}, \tau_{\tilde{y}+1,n})$, and it may be found by choosing $\alpha_0 = \tau_{a+1,n}$ if $|v_n(\tau_{a+1,n})| > |v_n(\tau_{\tilde{y}+1,n})|$, and $\alpha_0 = \tau_{\tilde{y}+1,n}$ if $|v_n(\tau_{a+1,n})| < |v_n(\tau_{\tilde{y}+1,n})|$;

139

- $\tau_{a+1,n} \geq \tau_{\tilde{y}+1,n}. \Rightarrow \Delta t_n \in (0, \tau_{\tilde{y}+1,n})$, and it may be found by choosing $\alpha_0 = 0$ if $|v_{0,n}| > |v_n(\tau_{\tilde{y}+1,n})|$, or $\alpha_0 = \tau_{\tilde{y}+1,n}$ if $|v_{0,n}| < |v_n(\tau_{\tilde{y}+1,n})|$;

- $\hat{y}_{0,n}\hat{y}_{\tilde{y}+1,n} = 0. \Rightarrow \Delta t_n = \hat{y}_{\tilde{y}+1,n}$;

- $\hat{y}_{0,n}\hat{y}_{\tilde{y}+1,n} > 0.$

  - $\hat{y}(\tau_{l,n}) = 0. \Rightarrow \Delta t_n = \tau_{l,n}$;
  - $\hat{y}(\tau_{l,n}) \neq 0, \ \Delta\tau_n < 0. \Rightarrow \tau_{a_{q+1},n} = \tau_{\tilde{y}_{q+1},n} + \Delta\tau_n$;

    - $\hat{y}_{\tilde{y}_q,n}\hat{y}_{a_{q+1},n} < 0. \Rightarrow \Delta t_n$ may be found by choosing $\alpha_0 = \tau_{\tilde{y}_q,n}$ if $|v_{\tilde{y}_q,n}| > |v_{a_{q+1},n}|$, or $\alpha_0 = \tau_{a_{q+1},n}$ otherwise (*Lemma* B.1);

    - $\hat{y}_{\tilde{y}_q,n}\hat{y}_{a_{q+1},n} = 0. \Rightarrow \Delta t_n = \tau_{a_{q+1},n}$;

    - $\hat{y}_{\tilde{y}_q,n}\hat{y}_{a_{q+1},n} > 0. \Rightarrow \Delta t_n \in (\tau_{a_{q+1},n}, \tau_{\tilde{y}_{q+1},n})$, and it may be found by choosing $\alpha_0 = \tau_{\tilde{y}_{q+1},n}$ if $|v_{\tilde{y}_{q+1},n}| > |v_{a_{q+1},n}|$, or $\alpha_0 = \tau_{a_{q+1},n}$ otherwise (*Lemma* B.1);

  - $\hat{y}(\tau_{l,n}) \neq 0, \ \Delta\tau_n = 0. \Rightarrow \tau_{a_q,n} = \tau_{\tilde{y}_q,n}$, and Δt_n may be found by choosing $\alpha_0 = \tau_{\tilde{y}_q,n}$ if $|v_{\tilde{y}_q,n}| > |v_{\tilde{y}_{q+1},n}|$, or $\alpha_0 = \tau_{\tilde{y}_{q+1},n}$ otherwise (*Lemma* B.1);
  - $\hat{y}(\tau_{l,n}) \neq 0, \ \Delta\tau_n > 0. \Rightarrow \tau_{a_q,n} = \tau_{\tilde{y}_q,n} + \Delta\tau_n$ (Fig. 5.11 (d));

    $\hat{y}_{\tilde{y}_q,n}\hat{y}_{a_q,n} < 0. \Rightarrow \Delta t_n$ may be found by choosing $\alpha_0 = \tau_{\tilde{y}_q,n}$ if $|v_{\tilde{y}_q,n}| > |v_{a_q,n}|$, or $\alpha_0 = \tau_{a_q,n}$ otherwise (*Lemma* B.1);

    $\hat{y}_{\tilde{y}_q,n}\hat{y}_{a_q,n} = 0. \Rightarrow \Delta t_n = \tau_{a_q,n}$;

    $\hat{y}_{\tilde{y}_q,n}\hat{y}_{a_q,n} > 0. \Rightarrow \Delta t_n \in (\tau_{a_q,n}, \tau_{\tilde{y}_{q+1},n})$, and it may be found by choosing $\alpha_0 = \tau_{\tilde{y}_{q+1},n}$ if $|v_{\tilde{y}_{q+1},n}| > |v_{a_q,n}|$, or $\alpha_0 = \tau_{a_q,n}$ otherwise (*Lemma* B.1);

2. $\hat{y}_{0,n}A_3 = 0. \Rightarrow \hat{y}_{0,n} = 0$ and $\Delta t_n = 0$, which means the length of the nth segment of the $R - y$ diagram is zero (Fig. 5.11 (b));

3. $\hat{y}_{0,n}A_3 > 0. \Rightarrow \hat{y}_n$ does not have any positive root (Fig. 5.11 (c));

2. $\tau_n^* > 0.$

   1. $\exists\tau_{v+1,n} \in (0, \tau_n^*]. \Rightarrow$ From the velocity analysis above, the first positive root $\tau_{v+1,n}$ of the velocity function is known. In order to find the roots of $\hat{y}_n$, the roots of the acceleration closest to $\tau_{v+1,n}$ are needed. This means to solve the equation $\tau_{a_q,n} = \tau_{v+1,n}$, which implicitly defines q, and then to get $\bar{q} = \lfloor q \rfloor$. In details,

- $C_1 \neq 0, C_2 = 0$.

$$\bar{q} = \left\lfloor \left| \frac{\omega_{d,n}}{\pi} \tau_{v+1,n} - \frac{1}{2} \right| \right\rfloor$$

- $C_1 = 0, C_2 \neq 0$.

$$\bar{q} = \left\lfloor \left| \frac{\omega_{d,n}}{\pi} \tau_{v+1,n} \right| \right\rfloor$$

- $C_1 \neq 0, C_2 \neq 0$.

$$\bar{q} = \left\lfloor \left| \frac{\omega_{d,n}}{\pi} \tau_{v+1,n} + \frac{1}{\pi} \arctan\left(\frac{C_1}{C_2}\right) \right| \right\rfloor$$

- $q = \bar{q}. \Rightarrow A_3 \neq 0$ and $\tau_{v+1,n}$ is a stationary point of inflexion.

  - $\hat{y}_{0,n}\hat{y}_{v+1,n} < 0. \Rightarrow \Delta t_n \in (0, \tau_{v+1,n}) \rightarrow \alpha_0 = \tau_{a_{\bar{q}-1},n}$
    (*Lemma* B.1, Fig. 5.11 (e));

  - $\hat{y}_{0,n}\hat{y}_{v+1,n} = 0$.

    $\hat{y}_{0,n} = 0. \Rightarrow \Delta t_n = 0$ (Fig. 5.11 (f));

    $\hat{y}_{0,n} \neq 0. \Rightarrow \Delta t_n = \tau_{v+1,n}$ (Fig. 5.11 (g));

  - $\hat{y}_{0,n}\hat{y}_{v+1,n} > 0$. The smallest root $\tau_{\tilde{y}_v,n}$ of $\tilde{y}_n$ such that $\tau_{\tilde{y}_v,n} > \tau_{v+1,n}$ is needed;

    $y_{0,n}A_3 < 0$ & $y_{v+1,n}y_n(\tau_{\tilde{y}_v,n}) < 0. \Rightarrow \Delta t_n$ may be found by choosing $\alpha_0 = \tau_{\tilde{y}_v,n}$;

    $y_{0,n}A_3 < 0$ & $y_{v+1,n}y_n(\tau_{\tilde{y}_v,n}) = 0. \Rightarrow \Delta t_n = \tau_{\tilde{y}_v,n}$;

    $y_{0,n}A_3 < 0$ & $y_{v+1,n}y_n(\tau_{\tilde{y}_v,n}) > 0. \Rightarrow \Delta t_n$ is close to $\tau_{l,n}$, and the analysis developed for the case $\tau_n^* \leq 0$ in a neighborhood of $\tau_{l,n}$ still applies (Fig. 5.11 (h));

    $y_{0,n}A_3 = 0. \Rightarrow \Delta t_n = 0$;

    $y_{0,n}A_3 > 0. \Rightarrow \hat{y}_n$ does not have any positive root
    (Fig. 5.11 (i));

- $q \neq \bar{q}$.

  - $\hat{y}_{0,n}\hat{y}_{v+1,n} < 0. \Rightarrow \Delta t_n \in (\tau_{0,n}, \tau_{v+1,n}) \rightarrow \alpha_0 = \tau_{a_{\bar{q}},n}$
    (*Lemma* B.1, Fig. 5.12 (a));

  - $\hat{y}_{0,n}\hat{y}_{v+1,n} = 0$.

$\hat{y}_{0,n} = 0. \Rightarrow$ Either $v_{0,n} \neq 0$ and $\Delta t_n = 0$, or $v_{0,n} = 0$ and there is a branch jump at $\tau_{0,n}$ (Fig. 5.12 (b)–5.12 (c));

$\hat{y}_{0,n} \neq 0. \Rightarrow$ There is a branch jump of the system configuration at $\delta t_n = \tau_{v+1,n}$ (Fig. 5.12 (d));

- $\hat{y}_{0,n}\hat{y}_{v+1,n} > 0. \Rightarrow$ There is a branch jump at $\tau_{v+1,n}$ (Fig. 5.12 (e));

2. $\nexists \tau_{v+1,n} \in (0, \tau_n^*]. \Rightarrow v_n$ does not have any positive root, and the analysis developed for the case $\tau_n^* \leq 0$ still applies.
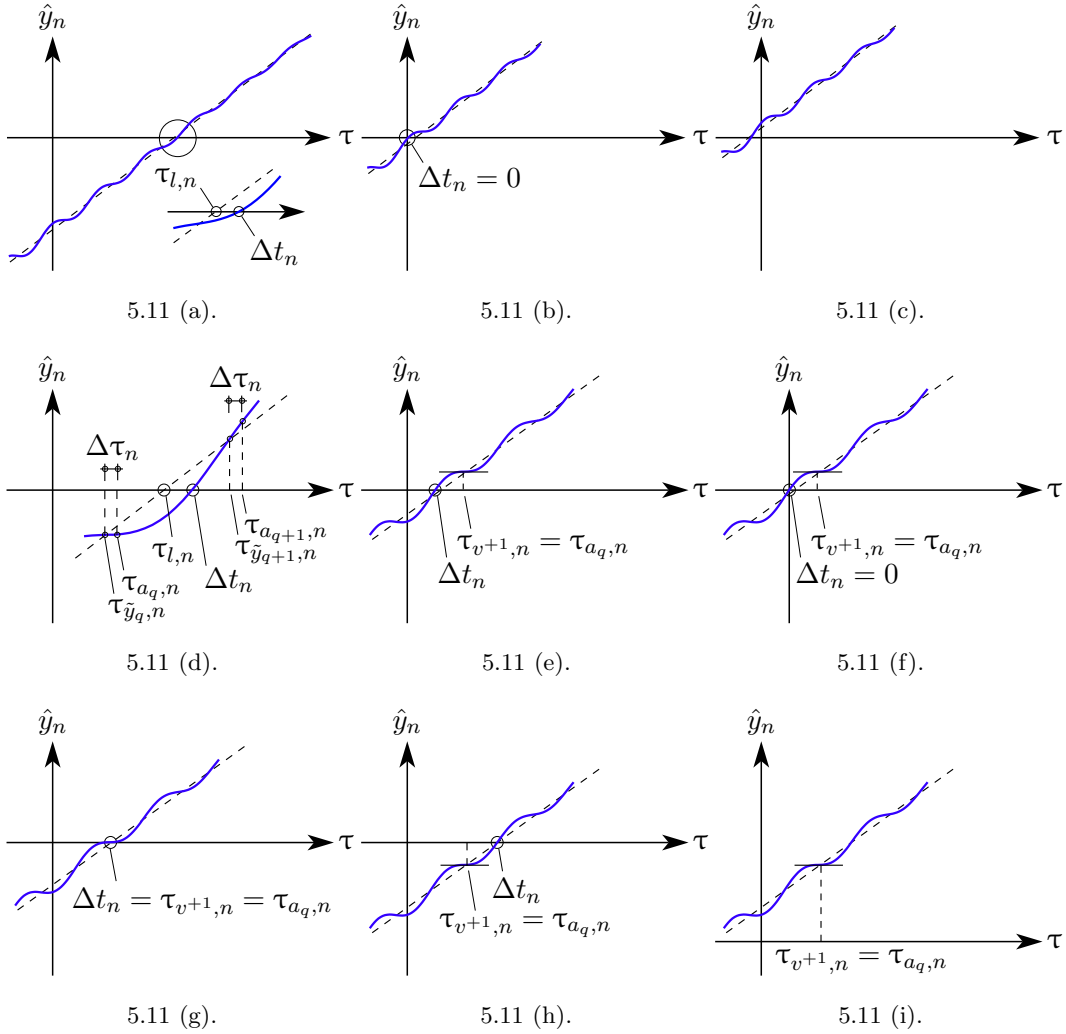
Fig. 5.11. Sinusoidal displacement function roots of a linear oscillator with positive damping coefficient.
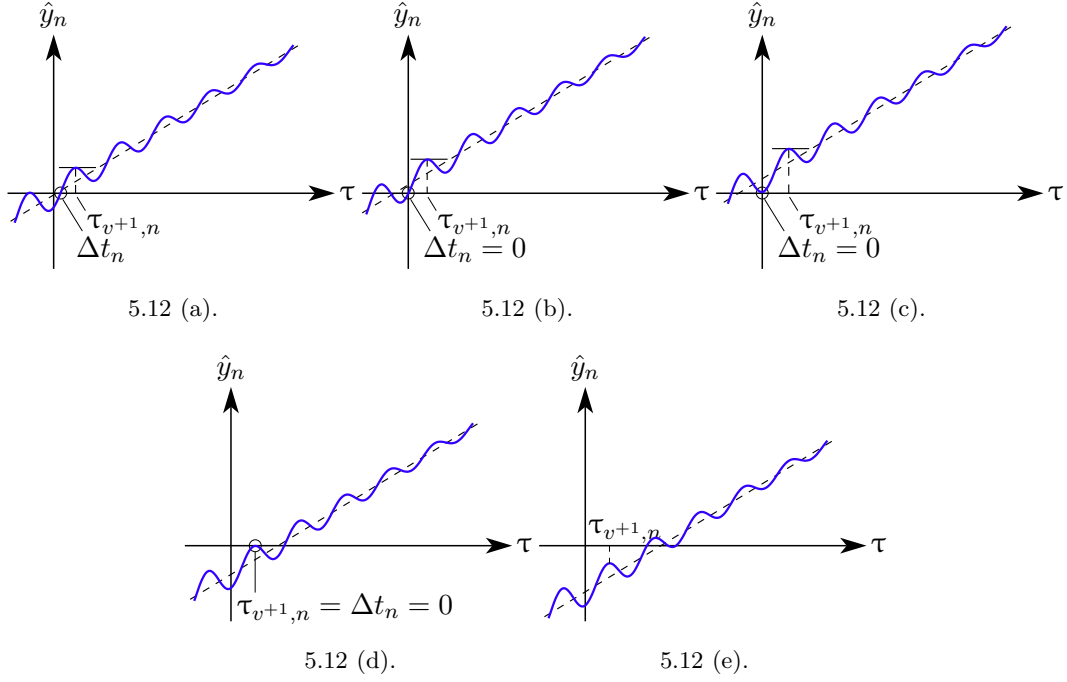
Fig. 5.12. Sinusoidal displacement function roots of a linear oscillator with positive damping coefficient.

5.4.5 Critically damped system with nonzero stiffness

From the Eqs. 5.51, 5.52, and 5.53 we get

$$y_n(\tau) = (C_0 + C_1\tau)e^{-\zeta_n\omega_n\tau} + C_2\tau + C_3 \tag{5.127}$$

$$C_0 = \frac{\mathbf{F}_{0,n}}{k_n} + 2\zeta_n \frac{F_{1,n}}{\omega_n k_n}$$

$$C_1 = \frac{\mathbf{F}_{0,n}}{k_n}\zeta_n\omega_n + \frac{F_{1,n}}{k_n}(2\zeta_n^2 - 1) + \dot{y}_{0,n}$$

$$C_2 = \frac{F_{1,n}}{k_n}$$

$$C_3 = y_{0,n} - \frac{\mathbf{F}_{0,n}}{k_n} - 2\zeta_n\frac{F_{1,n}}{\omega_n k_n}$$

$$v_n(\tau) = [-\zeta_n\omega_n C_0 + (1 - \zeta_n\omega_n\tau)C_1]e^{-\zeta_n\omega_n\tau} + C_2 \tag{5.128}$$

$$a_n(\tau) = [-\zeta_n\omega_n C_1 + (\zeta_n\omega_n)^2 C_0 + (\zeta_n\omega_n)^2 C_1\tau - \zeta_n\omega_n C_1]e^{-\zeta_n\omega_n\tau} =$$
$$= [(\zeta_n\omega_n)^2 C_0 - 2\zeta_n\omega_n C_1 + (\zeta_n\omega_n)^2 C_1\tau]e^{-\zeta_n\omega_n\tau} \tag{5.129}$$

$$j_n(\tau) = [(\zeta_n\omega_n)^2 C_1 - (\zeta_n\omega_n)^3 C_0 + 2(\zeta_n\omega_n)^2 C_1 - (\zeta_n\omega_n)^3 C_1\tau]e^{-\zeta_n\omega_n\tau} =$$
$$= [3(\zeta_n\omega_n)^2 C_1 - (\zeta_n\omega_n)^3 C_0 - (\zeta_n\omega_n)^3 C_1\tau]e^{-\zeta_n\omega_n\tau} \qquad (5.130)$$

Also, from the Eqs. (5.57) and (5.127), we get

$$\hat{y}_n(\tau) = y_n(\tau) - \left(y_{0,n} + \frac{\Delta R_n}{k_n}\right) = (C_0 + C_1\tau)e^{-\zeta_n\omega_n\tau} + C_2\tau + \hat{C}_3 \qquad (5.131)$$

$$\hat{C}_3 = C_3 - \left(y_{0,n} + \frac{\Delta R_n}{k_n}\right) \qquad (5.132)$$

It is worth noting the behavior of $\hat{y}_n$ and v_n when $\tau \to \pm\infty$,

$$\lim_{\tau\to+\infty} \hat{y}_n(\tau) \overset{c_n\leq 0}{=} \begin{cases} +\hat{C}_3, & C_0 = C_1 = C_2 = 0 \\ +\operatorname{sgn}(C_2)\cdot\infty, & C_0 = C_1 = 0,\ C_2 \neq 0 \\ +\operatorname{sgn}(C_0)\cdot\infty, & C_0 \neq 0,\ C_1 = 0 \\ +\operatorname{sgn}(C_1)\cdot\infty, & C_1 \neq 0 \end{cases} \qquad (5.133)$$

$$\lim_{\tau\to-\infty} \hat{y}_n(\tau) \overset{c_n\leq 0}{=} \begin{cases} +\hat{C}_3, & C_2 = 0 \\ -\operatorname{sgn}(C_2)\cdot\infty, & C_2 \neq 0 \end{cases} \qquad (5.134)$$

$$\lim_{\tau\to+\infty} \hat{y}_n(\tau) \overset{c_n\geq 0}{=} \begin{cases} +\hat{C}_3, & C_2 = 0 \\ +\operatorname{sgn}(C_2)\cdot\infty, & C_2 \neq 0 \end{cases} \qquad (5.135)$$

$$\lim_{\tau\to-\infty} \hat{y}_n(\tau) \overset{c_n\geq 0}{=} \begin{cases} +\hat{C}_3, & C_0 = C_1 = C_2 = 0 \\ -\operatorname{sgn}(C_2)\cdot\infty, & C_0 = C_1 = 0,\ C_2 \neq 0 \\ +\operatorname{sgn}(C_0)\cdot\infty, & C_0 \neq 0,\ C_1 = 0 \\ -\operatorname{sgn}(C_1)\cdot\infty, & C_1 \neq 0 \end{cases} \qquad (5.136)$$

$$\lim_{\tau\to+\infty} v_n(\tau) \overset{c_n\leq 0}{=} \begin{cases} +C_2, & C_0 = C_1 = 0 \\ +\operatorname{sgn}(C_0)\cdot\infty, & C_0 \neq 0,\ C_1 = 0 \\ +\operatorname{sgn}(C_1)\cdot\infty, & C_1 \neq 0 \end{cases} \qquad (5.137)$$

$$\lim_{\tau\to-\infty} v_n(\tau) \overset{c_n\leq 0}{=} C_2 \qquad (5.138)$$

$$\lim_{\tau\to+\infty} v_n(\tau) \overset{c_n\geq 0}{=} C_2 \qquad (5.139)$$

144

$$\lim_{\tau \to -\infty} v_n(\tau) \overset{c_n \geq 0}{=} \begin{cases} + C_2, & C_0 = C_1 = 0 \\ - \operatorname{sgn}(C_0) \cdot \infty, & C_0 \neq 0, \ C_1 = 0 \\ + \operatorname{sgn}(C_1) \cdot \infty, & C_1 \neq 0 \end{cases} \qquad (5.140)$$

The roots of the jerk function depend on the constants C_0 and C_1,

- $C_0 = C_1 = 0. \Rightarrow j(\tau_{j,n}) = 0, \ \forall \tau_{j,n} \in \mathbb{R}$;

- $C_0 \neq 0, C_1 = 0. \Rightarrow j(\tau_{j,n}) \neq 0, \ \forall \tau_{j,n} \in \mathbb{R}$;

- $C_1 \neq 0.$

$$j(\tau_{j,n}) = 0 \ \Leftrightarrow \ [3(\zeta_n \omega_n)^2 C_1 - (\zeta_n \omega_n)^3 C_0 - (\zeta_n \omega_n)^3 C_1 \tau_{j,n}] = 0$$

$$3C_1 - \zeta_n \omega_n C_0 - \zeta_n \omega_n C_1 \tau_{j,n} = 0 \ \Rightarrow \ \tau_{j,n} = \frac{3}{\zeta_n \omega_n} - \frac{C_0}{C_1}$$

The roots of the acceleration function depend on the constants C_0 and C_1 as well,

- $C_0 = C_1 = 0. \Rightarrow a(\tau_{a,n}) = 0, \ \forall \tau_{a,n} \in \mathbb{R}$;

- $C_0 \neq 0, C_1 = 0. \Rightarrow a(\tau_{a,n}) \neq 0, \ \forall \tau_{a,n} \in \mathbb{R}$;

- $C_1 \neq 0.$

$$a(\tau_{a,n}) = 0 \ \Leftrightarrow \ [(\zeta_n \omega_n)^2 C_0 - 2\zeta_n \omega_n C_1 + (\zeta_n \omega_n)^2 C_1 \tau_{a,n}] = 0$$

$$\zeta_n \omega_n C_0 - 2C_1 + \zeta_n \omega_n C_1 \tau_{a,n} = 0 \ \Rightarrow \ \tau_{a,n} = \frac{2}{\zeta_n \omega_n} - \frac{C_0}{C_1}$$

By recalling the Eqs. (5.128) and (5.137)–(5.140), the roots of v_n depend on the constants $C_{0,1,2}$ as it follow,

1. $C_2 = 0. \Rightarrow v_n(\tau_{v,n}) = 0 \ \Leftrightarrow \ -\zeta_n \omega_n C_0 + (1 - \zeta_n \omega_n \tau_{v,n}) C_1 = 0 \ \Leftrightarrow \ \tau_{v,n} C_1 = \dfrac{C_1}{\zeta_n \omega_n} - C_0$;

   1. $C_0 = C_1 = 0. \Rightarrow v_n(\tau) = 0, \ \forall \tau \in \mathbb{R}$;

   2. $C_0 \neq 0, C_1 = 0. \Rightarrow v_n(\tau) \neq 0, \ \forall \tau \in \mathbb{R}$;

3. $C_1 \neq 0. \Rightarrow \tau_{v,n} = \dfrac{1}{\zeta_n \omega_n} - \dfrac{C_0}{C_1}$;

2. $C_2 \neq 0$.

    1. $C_0 = C_1 = 0. \Rightarrow v_n(\tau) = C_2, \ \forall \tau \in \mathbb{R}$;

    2. $C_0 \neq 0, C_1 = 0. \Rightarrow v(\tau) = -\zeta_n \omega_n C_0 e^{-\zeta_n \omega_n \tau} + C_2$, and

$$v_n(\tau_{v,n}) = 0 \ \Leftrightarrow \ e^{-\zeta_n \omega_n \tau_{v,n}} = \frac{1}{\zeta_n \omega_n} \frac{C_2}{C_0}$$

    1. $c_n C_0 C_2 < 0. \Rightarrow v_n(\tau) \neq 0 \ \forall \tau \in \mathbb{R}$;

    2. $c_n C_0 C_2 > 0. \Rightarrow \tau_{v,n} = -\dfrac{1}{\zeta_n \omega_n} \ln \left(\dfrac{1}{\zeta_n \omega_n} \dfrac{C_0}{C_2} \right)$;

3. $C_1 \neq 0$.

$$\tau_{a,n} = \frac{2}{\zeta_n \omega_n} - \frac{C_0}{C_1}, \quad \tau_{j,n} = \frac{3}{\zeta_n \omega_n} - \frac{C_0}{C_1}$$

$$v_{a,n} = v_n(\tau_{a,n}) = \left[-\zeta_n \omega_n C_0 + C_1 \left(1 - \zeta_n \omega_n \left(\frac{2}{\zeta_n \omega_n} - \frac{C_0}{C_1} \right) \right) \right] \cdot$$

$$\cdot \exp \left(-\zeta_n \omega_n \left(\frac{2}{\zeta_n \omega_n} - \frac{C_0}{C_1} \right) \right) + C_2$$

$$v_{a,n} = \left[-\zeta_n \omega_n C_0 + C_1 \left(1 - 2 + \zeta_n \omega_n \frac{C_0}{C_1} \right) \right] \exp \left(-2 + \zeta_n \omega_n \frac{C_0}{C_1} \right) + C_2$$

$$= C_2 - C_1 \exp \left(\zeta_n \omega_n \frac{C_0}{C_1} - 2 \right)$$

$$C_1 \cdot v_{a,n} = C_1 C_2 - C_1^2 \exp \left(\zeta_n \omega_n \frac{C_0}{C_1} - 2 \right)$$

    1. $c_n < 0. \Rightarrow \tau_{a,n} > \tau_{j,n}$, $\lim_{\tau \to +\infty} v_n(\tau) = \mathrm{sgn}(C_1) \cdot \infty$, $\lim_{\tau \to -\infty} v_n(\tau) = C_2$;

        1. $C_1 C_2 < 0. \Rightarrow v_n$ has one root $\tau_{v,n}$ (Fig. 5.3 (j)), which may be found by choosing $\alpha_0 > \tau_a$ (*Lemma* B.1);

        2. $C_1 C_2 > 0$.

- $C_1 v_{a,n} < 0. \Rightarrow v_n$ has two real roots (Fig. 5.3 (g)). $\tau_{v_1,n}$ may be found by $\alpha_0 = \tau_{j,n}$, and $\tau_{v_2,n}$ may be found by $\alpha_0 > \tau_{a,n}$ (*Lemma* B.1);

- $C_1 v_{a,n} = 0. \Rightarrow v_n$ has one root $\tau_{v,n} = \tau_{a,n}$ (Fig. 5.3 (h));

- $C_1 v_{a,n} > 0. \Rightarrow v_n$ does not have any real root (Fig. 5.3 (i));

2. $c_n > 0. \Rightarrow \tau_{a,n} < \tau_{j,n}$, $\lim_{\tau \to +\infty} v_n(\tau) = C_2$, $\lim_{\tau \to -\infty} v_n(\tau) = \operatorname{sgn}(C_1) \cdot \infty$;

     1. $C_1 C_2 < 0. \Rightarrow v_n$ has one root $\tau_{v,n}$ (Fig. 5.3 (j)), which may be found by choosing $\alpha_0 < \tau_a$ (*Lemma* B.1);

     2. $C_1 C_2 > 0. \Rightarrow$

- $C_1 v_{a,n} < 0. \Rightarrow v_n$ has two real roots (Fig. 5.4 (g)). $\tau_{v_1,n}$ may be found by $\alpha_0 < \tau_{a,n}$, and $\tau_{v_2,n}$ may be found by $\alpha_0 = \tau_{j,n}$ (*Lemma* B.1);

- $C_1 v_{a,n} = 0. \Rightarrow v_n$ has one root $\tau_{v,n} = \tau_{a,n}$ (Fig. 5.4 (h));

- $C_1 v_{a,n} > 0. \Rightarrow v_n$ does not have any real root (Fig. 5.4 (i)).

From the Eqs. 5.57 and 5.141, we get

$$\hat{y}_n(\Delta t_n) = (C_0 + C_1 \Delta t_n) e^{-\zeta_n \omega_n \Delta t_n} + C_2 \Delta t_n + \hat{C}_3 = 0, \qquad (5.141)$$

and the solutions of this equation depend on the constants C_0, C_1, C_2, $\hat{C}_3$,

1. $C_2 = 0$.

     1. $C_0 = C_1 = 0$.

         1. $\hat{C}_3 = 0. \Rightarrow \hat{y}(\tau) = 0, \ \forall \tau \in \mathbb{R}$;

         2. $\hat{C}_3 \neq 0. \Rightarrow \hat{y}(\tau) \neq 0, \ \forall \tau \in \mathbb{R}$;

     2. $C_0 \neq 0, C_1 = 0. \Rightarrow \hat{y}(\Delta t_n) = C_0 e^{-\zeta_n \omega_n \Delta t_n} + \hat{C}_3 = 0$;

         1. $C_0 \hat{C}_3 < 0. \Rightarrow \Delta t_n = -\dfrac{1}{\zeta_n \omega_n} \ln \left(-\dfrac{\hat{C}_3}{C_0} \right)$;

         2. $C_0 \hat{C}_3 \geq 0. \Rightarrow y(\tau) \neq 0 \ \forall \tau \in \mathbb{R}$;

     3. $C_1 \neq 0. \Rightarrow \tau_{v,n} = \dfrac{1}{\zeta_n \omega_n} - \dfrac{C_0}{C_1}$, $\tau_{a,n} = \dfrac{2}{\zeta_n \omega_n} - \dfrac{C_0}{C_1}$;

$$\hat{y}_n(\tau_{v,n}) = \left[C_0 + C_1 \left(\frac{1}{\zeta_n \omega_n} - \frac{C_0}{C_1} \right) \right] \exp\left(-\zeta_n \omega_n \left(\frac{1}{\zeta_n \omega_n} - \frac{C_0}{C_1} \right) \right) +$$

$$+ C_2 \left(\frac{1}{\zeta_n \omega_n} - \frac{C_0}{C_1} \right) + \hat{C}_3$$

$$\hat{y}_{v,n} = \hat{y}_n(\tau_{v,n}) = \frac{C_1}{\zeta_n \omega_n} \exp\left(\zeta_n \omega_n \frac{C_0}{C_1} - 1 \right) + C_2 \left(\frac{1}{\zeta_n \omega_n} - \frac{C_0}{C_1} \right) + \hat{C}_3$$

$$= \frac{C_1}{\zeta_n \omega_n} \exp\left(\zeta_n \omega_n \frac{C_0}{C_1} - 1 \right) + \hat{C}_3$$

$$C_1 \hat{y}_{v,n} = \frac{C_1^2}{\zeta_n \omega_n} \exp\left(\zeta_n \omega_n \frac{C_0}{C_1} - 1 \right) + C_1 \hat{C}_3$$

1. $c_n < 0. \Rightarrow \tau_{v,n} > \tau_{a,n}$, $\lim_{\tau \to +\infty} \hat{y}_n = \text{sgn}(C_1) \cdot \infty$, $\lim_{\tau \to -\infty} \hat{y}_n = \hat{C}_3$;

   1. $C_1 \hat{C}_3 \le 0. \Rightarrow \hat{y}_n$ has one real root Δt_n (Fig. 5.4 (m)), which may be found by choosing $\alpha_0 > \tau_{v,n}$ (*Lemma* B.1);

   2. $C_1 \hat{C}_3 > 0.$

      - $C_1 \hat{y}_{v,n} < 0. \Rightarrow \hat{y}_n$ has two real roots, $\Delta t_{1,n}$ and $\Delta t_{2,n}$ (as shown in Fig. 5.4 (j)). The former may be found by choosing $\alpha_0 = \tau_{a,n}$, while the latter comes from $\alpha_0 > \tau_{v,n}$ (*Lemma* B.1);

      - $C_1 \hat{y}_{v,n} = 0. \Rightarrow \hat{y}_n$ has one real root, $\Delta t_n = \tau_{v,n}$ (Fig. 5.4 (k));

      - $C_1 \hat{y}_{v,n} > 0. \Rightarrow \hat{y}_n$ does not have any real root (Fig. 5.4 (l));

2. $c_n > 0. \Rightarrow \tau_{v,n} < \tau_{a,n}$, $\lim_{\tau \to +\infty} \hat{y}_n = \hat{C}_3$, $\lim_{\tau \to -\infty} \hat{y}_n = -\text{sgn}(C_1) \cdot \infty$;

   1. $C_1 \hat{C}_3 < 0.$

      - $C_1 \hat{y}_{v,n} < 0. \Rightarrow \hat{y}_n$ does not have any real root (Fig. 5.4 (l));

      - $C_1 \hat{y}_{v,n} = 0. \Rightarrow \Delta t_n = \tau_{v,n}$ (Fig. 5.4 (k));

      - $C_1 \hat{y}_{v,n} > 0. \Rightarrow \hat{y}_n$ has two real roots, $\Delta t_{1,n}$ and $\Delta t_{2,n}$ (as shown in Fig. 5.4 (j)). The former may be found by choosing $\alpha_0 < \tau_{v,n}$, while the latter comes from $\alpha_0 = \tau_{a,n}$ (*Lemma* B.1);

   2. $C_1 \hat{C}_3 \ge 0. \Rightarrow C_1 \hat{y}_{v,n} > 0 \Rightarrow \hat{y}$ has one real root Δt_n (as shown in Fig. 5.4 (m)), which may be found by choosing $\alpha_0 < \tau_{v,n}$ (*Lemma* B.1);

2. $C_2 \neq 0$.

    1. $C_0 = C_1 = 0. \Rightarrow \Delta t_n = -\hat{C}_3/C_2$;

    2. $C_0 \neq 0, C_1 = 0. \Rightarrow a_n(\tau), j_n(\tau) \neq 0 \ \forall \tau \in \mathbb{R}$, thus v_n is strictly monotone everywhere. Also,

$$\lim_{\tau \to +\infty} \hat{y} = \begin{cases} + \operatorname{sgn}(C_0) \cdot \infty, & c_n < 0 \\ + \operatorname{sgn}(C_2) \cdot \infty, & c_n > 0 \end{cases} \tag{5.142a}$$

$$\lim_{\tau \to -\infty} \hat{y} = \begin{cases} - \operatorname{sgn}(C_2) \cdot \infty, & c_n < 0 \\ + \operatorname{sgn}(C_0) \cdot \infty, & c_n > 0 \end{cases} \tag{5.142b}$$

        1. $c_n C_0 C_2 < 0. \Rightarrow v_n$ does not have any real root, thus $\hat{y}_n$ is strictly monotone (Fig. 5.4 (d)). Also, since $\hat{y}_n$ is continuous and recalling the Eq. 5.142, we may state that $\hat{y}_n$ has a unique root Δt_n, which may be found for any initial guess $\alpha_0 \in \mathbb{R}$ (*Lemma* B.2);

        2. $c_n C_0 C_2 > 0. \Rightarrow a_n(\tau) \neq 0 \ \forall \tau \in \mathbb{R}$ and $v_n(\tau)$ has one root $\tau_{v,n}$;

            1. $\hat{y}_{v,n} C_0 < 0. \Rightarrow \hat{y}_n$ has two roots (Fig. 5.4 (a)), $\Delta t_{1,n}$ from $\alpha_0 < \tau_{v,n}$ and $\Delta t_{2,n}$ from $\alpha_0 > \tau_{v,n}$ (*Lemma* B.4);

            2. $\hat{y}_{v,n} C_0 = 0. \Rightarrow \hat{y}_n$ has one root $\Delta t_n = \tau_{v,n}$ (Fig. 5.4 (b));

            3. $\hat{y}_{v,n} C_0 > 0. \Rightarrow \hat{y}_n$ does not have any real root (Fig. 5.4 (c));

3. $C_1 \neq 0$.

$$\tau_{a,n} = \frac{2}{\zeta_n \omega_n} - \frac{C_0}{C_1}, \quad \tau_{j,n} = \frac{3}{\zeta_n \omega_n} - \frac{C_0}{C_1}$$

$$\lim_{\tau \to +\infty} \hat{y} = \begin{cases} + \operatorname{sgn}(C_1) \cdot \infty, & c_n < 0 \\ + \operatorname{sgn}(C_2) \cdot \infty, & c_n > 0 \end{cases}$$

$$\lim_{\tau \to -\infty} \hat{y} = \begin{cases} - \operatorname{sgn}(C_2) \cdot \infty, & c_n < 0 \\ - \operatorname{sgn}(C_1) \cdot \infty, & c_n > 0 \end{cases}$$

    1. $c_n < 0. \Rightarrow \tau_{a,n} > \tau_{j,n}$;

        1. $C_1 C_2 < 0. \Rightarrow v_n$ has one root $\tau_{v,n} > \tau_{a,n} > \tau_{j,n}$;

           - $\hat{y}_{v,n} C_1 < 0. \Rightarrow \hat{y}_{v,n}$ has two roots (Fig. 5.4 (g)), $\Delta t_{1,n}$ from $\alpha_0 = \tau_{a,n}$ and $\Delta t_{2,n}$ from $\alpha_0 > \tau_{v,n}$ (*Lemma* B.1);

           - $\hat{y}_{v,n} C_1 = 0. \Rightarrow \hat{y}_{v,n}$ has one root $\Delta t_n = \tau_{v,n}$ (Fig. 5.4 (h));

           - $\hat{y}_{v,n} C_1 > 0. \Rightarrow \hat{y}_{v,n}$ does not have any real root (Fig. 5.4 (i));

2. $C_1 C_2 > 0$.

   - $C_1 v_{a,n} < 0. \Rightarrow \tau_{v_1,n}$ and $\tau_{v_2,n}$ are the roots of v_n. Let $\hat{y}_{v_1,n} = \hat{y}_{(\tau_{v_1,n})}$ and $\hat{y}_{v_2,n} = \hat{y}_{(\tau_{v_2,n})}$;

      - $\hat{y}_{v_1,n} \hat{y}_{v_2,n} < 0. \Rightarrow \hat{y}_n$ has three roots (Fig. 5.5 (a)), $\Delta t_{1,n}$ from $\alpha_0 < \tau_{v_1,n}$, $\Delta t_{2,n}$ from $\alpha_0 = \tau_{a,n}$, and $\Delta t_{3,n}$ from $\alpha_0 > \tau_{v_2,n}$ (*Lemma* B.1);

      - $\hat{y}_{v_1,n} \hat{y}_{v_2,n} = 0. \Rightarrow \hat{y}_n$ has two roots (Fig. 5.5 (b));

        $\hat{y}_{v_1,n} = 0. \Rightarrow \Delta t_{1,n} = \tau_{v_1,n}$ and $\Delta t_{2,n}$ is from $\alpha_0 > \tau_{v_2,n}$;

        $\hat{y}_{v_1,n} \neq 0. \Rightarrow \Delta t_{1,n}$ is from $\alpha_0 < \tau_{v_1,n}$ and $\Delta t_{2,n} = \tau_{v_2,n}$;

      - $\hat{y}_{v_1,n} \hat{y}_{v_2,n} > 0. \Rightarrow \hat{y}_n$ has one root Δt_n (Fig. 5.5 (c)), which may be found by an appropriate choice of α_0;

        $\hat{y}_{v_1,n} C_1 < 0. \Rightarrow \alpha_0 > \tau_{v_2,n}$;

        $\hat{y}_{v_1,n} C_1 > 0. \Rightarrow \alpha_0 < \tau_{v_1,n}$;

   - $C_1 v_{a,n} = 0. \Rightarrow \tau_{v,n} = \tau_{a,n} \neq \tau_{j,n}$ is an inflexion point of $\hat{y}_n$ (Fig. 5.5 (d));

      - $y_{a,n} C_1 < 0. \Rightarrow \Delta t_n$ is from $\alpha_0 > \tau_{a,n}$ (*Lemma* B.1);

      - $y_{a,n} C_1 = 0. \Rightarrow \Delta t_n = \tau_{a,n}$ (*Lemma* B.1);

      - $y_{a,n} C_1 > 0. \Rightarrow \Delta t_n$ is from $\alpha_0 < \tau_{a,n}$ (*Lemma* B.1);

   - $C_1 v_{a,n} > 0. \Rightarrow v_n$ does not have any real root. Also, $\hat{y}_n$ has one real root Δt_n (Fig. 5.5 (e)), which may be found by choosing $\alpha_0 = \tau_{a,n}$ (*Lemma* B.3);

2. $c_n > 0. \Rightarrow \tau_{a,n} < \tau_{j,n}$;

  1. $C_1 C_2 < 0. \Rightarrow v_n$ has a unique root $\tau_{v,n} < \tau_{a,n}$;

   - $\hat{y}_{v,n} C_1 < 0. \Rightarrow \hat{y}_n$ has no real roots (Fig. 5.4 (i));

   - $\hat{y}_{v,n} C_1 = 0. \Rightarrow \Delta t_n = \tau_{v,n}$ (Fig. 5.4 (h));

   - $\hat{y}_{v,n} C_1 > 0. \Rightarrow \hat{y}_n$ has two roots (Fig. 5.4 (g)), $\Delta t_{1,n}$ from $\alpha_0 < \tau_{v,n}$ and $\Delta t_{2,n}$ from $\alpha_0 = \tau_{a,n}$ (*Lemma* B.1);

  2. $C_1 C_2 > 0$.

   - $C_1 v_{a,n} < 0. \Rightarrow v_n$ has two roots, $\tau_{v_1,n}$ and $\tau_{v_1,n}$. Let $\tilde{y}_{v_1,n} = \tilde{y}_n(\tau_{v_1,n})$ and $\tilde{y}_{v_2,n} = \tilde{y}_n(\tau_{v_2,n})$;

      - $\hat{y}_{v_1,n} \hat{y}_{v_2,n} < 0. \Rightarrow \hat{y}_n$ has three roots, $\Delta t_{1,n}$ from $\alpha_0 < \tau_{v_1,n}$, $\Delta t_{2,n}$ from $\alpha_0 = \tau_{a,n}$, and $\Delta t_{3,n}$ from $\alpha_0 > \tau_{v_2,n}$ (Fig. 5.5 (a), *Lemma* B.1);

- $\hat{y}_{v_1,n}\hat{y}_{v_2,n} = 0.$ $\Rightarrow$ $\hat{y}_n$ has two roots (Fig. 5.5 (b));

$\hat{y}_{v_1,n} = 0.$ $\Rightarrow$ the roots are $\Delta t_{1,n} = \tau_{v_1,n}$ and $\Delta t_{2,n}$ from $\alpha_0 > \tau_{v_2,n}$ (*Lemma* B.1);

$\hat{y}_{v_1,n} \neq 0.$ $\Rightarrow$ the roots are $\Delta t_{1,n}$ from $\alpha_0 < \tau_{v_1,n}$ and $\Delta t_{2,n} = \tau_{v_2,n}$ (*Lemma* B.1);

- $\hat{y}_{v_1,n}\hat{y}_{v_2,n} > 0.$ $\Rightarrow$ $\hat{y}_n$ has one root (Fig. 5.5 (c));

$\hat{y}_{v_1,n}C_1 < 0.$ $\Rightarrow$ Δt_n is from $\alpha_0 < \tau_{v_1,n}$ (*Lemma* B.1);

$\hat{y}_{v_1,n}C_1 > 0.$ $\Rightarrow$ Δt_n is from $\alpha_0 > \tau_{v_2,n}$ (*Lemma* B.1);

- $C_1 v_{a,n} = 0.$ $\Rightarrow$ v_n has one root $\tau_{v,n} = \tau_{a,n}$ (stationary point of inflexion, Fig. 5.5 (d));

  - $\hat{y}_{a,n}C_1 < 0.$ $\Rightarrow$ Δt_n is from $\alpha_0 < \tau_{a,n}$ (*Lemma* B.1);

  - $\hat{y}_{a,n}C_1 = 0.$ $\Rightarrow$ $\Delta t_n = \tau_{a,n}$;

  - $\hat{y}_{a,n}C_1 > 0.$ $\Rightarrow$ Δt_n is from $\alpha_0 > \tau_{a,n}$ (*Lemma* B.1);

- $C_1 v_{a,n} > 0.$ $\Rightarrow$ v_n does not have roots, and $\hat{y}_n$ has one root from $\alpha_0 = \tau_{a,n}$ (Fig. 5.5 (e), *Lemma* B.3).

In order to get the actual time δt_n when the spring stiffness does change, in case of multiple solutions $\tau_{v_q,n}$ and $\Delta t_{q,n}$, $q = 1, 2, \ldots$, the minimum positive one, whether it exist, is needed.

5.5 Hysteresis cycle branch finding

Once a break point location in the time domain is known, in order to update the stiffness value the only information still needed is what path of the $R - y$ diagram is followed by the spring–mass system right after that break point. As shown in Fig. 5.1, the $R - y$ diagram is made of two branches. One represents the spring configuration while $y(t)$ is monotonically increasing, and the other one applies when $y(t)$ is monotonically decreasing. When the velocity sign changes, the system configuration jumps instantaneously from one branch to another. In order to decide when this happens, it is necessary to analyze the displacement function and its derivatives when the velocity drops to zero. Let us suppose that $y_n(0) = y_{0,n}$, $\dot{y}_n(0) = \dot{y}_{0,n}$, $R_n(0) = R_{0,n}$, and $\mathcal{D}_n(0) = \mathcal{D}_{0,n}$ is a set of initial conditions at $\tau = 0$.

Then, from the Eqs. (5.6) and (5.7a), for any $\tau_x \in [0, t_{0,n+1} - t_{0,n}]$ we have

$$\ddot{y}_n(\tau) = \frac{1}{m} \left(F_{0,n} - R_{0,n} - D_{0,n} + k_n y_{0,n} + c_n \dot{y}_{0,n} - k_n y_n(\tau) - c_n \dot{y}_n(\tau) + F_{1,n}\tau \right)$$

$$\ddot{y}_n(\tau_x) = \frac{1}{m} \left(F_{0,n} - (R_{0,n} + k_n(y_n(\tau_x) - y_{0,n}))) - \right.$$
$$\left. - (D_{0,n} + c_n(\dot{y}_n(\tau_x) - \dot{y}_{0,n})) + F_{1,n}\tau_x \right)$$

$$\ddot{y}_n(\tau_x) = \frac{1}{m} \left(F_{0,n} - R_n(\tau_x) - D_n(\tau_x) + F_{1,n}\tau_x \right) \tag{5.143a}$$

$$y_n^{(3)}(\tau) = \frac{1}{m} \left(F_{1,n} - k_n \dot{y}_n(\tau) - c_n \ddot{y}_n(\tau) \right)$$

$$y_n^{(3)}(\tau_x) = \frac{1}{m} \left(F_{1,n} - k_n \dot{y}_n(\tau_x) - c_n \ddot{y}_n(\tau_x) \right) \tag{5.143b}$$

$$y_n^{(4)}(\tau) = -\frac{1}{m} \left(k_n \ddot{y}_n(\tau) + c_n y_n^{(3)}(\tau) \right)$$

$$y_n^{(4)}(\tau_x) = -\frac{1}{m} \left(k_n \ddot{y}_{\tau_0,n} + c_n y_{\tau_0,n}^{(3)} \right) \tag{5.143c}$$

$$\vdots$$

$$y_n^{(q)}(\tau) = -\frac{1}{m} \left(k_n y_n^{(q-2)}(\tau) + c_n y_n^{(q-1)}(\tau) \right), \quad q \geq 4$$

$$y_n^{(q)}(\tau_x) = -\frac{1}{m} \left(k_n y_{\tau_0,n}^{(q-2)} + c_n y_{\tau_0,n}^{(q-1)} \right), \quad q \geq 4 \tag{5.143d}$$

where $y_n^{(q)}(\tau)$ is the qth derivative of the displacement function. Now let us expand $y_n(\tau)$ in a Taylor series, in a neighborhood of $\tau = \tau_x$:

$$y_n(\tau) = y_{\tau_x,n} + \dot{y}_{\tau_x,n}(\tau - \tau_x) + \frac{1}{2}\ddot{y}_{\tau_x,n}(\tau - \tau_x)^2 + \frac{1}{6} y_{\tau_x,n}^{(3)}(\tau - \tau_x)^3 + \dots \tag{5.144}$$

$$y_{\tau_x,n} = y_n(\tau_x), \ \dot{y}_{\tau_x,n} = \dot{y}_n(\tau_x), \ \ddot{y}_{\tau_x,n} = \ddot{y}_n(\tau_x), \ y_{\tau_x,n}^{(3)} = y_n^{(3)}(\tau_x)$$

For any τ close enough to τ_x, the function behavior is established by the firs non zero derivative $y_{\tau_x,n}^{(q)}$ into the Eq. (5.144), $\forall q \geq 1$. Also, the Eq. (5.143d) shows that, whether $\dot{y}_{\tau_x,n} = \ddot{y}_{\tau_x,n} = y_{\tau_x,n}^{(3)} = 0$, then $y_{\tau_x,n}^{(q)} = 0 \ \forall q \geq 4$. This implies that only the first three derivatives of $y_n(\tau)$ need to be surveyed. If, for any $\tau_x \in \mathbb{R}$, we define a

function $Y(\tau_x)$ as

$$Y(\tau_x) = \begin{cases} \text{sgn}(\dot{y}_{\tau_x,n}), & \text{if } \dot{y}_{\tau_x,n} \neq 0 \\ 2 \cdot \text{sgn}(\ddot{y}_{\tau_x,n}), & \text{if } \dot{y}_{\tau_x,n} = 0, \ \ddot{y}_{\tau_x,n} \neq 0 \\ 3 \cdot \text{sgn}(y_{\tau_x,n}^{(3)}), & \text{if } \dot{y}_{\tau_x,n} = \ddot{y}_{\tau_x,n} = 0, \ y_{\tau_x,n}^{(3)} \neq 0 \\ 0, & \text{if } \dot{y}_{\tau_x,n} = \ddot{y}_{\tau_x,n} = y_{\tau_x,n}^{(3)} = 0 \end{cases} \tag{5.145}$$

we may state that, when $Y(\tau_x) = 1$, $y_n(\tau)$ is monotonically increasing in a neighborhood of such point (Fig. 5.1, branch (a)), while if $Y(\tau_x) = -1$, $y_n(\tau)$ is monotonically decreasing in a neighborhood of τ_x (Fig. 5.1, branch (b)). When $Y(\tau_x) = \pm 2$, $y_n(\tau)$ has a local minimum or maximum at $\tau = \tau_x$, which implies a jump of the system configuration from one branch of the $R - y$ diagram to the other one; when $Y(\tau_x) = 3$, $y_n(\tau)$ has a stationary point of inflexion at $\tau = \tau_x$, and it is monotonically increasing in a neighborhood of such point (branch (a)), while if $Y(\tau_x) = -3$, $y_n(\tau)$ is monotonically decreasing in a neighborhood of τ_x (branch (b)). Finally, when $Y(\tau_x) = 0$, $y_n(\tau) = y_n(\tau_x) = \text{constant}$. In the last case, at $\tau = \tau_x$ the system is in a condition of a static equilibrium, which holds until the external excitation changes. Indeed, from the Eqs. (5.143a), (5.143b), and (5.145) we get $F_{0,n} = R_n(\tau_x) + \mathcal{D}_n(\tau_x)$ and $F_{1,n} = 0$, which means the external force $F_n(\tau) = F_{0,n} + F_{1,n}\tau$ is constant in time and balanced by the internal force $R_n(\tau_x) + \mathcal{D}_n(\tau_x)$. Thus, since $\dot{y}(\tau_x) = 0$, the system is motionless and, unless the external force changes, the dynamic analysis is ended.

Now let us suppose that during an infinitesimal interval $[\tau_x, \tau_x + d\tau]$ the spring stiffness goes to $\pm\infty$. This means the oscillator velocity drops to zero instantaneously. The spring force jumps to the value $R_n(\tau_x + d\tau) = \min\{F_{0,n}, R_{0,n+1}\}$ if $k_n \to +\infty$, and to the value $R_n(\tau_x + d\tau) = \max\{F_{0,n}, R_{0,n+1}\}$ if $k_n \to -\infty$. Then, recalling the Eqs. (5.143a)–(5.143a), we get

$$y_n(\tau_x + d\tau) = y(\tau_x), \qquad \dot{y}_n(\tau_x + d\tau) = 0 \tag{5.146}$$

$$\ddot{y}_n(\tau_x + d\tau) = \frac{1}{m}\left(F_{0,n} - R_n(\tau_x + d\tau) - \mathcal{D}_n(\tau_x + d\tau) + F_{1,n}\tau_x\right)$$

$$y_n^{(3)}(\tau_x + d\tau) = \frac{1}{m}\left(F_{1,n} - c_n\ddot{y}_n(\tau_x + d\tau)\right)$$

$$R_n(\tau_x + d\tau) = \begin{cases} \min\{F_{0,n}, R_{0,n+1}\}, & \text{if } k_n \to +\infty \\ \max\{F_{0,n}, R_{0,n+1}\}, & \text{if } k_n \to -\infty \end{cases} \tag{5.147}$$

The value of $Y(\tau_x)$ may be found from the Eqs. (5.146) and (5.147). As discussed above, the system configuration undergoes a branch jump if and only if $Y(\tau_x) = \pm 2$.

5.6 Non linear modeling of reinforced concrete members

In this section, a simple application of the non linear oscillator so far described is shown. A reinforced concrete column under axial dynamic load from Eq. (4.1) is considered. The dynamic behavior of such structural member depends upon the constitutive laws of the concrete and reinforcing steel bars it is made of. Since both materials have non linear and strain rate dependent stress–strain constitutive laws, a displacement and velocity dependent spring needs to be introduced within the equivalent structural model. This further complication may be easily got over by knowing the roots of any function resulting from the sum of the oscillator velocity function plus a constant, in analogy with what seen for the displacement function. It may be noted that such issue does not require any further theoretical work concerning the root seeking.

Concrete in compression may be modeled according to Scott *et al.* [25],

$$f_c = K f_c' \left[\frac{2\varepsilon_c}{0.002K} - \left(\frac{2\varepsilon_c}{0.002K} \right)^2 \right], \qquad \varepsilon_c \leq 0.002K$$

$$f_c = K f_c' [1 - Z_m(\varepsilon_c - 0.002K)], \ \ f_c \geq 0.2K f_c', \qquad \varepsilon_c > 0.002K$$

$$K = 1.25 \left(1 + \frac{\varrho_s f_{yh}}{f_c'} \right)$$

$$Z_m = \frac{1.25 \cdot 0.5}{\dfrac{3 + 0.29 f_c'}{145 f_c' - 1000} + \dfrac{3}{4} \varrho_s \sqrt{\dfrac{h''}{S_h}} - 0.002K}$$

where

- ε_c is the longitudinal strain in concrete;

- f_c is the longitudinal stress in concrete;

- f_c' is the concrete compressive cylinder strength;

154

- f_{yh} is the yield strength of hoop reinforcement;

- ϱ_s is the ratio of volume of hoop reinforcement to volume of concrete core measured to outside the hoops;

- h'' is the width of concrete core measured to outside of the peripheral hoop;

- S_h is the center–to–center spacing of hoop sets;

- the multiplying factor 1.25, applied to the peak stress, the strain at the peak stress, and the slope of the falling branch, has the purpose to adapt the stress–strain relation for high strain rates.

For concrete in tension, the stress–strain diagram proposed by Carreira and Chu [71] for static loads may be adopted,

$$f_{ts} = f'_t \frac{\Upsilon \dfrac{\varepsilon_t}{\varepsilon'_t}}{\Upsilon - 1 + \left(\dfrac{\varepsilon_t}{\varepsilon'_t}\right)^\Upsilon}$$

in which

- f_{ts} is the stress corresponding to the strain ε_t in case of static load;

- f'_t is the tensile strength. Depending on the degree of cracking, it may be assumed between 0.29 and 0.37 $\sqrt{f'_c}$ in MPa;

- ε'_t is the strain corresponding to the maximum stress f'_t. For cracked concrete sections, it may be taken as 1/10 of ε'_c (for design purposes $\varepsilon'_c = 0.002$ is recommended);

- Υ may be assumed according to Carreira and Chu [72],

$$\Upsilon = \left(\frac{f'_c}{32.4}\right)^3 + 1.55$$

In order to take into account the strain rate effects on concrete in tension, the dynamic increase factor suggested by Malvar and Ross [31] is adopted,

$$\text{DIF} = \frac{f_{td}}{f_{ts}} = \left(\frac{\dot{\varepsilon}_t}{\dot{\varepsilon}_{ts}}\right)^{\delta}, \qquad\qquad \dot{\varepsilon}_t \leq 1 \text{ s}^{-1}$$

$$\text{DIF} = \frac{f_{td}}{f_{ts}} = \beta \left(\frac{\dot{\varepsilon}_t}{\dot{\varepsilon}_{ts}}\right)^{\frac{1}{3}}, \qquad\qquad \dot{\varepsilon}_c > 1 \text{ s}^{-1}$$

where

- f_{td} and f_{ts} represent the dynamic and static tensile stress in concrete, respectively;

- DIF is the dynamic increase factor;

- $\dot{\varepsilon}_t$ and $\dot{\varepsilon}_{ts}$ are the current strain rate (up to 10^4 s^{-1}) and the static strain rate ($10^{-5} \sim 10^{-6}$ s^{-1});

- $\beta = e^{6\delta - 2}, \quad \delta = 1/[1 + 8(f_c'/f_{c0}')]$;

- f_{c0}' is a fraction of concrete strength in compression (10 Mpa).

The stress–strain relation of reinforcing steel bars is assumed to be elastic–perfectly plastic,

$$f_{sd} = \text{DIF} \cdot E_s \cdot \varepsilon_s, \qquad\qquad 0 \leq \varepsilon_s \leq \varepsilon_y$$

$$f_{sd} = \text{DIF} \cdot E_s \cdot \varepsilon_y, \qquad\qquad \varepsilon_s > \varepsilon_y$$

where f_{sd} is the dynamic stress in steel bars, ε_s is the corresponding strain, E_s is the modulus of elasticity of steel, ε_y is the yield strain of steel, and DIF is the dynamic increase factor given by Malvar [41],

$$\text{DIF} = \left(\frac{\dot{\varepsilon}_s}{10^{-4}}\right)^{0.074 - 0.04(f_y/414)}$$

f_y being the static yield stress and $\dot{\varepsilon}_s$ the strain rate in steel.

By integrating the stress σ over the gross cross–section area and the strain ε over the span length L of the column, the axial force N and the axial displacement y of one end of the member may be derived. For a clamped column under a uniform pressure p acting in axial direction on the free end of such element, we get
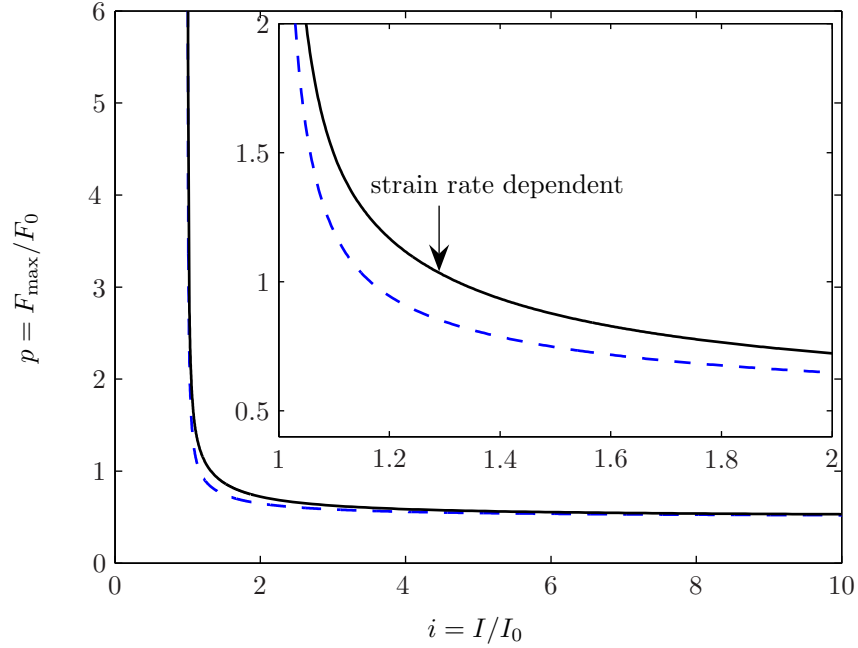
Fig. 5.13. Pressure–impulse diagrams for a reinforced concrete column under exponentially decaying axial load ($\lambda = 1$, $\gamma = 3$). The dashed curve is calculated without takeing into account strain rate effects on material constitutive laws; the solid curve is strain rate dependent.

$$N = \int_A \sigma(\varepsilon)\,dA = p \cdot A, \quad y = \int_0^L \varepsilon\,dx = L \cdot \varepsilon,$$

where A is the gross cross–section area of the column. This way, it is straightforward to get a force–displacement relationship for any stress–strain constitutive law reported above. In case of a column made of concrete with $f_c' = 30.48$ MPa and grade 60 reinforcing steel bars (yield and ultimate strength equal to 475 MPa and 750 MPa respectively), Fig. 5.13 shows the pressure–impulse curve induced by a loading function derived from the Eq. (4.1),

$$F(t) = \begin{cases} F_{\max}\left(1 - \dfrac{t}{t_d}\right)\exp\left(-3\dfrac{t}{t_d}\right) & \text{for} \quad 0 \le t \le t_d \\[2em] 0 & \text{for} \quad t > t_d \end{cases}$$

$$F(t) = P(t) \cdot A, \quad F_{\max} = P_{\max} \cdot A$$

where P is the pressure acting on the free end exposed to the blast, $P_{\max}$ is the peak overpressure, and the shape parameters λ and γ are set equal to 1 and 3 respectively. It may be noted that the enhanced strength of steel and concrete under high strain rate affects the structural response and the pressure–impulse diagram. Indeed, if

strain rate effects on material properties are taken into account, the resultant p–i curve is shifted up and to the right (Fig. 5.13).

Chapter 6

Conclusions and Recommendations

The linear oscillator described in chapter 4 is useful for predicting the overall response of structural members when the elastic deformations are dominant. Such linear model is obviously not capable to capture the actual behavior a structure which undergoes plastic deformations due to material nonlinearity. On the other hand, whenever the plastic deformation is negligible, a simple elastic analysis may represent an easy way to establish the structural response without any appreciable computational effort. However, in order to improve such model, some issues need further investigations. Many properties of the envelope function still need to be proved, such as the localization of the transition point. The response curve expression used in § 4.3.3 produces low residuals for the fitted curve, whose input data are generated by computer experiments. The notable complexity of such expression suggests to investigate simplified analytical forms for isodamage curves. Simple hyperbolic functions seem suitable to fit the data of these diagrams. However, for some load shapes, curves with sufficiently low values of residuals can not be obtained when only two parameters m_1 and m_2 are used. An improvement in that direction might be reached by using a linear combination of hyperbolic function powers, as it was done for the transient response spectrum. Lower values of the sum of squared deviations could allow the isodamage curves to collapse into an unique chart in the effective space, for any value of λ and γ. The influence of a given choice of the spectrum domain and set of constants $n_0, n_1, \ldots, n_4$ on the isodamage curve coefficients is also an issue worth of further investigations.

Genetic algorithms seemed to perform very well when used to get the response spectra and isodamage curves, since predicted the structural response with a good

accuracy and a low computational effort. Their peculiar flexibility and adaptability to any sort of optimization problem make them a useful tool in order to validate results from any analytical model.

A non linear, low time consuming, oscillator has been described in chapter 5. It represents a simple design tool capable to correctly evaluate the order of magnitude of the structural response of elements under high speed dynamic loads, such as the ones yield by shock waves from condensed high explosive detonations. The brief overview regarding loading/strain rate effects on the strength of building materials clearly showed that, under blast loads, such effects are relevant. Hence the necessity of takeing into account two aspects usually neglected in any simplified dynamic analysis: the material non linearity and the strain rate effects on the material constitutive laws. Such tasks are accomplished by the proposed non linear model through a wise application of the Newton–Raphson method, which always ensure a rate of convergence at least quadratic.

Any structural model described in the preset dissertation is based on a maximum displacement failure criterion. Thereafter, for a flexional problem, only global bending failure modes may be considered. However, many tests conducted over the years showed shear induced failure mechanisms, since the shear force caused by the short duration overpressure from a blast wave is many times higher than the shear force associated with flexural failure modes. The high shear stresses involved may lead to a global shear failure before any noticeable bending deformations. Such phenomenon point out the necessity to incorporate shear failure criteria in future structural models.

Any time flexural problems have been dealt with by single degree of freedom model considerations, the first mode deformed shape has been assumed in order to get an energetically equivalent SDOF system. This approach, although frequently used, is limited by the fact that suitable shape functions may be suggested without any previous finite element analysis only for very simple geometries and boundary conditions. Further investigations in this field may aim to predict the actual deformed shape with better accuracy.

Since SDOF models have the fundamental disadvantage of providing information only for one point of an actual structure, the analytical and numerical techniques developed in this thesis might be used to make up a multi degree of freedom model. After uncoupling the motion equations of any oscillator, the problem might be treated as that of many independent SDOF models.

Appendix A

Newton–Raphson Method

According to Mathews and Fink [73], if we assume that $f \in C^2 : [a, b] \to \mathbb{R}$, and there exist a number $\alpha \in [a, b]$ such that $f(\alpha) = 0$ and $f'(\alpha) \neq 0$, then there exist a $\delta > 0$ such that the sequence $\{\alpha_i\}_{i=0}^{\infty}$ defined by the iteration

$$\alpha_i = g(\alpha_{i-1}) = \alpha_{i-1} - \frac{f(\alpha_{i-1})}{f'(\alpha_{i-1})} \quad \text{for } i = 1, 2, \dots \tag{A.1}$$

will converge to α for any initial approximation $\alpha_0 \in [\alpha - \delta, \alpha + \delta]$.
The function $g(x)$ defined by formula

$$g(x) = x - \frac{f(x)}{f'(x)} \tag{A.2}$$

is called Newton–Raphson iteration function. Since $f(\alpha) = 0$, $g(\alpha) = \alpha$. This means the Newton–Raphson iteration for finding the root of the equation $f(x) = 0$ is accomplished by finding a fixed point of the function $g(x)$.

The proof of this theorem shows a general convergence criterion for any iterative method defined by the statement $\alpha_{i+1} = g(\alpha_i)$,

$$|g'(x)| < 1, \quad \forall x \in [\alpha - \delta, \alpha + \delta] \tag{A.3}$$

According to Hoffman [74], the Eq. (A.3) may be regarded as:

$$\left| \frac{\varepsilon_{i+1}}{\varepsilon_i} \right| = \left| \frac{f(x) f''(x)}{[f'(x)]^2} \right| \leq 1, \quad \forall x \in [\alpha_i, \alpha] \tag{A.4}$$

where $\varepsilon_i = \alpha_i - \alpha$ denote the ith error.

A.1 Speed of convergence

In order to discuss the rate of convergence of the Newton–Raphson method, it is useful to recall some concepts of error analysis. Suppose that $\hat{\alpha}$ is an approximation to α. The *absolute error* is $\varepsilon_\alpha = |\alpha - \hat{\alpha}|$, and the *relative error* is $r_\alpha = |\alpha - \hat{\alpha}|/|\alpha|$, provided that $\alpha \neq 0$. Also, the number $\hat{\alpha}$ is said to approximate α to d significant digits if d is the largest positive integer for which

$$\left| \frac{\alpha - \hat{\alpha}}{\alpha} \right| < \frac{10^{-d}}{2} \tag{A.5}$$

On the other hand, $\hat{\alpha}$ is said to approximate α to d decimal places if d is the largest positive integer for which

$$|\alpha - \hat{\alpha}| < \frac{10^{-d}}{2} \tag{A.6}$$

Now let us assume that $\{\alpha_i\}_{i=0}^\infty$ converges to α and set $\varepsilon_i = \alpha - \alpha_i$ for $i \geq 0$. If there exist two constants $C \neq 0$ and $\Gamma > 0$ such that

$$\lim_{i \to \infty} \frac{|\alpha - \alpha_{i+1}|}{|\alpha - \alpha_i|^\Gamma} = C \tag{A.7}$$

than the sequence is said to converge to α with order of convergence Γ. C is called asymptotic error constant. The larger is Γ, the faster the sequence converges. If $\Gamma = 1$, the convergence of $\{\alpha_i\}_{i=0}^\infty$ is called linear, while if $\Gamma = 2$ the convergence of $\{\alpha_i\}_{i=0}^\infty$ is called quadratic.

It might be shown that the order of convergence of the sequence defined by the Newton–Raphson itaration depends on the order of the root such sequence converges to. Assuming that $f(x)$ and its derivative $f'(x), \ldots, f^{(M)}(x)$ are defined and continuous on a neighborhood of $x = \alpha$, $f(x)$ has a root of order M at $x = \alpha$ if and only if

$$f(\alpha) = 0, f'(\alpha) = 0, \ldots, f^{(M-1)}(\alpha) = 0, \text{ and } f^{(M)}(\alpha) \neq 0$$

A root of order $M = 1$ is called *simple root*, and if $M > 1$ it is called a *multiple root*. According to Bercovier [75], if we assume α is a simple root, we get

$$f(\alpha) = f(\alpha_i) + f'(\alpha_i)(\alpha - \alpha_i) + \frac{1}{2}f''(\xi)(\alpha - \alpha_i)^2, \quad \xi \text{ between } \alpha_i \text{ and } \alpha$$

$$\alpha - \alpha_i + \frac{f(\alpha_i)}{f'(\alpha_i)} = -\frac{(\alpha - \alpha_i)^2 f''(\xi)}{2f'(\alpha_i)} \quad \Rightarrow \quad \alpha - \alpha_{i+1} = -\frac{(\alpha - \alpha_i)^2 f''(\xi)}{2f'(\alpha_i)}$$

$$\frac{|\varepsilon_{i+1}|}{|\varepsilon_i|^2} = \frac{|f''(\xi)|}{2|f'(\alpha_i)|} \quad \Rightarrow \quad \lim_{i \to \infty} \frac{|\varepsilon_{i+1}|}{|\varepsilon_i|^2} = \frac{1}{2}\left|\frac{f''(\alpha)}{f'(\alpha)}\right|, \ f'(\alpha) \neq 0.$$

Therefore, in case of a simple root α, the Newton's method converges at least quadratically, with asymptotic error constant $|f''(\alpha)|/|2f'(\alpha)|$. This means that, at each iteration, the number of the accurate significant digits doubles. It is worth noting that, in case of $f''(\alpha) = 0$, the order of convergence is higher.

In case $f(x)$ has a root of algebraic multiplicity M at $x = \alpha$, then there exists a continuous function $h(x)$ such that $f(x)$ may be expressed as the product

$$f(x) = (x - \alpha)^M h(x), \quad h(\alpha) \neq 0 \tag{A.8}$$

Also, the firs derivative is

$$f'(x) = (x - \alpha)^{M-1}\left[(x - \alpha)h'(x) + Mh(x)\right] \tag{A.9}$$

which vanishes at $x = \alpha \ \forall M > 1$. Hence the requirement that α be simple for the method to be quadratically convergent. Otherwise, if α is not simple, we have

$$\alpha_{i+1} - \alpha = \alpha_i - \alpha - \frac{f(\alpha_i)}{f'(\alpha_i)} = \alpha_i - \alpha - \frac{(\alpha_i - \alpha)h(\alpha_i)}{(\alpha_i - \alpha)h'(\alpha_i) + Mh(\alpha_i)}$$

$$\left|\frac{\alpha_{i+1} - \alpha}{\alpha_i - \alpha}\right| = \left|1 - \frac{h(\alpha_i)}{(\alpha_i - \alpha)h'(\alpha_i) + Mh(\alpha_i)}\right|$$

$$\Rightarrow \quad \lim_{i \to \infty} \frac{|\varepsilon_{i+1}|}{|\varepsilon_i|} = \left|1 - \frac{h(\alpha)}{Mh(\alpha)}\right| = \frac{M-1}{M}, \ M \geq 2$$

So, the order of convergence of multiple roots is only linear and, as M gets bigger, the convergence slows down since the asymptotic error constant $(M-1)/M \to 1$. However, the function $q(x) = f(x)/f'(x)$ always has simple roots. Ideed,

$$q(x) = \frac{(x - \alpha)h(x)}{(x - \alpha)h'(x) - Mh(x)} \quad \Rightarrow \quad q(\alpha) = 0$$

$$q'(x) = \frac{[(x-\alpha)h'(x) + Mh(x)][(x-\alpha)h'(x) + h(x)]}{[(x-\alpha)h'(x) + Mh(x)]^2} -$$

$$-\frac{(x-\alpha)h(x)[(x-\alpha)h''(x) + (M+1)h'(x)]}{[(x-\alpha)h'(x) + Mh(x)]^2} \quad \Rightarrow \quad q'(\alpha) = \frac{1}{M} \neq 0$$

Hence, the Newton's method applied to $q(x)$ leads to the modified Newton's method

$$\alpha_{i+1} = \alpha_i - \frac{q(\alpha_i)}{q'(\alpha_i)}$$

$$q'(\alpha_i) = \frac{f'(\alpha_i)^2 - f(\alpha_i)f''(\alpha_i)}{[f'(\alpha_i)]^2}$$

$$\frac{q(\alpha_i)}{q'(\alpha_i)} = \frac{f(\alpha_i)f'(\alpha_i)}{f'(\alpha_i)^2 - f(\alpha_i)f''(\alpha_i)}$$

$$\alpha_{i+1} = \alpha_i - \frac{f(\alpha_i)f'(\alpha_i)}{f'(\alpha_i)^2 - f(\alpha_i)f''(\alpha_i)}$$

which is quadratically convergent to a root of any multiplicity, but requires more computational effort due to the evaluation of $f''(\alpha_i)$. Alternatively, it may be noted that if $f(x) = K(x-\alpha)^M$ for some constant K, then $f'(x) = KM(x-\alpha)^{M-1}$, $f(x)/f'(x) = (x-\alpha)/M$, and $\alpha = x - Mf(x)/f'(x)$ $\forall x \in \mathbb{R}$. In a general case of multiple root, this becomes an approximation rather than an equality, and we get another modified Newton's method,

$$\alpha_{i+1} = \alpha_i - M\frac{f(\alpha_i)}{f'(\alpha_i)} \tag{A.10}$$

which does not require a calculation of $f''(\alpha_i)$, but it does require the calculation of the algebraic multiplicity M from

$$\left|\frac{\varepsilon_{i+1}}{\varepsilon_i}\right| \approx \frac{M-1}{M}$$

where ε_i and ε_{i+1} come from the Newton's method. This way, a quadratic convergence is still guaranteed. By recalling the Eqs. (A.8), (A.9), and (A.10), we have

$$\alpha_{i+1} - \alpha = \alpha_i - \alpha - M\frac{f(\alpha_i)}{f'(\alpha_i)} = \alpha_i - \alpha - M\frac{(\alpha_i - \alpha)h(\alpha_i)}{(\alpha_i - \alpha)h'(\alpha_i) + Mh(\alpha_i)}$$

$$\frac{\alpha_{i+1} - \alpha}{(\alpha_i - \alpha)^2} = \frac{\varepsilon_{i+1}}{\varepsilon_i^2} = \frac{1}{\alpha_i - \alpha} - M\frac{h(\alpha_i)}{(\alpha_i - \alpha)^2 h'(\alpha_i) + M(\alpha_i - \alpha)h(\alpha_i)}$$

$$\frac{\varepsilon_{i+1}}{\varepsilon_i^2} = \frac{1 - M\dfrac{h(\alpha_i)}{(\alpha_i - \alpha)h'(\alpha_i) + Mh(\alpha_i)}}{\alpha_i - \alpha}$$

$$\lim_{i \to \infty}\frac{\varepsilon_{i+1}}{\varepsilon_i^2} = \lim_{\alpha_i \to \alpha}\frac{1 - \dfrac{Mh(\alpha_i)}{(\alpha_i - \alpha)h'(\alpha_i) + Mh(\alpha_i)}}{\alpha_i - \alpha} =$$

$$\overset{H}{=} \lim_{\alpha_i \to \alpha}\frac{-Mh'(\alpha_i)[(\alpha_i - \alpha)h'(\alpha_i) + Mh(\alpha_i)]}{[(\alpha_i - \alpha)h'(\alpha_i) + Mh(\alpha_i)]^2} -$$

$$- \lim_{\alpha_i \to \alpha}\frac{Mh(\alpha_i)[(M + 1)h'(\alpha_i) + (\alpha_i - \alpha)h''(\alpha_i)]}{[(\alpha_i - \alpha)h'(\alpha_i) + Mh(\alpha_i)]^2} =$$

$$= -\frac{2M^2 h(\alpha)h'(\alpha) + Mh(\alpha)h'(\alpha)}{M^2 h^2(\alpha)} = \frac{M(2M + 1)h(\alpha)h'(\alpha)}{M^2 h^2(\alpha)} = \frac{2M + 1}{M}\frac{h'(\alpha)}{h(\alpha)}$$

$$\Rightarrow \quad \lim_{i \to \infty}\frac{|\varepsilon_{i+1}|}{|\varepsilon_i|^2} = \frac{2M + 1}{M}\left|\frac{h'(\alpha)}{h(\alpha)}\right|, \ h(\alpha) \neq 0$$

which proves that the order of convergence is 2 in case of $h'(\alpha) \neq 0$, and higher otherwise.

In order to establish a general criterion to evaluate the rate of convergence of the Newton's method, we may use the efficiency index suggested by Antia [76],

$$EI = \Gamma^{1/\theta},$$

where Γ is the order of convergence and θ is the cost per iteration, measured in units of cost required for the function evaluation (e.g., two function evaluations in each step imply $\theta = 2$). For secant iteration, it would be $\theta = 1$, since only the value of the function is required, while for the Newton's method $\theta = 1 + \chi$, where χ is the relative cost of evaluating $f'(x)$. Thus,

$$EI_S \approx 1.618, \qquad\qquad \text{for a secant iteration}$$

$$EI_N = \Gamma^{1/(1+\chi)}, \qquad\qquad \text{for a Newton's iteration}$$

Hence, if $\Gamma = 2$ and $\chi < 0.44$, the Newton's method is more efficient, otherwise the secant method should converge faster. If $f(x)$ is a polynomial, then an evaluation of $f'(x)$ is almost as costly as an evaluation of $f(x)$, and $\chi \approx 1$. Therefore, for polynomials, the secant method would be more efficient. However, if $f(x)$ involves exponential or trigonometric functions, then often the evaluation of $f'(x)$ may not require much more extra effort, provided that relevant information is preserved. In all the cases surveyed in § 5.4, the Newton's method is applied in a way such that $\Gamma \geq 2$, and trigonometric or exponential functions are always involved. Therefore, the efficiency index should be at least as high as for the secant method.

A.2   Convergence criteria

The iterative process of the Newton's method may be stopped when one of the following inequalities is satisfied,

$$\left| \frac{\alpha_{i+1} - \alpha}{\alpha} \right| \leq e_1 \tag{A.11}$$

$$|\alpha_{i+1} - \alpha| \leq e_2 \tag{A.12}$$

$$|f(\alpha_{i+1})| \leq e_3 \tag{A.13}$$

where e_1, e_2, and e_3 represent the accuracy required. If the firs criterion is chosen and $e_1 = 10^{-d}/2$, we get the root α with an accuracy of at least d significant digits. On the other hand, if the second criterion is chosen and $e_2 = 10^{-d}/2$, α has d decimal places at least correct. As far as the third criterion is concerned, the accuracy regards the function value instead of the root numerical value. If we set $e_3 = 10^{-d}/2$, we get at least d accurate decimal places of the function value, which means $d + 1$ significant figures of accuracy.

Since the value of α is unknown, the Eqs. (A.11) and Eqs. (A.12) are practical useless. Instead, the absolute and relative errors of the root value may be approximated as it follows:

$$\left| \frac{\alpha_{i+1} - \alpha_i}{\alpha_{i+1}} \right| \leq e_1 \tag{A.14}$$

$$|\alpha_{i+1} - \alpha_i| \leq e_2 \tag{A.15}$$

166

A.3   Drawbacks

The Newton–Raphson method may be derived from the Taylor series, truncated after the second term

$$f(\alpha_{i+1}) = f(\alpha_i) + f'(\alpha_i)(\alpha_{i+1} - \alpha_i) + \ldots \tag{A.16}$$

This method has excellent local convergence proprieties, but its global convergence proprieties may be really poor, due to the neglect of the higher order terms in the Taylor series of the Eq. (A.16). A more accurate extension of this technique is the Newton's second order method, which truncates the Taylor series after the third term to yield the equation

$$f(\alpha_{i+1}) = f(\alpha_i) + f'(\alpha_i)(\alpha_{i+1} - \alpha_i) + \frac{1}{2}f''(\alpha_i)(\alpha_{i+1} - \alpha_i)^2 + \cdots = 0 \tag{A.17}$$

This is a quadratic equation in $\alpha_{i+1} - \alpha_i$, whose solution is given by

$$\alpha_{i+1} - \alpha_i = \frac{-f'(\alpha_i) \pm \sqrt{[f'(\alpha_i)]^2 - 2f(\alpha_i)f''(\alpha_i)}}{f''(\alpha_i)}$$

The general iterative formula for this method would be

$$\alpha_{i+1}^+ = \alpha_i - \frac{f'(\alpha_i)}{f''(\alpha_i)} + \frac{\sqrt{[f'(\alpha_i)]^2 - 2f(\alpha_i)f''(\alpha_i)}}{f''(\alpha_i)} \tag{A.18a}$$

$$\alpha_{i+1}^- = \alpha_i - \frac{f'(\alpha_i)}{f''(\alpha_i)} - \frac{\sqrt{[f'(\alpha_i)]^2 - 2f(\alpha_i)f''(\alpha_i)}}{f''(\alpha_i)} \tag{A.18b}$$

and the choice between (A.18a) and (A.18b) would be determined by exploring bot values of α_{i+1}^+ and α_{i+1}^-, determining which one results in the function $f(\alpha_{i+1}^+)$ or $f(\alpha_{i+1}^-)$ being closer to zero. This procedure requires the evaluation of $f''(x)$ and the solution of a quadratic solution for $\Delta\alpha_i = \alpha_{i+1} - \alpha_i$, and it is not widely used. On the other hand, if the usual Newton–Raphson method is applied, it might be necessary to bracket the solution within a closed interval and ensure that successive approximations remain within such interval. The more common disadvantages of this method are reported below.

- Division by zero (Fig.A.1 (a)). If an iteration value α_i is such that $f'(\alpha_i) \cong 0$, then one may face a division by zero or a near–zero number. This will give a large magnitude for the next value α_{i+1};
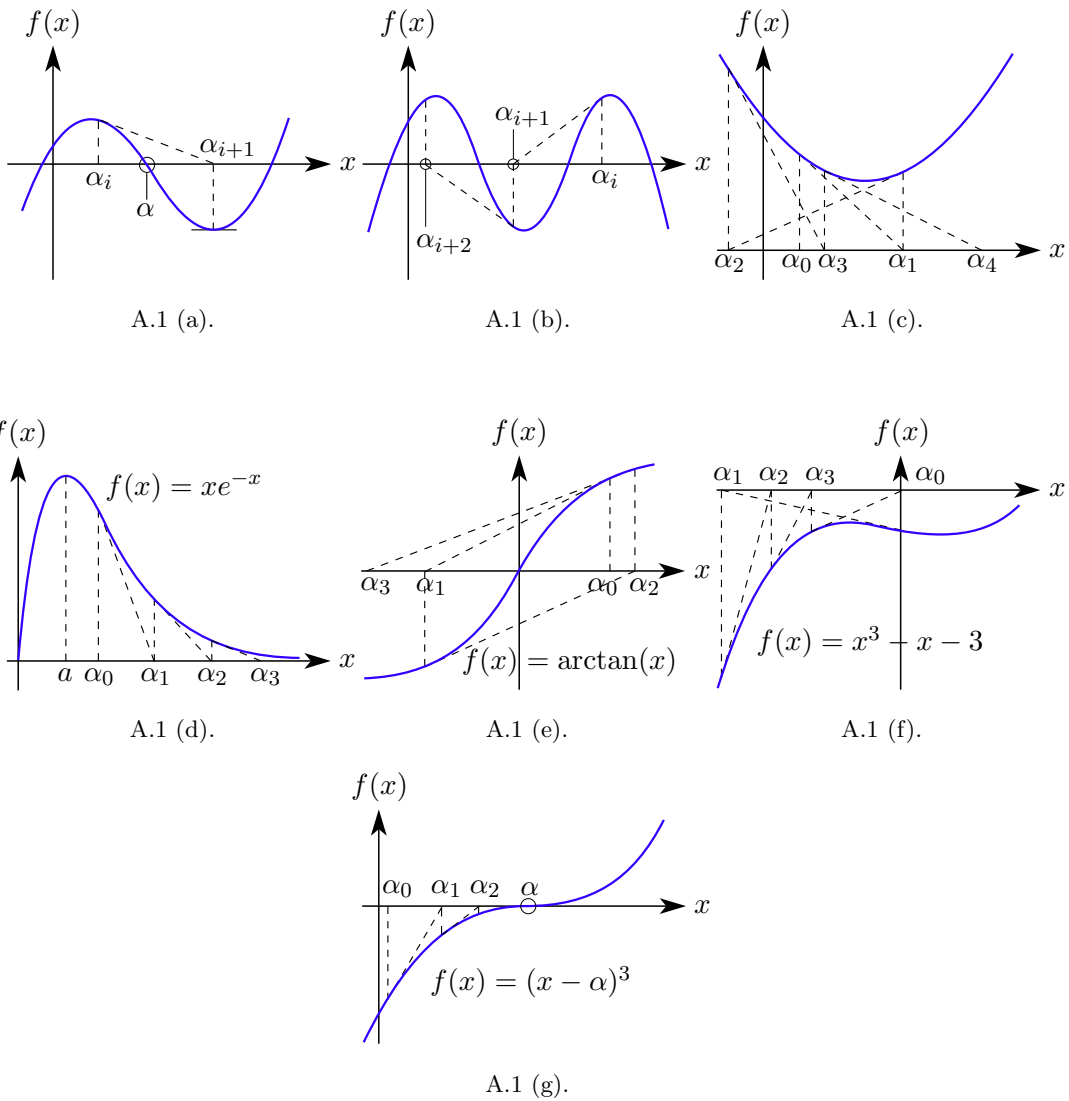
Fig. A.1. Newton–Raphson drawbacks.

- root jumping (Fig.A.1 (b)). In some cases where the function $f(x)$ is oscillating and has a number of roots, one may choose an initial guess close to a root. However, the guesses may jump and converge to another root;

- oscillations near local minimum or maximum (Fig.A.1 (c)). Iteration results may oscillate about a local minimum or maximum without converging on a root but converging on the local extremum. Eventually, it may lead to division by zero and may diverge;

- divergent sequence (Fig.A.1 (d)). Suppose that $f(x)$ is positive and monotonically decreasing on the unbounded interval $[a, \infty)$ and $\alpha_0 > a$. Then the sequence $\{\alpha_i\}_{i=0}^{\infty}$ might diverge to ∞. For example, it could be $f(x) = xe^{-x}$ and $\alpha_0 = 2$. This particular function has another problem, because the value of $f(x)$ goes to zero rapidly as x gets large, and some α_i could be eventually mistaken for a root;

- divergent oscillating sequence (Fig.A.1 (e)). When $|g'(x)| \geq 1$ on an interval containing the root α and the initial guess is chosen too far from such root, there is a chance of divergent oscillation. For example, let $f(x) = \arctan(x)$ and $\alpha_0 = 1.45$;

- cycling (Fig.A.1 (f)). It occurs when the terms in the sequence $\{\alpha_i\}_{i=0}^{\infty}$ tend to repeat or almost repeat. For example, $f(x) = x^3 - x - 3$ and $\alpha_0 = 0$;

- evaluation of the first derivative $f'(x)$. In general, the evaluation of the first derivative requires an extra effort compared to other numerical techniques, like the secant method. Also, when the function $f(x)$ is a general non linear relationship between an input x and an output $f(x)$, $f'(x)$ can not be determined analytically. In that case, $f'(x)$ may be estimated numerically by evaluating $f(x)$ at α_i and $\alpha_i + \delta$, and approximating $f'(x)$ as

$$f'(x) = \frac{f(\alpha_i + \delta) - f(\alpha_i)}{\delta}$$

This procedure doubles the number of function evaluations at each iteration, but the evaluation of $f'(x)$ is no longer necessary. If δ is small, round–off error are introduced, while if δ is too large, the convergence rate decreases. This process is called *approximate Newton method*. In some cases, the efficiency of the Newton's method is increased by using the same value of $f'(x)$ at each iteration. As long as the sign of $f'(x)$ does not change, the iterates α_i move

toward the root α, but the second order convergence is lost. However, in problems where the evaluation of $f'(x)$ is more costly than the evaluation of $f(x)$, this procedure may be more efficient, for example in case of a system of nonlinear equations. This procedure is called the lagged Newton's method.

- slow convergence in case of multiple roots (Fig.A.1 (g)). As seen above, in case of roots of algebraic multiplicity $M > 1$, the order of convergence drops to 1, and the bigger is M the lower is the speed of convergence.

In order to avoid all the drawbacks reported above, in the following appendix some lemmas are developed. Under the assumptions of such lemmas, the Newton–Raphson method always converges quadratically to the sought root. It should be noted that a multiple root problem is not dealt with in § 5.4. Any root is bracketed throw a check of the function sign, excepted when such function has an unique root on $\mathbb{R}$ and the second derivative sign changes no more than once. Also, a good initial guess is always located.

Appendix B

Applications of the Newton–Raphson Method

B.1 *Lemma*

Let $f(x)$ be a function such that:

- $f \in C^2 : [a, b] \to \mathbb{R}$;

- $f(a)f(b) < 0$;

- $f'(x) \neq 0 \; \forall x \in (a, b)$;

- $f''(x) \neq 0 \; \forall x \in (a, b)$;

- $\alpha_0 \in [a, b], \; g(\alpha_0) \in [a, b]$;

where $g(\alpha_0) = \alpha_0 - f(\alpha_0)/f'(\alpha_0) = \alpha_1$. Then f has an unique root $\alpha \in (a, b)$, and the sequence $\{\alpha_i\}_{i=1}^{\infty}$ such that $\alpha_{i+1} = \alpha_i - f(\alpha_i)/f'(\alpha_i), \; i = 0, 1, \ldots$ converges to α.

Proof. Let us suppose $f(a) < 0$ and $f''(x) > 0 \; \forall x \in (a, b)$. Then, according to the second hypothesis, it must be $f(b) > 0$. By applying the Bolzano theorem, there exist $\alpha \in (a, b)$ such that $f(\alpha) = 0$. Also, since f is strictly monotone in (a, b), α is the unique zero in $[a, b]$, and $f(x) < 0 \; \forall x \in [a, \alpha), \; f(x) > 0 \; \forall x \in (\alpha, b]$. According to Fitzpatrick [77], by applying the Lagrange reminder theorem it is easy to show that

$$f(b) = f(\alpha) + f'(\xi)(b - \alpha) = f'(\xi)(b - \alpha) > 0 \; \Rightarrow \; f'(\xi) > 0, \; \xi \in [\alpha, b]$$

Therefore, according to the 3$^{\text{rd}}$ hypothesis, $f'(x) > 0 \; \forall x \in (a, b)$ and, because of the continuity of f', $f'(a) \geq 0$ and $f'(b) \geq 0$.

Recalling the definition of the Newton–Raphson iteration function, $g(x) = x - f(x)/f'(x)$, it may be shown that $\forall x \in [a, b]$ such that $f'(x) \neq 0$, $g(x) > a$. Indeed, for some $\xi \in [a, x]$, we have

$$f(a) < \frac{1}{2} f''(\xi)(x - a)^2$$

$$f(a) + f'(a)(x - a) < f'(a)(x - a) + \frac{1}{2} f''(\xi)(x - a)^2$$

$$f(a) + f'(a)(x - a) + \frac{1}{2} f''(\xi)(x - a)^2 < f'(a)(x - a) + f''(\xi)(x - a)^2$$

$$f(x) < f'(x)(x - a)$$

$$\frac{f(x)}{f'(x)} < x - a$$

$$x - \frac{f(x)}{f'(x)} = g(x) > a \tag{B.1}$$

Now let $\alpha_0 \in [a, b]$ be an initial guess such that $\alpha_1 = \alpha_0 - f(\alpha_0)/f'(\alpha_0) \in [a, b]$. From the Eq. (B.1) we have $\alpha_1 > a$, thus $\alpha_1 \in (a, b]$ and $f'(\alpha_1) \neq 0$. Indeed, if $\bar{x} = (\alpha_1 - a)/2$, according to assumptions above it is $f'(x) > 0 \; \forall x \in (a, b)$ and $f''(x) \geq 0 \; \forall x \in [a, b]$; therefore

$$f'(\alpha_1) = f'(\bar{x}) + f''(\xi)(\alpha_1 - \bar{x}) > 0, \; \xi \in [\bar{x}, \alpha_1]$$

Also,

$$f(\alpha_1) = f(\alpha_0) + f'(\alpha_0)(\alpha_1 - \alpha_0) + \frac{1}{2} f''(\xi_{0,1})(\alpha_1 - \alpha_0)^2$$

$$= \frac{1}{2} f''(\xi_{0,1})(\alpha_1 - \alpha_0)^2 \geq 0, \quad \xi_{0,1} \text{ between } \alpha_0 \text{ and } \alpha_1$$

$$\alpha_2 = \alpha_1 - \frac{f(\alpha_1)}{f'(\alpha_1)} \leq \alpha_1$$

If we suppose $\alpha_i \in (a, b]$, $f'(\alpha_i) > 0$, and $f(\alpha_i) \geq 0$, we get

172

$$\alpha_{i+1} = \alpha_i - \frac{f(\alpha_i)}{f'(\alpha_i)} \le \alpha_i \le b$$

and by recalling the Eq. (B.1), $\alpha_{i+1} > a \ \Rightarrow \ \alpha_{i+1} \in (a, b]$

$$f'(\alpha_{i+1}) = f'(x_i) + f''(\xi)(\alpha_{i+1} - x_i) > 0, \ x_i = \frac{\alpha_{i+1} - a}{2}, \ \xi \in [x_i, \alpha_{i+1}]$$

$$f(\alpha_{i+1}) = f(\alpha_i) + f'(\alpha_i)(\alpha_{i+1} - \alpha_i) + \frac{1}{2}f''(\xi_{i,i+1})(\alpha_{i+1} - \alpha_i)^2$$

$$f(\alpha_{i+1}) = \frac{1}{2}f''(\xi_{i,i+1})(\alpha_{i+1} - \alpha_i)^2 \ge 0, \quad \xi_{i,i+1} \text{ between } \alpha_i \text{ and } \alpha_{i+1}$$

By the induction principle we may conclude that, if $g(\alpha_0) \in [a, b]$, then $\alpha_i \in (a, b]$, $f'(\alpha_i) > 0$, and $f(\alpha_i) \ge 0$, $\forall i \in \mathbb{N}$. Moreover, $\alpha_{i+1} \le \alpha_i, \ i = 1, 2, \ldots$

According to Buchanan and Turner [78], from the analysis of g' we get

$$g'(x) = \frac{f(x)f''(x)}{(f'(x))^2} \begin{cases} < 0, \ \forall x \in (a, \alpha) \\ = 0, \ x = \alpha \\ > 0, \ \forall x \in (\alpha, b) \end{cases}$$

and because of the continuity of f'', $g'(b) \ge 0$. Since $g(x) \in (a, b] \ \forall x = \alpha_0, \alpha_1, \ldots,$ we may write

$$g(x) - \alpha = g(x) - g(\alpha) = g'(\xi)(x - \alpha) \ge 0, \quad \text{for some } \xi \text{ betwee } x \text{ and } \alpha,$$

but $g(x) \ge \alpha \ \Rightarrow \ \alpha_i \ge \alpha, \ i = 1, 2, \ldots$

Therefore $\alpha \le \alpha_{i+1} \le \alpha_i \le \alpha_1 \ \forall i = 1, 2, \ldots$, that is the sequence $\{\alpha_i\}_{i=1}^{\infty}$ is bounded and monotone, and thus convergent.

Now let r be the limit of the sequence $\{\alpha_i\}_{i=1}^{\infty}$,

$$r = \lim_{i \to \infty} \alpha_i$$

It is clear that r is nothing but the limit of a sequence generated by the fixed–point iteration function g which, as well known, may only converge to the fixed point $r = g(r)$. Indeed, by applying the continuity of g, we get

$$g(r) = g(\lim_{i \to \infty} \alpha_i) = \lim_{i \to \infty} g(\alpha_i) = \lim_{i \to \infty} \alpha_{i+1} = \lim_{i \to \infty} \alpha_i = r$$

173

but

$$g(r) = r \quad \Rightarrow \quad f(r) = 0 \quad \Rightarrow \quad r = \alpha$$

This proves that the sequence $\{\alpha_i\}_{i=1}^{\infty}$ converges to the root α.

Remark 1. Since $f''(x) \neq 0 \ \forall x \in (a, b)$ and $a \neq b$, $f'(x)$ is strictly monotone in (a, b) and $f'(a) \neq f'(b)$. Let α_0 be an initial guess such that $\alpha_0 = a$ if $|f'(a)| > |f'(b)|$, and $\alpha_0 = b$ if $|f'(a)| < |f'(b)|$. Then, the sequence $\{\alpha_i\}_{i=1}^{\infty}$, $\alpha_{i+1} = g(\alpha_i)$, $i = 0, 1, \ldots$, converges to α. For example, in case of $f(a) < 0$ and $f''(x) > 0 \ \forall x \in (a, b)$, we get $f'(x) > 0 \ \forall x \in (a, b)$ and $f'(x)$ monotonically increasing on (a, b). This means $|f'(a)| < |f'(b)|$, therefore $\alpha_0 = b$, and

$$\alpha_1 = g(b) = b - \frac{f(b) > 0}{f'(b) > 0} < b$$

Also, by recalling the Eq. (B.1), we have $g(b) > a$, thus $g(b) \in (a, b)$, and the sequence started by $\alpha_0 = b$ converges to the unique root α.

Remark 2. Whether $f(a) < 0$, $f''(x) > 0 \ \forall x \in (a, b)$, $|f'(a)| < |f'(b)|$, and $b \to +\infty$, the fifth hypothesis is satisfied $\forall \alpha_0 > a$. Indeed, because of the Eq. (B.1), it is $g(\alpha_0) > a$, and of course it is $g(\alpha_0) < b = +\infty$, thus $g(\alpha_0) \in (a, b)$, and the sequence $\{\alpha_i\}_{i=1}^{\infty}$ converges to α.

Remark 3. This *Lemma* has been proved under the assumptions $f(a) < 0$ & $f''(x) > 0 \ \forall x \in (a, b)$. Under different assumptions ($f(a) < 0$ & $f''(x) < 0 \ \forall x \in (a, b)$, $f(a) > 0$ & $f''(x) > 0 \ \forall x \in (a, b)$, $f(a) > 0$ & $f''(x) < 0 \ \forall x \in (a, b)$), the proof may be given in the same way as seen above.

B.2 *Lemma*

Let $f(x)$ be a function such that:

- $f \in C^2 : \mathbb{R} \to \mathbb{R}$;

- $f(\alpha) = 0$;

- $f'(x) \neq 0 \ \forall x \in \mathbb{R}$;

- $f''(x) \neq 0 \ \forall x \in \mathbb{R}$.

Then, the sequence $\{\alpha_i\}_{i=1}^{\infty}$ such that $\alpha_{i+1} = \alpha_i - f(\alpha_i)/f'(\alpha_i)$, $i = 0, 1, \ldots$, converges to α for any choice of the initial guess $\alpha_0 \in \mathbb{R}$.

Proof. According to Fitzpatrick [77], by applying the Lagrange reminder theorem, for some ξ between x and α we have

$$f(x) = f(\alpha) + f'(\xi)(x - \alpha) = f'(\xi)(x - \alpha) \neq 0, \ \forall x \neq \alpha$$

which means the root α is unique. Also,

$$(x - \alpha)f(x)f'(\xi) > 0, \ \forall x \neq \alpha$$
$$\text{sgn}[(x - \alpha)f(x)f'(\xi)] = 1, \ \forall x \neq \alpha$$
$$\text{sgn}[(x - \alpha)f(x)] = \text{sgn}(f'), \ \forall x \neq \alpha$$

and since f is strictly monotone, for any ξ between x and α, $\xi \neq \alpha$, we get

$$\text{sgn}[(x - \alpha)f(\xi)] = \text{sgn}(f'), \ \forall x \neq \alpha \tag{B.2}$$

According to Mathews and Fink [73], since α is the unique root, $g(x) = x \Leftrightarrow x = \alpha$. Then, from Eq. (B.2), for some ξ between x and α, $\xi \neq \alpha$, we get

$$g(x) - \alpha = g(x) - g(\alpha) = g'(\xi)(x - \alpha) = \frac{f(\xi)f''(\xi)}{[f'(\xi)]^2}(x - \alpha)$$
$$\text{sgn}[g(x) - \alpha] = \text{sgn}[f(\xi)(x - \alpha)]\,\text{sgn}[f''(\xi)] = \text{sgn}(f')\,\text{sgn}(f'')$$
$$\text{sgn}[g(x) - \alpha] = \text{sgn}(f'f''), \ \forall x \neq \alpha \tag{B.3}$$

$$f'f'' > 0 \ \Rightarrow \ g(x) > \alpha, \ \forall x \neq \alpha$$
$$f'f'' < 0 \ \Rightarrow \ g(x) < \alpha, \ \forall x \neq \alpha \tag{B.4}$$

Again, since α is unique, by recalling the Eq. (B.3), for any initial guess $\alpha_0 \neq \alpha$ we may write

$$\alpha_1 = \alpha_0 - \frac{f(\alpha_0)}{f'(\alpha_0)} \neq \alpha, \ \alpha_1 \in \mathbb{R}$$
$$f(\alpha_1) = f(\alpha) + f'(\xi)(\alpha_1 - \alpha) = f'(\xi)(\alpha_1 - \alpha), \ \xi \text{ between } \alpha \text{ and } \alpha_1$$
$$\text{sgn}[f(\alpha_1)] = \text{sgn}(f')\,\text{sgn}(\alpha_1 - \alpha) = \text{sgn}(f')\,\text{sgn}(f')\,\text{sgn}(f'')$$
$$\text{sgn}[f(\alpha_1)] = \text{sgn}(f'') \tag{B.5}$$

and

$$\alpha_2 = \alpha_1 - \frac{f(\alpha_1)}{f'(\alpha_1)} \neq \alpha, \ \alpha_2 \in \mathbb{R}$$

$$\mathrm{sgn}(\alpha_2 - \alpha_1) = -\frac{\mathrm{sgn}[f(\alpha_1)]}{\mathrm{sgn}(f')} = -\mathrm{sgn}(f'f'')$$

Now let us take $\alpha_i \neq \alpha$. We have

$$f(\alpha_i) = f(\alpha) + f'(\xi)(\alpha_i - \alpha) = f'(\xi)(\alpha_i - \alpha)$$

$$\mathrm{sgn}[f(\alpha_i)] = \mathrm{sgn}(f') \, \mathrm{sgn}(\alpha_i - \alpha) = \mathrm{sgn}(f') \, \mathrm{sgn}(f') \, \mathrm{sgn}(f'')$$

$$\mathrm{sgn}[f(\alpha_i)] = \mathrm{sgn}(f'')$$

$$\alpha_{i+1} = \alpha_i - \frac{f(\alpha_i)}{f'(\alpha_i)} \neq \alpha, \ \alpha_{i+1} \in \mathbb{R}$$

$$\mathrm{sgn}(\alpha_{i+1} - \alpha_i) = -\frac{\mathrm{sgn}[f(\alpha_i)]}{\mathrm{sgn}(f')} = -\mathrm{sgn}(f'f'')$$

therefore, for any choice of $\alpha_0 \neq 0$ we may write

$$\mathrm{sgn}(\alpha_{i+1} - \alpha_i) = -\mathrm{sgn}(f'f''), \ i = 1, 2, \ldots$$

$$f'f'' > 0 \ \Rightarrow \ \alpha_{i+1} < \alpha_i$$
$$f'f'' < 0 \ \Rightarrow \ \alpha_{i+1} > \alpha_i, \quad i = 1, 2, \ldots \tag{B.6}$$

Thus, from Eqs. (B.4) and (B.6), we may conclude

$$f'f'' > 0 \ \Rightarrow \ \alpha < \alpha_i < \alpha_1$$
$$f'f'' < 0 \ \Rightarrow \ \alpha_1 < \alpha_i < \alpha \quad i = 1, 2, \ldots$$

This prove that the sequence $\{\alpha_i\}_{i=1}^{\infty}$ is bounded and monotone, and thus convergent. Also, by noting that $\{\alpha_i\}_{i=1}^{\infty}$ is nothing but the sequence generated by the fixed–point iteration function g, we may conclude that this sequence converges to the fixed point $r = g(r)$, which means $f(r) = 0$. Therefore $r = \alpha$.

B.3 *Lemma*

Let $f(x)$ be a function such that:

- $f \in C^2 : \mathbb{R} \to \mathbb{R}$;

- $f(\alpha) = 0$;

- $f'(x) \neq 0 \; \forall x \in \mathbb{R}$;

- $f''(x_c) = 0$ and $f''(x) \neq 0 \; \forall x \neq x_c, \; x_c \neq \alpha$.

Then, the sequence $\{\alpha_i\}_{i=1}^{\infty}$ such that $\alpha_0 = x_c$ and $\alpha_{i+1} = \alpha_i - f(\alpha_i)/f'(\alpha_i)$, $i = 0, 1, \ldots$ converges to α.

Proof. Since f' never vanish, f is strictly monotone and the root α is unique. Whether $f(x_c)f'(x_c) > 0$, the first four hypotheses of *Lemma* B.1 are satisfied by imposing $a \to -\infty$ and $b = x_c$. Thus, for any $\alpha_0 \in [a, b]$ such that $g(\alpha_0) \in [a, b]$, the sequence $\{\alpha_i\}_{i=1}^{\infty}$, $\alpha_{i+1} = \alpha_i - f(\alpha_i)/f'(\alpha_i)$, $i = 0, 1, \ldots$, converges to α. For example, it could be $\alpha_0 = x_c$ (see remark 2 of *Lemma* B.1).

In case of $f(x_c)f'(x_c) < 0$, the hypotheses of *Lemma* B.1 are satisfied by imposing $a = x_c$ and $b \to +\infty$, and the sequence $\{\alpha_i\}_{i=1}^{\infty}$ converges to α for any $\alpha_0 \in [a, b]$ such that $g(\alpha_0) \in [a, b]$. Again, it could be $\alpha_0 = x_c$.

B.4 *Lemma*

Let $f(x)$ be a function such that:

- $f \in C^2 : \mathbb{R} \to \mathbb{R}$;

- $f'(x_s) = 0$ and $f'(x) \neq 0 \; \forall x \neq x_s$;

- $f''(x)f(x_s) < 0 \; \forall x \in \mathbb{R}$.

Then, $f(x)$ has two real roots, $\alpha < x_s$ and $\beta > x_s$, as shown in Fig. B.1, and the Newton–Raphson method converges to one of them for any choice of the initial guess $\alpha_0 \neq x_s$. The root r found depends on the value of α_0: if $\alpha_0 < x_s \Rightarrow r = \alpha$, if $\alpha_0 > x_s \Rightarrow r = \beta$.

Proof. According to Fitzpatrick [77], by applying the Lagrange reminder theorem we get
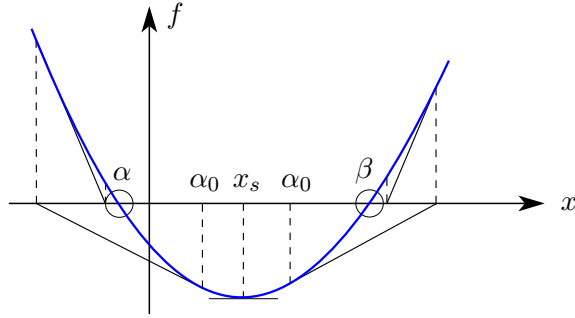
Fig. B.1. Newton–Raphson method under *Lemma* B.4 hypotheses.

$$f(x) = f(x_s) + f'(x_s)(x - x_s) + \frac{1}{2} f''(\xi)(x - x_s)^2$$

$$f(x) = f(x_s) + \frac{1}{2} f''(\xi)(x - x_s)^2, \ \xi \text{ between } x \text{ and } x_s$$

thus,

$$\lim_{x \to \pm\infty} f(x) = \lim_{x \to \pm\infty} \left(f(x_s) + \frac{1}{2} f''(\xi)(x - x_s)^2 \right) =$$

$$= f(x_s) \left(1 + \frac{1}{2} \lim_{x \to \pm\infty} \frac{f''(\xi)}{f(x_s)} (x - x_s)^2 \right) = -\text{sgn}(f(x_s)) \cdot \infty$$

and because of the continuity of f, there exist x^- and x^+ such that $\text{sgn}(f(x^-)) = \text{sgn}(f(x^+)) = -\text{sgn}(f(x_s))$. Also, f is strictly monotone within the subintervals $[x^-, x_s)$ and $(x_s, x^+]$, thus, by Bolzano theorem, there exist an unique $\alpha \in (x^-, x_s)$ and an unique $\beta \in (x_s, x^+)$ such that $f(\alpha) = f(\beta) = 0$. Finally, it should be noted that f satisfies the first four hypotheses of *Lemma* B.1 within those sub–domains, and by recalling the remark 2 of such lemma we may conclude that the sequence $\{\alpha_i\}_{i=1}^{\infty}$ converges to $\alpha \ \forall \, \alpha_0 < x_s$, and to $\beta \ \forall \, \alpha_0 > x_s$.

178

Appendix C

Trigonometric Identities

The periodic part of the displacement function y_n from the Eq. (5.43) can be put in the form

$$\tilde{y}_n(\tau) = e^{-\zeta_n \omega_n \tau} [A_1 \cos(\omega_{d,n} \tau) + A_2 \sin(\omega_{d,n} \tau)] = e^{-\zeta_n \omega_n \tau} A \cos(\omega_{d,n} \tau + \phi_y) \quad (C.1)$$

where $\bar{A} = A e^{-\zeta_n \omega_n \tau}$ and ϕ_y represent the vibration amplitude and the phase angle respectively. In order to find these constants, from the Eq. (C.1), we get

$$A \cos(\omega_{d,n} \tau + \phi_y) = A[\cos(\omega_{d,n} \tau) \cos \phi_y - \sin(\omega_{d,n} \tau) \sin \phi_y]$$

$$\begin{cases} A \cos \phi_y = +A_1 \\ A \sin \phi_y = -A_2 \end{cases} \Rightarrow \begin{cases} A^2 = A_1^2 + A_2^2 \\ \tan \phi_y = -\dfrac{A_2}{A_1} \end{cases} \Rightarrow \begin{cases} A = \pm\sqrt{A_1^2 + A_2^2} \\ \phi_y = \begin{cases} -\arctan\left(\dfrac{A_2}{A_1}\right) \\ \pi - \arctan\left(\dfrac{A_2}{A_1}\right) \end{cases} \end{cases}$$

If we assume $A = \sqrt{A_1^2 + A_2^2}$, we get

$$\sin \phi_y = -\frac{A_2}{\sqrt{A_1^2 + A_2^2}}, \quad \cos \phi_y = \frac{A_1}{\sqrt{A_1^2 + A_2^2}}.$$

Indeed,

$$
\begin{cases}
A \cos \phi_y = \sqrt{A_1^2 + A_2^2} \, \dfrac{A_1}{\sqrt{A_1^2 + A_2^2}} = A_1 \\[4mm]
A \sin \phi_y = \sqrt{A_1^2 + A_2^2} \left(-\dfrac{A_2}{\sqrt{A_1^2 + A_2^2}} \right) = -A_2
\end{cases}
$$

In order to pick a value for ϕ_y, the following cases must be considered,

- $A_1 < 0. \Rightarrow \cos \phi_y < 0 \;\Rightarrow\; \phi_y = \pi - \arctan\left(\dfrac{A_2}{A_1}\right)$;

- $A_1 > 0. \Rightarrow \cos \phi_y > 0 \;\Rightarrow\; \phi_y = -\arctan\left(\dfrac{A_2}{A_1}\right)$;

- $A_1 = 0. \Rightarrow \cos \phi_y = 0$;

  - $A_2 < 0. \Rightarrow \sin \phi_y = 1 \;\Rightarrow\; \phi_y = \dfrac{\pi}{2}$;
  - $A_2 = 0. \Rightarrow \tilde{y}_n \equiv 0$;
  - $A_2 > 0. \Rightarrow \sin \phi_y = -1 \;\Rightarrow\; \phi_y = -\dfrac{\pi}{2}$.

The velocity function may be represented as seen for the displacements,

$$
\begin{aligned}
v_n(\tau) &= e^{-\zeta_n \omega_n \tau} \left[B_1 \cos(\omega_{d,n}\tau) + B_2 \sin(\omega_{d,n}\tau) + A_3 \right] = \\
&= e^{-\zeta_n \omega_n \tau} B \cos(\omega_{d,n}\tau + \phi_v) + A_3
\end{aligned}
\qquad \text{(C.2)}
$$

where $B = \sqrt{B_1^2 + B_2^2}$ and ϕ_v depends on the sign of B_1 and B_2,

- $B_1 < 0. \Rightarrow \cos \phi_v < 0 \;\Rightarrow\; \phi_v = \pi - \arctan\left(\dfrac{B_2}{B_1}\right)$;

- $B_1 > 0. \Rightarrow \cos \phi_v > 0 \;\Rightarrow\; \phi_v = -\arctan\left(\dfrac{B_2}{B_1}\right)$;

- $B_1 = 0. \Rightarrow \cos \phi_v = 0$;

  - $B_2 < 0. \Rightarrow \sin \phi_v = 1 \;\Rightarrow\; \phi_v = \dfrac{\pi}{2}$;
  - $B_2 = 0. \Rightarrow v_n \equiv 0$;

- $B_2 > 0. \Rightarrow \sin\phi_v = -1 \Rightarrow \phi_v = -\dfrac{\pi}{2}$.

As far as the acceleration is considered, we have

$$a_n(\tau) = e^{-\zeta_n\omega_n\tau}[C_1\cos(\omega_{d,n}\tau) + C_2\sin(\omega_{d,n}\tau)] = e^{-\zeta_n\omega_n\tau}C\cos(\omega_{d,n}\tau + \phi_a)$$

$$C = \sqrt{C_1^2 + C_2^2} \tag{C.3}$$

- $C_1 < 0. \Rightarrow \cos\phi_a < 0 \Rightarrow \phi_a = \pi - \arctan\left(\dfrac{C_2}{C_1}\right)$;

- $C_1 > 0. \Rightarrow \cos\phi_a > 0 \Rightarrow \phi_a = -\arctan\left(\dfrac{C_2}{C_1}\right)$;

- $C_1 = 0. \Rightarrow \cos\phi_a = 0$;

  - $C_2 < 0. \Rightarrow \sin\phi_a = 1 \Rightarrow \phi_a = \dfrac{\pi}{2}$;
  - $C_2 = 0. \Rightarrow a_n \equiv 0$;
  - $C_2 > 0. \Rightarrow \sin\phi_a = -1 \Rightarrow \phi_a = -\dfrac{\pi}{2}$.

This time the phase angle depends on the ratio C_2/C_1, and in order to establish a relationship between ϕ_y and ϕ_a, C_1 and C_2 may be expressed in terms of A_1 and A_2,

$$
\begin{aligned}
C_1 &= -\zeta_n\omega_n B_1 + \omega_{d,n}B_2 = \\
&= -\zeta_n\omega_n(-\zeta_n\omega_n A_1 + \omega_{d,n}A_2) + \omega_{d,n}(-\zeta_n\omega_n A_2 - \omega_{d,n}A_1) = \\
&= (\zeta_n^2\omega_n^2 - \omega_{d,n}^2)A_1 - 2\zeta_n\omega_n\omega_{d,n}A_2 = \omega_n^2[(2\zeta_n^2 - 1)A_1 - 2\zeta_n\sqrt{1 - \zeta_n^2}A_2]
\end{aligned}
$$

$$
\begin{aligned}
C_2 &= -\zeta_n\omega_n B_2 - \omega_{d,n}B_1 = \\
&= -\zeta_n\omega_n(-\zeta_n\omega_n A_2 - \omega_{d,n}A_1) - \omega_{d,n}(-\zeta_n\omega_n A_1 + \omega_{d,n}A_2) = \\
&= \zeta_n^2\omega_n^2 A_2 + 2\zeta_n\omega_n\omega_{d,n}A_1 - \omega_{d,n}^2 A_2 = A_2(\zeta_n^2\omega_n^2 - \omega_{d,n}^2) + 2\zeta_n\omega_n\omega_{d,n}A_1 = \\
&= \omega_n^2[(2\zeta_n^2 - 1)A_2 + 2\zeta_n\sqrt{1 - \zeta_n^2}A_1]
\end{aligned}
$$

In case of $\zeta_n = 0$, from the two equations above we get

$$C_1 = -\omega_n^2 A_1, \quad C_2 = -\omega_n^2 A_2 \quad \Rightarrow \quad \frac{C_2}{C_1} = \frac{A_2}{A_1} \tag{C.4}$$

181

Since $\omega_n^2 = k_n/m$, when the stiffness is positive, we get

$$A_i < 0 \;\Leftrightarrow\; C_i > 0, \; i = 1, 2$$
$$A_i = 0 \;\Leftrightarrow\; C_i = 0, \; i = 1, 2$$
$$A_i > 0 \;\Leftrightarrow\; C_i < 0, \; i = 1, 2$$

which means that between the functions $\tilde{y}_n$ and a_n there is a phase shift $\Delta\phi = \phi_y - \phi_a = \pi$.

Bibliography

[1] G.F. Kinney, K.J. Graham, *Explosive shocks in air*, Springer–Verlag, New York, 1985.

[2] P.D. Smith, J.G. Hetherington, *Blast and Ballistic Loading of Structures*, Butterworth–Heinemann Ltd., London, 1994.

[3] W.E. Baker, P.A. Cox, P.S. Westine, J.J. Kulesz, R.A. Strehlow, *Explosion Hazards and Evaluation*, Elsevier, London, 1983.

[4] W.E. Baker, *Explosions in air*, University of Texas Press, Austin, 1973.

[5] N.M. Newmark, An engineering approach to blast resistant design, *Proceedings of ASCE*, Vol. 79, 1953.

[6] US Department of the Army Technical Manual, *Design of structures to resist the effects of accidental explosions*, TM 5–1300 (1990).

[7] H.W. Liepmann, A.Roshko, *Elements of Gas Dynamics*, Wiley, New York, 1957.

[8] H.L. Brode, Numerical solutions of spherical blast waves, *Journal of Applied Physics* 26 (6) (1955) 766–775.

[9] US Department of the Army Technical Manual, *Fundamentals of Protective Design for Conventional Weapons*, TM 5–855–1 (1986).

[10] B. Hopkinson, British ordnance board minutes 13565 (1915).

[11] C. Cranz, *Lehrbuch der Ballistik*, Springer–Verlag, Berlin, 1926.

[12] N.M. Newmark, R.J. Hansen, *Design of blast–resistant structures*, Vol. III of *Shock and Vibration Handbook*, McGraw–Hill, 1961.

[13] C.A. Mills, The design of concrete structures to resit explosions and weapon effects, *Proceedings of the 1st International Conference on concrete for hazard protections*, Edinburgh, 1987, pp. 61–73.

[14] J.E. Crawford, J. Karagozian, The behaviour and design of conventional structural components which are to resist blast loadings, Tech. Rep. TR–95–52.1, Karagozian & Case, Glendale, CA (1995).

[15] N.M. Newmark, External blast, *Proceedings of the International Conference on the planning and design of tall buildings*, Vol. 79, ASCE, 1972.

[16] G.C. Mays, P.D. Smith, *Blast Effects on Buildings – Design of Buildings to Optimize Resistance to Blast Loading*, Thomas Telford, London, 1995.

[17] J.R. Britt, J.L. Drake, M.B. Cobb, J.P. Mobley, *BLASTINW User's Manual ARA 5986–2 Contract DACA39-86-M-0213 for USAE Waterways Experiment Station*, Applied Research Associates Inc. (April 1986).

[18] J.R. Britt, J.L. Drake, M.B. Cobb, J.P. Mobley, *CHAMBERM User's Manual ARA 5986–1 Contract DACA39-86-M-0213 for USAE Waterways Experiment Station*, Applied Research Associates Inc. (April 1986).

[19] A.F.F. Tolba, Response of FRP–retrofitted reinforced concrete panels to blast loading, Ph.D. thesis, Department of Civil and Environmental Engineering, Carleton University, Ottawa, Canada (2001).

[20] S.C. Woodson, *Response of slabs: in plane forces and shear effects*, Structural concrete slabs under impulsive loads, Research Library, U.S. Army Engineer Waterways Experiment Station, Vicksburg, Mississippi, 1993, pp. 51–68.

[21] F. Toutlemonde, C. Boulay, Shock–tube tests of concrete slabs, *Materials and Structures* 26 (1993) 38–42.

[22] F. Toutlemonde, C. Boulay, *Dynamic failure modes of concrete slabs: experimental evidence and questions*, Structural concrete slabs under impulsive loads, Research Library, U.S. Army Engineer Waterways Experiment Station, Vicksburg, Mississippi, 1993, pp. 69–78.

[23] A. Watson, *Experimental analysis in the laboratory and in the field: approaches, observations, needs*, Structural concrete slabs under impulsive loads, Research Library, U.S. Army Engineer Waterways Experiment Station, Vicksburg, Mississippi, 1993, pp. 81–96.

[24] J.M. Biggs, *Introduction to Structural Dynamics*, McGraw–Hill, New York, 1964.

[25] B.D. Scott, R. Park, M.J.N. Priestley, Stress strain behaviour of concrete confined by overlapping hoops at low and high strain rates, *ACI Journal* 79 (2) (1982) 13–27.

[26] D. Bogosian, Parametric analysis of 12–inch substantial dividing walls, Tech. Rep. TR–94–20, Karagozian & Case, Glendale, CA (1994).

[27] H. Langberg, *Response of concrete structures subjected to close–in detonations*, Structural concrete slabs under impulsive loads, Research Library, U.S. Army Engineer Waterways Experiment Station, Vicksburg, Mississippi, 1993, pp. 5–14.

[28] P.H. Bischoff, S.H. Perry, Compressive behaviour of concrete at high strain rates, *Materials and Structures* 24 (1991) 425–450.

[29] M. Johansson, Structural behaviour of concrete frame corners of civil defence shelters, Ph.D. thesis, Department of Structural Engineering, Chalmers University of technology, Goteborg, Sweden (2000).

[30] L.E. Murr, *Metallurgical effects of shock and high-strain rate loading*, Materials at high strain rates, Elsevier Applied Science, Essex, England, 1987, pp. 1–46.

[31] L.J. Malvar, C.A. Ross, Review of strain rate effects for concrete in tension, *ACI Materials Journal* 95 (6) (1998) 735–739.

[32] D.A. Abrams, The effect of rate of application of load on the compressive strength of concrete, *Proceedings of ASTM*, Vol. 17, 1917, pp. 364–365.

[33] D. Watstein, Effect of straining rate on the compressive strength and elastic properties of concrete, *ACI Journal* 49 (8) (1953) 729–744.

[34] B.L. Atchley, H.L. Furr, Strength and energy absorption capabilities of plain concrete under dynamic and static loadings, *ACI Journal* 64 (1967) 745–756.

[35] P.R. Sparks, J.B. Menzies, The effect of rate of loading upon the static and fatigue strengths of plain concrete in compression, *Magazine of Concrete Research* 25 (83) (1973) 73–80.

[36] D.C. Spooner, Stress-strain-time relationships for concrete, *Magazine of Concrete Research* 23 (75/76) (1971) 127–131.

[37] M. Wakabayshi, T. Nakamura, N. Yoshida, S. Iwai, Y. Watanabe, Dynamic loading effects on the structural performance of concrete and steel materials and beams, *Proceedings of the 7th World Conference on Earthquake Engineering*, Vol. 6, Istanbul, Turkey, 1980, pp. 271–278.

[38] G.H. Norris, R.J. Hansen, M.J.Holly, J.M. Biggs, S. Namyet, J.K. Minami, *Structural design for dynamic loads*, McGraw–Hill, New York, 1959.

[39] A.R. Dowling, J. Harding, Tensile properties of mild steel under high strain rates, *Proceedings of the 1st HERF Conference*, Vol. 2, University of Denver, 1967.

[40] W. Keenan, A. Feldman, *The yield strength of intermediate grade reinforcing bars under rapid loading*, Naval Civil Engineering Laboratory, California, 1983.

[41] L.J. Malvar, Review of static and dynamic properties of steel reinforcing bars, *ACI Materials Journal* 95 (5) (1998) 609–616.

[42] J. Penzien, R.J. Hansen, Static and dynamic elatic behavior of reinforced concrete beams, *Journal of the ACI* 25 (7) (1954) 545–567.

[43] V.V. Bertero, D. Rea, S. Mahin, M.B. Atalay, Rate of loading effects on uncracked and repaired reinforced concrete members, *Proceedings of the 5th World Conference on Earthquake Engineering*, Vol. 1, Rome, 1973, pp. 1461–1470.

[44] J. Takeda, H. Tachikawa, Deformation and fracture of concrete subjected to dynamic load, *Proceedings of the International Conference on Mechanical Behaviour of Materials*, Vol. 4, Kyoto, Japan, 1971, pp. 267–277.

[45] T.P. Chang, Dynamic response of space structures under random excitation, *Computers and Structures* 48 (4) (1993) 575–582.

[46] Q.M. Li, H. Meng, Pressure–impulse diagram for blast loads based on dimensional analysis and single–degree–of–freedom model, *Journal of Engineering Mechanics* 128 (1) (2002) 87–92.

[47] Q.M. Li, H. Meng, Pulse loading shape effects on pressure–impulse diagram of an elasti–plastic, single–degree–of–freedom structural model, *International Journal of Mechanical Sciences* 44 (2002) 1985–1998.

[48] M.Y.H. Bangash, *Impact and Explosion-Analysis and Design*, Blackwell Scientific Publication, Oxford, 1993.

186

[49] T. Krauthammer, Blast mitigation technologies: developments and numerical considerations for behaviour assessment and design, *Proc. Int. Conf. on Structures Under Shock and Impact, SUSI*, Computational Mechanics Inc., 1998, pp. 3–12.

[50] G.R. Abrahamson, H.E. Lindberg, Peak load–impulse characterization of critical pulse loads in structural dynamics, *Nuclear Engineering and Design* 37 (1976) 35–46.

[51] G.K. Schleyer, S.S. Hsu, A modelling scheme for predicting the response of elastic–plastic structures to pulse pressure loading, *International Journal of Impact Engineering* 24 (2000) 759–777.

[52] Q.M. Li, N. Jones, Blast loading of fully clamped circular plates with transverse shear effects, *International Journal of Solids and Structures* 31 (14) (1994) 1861–1876.

[53] Q.M. Li, N. Jones, Blast loading of a 'short' cylindrical shell with transverse shear effects, *International Journal of Impact Engineering* 16 (2) (1995) 331–353.

[54] Q.M. Li, N. Jones, Blast loading of fully clamped beams with transverse shear effects, *Mechanics of Structures and Machines* 23 (1) (1995) 59–86.

[55] C.K. Youngdahl, Correlation parameters for eliminating the effect of pulse shape on dynamic plastic deformation, *ASME Journal of Applied Mechanics* 37 (1970) 744–752.

[56] C.K. Youngdahl, Dynamic plastic deformation of circular cylindrical shells, *ASME Journal of Applied Mechanics* 39 (1972) 746–750.

[57] C.K. Youngdahl, The interaction between pulse shape and strain hardening in dynamic plastic response, *International Journal of Impact Engineering* 7 (1988) 55–70.

[58] G. Zhu, Y.G. Huang, T.X. Yu, R. Wang, Estimation of the plastic structural response under impact, *International Journal of Impact Engineering* 4 (4) (1986) 271–282.

[59] M. Campidelli, E. Viola, An analytical–numerical method to analyze single degree of freedom models under airblast loading, *Journal of Sound and Vibration* 302 (2007) 260–286.

[60] Eurocode 1, Basis of design and actions on structures – Part 2–7: Actions on structures – Accidental actions due to impact and explosions, *UNI ENV 1991-2-7* (September 2000).

[61] H.J. Hansen, A. Kristensen, L. Damkilde, U. Thygesen, Structural analysis of offshore structures exposed to blast loads, *NSCM 15 – 15th Nordic Seminar on Computational Mechanics*, 2002, pp. 237–240.

[62] B.W. Lindgren, *Statistical Theory*, Macmillan, New York, 1976.

[63] J.R. Florek, H. Benaroya, Pulse–pressure loading effects on aviation and general engineering structures—review, *Journal of Sound and Vibration* 284 (2005) 421–453.

[64] S. Boyd, L. Vandenberghe, *Convex Optimization*, Cambridge University Press, 2004.

[65] J. Nocedal, S.J. Wright, *Numerical Optimization*, Springer, 2006.

[66] P.Y. Papalambros, D.J. Wilde, *Principles of Optimal Design: Modeling and Computation*, Cambridge University Press, 2000.

[67] The MathWorks Inc., 3 Apple Hill Drive Natick (MA), *Genetic Algorithm and Direct Search Toolbox User's Guide*, 2nd Edition (September 2007).

[68] M. Tomassini, *A survey of genetic algorithms*, Vol. III of *Annual Reviews of Computational Physics*, World Scientific, 1995, pp. 87–118.

[69] M. Campidelli, D. Bruno, E. Viola, Effetto della forma di carico di esplosioni detonanti sulla risposta di un oscillatore ad un grado di libertà, *Atti - XVI Convegno Italiano di Meccanica Computazionale*, XVI Convegno Italiano di Meccanica Computazionale, 2006, p. 24.

[70] R.W.D. Nickalls, A new approach to solving the cubic: Cardan's solution revealed, *The Mathematical Gazette* 77 (November 1993) 354–359.

[71] D.J. Carreira, K.H. Chu, Stress strain relationship for reinforced concrete in tension, *ACI Journal* 83 (3) (1986) 21–28.

[72] D.J. Carreira, K.H. Chu, Stress strain relationship for plain concrete in compression, *ACI Journal* 82 (72) (1985) 797–804.

[73] J.H. Mathews, K.D. Fink, *Numerical Methods Using MATLAB*, 3rd Edition, Prentice Hall, New Jersey, 1999.

[74] J.D. Hoffman, *Numerical Methods for Engineers and Scientists*, Marcel Dekker Inc., New York, 2001.

[75] M. Bercovier, *Numerical Solution Of Nonlinear Algebraic Equations*, `http://www.cs.huji.ac.il/course/2004/scicomp/`, lecture on Newton's method (2004).

[76] H.M. Antia, *Numerical Methods for Scientists and Engineers*, 2nd Edition, Birkhäuser Verlag, Boston, 2002.

[77] P.M. Fitzpatrick, *Advanced Calculus*, International Thomson Publishing Inc., Boston, 1996.

[78] J.L. Buchanan, P.R. Turner, *Numerical Methods and Analysis*, McGraw-Hill Inc., New York, 1992.